NORTH-WEST UNIVERSITY
YUNIBESITI YA BOKONE-BOPHIRIMA
NOORDWES-UNIVERSITEIT
POTCHEFSTROOMKAMPUS

Air quality in the Johannesburg-Pretoria megacity, its regional influence and identification of parameters that could mitigate pollution

ASM Lourens

MSc

Dissertation submitted in fulfilment of the requirements for the degree *Philosophiae Doctor* in Environmental Sciences at the Potchefstroom Campus of the North-West University

Supervisor: Dr JP Beukes

Co-supervisors: Dr TM Butler and Dr PG van Zyl

November 2012

Potchefstroom

Acknowledgements

“Have I not commanded you? Be strong and courageous. Do not be frightened, and do not be dismayed, for the LORD your God is with you wherever you go.” Joshua 1:9

Firstly, I want to thank my Heavenly Father, who enabled me with health, understanding and courage to complete this study.

I also want to acknowledge everyone who was and is part of my life. A special thank you to the following:

- Wouter, for your never-ending love, support and encouragement through the hard times of this study.
- My family and friends for their support, encouragement and understanding during this period.
- My parents, Wessel and Barbara Lourens, who believe in me.
- My mentors, Drs. JP Beukes, PG van Zyl and TM Butler for their support, encouragement, guidance, positive attitude and who were always available to assist me. No words can really express my gratitude.
- Dr GD Fourie, from Sasol, and Dr MG Lawrence, from the Max-Planck Institute for their financial contribution and also scientific inputs in this study.
- Grizelda du Toit for assisting me during the sampling.

Thank you

Sandra

Abstract

A megacity is generally defined as a city that, together with its suburbs or recognised metropolitan area, has a total population of more than 10 million people. Air pollution in megacities is a major concern due to large increases of populations over the past decades. Increases of air pollution result from more anthropogenic emission sources in megacities, which include energy production, transportation, industrial activities and domestic fuel burning. In the developing parts of Africa, urbanisation is increasing rapidly, with growth rates of populations in cities of up to 5% per annum. The major driving forces for these population increases in African countries can be attributed to population growth, natural disasters and armed ethnic conflicts. In South Africa, 62% of the total population lived in cities in 2010. The rate of urbanisation growth is predicted to be 1.2% per annum.

The largest urbanised city in South Africa is the Johannesburg-Pretoria conurbation (referred to as Jhb-Pta megacity) that has more than 10 million inhabitants. Johannesburg is considered to be the central hub of economic activities and -growth in South Africa. The larger conurbation includes all the suburbs of Johannesburg and Pretoria. In South Africa, household combustion and traffic emissions are major sources of pollutants in urbanised areas. The major pollutants emitted from these activities include nitrogen oxide (NO), nitrogen dioxide (NO_2), sulphur dioxide (SO_2), carbon monoxide (CO), particular matter (PM) and various organic compounds. The Jhb-Pta megacity is also located relatively close to large industrialised regions in South Africa, i.e. the Mpumalanga Highveld and the Vaal Triangle.

Very few air quality modelling studies have been conducted for the Jhb-Pta megacity. According to the knowledge of the author, no literature existed in peer-reviewed publications at the time of the study. An in-depth modelling study was therefore conducted to assess the current state of air quality within the Jhb-Pta megacity. The main objectives were to optimise an existing photochemical box model for the Jhb-Pta megacity and to utilise the model to investigate the photochemical processes in the Jhb-Pta megacity and surrounding areas. In this investigation, ground-based measurements of criteria atmospheric pollutant species representative of the Jhb-Pta megacity were obtained to utilise as input data in the model, as well as to compare to results determined with the model. From the ground-based measurements, the possible

contribution of the Jhb-Pta megacity to the NO_2 hotspot observed over the South African Highveld from satellite retrievals was also contextualised.

Five ground-based monitoring sites were situated strategically within the boundaries of the Jhb-Pta megacity to measure the direct influences of urban air pollution, e.g. traffic emissions, biomass burning and residential pollution. One measurement site was situated outside the modelling domain in order to collect rural background data in close proximity to the Jhb-Pta megacity. All the air quality stations continuously measured the criteria pollutants NO_x, SO_2 and O_3. In addition, benzene, toluene, ethylbenzene and xylene (BTEX) were measured at four sites. Passive sampling of NO_x, SO_2, O_3 and BTEX was also conducted in March and April 2010. Active data was obtained for March to May 2009, since no active measurements were available for the same year that passive sampling was performed due to logistical reasons. Meteorological parameters that included temperature, pressure and relative humidity were also measured at the monitoring stations

Ground-based measurements provided a good indication of the state of the air quality in the Jhb-Pta megacity. The air quality levels of NO_2, SO_2, O_3 and BTEX could be compared to other cities in the world. A distinct diurnal cycle was observed for NO_2 at most of the stations. An early morning peak between 6:00 and 9:00 coincided with the time that commuters travel to work, whereas an evening peak between 18:00 and 21:00 could be attributed to traffic emissions and household combustion. Levels of O_3, which is a secondary pollutant, peaked between 13:00 and 15:00. This diurnal pattern could be attributed to the photochemical formation of O_3 from precursor species NO and VOCs. Toluene was predominantly higher than the other BTEX species. Benzene and xylene concentrations were in the same order, while the lowest levels were measured for ethyl benzene

Ground-based measurements also indicated that the NO_2 Highveld hotspot, which is well known in the international science community due to its prominence in satellite images, is accompanied by a second hotspot over the Jhb-Pta megacity. Peak NO_2 pollution levels in the Jhb-Pta megacity exceeded the maximum daily Highveld values during the morning and evening rush hours. This result is significant for the more than 10 million people living in the Jhb-Pta megacity. Although satellite instruments have been extremely valuable in pointing out global hotspots, a limitation of satellite retrievals due to their specific overpass times has been presented.

Chemical processes in the Jhb-Pta megacity were investigated by utilising an existing photochemical box model, i.e. MECCA-MCM. This model was further developed in this study and was termed the MECCA-MCM-UPWIND model. This model included horizontal and vertical mixing processes in the atmosphere. These processes were included to simulate the advection of upwind air masses into the modelling domain, as well as the entrainment from the troposphere resulting from the diurnal mixing layer (ML) height variation. Three processes, i.e. horizontal mixing, vertical mixing and ML height variation, were built into the MECCA-MCM-UPWIND model. The model was tested and evaluated to determine the efficiency of the model to represent atmospheric mixing processes. MECCA-MCM-UPWIND simulated horizontal mixing, vertical entrainment and ML height variations as expected.

The input data for the model runs for the Jhb-Pta megacity modelling runs were either obtained from ground-based measurements or literature. Input data included meteorology, emission inventory, ML height and mixing ratios of the atmospheric chemical species. The chemical composition of the air mass entering the Jhb-Pta megacity was determined with MECCA-MCM-UPWIND. The concentrations and diurnal variability of criteria pollutant species were well predicted with the MECCA-MCM-UPWIND model. The day-time chemistry, especially, compared well, while slight under-predictions were observed for the night-time chemistry for most of the species. The differences observed between modelled and measured data could partially be ascribed to uncertainties associated with some of the input data obtained from literature used.

The MECCA-MCM-UPWIND model was used to perform sensitivity studies on the influence of different parameters on O_3 levels in the Jhb-Pta megacity. Possible scenarios to alter or mitigate pollution were also investigated. The results from the sensitivity analyses showed that O_3 mixing ratios decreased within the Jhb-Pta megacity with increasing wind speeds. The contribution of local emissions to the change in the concentration of pollutants is reduced at higher wind speeds. It also indicated that the Mpumalanga Highveld can potentially be a source of NO_x in the Jhb-Pta megacity that can lead to the titration of O_3. This also implies that if the air quality of the surrounding area improves, the concentration of the secondary pollutant O_3 will increase in the Jhb-Pta megacity due to the decrease in the titration of O_3. Sensitivity analyses also indicated that the Jhb-Pta megacity is a VOC-limited (or NO_x-saturated) regime. Therefore, O_3 reduction in the Jhb-Pta megacity will mostly be effective if VOC emissions are reduced. The same effect was observed in various cities world-wide where O_3 increased when NO_x emissions

were reduced during emission control strategies. The effect of reducing vehicular emissions in the Jhb-Pta megacity on the instantaneous production of O_3 was also investigated. A significant increase of approximately 23ppb O_3 production was observed when changing from Euro-0 to Euro-3 vehicles with lower emissions of VOCs, NO_x and CO. This compares with other modelled sensitivity studies of traffic emissions that also predict that future urban O_3 concentrations will increase in many cities by 2050 due to the reduction in the NO_x titration of O_3 despite the implementation of O_3 control regulations

Keywords

Johannesburg-Pretoria megacity, air pollution, passive sampling, active sampling, South African Highveld hotspot, satellite retrievals, photochemical box model

Table of contents

Chapter 3
Contextualising the NO_2 hotspot over South Africa

Chapter 4
Model development

Chapter 5

Model results

Chapter 6
Project evaluation and future perspectives

Annex

List of figures

Chapter 1

Chapter 2

Chapter 3

Chapter 4

Chapter 5

List of tables

Chapter 1

Chapter 2

Chapter 3

Chapter 4

Chapter 5

Graphical layout of Chapter 1

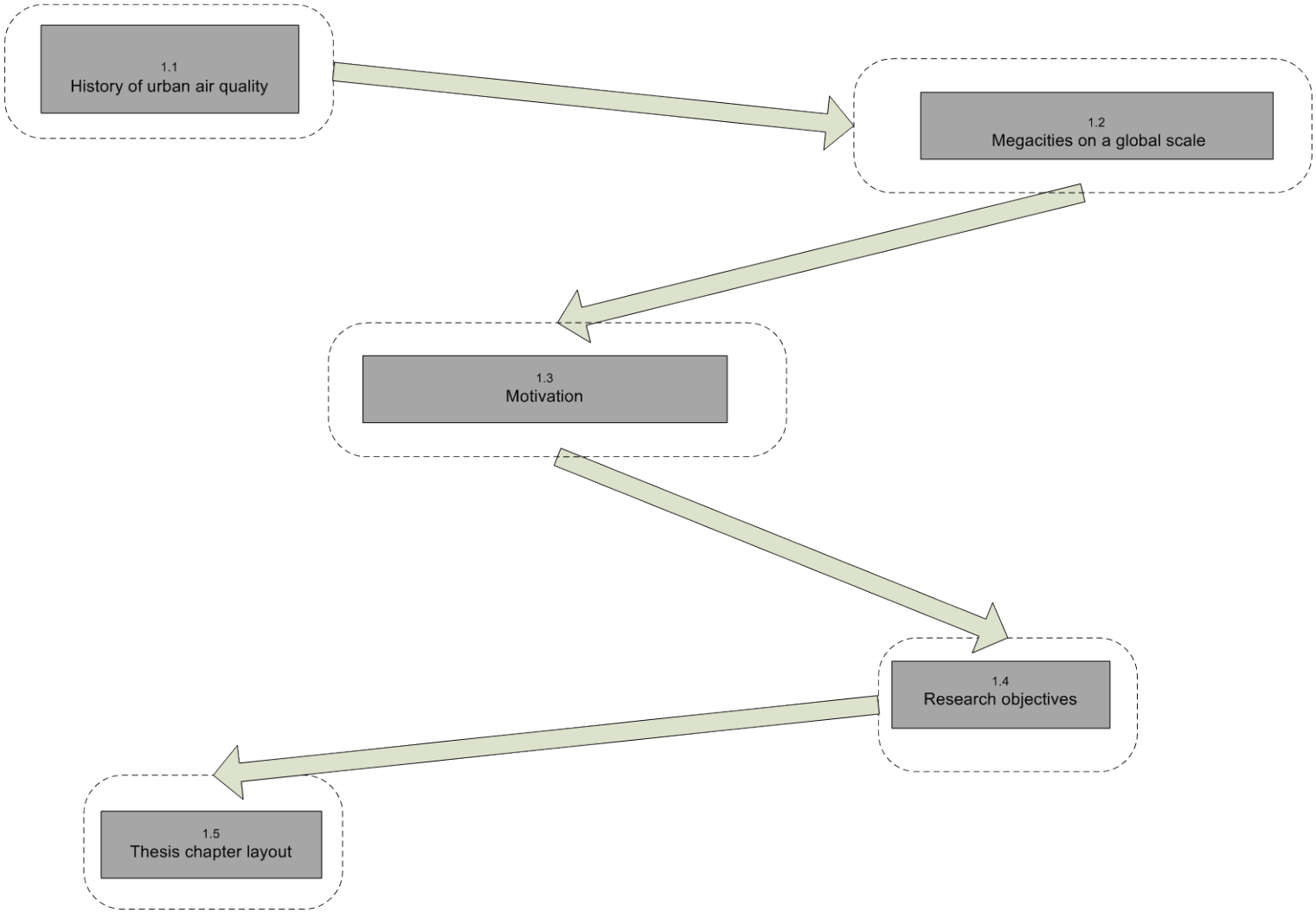

Chapter 1:
Introduction and Motivation

1.1. HISTORY OF URBAN AIR QUALITY

Throughout centuries cities have been known as places with the highest concentration of people, resources and activities. In ancient times already these activities caused significant air pollution problems and it was well-known that smog drew negative connotations (Brimblecombe, 2011). Since people were less critical about their living conditions in those times, they were unaware that air pollution is not only regionally specific, but are enacted on all geographical and temporal scales (Chow *et al.*, 2002). Impacts of air pollution can range from "here-and-now" problems (e.g. health and material damage), to regional phenomena (e.g. acidification and forest die back within decades) and to global impacts that can over centuries change the conditions for humans and nature across the entire globe (Fenger, 1999).

Laws controlling air pollution was created as early as in 1306 when Edward I of England prohibited the burning of sea coal in craftsman furnaces, because of the foul-smelling fumes produced (Vallero, 1994). Centuries later Elizabeth I banned, for similar aesthetic reasons, the burning of coal in London while parliament was in session (Anon., 2010). These anecdotes indicate that air pollution was considered as a nuisance rather than a threat to human health.

It was only after World War II that awareness of air pollution and its effects increased when scientist and amateur enthusiasts started semi-quantitative evaluations of air pollution (Fenger, 1999). Some of the early studies included recording material damage, as well as impacts on human health and vegetation. There was also an attempt to develop a simplified dispersion model by using the known consumption of fuels and raw materials within a confined area (Brimblecombe, 1987). However, air pollution was still mostly ignored as a health threat and only considered a real problem when crisis proportions were reached. Some of the major pre and post World War II air pollution episodes are listed in the table below.

Table 1.1: Major air pollution episodes (adopted from Fenger, 1999; Brimblecombe, 1987).

Air Pollution episode	Date	Cause	Consequences
Meuse River Valley, Belgium	1930	Thermal inversion trapped fog over a 15 mile stretch of the valley.	63 people died and thousands sick
Donora, Pennsylvania	1948	High concentrations of toxic gases coupled with temperature inversion and foggy weather.	20 people died due to cardiac and respiratory disease, while approximately half of the town's 12,000 residents complained of cough, respiratory tract irritation, chest pain, headaches, nausea and vomiting.
Poza Rica, Mexico	1950	Natural gas plant inadvertently released hydrogen sulphide coupled with temperature inversion and foggy weather.	22 people died and 320 were hospitalised.
London, England "London Smog"	1952	A five day temperature inversion trapped deadly acid aerosols in the atmosphere.	Over 4,000 fell ill to bronchitis, pneumonia, and respiratory and cardiac disease and over 3,000 died (Ministry of Health, 1954).

It was only during the last century that the direct measurement of air pollution increased. The continuous measurements of time series data only became more common in the 1970s. Different international programmes have also been initiated to monitor air pollution on a continuous basis. In 1972 during the United Nations (UN) Conference on the Environment in

Stockholm the UN Environmental Programme (UNEP) in collaboration with the World Health Organisation (WHO) was created to address the problems associated with air quality, which was exemplified by the 1952 London Smog event (Table 1.1). Since 1974 UNEP and WHO have collaborated in establishing a Global Environment Monitoring System (GEMS) urban air pollution monitoring network (GEMS/Air) (Mage *et al.*, 1996; UNEP., 1991). Concentrations and trends of air pollutants in selected countries have also been reported yearly by the Organisation for Economic Co-operation and Development (OECD). Since these initiatives many more networks have been set up around the world to monitor and measure air pollutants in different regions.

1.2. MEGACITIES ON GLOBAL SCALE

With the population increase after World War II, the amount and size of large cities have increased dramatically, since more people moved to urban regions where prospects of work and money were available. London was in 1800 the only major city in the world with a population of 1 million people (Molina & Molina 2004). In 1800 the average population of the 100 largest cities was 200,000, which increased to 2.1 million in 1950, 5 million in 1990 and 7.7 million people in 2002 (Division, 2009; Molina & Molina, 2004). In the beginning of the 20th century there were three cities with a population of 1 million people, while currently there are 281 cities of this magnitude (Molina & Molina, 2004; Division, 2009). Table 1.2 shows the distribution of global population by size of settlement (1950-2050) (Division, 2009). The world's population has more than doubled since World War II from 2.5 billion to 5.9 billion in mid-1998 (Fenger, 1999) and is expected to grow to more than 9 billion in 2050 as indicated in Table 1.2.

Table 1.2: Distribution of global population by size of settlement (1950-2030) (Division, 2009).

	Population (billion)					
Major Area	**1950**	**1975**	**2000**	**2005**	**2010**	**2050**
Global population						
World	2.52	4.07	6.07	6.46	6.95	9.08
More developed regions	0.81	1.05	1.18	1.20	1.22	1.26
Less developed regions	1.71	3.02	4.88	5.22	5.66	7.70
Urban population						
World	0.73	1.52	2.86	3.16	3.48	6.28
More developed regions	0.43	0.70	0.88	0.89	0.92	1.09
Less developed regions	0.31	0.81	1.97	2.22	2.55	5.10
Rural population						
World	1.8	2.5	3.21	3.3	3.47	2.8
More developed regions	0.38	0.34	0.31	0.31	0.30	0.17
Less developed regions	1.4	2.21	2.9	3.0	3.11	2.6

In 2000 nearly half of the world's population lived in urban areas and it is expected to grow by two percent per year during the next three decades (Division, 2009). Since World War II the global level of urbanisation, which is defined as the fraction of people living in settlements with more than 2000 inhabitants, has risen from <30% to 44% (Fenger, 1999). In the more developed countries the fraction of people currently living in urban areas is now on average 73% and in less developed countries 36% (Bureau, 1998). It is estimated that the urban population in less developed regions will double from 2 billion to 3.9 billion inhabitants. It is predicted that by the year 2030 almost 80% of the world's population will be living in urban

centres and the sharpest rise will be in the developing regions, with the largest increase predicted for Africa (Gurjar *et al.,* 2007; Economist, 2010).

A megacity is defined by Molina & Molina (2004) as a general term for cities that together with their suburbs or recognised metropolitan area have a total population in excess of 10 million people. In 1950 New York and Tokyo were considered to be the only Megacities. That number grew to three (Tokyo, New York Mexico City) by 1975, to 19 by 2007, 20 by 2010 and its estimated to reach 24 by 2015 (Division, 2009).

Air pollution in Megacities has increased as a result of more anthropogenic emission sources, which include energy production, transportation, industrial activities and domestic fuel burning (Molina & Molina 2004). Since the majority of energy has been derived from fossil fuels, (initially without flue gas cleaning) emissions from combustion processes have been a major source of air pollution in many cities (Molina & Molina 2004). The distribution of the sources varies from city to city depending on which source play a more important role. In South Africa household combustion and traffic emissions are major sources. The major pollutants emitted from these activities include nitrogen oxide (NO), nitrogen dioxide (NO_2), sulphur dioxide (SO_2), carbon monoxide (CO), particular matter (PM), and various organic compounds.

The above-mentioned anthropogenic emissions emitted from large urban centres not only change the composition of the atmosphere, but can also undergo various chemical reactions to form secondary pollutants (Atkinson, 2000). Since 1950 the global emission of sulphur oxides in urban areas have more than doubled and the emission of nitrogen oxides have increased by a factor of four (Fenger, 1999). A challenge that Megacities face is how to reduce the adverse environmental impacts and other negative effects associated with transportation without giving up the benefits of mobility (Division, 2009; Molina & Molina, 2004).

1.3. MOTIVATION

Air pollution has been monitored for some years in the larger African cities such as Cairo, Alexandria, Nairobi and Johannesburg, while there is increasing awareness of the need for air quality management (Mage *et al.*, 1996; UNEP., 1991) in Africa. Urbanisation, however, is increasing rapidly in Africa, especially in the least developed countries with growth rates of up to five percent per year. The driving force is a mixture of population growth, natural disasters and armed ethnic conflicts. Currently 38% of Africa's population is living in urban areas and it is

estimated that by 2030, 54% will be living in urban areas (EPA, 2011). According to Laakso et al. (2008) Africa is one of the least studied continents in the world with respect to air quality.

South Africa is one of the three largest emitters of greenhouse gases on the African continent with 99.4 million metric ton (MMT) carbon or 42% of Africa's total carbon emissions (EPA, 2011). These emissions are mainly from industrialised areas and urban settlements. With regard to urbanisation, 62% of the total South African population already lived in cities in 2010, with a predicted urbanisation rate of 1.2% per annum (Economist, 2010). The government will face major environmental challenges during such a rapid rate of urbanisation, which include food and water shortages, poor infrastructure, lack of housing and water, as well as problems associated with air pollution. South Africa is unique in terms of the spatial distribution of industries and urban settlements since the largest urbanised city in South Africa the Johannesburg-Pretoria conurbation, is located relatively close to the most industrialised regions, i.e. the Mpumalanga Highveld and the Vaal Triangle. Johannesburg is the central hub of economic activities and -growth in South Africa. The city of Johannesburg alone has a population of approximately 3.8 million (Anon, 2008). The larger conurbation that includes all the suburbs of Johannesburg, as well as Pretoria has more than 10 million inhabitants (Anon, 2010). The Johannesburg-Pretoria conurbation will be referred to as the *Jhb-Pta megacity* throughout the thesis. Figure 1.1 illustrates the study area in context of South Africa.

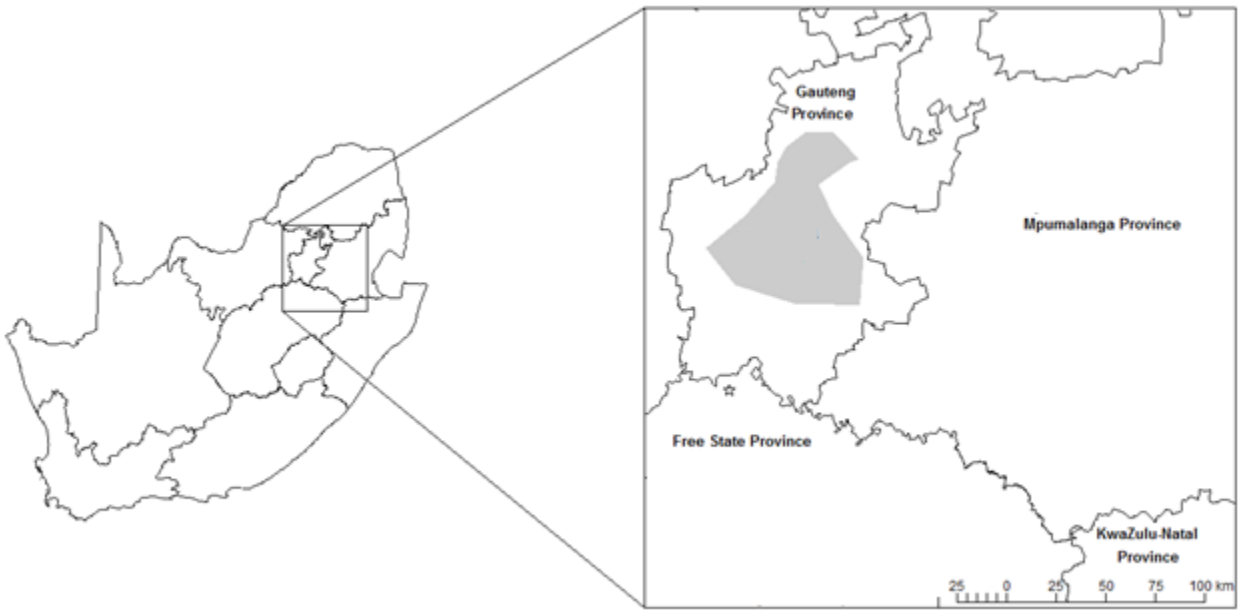

Figure 1.1: The study area with the grey indicates the Jhb-Pta megacity. The Mpumalanga Highveld is east of the study area in the Mpumalanga Province. The Vaal Triangle is south of the study area in the Free State Province.

Various studies have been conducted on atmospheric ozone (O_3), nitrogen oxides (NO_x), sulphur dioxide (SO_2) and aerosols in certain parts of southern Africa (e.g. Tyson *et al.,* 1997; Diab *et al.,* 2003; Swap *et al.,* 2002, Laakso *et al.,* 2008). However, very few air quality modelling studies have been conducted for the Jhb-Pta megacity and according to current knowledge of the author, none has been published in the peer reviewed public domain. Dispersion modelling within South Africa is mainly performed by industrial companies and governmental authorities, as well as to some extent by parastatals such as the Council for Scientific Industrial Research (CSIR) that are partially funded by government. Industrial companies are usually required to conduct dispersion modeling for regulatory purposes to ensure that their emissions are below standard concentrations. Therefore a need exist to conduct an in-depth air quality study within the Jhb-Pta megacity, specifically within a modeling framework

1.4. RESEARCH OBJECTIVES

The focus of this study was twofold. The first was to investigate the air quality in the Jhb-Pta megacity, while the second was to investigate the chemical processes in the urban atmosphere by utilising an atmospheric model. In order to achieve these general objectives, current

representative ground-based measurements were required, as well as a photochemical box model with a comprehensive chemical scheme suitable for the Jhb-Pta megacity. Data for 2009 and 2010 was utilised as input parameters in the model, in order to assist in testing and evaluation of the box model.

The specific objectives for the study were to:

1. determine the current air quality in the Jhb-Pta megacity and obtain model input data through

    a. establishment of an ambient BTEX, NO_2, SO_2 and O_3 passive sampling network at measurement sites in and around the Jhb-Pta megacity that operated for a period of at least two months;

    b. conduct active BTEX measurements at some of the sites for 8-hour sample intervals for two consecutive days during each month of sampling.

2. contextualising the possible contribution of the Jhb-Pta megacity to the NO_2 hotspot seen over the South African Highveld from satellite retrievals.

3. optimise an existing photochemical box model MECCA (Module Effective Calculating the Chemistry of the Atmosphere) for the Jhb-Pta megacity of South Africa, by utilising the data collected for Objective 1 and 2.

4. utilise the measured data and model to investigate the photochemical processes in the Jhb- Pta megacity and surrounding areas.

1.5. THESIS LAYOUT

This thesis deviates somewhat from the more traditional chapter layout, i.e. presenting literature, experimental and results/discussions in different chapters. Each chapter will endeavour to cover a specific objective completely with relevant literature, experimental methods utilised and results/discussions presented. However, each chapter still forms part of the main storyline i.e. assessment of air quality in the Jhb-Pta megacity. In Chapter 2, the current state of air quality in the Jhb-Pta megacity is considered, through the review of relevant literature and the presentation of results of the measurement campaigns conducted (Objective

1). In chapter three, the spatial area considered is zoomed out from the Jhb-Pta megacity to include the surrounding areas as well. This was conducted to contextualise the contribution of the Jhb-Pta megacity to the well-known South African Highveld NO_2 hotspot (Objective 2). Chapter 4 & 5 utilise the measurement results obtained in Chapter 2 & 3 as input parameters for a photochemical box model (Objective 3) to better understand quality in the megacity and its contributing effects on the surrounding areas (Objective 4).

REFERENCE

ATKINSON, R. 2000. Atmospheric chemistry of VOCs and NOx. *Atmospheric Environment*, 34:2063-2101.

ANON. 2008. *Statisctics South Africa*.

ANON. 2010. *Statistics South Africa: Statisical release PO301*.

ANON. 2010. Air Pollution Control Orientation Course (Environmental Protection Agency). Date of access: 30 November 2011. <http://www.epa.gov/apti/course422/apc1.html>

BRIMBLECOMBE, P. 1987. The Big Smoke. A History of Air Pollution in London Since Medieval times. London: Methuen.

BRIMBLECOMBE, P. 2011. A History of the Causes and Consequences of Air Pollution. *In*: OUANTE, M., EBINGHAUS, R. & FLOSER, G., eds. *Presistent Pollution- Past, Present and Future*, Dordrecht London New York: Springer Heidelber.

BUREAU, Population Reference. 1998. *Demographic data and estimates for the countries and regions of the World*. Washington D.C.

CHOW, J.C., ENGELBRECHT, J.P., WATSON, J.G., WILSON, W.E., N.H., Frank & ZHU, T. 2002. Designing Monitoring Networks for Represent Outdoor Human Exposure. *Chemopshere*, 49(9):961-978.

DIAB, R.D., RAGHUNANDAN, A., THOMPSON, A.M. & THOURET, V. 2003. Classification of tropospheric ozone profile over Johannesburg based on mozaic aircraft data. *Atmospheric Chemistry and Physics*, 3:713-723.

DIVISION, United Nations Population. 2009. World Urbaniation Prospects: The 2009 Revision. Date of access: 30 November 2011. <http://esa.un.org/unpd/wup/index.htm>

ECONOMIST, The. 2010. Economist. http://www.economist.com/theworldin/2010 Date of access: 20 November 2011.

EPA. 2011. International Programme: Africa Air Quality. Date of access: 3 December 2011. <http://www.epa.gov/international/air/africa.htm>

FELLENBERG, G. 1997. The chemistry of pollution. Chichester: Wiley.

FENGER, J. 1999. Urban air quality. *Atmospheric Environment*, 33:4877-4900.
GURJAR, B.R., BUTLER, T.M., LAWRENCE, M.G. & LELIEVELD, J. 2007. Evaluation of emissions and
air quality in megacities. *Atmospheric Environment*, 42:1593-1606.

LAAKSO, L., AALTO, P.P., PETAJA, T., NIEMINEN, T., POHJA, T., SILVOLA, E., KULMALA, M., KGABI, N., MOLEFE, M., MABASO, D., PHATATSE, D., PIENAAR, K. & KERMINEN, V.M. 2008. Basic characteristics of atmospheric particels, trace gases and meteorology in a relatively clean Southern African Savannah environment. *Atmospheric Chemistry and Physics*, 8(16):4823-4839.

MAGE, D., OZOLINS, G., PETERSON, P., WEBSTER, A., ORTHOFER, R., VANDERWEERD, V. & GWYNNE, M. 1996. Urban air pollution in Megacities of the world. *Atmospheric Environment*, 30(5):681-686.

MOLINA, M.J. & MOLINA, L.T. 2004. Megacities and amospheric pollution. *Journal of Air and Waste Management*, 54:644-680.

SWAP, R.J., ANNEGRAM, H.J., SUTTLES, J.T., KING, M.D., PLATNICK, S., PRIVETTE, J.L. & SCHOLES, R.J. 2003. Africa burning: A thematic analysis of the Southern African Regional Science Initiative (SAFARI 2000). *Journal of Geophysical Research*, 108(D13):1-13.

TYSON, P.D. 1997. Atmospheric transport of aerosols and trace gases over southern Africa. *Physical geopgraphy*, 21(1):79-101.

UNEP. 1991. Urban air pollution. (*In* United Nations Environment Programm. Nairobi. p. Library No. 4.)

VALLERO, D. 1994. Fundamentals of Air Pollution. California: Academic Press.

Graphical layout of Chapter 2

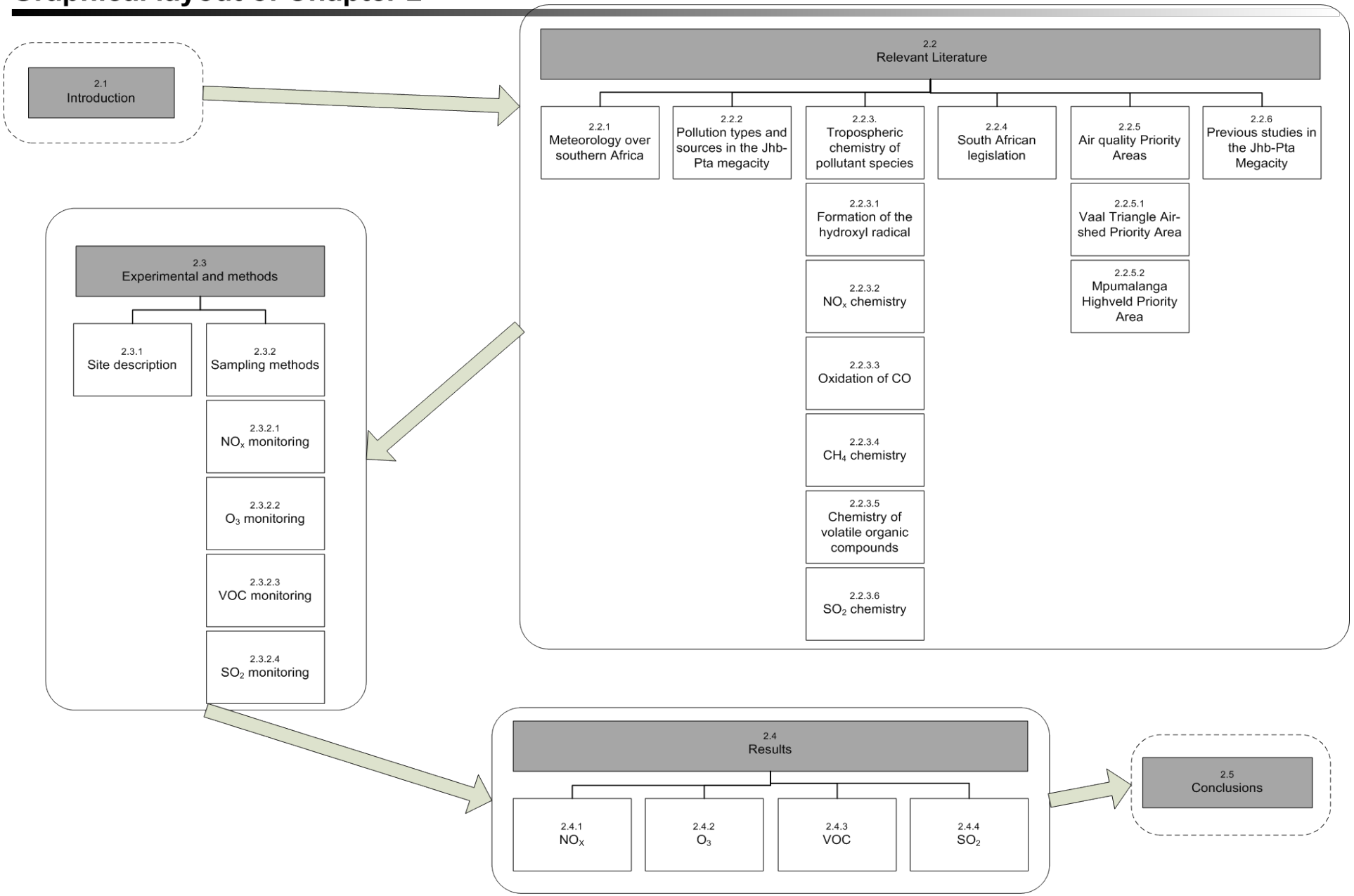

Chapter 2:

Air quality within the Jhb-Pta megacity of South Africa

2.1. INTRODUCTION

Measurement campaigns were conducted in the Jhb-Pta megacity to obtain information of the current status of air quality within the Jhb-Pta megacity (objective 1, Chapter 2). This data collected could also be used to contextualise the contribution of the Jhb-Pta megacity to the NO_2 hotspot observed over the South African Highveld from satellite retrievals (objective 2, Chapter 3), while the main purpose of collecting the data was to obtain a representative dataset to use for modelling purposes (objective 3 and 4, Chapter 4 and 5).

The above-mentioned measurement campaigns in the Jhb-Pta megacity were not conducted to obtain spatial and temporal distributions of pollutions at ground-level (in situ) in the Jhb-Pta megacity, but rather to get a snap shot of the air quality in the Jhb-Pta megacity. This data will then be used as input into the modelling study discussed in Chapters 4 and 5.

2.2. RELEVENT LITERATURE

2.2.1. Meteorology over southern Africa

Southern Africa is situated in the subtropical high-pressure belt that circles the globe between 25°S and 30°S and is influenced by several high-pressure cells. Anti-cyclonic conditions prevail over southern Africa throughout most of the year. This is due to the dominance of three high pressure cells, i.e. the South Atlantic high-pressure cell off the west coast, the South Indian high-pressure cell off the east coast and the continental high-pressure cell over the interior as indicated in Figure 2.1.

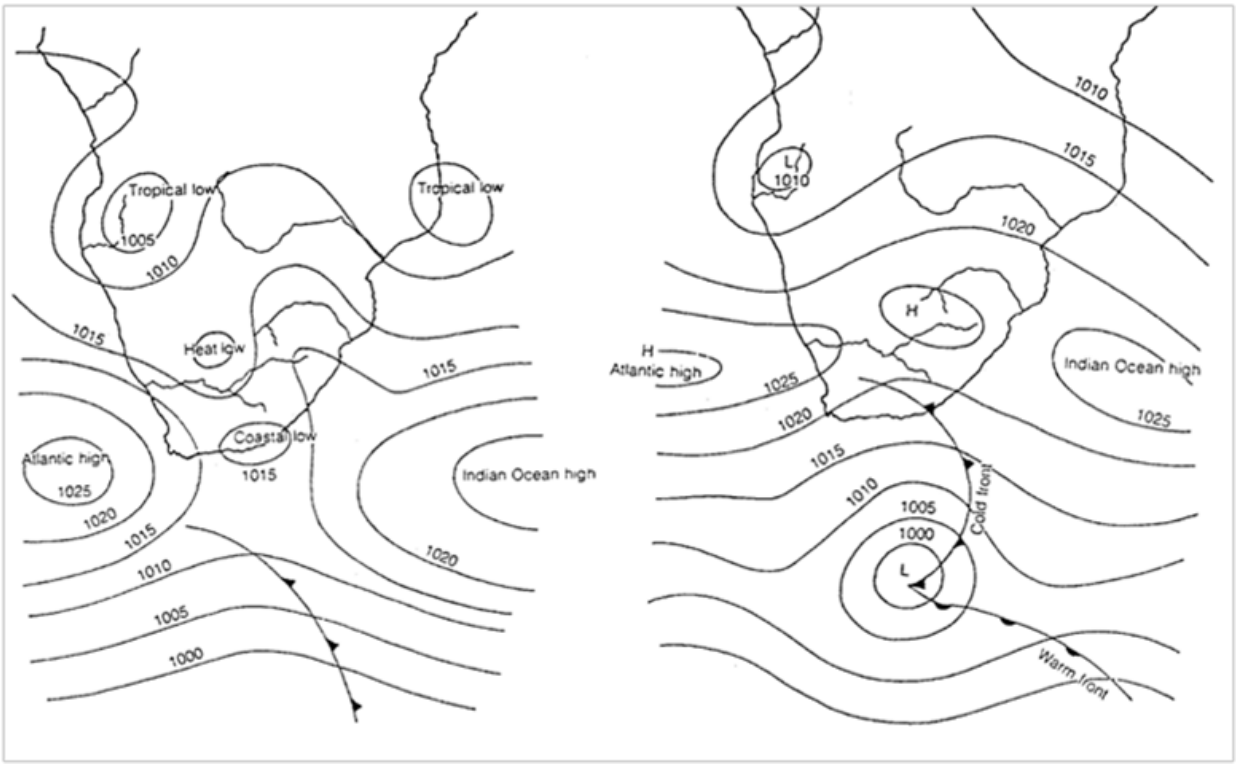

(a) **(b)**

Figure 2.1: General seasonal circulation over southern Africa (Sandham, 2008; Tyson, 1996) (a) the basic elements in the pattern of pressure distribution for mid-summer and (b) the basic elements in the pattern of pressure distribution for mid-winter.

In the summer the anti-cyclonic belt weakens and shifts southwards, allowing the tropical easterly flow to be prevalent over southern Africa during this period. Low air pressure conditions prevail over the interior with generally unstable meteorological conditions, which increase the vertical motion and dispersion of pollutants in the atmosphere (Tyson *et al.*, 1996). The first elevated inversion layer increases up to between four and five km over the plateau, while polluted air masses from urban and industrial areas affect suburban and rural areas in the direction of the prevailing wind across considerable distances.

During winter, however, stable conditions with low wind speeds prevail over most parts of southern Africa. Winters are characterised by the formation of inversion layers inhibiting vertical atmospheric mixing that generally weakens removal processes and effectively trap pollutants between these layers. The first elevated inversion layer is located at an altitude of three km over the plateau. Pollutants emitted near the surface of the earth accumulate in the boundary layer

where humans live. This is the region of the atmosphere in which pollution build-up is of most concern. Pollutants that escape the boundary layer can travel horizontally for long distances before they are removed from the atmosphere though various processes. The mixing layer (ML) is one of the key parameters that define the volume of air in which pollutants are mixed. On non-rainy days when stable conditions are associated with anti-cyclonic recirculation, haze layers are formed (Cosijn & Tyson, 1996; Garstang *et al.*, 1996) that potentially causes severe pollution problems (Tyson & Preston-Whyte, 2000). This is of particular concern within the context of Jhb-Pta megacity pollution, as considered in this thesis.

Atmospheric transport of anthropogenic emissions has been the subject of various scientific investigations over the past two decades in South Africa. Four major synoptic circulation types were defined in previous studies conducted on atmospheric circulation over southern Africa (Krishnamurti *et al.*, 1993; Garstang *et al.*, 1996; Piketh & Walton, 2004). These types include: the semi-permanent subtropical continental anticyclones, transient mid-latitude ridging anticyclones, westerly baroclinic disturbances and baratropic quasi-stationary tropical easterly disturbances. Figure 2.2 shows the major air transport pathways as determined by Freiman & Piketh (2003).

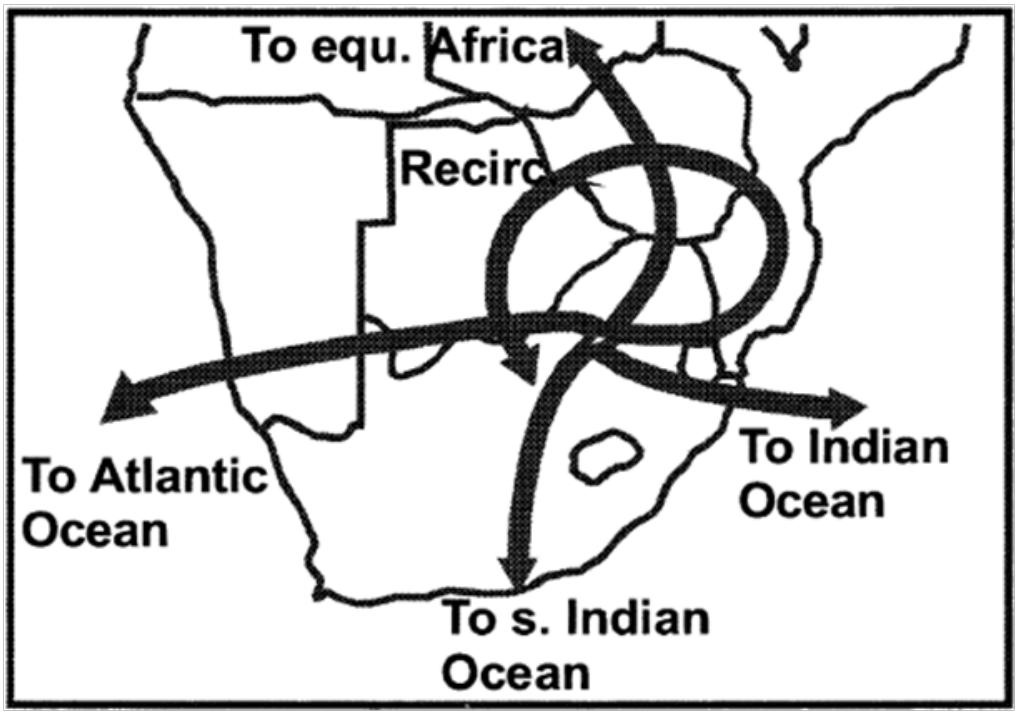

Figure 2.2: The main air transport pathways out of the Highveld (adopted from Freiman & Piketh, 2003).

The Jhb-Pta megacity investigated in this study is located around a series of low, rocky ridges at altitudes between 1500-1800m above mean sea level (AMSL). High pressure cells occur most of the time over the Gauteng region in summer and winter. The average temperature of the Jhb-Pta megacity is usually fairly mild due to the city's high altitude with an average temperature of 22.4°C. Winters are cold and dry with average maximum temperatures of 19°C and average minimum temperatures of 4°C that sometimes drop below freezing point. Summer months are warm and wet. An averaged summer day in January is 25°C with high temperatures reaching 35°C and minimum temperatures of 16°C. Rainfall averages is ca. 710 mm per annum, occurring almost exclusively during summer and mainly in the form of late afternoon showers (Mathee & Von Schirnding, 2003).

The Jhb-Pta megacity is situated on the Highveld within the Gauteng Province. The South African Highveld includes the North West and Gauteng provinces, as well as substantial fractions of the Mpumalanga, Northern Cape, Limpopo and Free State provinces. The Highveld is bordered by the Bushveld (hotter savannah with more trees) and the Lowveld (more tropical, lower lying region) in the north and northeast, the Drakensberg mountains to the east and

southeast, the Kalahari Desert in the north and west (continuing into Botswana and Namibia), and the Great Karoo to the southwest. The Highveld covers an area of almost 400,000 km² that is ca. 30% of South Africa's surface area.

2.2.2. Pollution types and sources in the Jhb-Pta megacity

Anthropogenic urban air pollution is caused mainly by two types of pollutants, i.e. the release of primary pollutants directly from sources (Godish, 2004) and the formation of secondary pollutants through chemical reactions of primary pollutants as indicated in Figure 2.3. Two main types of reactions result in the formation of secondary pollutant species, i.e. oxidation reactions and photochemical chain reactions (Figure 2.3). Of the pollutants that are either primary emitted or secondary formed, there are six so-called “criteria air pollutants” established by the Clean Air Act of 1970 in the United States of America. These criteria pollutants are particular matter (PM), tropospheric ozone (O_3), carbon monoxide (CO), sulfur dioxide (SO_2), nitrogen dioxide (NO_2) and lead (Pb). These species have since been adopted by most countries as species that are governed under ambient air quality legislation. South African ambient air quality standards also include these criteria pollutants (NEMA, 2004). A major problem in many cities is the formation of O_3 through photochemical reactions of NO_x (NO and NO_2) and various hydrocarbon (HC) species.

TYPE OF REACTION	PRIMARY POLLUTANT	SECONDARY POLLUTANTS	UNPOLLUTED ATMOSPHERE

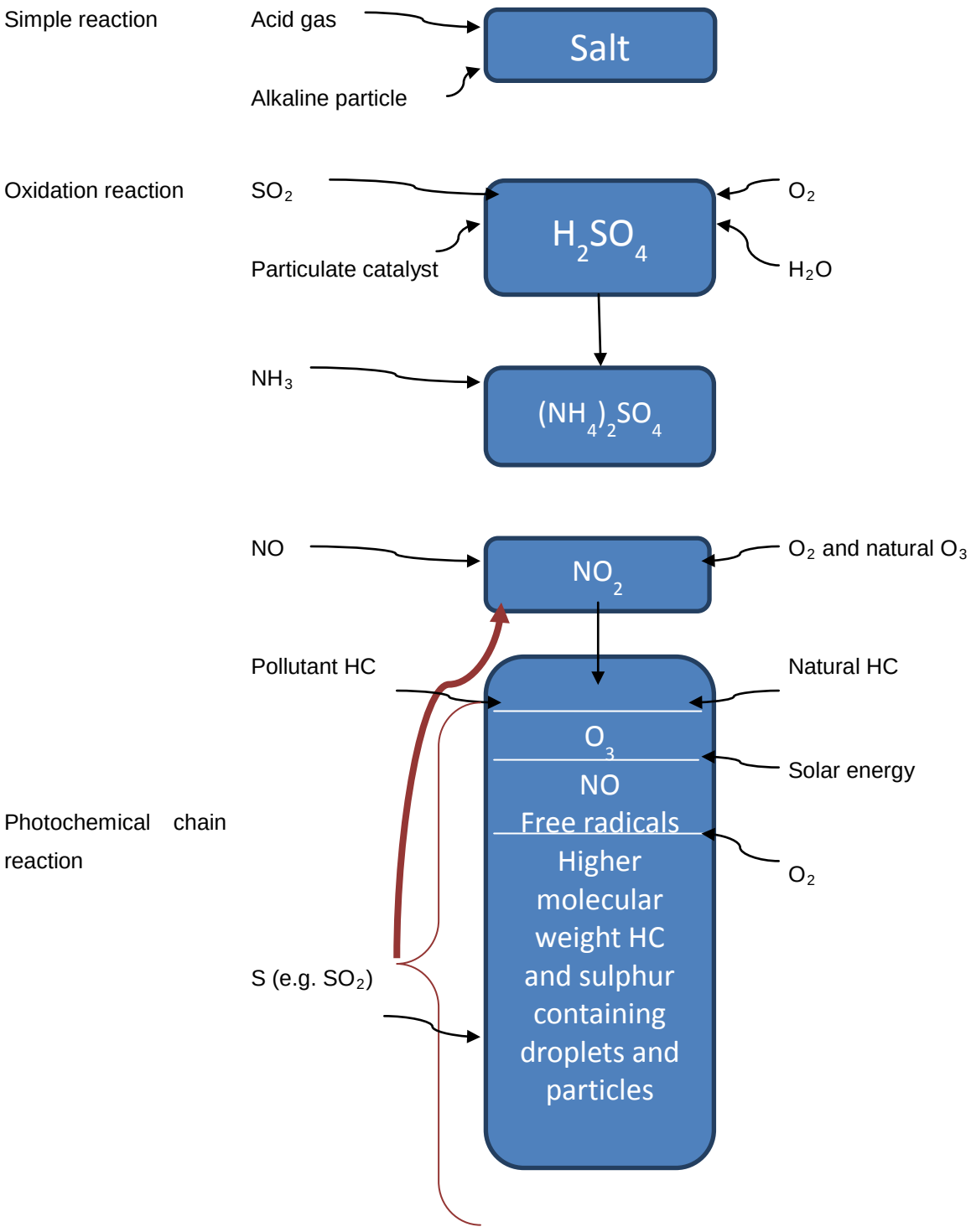

Figure 2.3: Types of reactions with primary and secondary pollutants. Adopted from Boubel et al. (1994).

Depending on the concentrations of these species in the atmosphere, as well as the time of exposure, there are several adverse environmental and health impacts associated with these species. Environmental impacts include acidification of soil and surface waters, damages to crops and native vegetation (Boubel *et al.*, 1994; Parra *et al.*, 2006) and climate change. Health impacts associated with these species include long-term effects such as pulmonary asthma and chronic bronchitis (Kampa & Castanas, 2008). Certain pollutant species are carcinogenic and are associated with leukaemia (Ma *et al.*, 2003)

There are three major sources of air pollution in the Jhb-Pta megacity, i.e. household combustion, industrial activities and vehicular emissions. Household combustion for space heating and cooking is primarily from low-income informal settlements in and around the city, which have their origin due to rapid and unplanned urbanisation over the past decades. These informal settlements have in the past been estimated to house half of the population of the Johannesburg city (Scorgie *et al.*, 2003). A large fraction of these households do not have access to electricity and relies on fuels such as coal, wood and kerosene for domestic purposes. The rapid urbanisation and the growth of informal settlements have resulted in backlogs in the distribution of basic services such as electricity and waste removal. As part of a national program almost 450,000 households have been given access to electricity annually since the 1990s. However, assessments have indicated that these informal households continue to use coal, wood and other polluting fuels for cooking and heating (Mathee & Von Schirnding, 2003). The main air pollutants emitted from the use of coal and wood for domestic burning are PM, SO_2, NO_2, CO and volatile organic compounds (VOCs). The sulphur content in coal can range between 0.5 and 3% of the mass, depending on the grade of coal used. The emission of these species from household combustion increases especially in winter, when indoor air quality may exceed international health standards.

The second major source of pollutants is industrial activities. The main industrial activities are mainly located in the southern part of the Jhb-Pta megacity. Several mining dumps are also currently being reprocessed in this region and are a major problem of dust emissions (DEA, 2006). The Vaal Triangle located 40 km south of the megacity and the Mpumalanga Highveld located 100 km east of the megacity, may also influence air quality in the megacity. These two areas are home to various industrial activities such as petrochemical, chemical, brick, tile, steel

and numerous other operations (Mathee & Von Schirnding, 2003). These two geographical areas will be discussed in more detail in Sections 2.2.5.1 and 2.2.5.2. Major air pollutants emitted from these industrial activities include SO_2, O_3, PM, CO. CH_4, NO_x and VOCs.

Vehicular emissions are the third major source of pollutants in the Jhb-Pta megacity. The megacity is the hub for local and international air travel (O.R. Tambo airport situated within the megacity) commercial and industrial travel that causes the railways and multi-lane freeways to carry high traffic volumes every day (Scorgie *et al.*, 2003). In South Africa the motor vehicle fleet are on average older than in developed countries. Most of the informal settlements are also located outside the city and workers therefore have to commute on a daily basis. The poor public transportation system that covers only parts of the city, has resulted in the formation of an informal mini-bus taxi industry that serves a large part of the community. Although legislation has been put into place to manage and regulate the taxi industry, many of the mini-bus vehicles used are poorly maintained. This situation results in elevated road accidents with high mortality and injury rates (Mathee & Von Schirnding, 2003), as well as an increase in air pollution in the Jhb-Pta megacity. The Jhb-Pta megacity also has a high road network density, with 9 224 km of roads. 93% of these are managed by local authorities of the megacity, while the other roads are managed by provincial governments. Approximately 12% of roads (1 217 km) in the Jhb-Pta megacity are gravel, with an estimate of 75% of these roads in informal settlements (Scorgie *et al.*, 2003) that causes high levels of particulate emissions.

High NO_x levels have been found in urban areas in the mornings and in the late afternoons, due to increased motor vehicle activities (Zavala *et al.*, 2009), as well as increases in household combustion. The majority of NO_x emissions are emitted in the form of non-toxic nitric acid (NO), which is subsequently oxidized in the atmosphere to NO_2. Atmospheric VOC pollutants are the result of incomplete combustion of fuels or are formed during other combustion process, including in vehicles. Aromatic HCs account for 20-40% of the total ambient VOCs in urban areas (Derwent *et al.*, 2002). The most important organic compounds in urban areas are benzene and substituted benzenes, alkenes, as well as polyaromatic hydrocarbons (PAH). CO is also the result of incomplete combustion, with motor vehicles and household combustion being the major sources thereof.

2.2.3. Tropospheric chemistry of pollutant species

In subsequent paragraphs an overview of the chemistry of the major gaseous pollutant species relevant to this investigation is presented. The key to understanding tropospheric chemistry begins with the formation of the hydroxyl radical ($HO^{\bullet}$) that is generated by O_3 photolysis. Since O_3 is a secondary pollutant that is formed through the chemical reaction of most of the major primary emitted atmospheric pollutants, O_3 chemistry is not discussed in a separate subsection.

2.2.3.1. Formation of the hydroxyl radical

Photolysis at wavelengths < 315 nm of low levels of O_3 present in the "clean" troposphere are considered to be the beginning of all the atmospheric oxidation reactions and the formation of the most important species in tropospheric chemistry, i.e. the hydroxyl radical ($HO^{\bullet}$). The $HO^{\bullet}$ initiate the degradation processes that remove almost all the oxidation trace gases emitted in the atmosphere. The process starts with the formation of ground state oxygen (O_2) and excited singlet oxygen atoms ($O(^1D)$) produced from O_3 by the reaction (Atkinson, 2000)

$$O_3 + h\upsilon \rightarrow O_2 + O(^1D) \qquad \text{R1}$$

The excited singlet state atom is reduced to the ground state and then rapidly combines with O_2 to reform O_3

$$O(^1D) + M \rightarrow O(^3P) + M \ (M = N_2 \text{ or } O_2) \qquad \text{R2}$$

$$O(^3P) + O_2 + M \rightarrow O_3 + M \qquad \text{R3}$$

Approximately 10% of the singlet $O(^1D)$ atoms reacts with H_2O to generate two $HO^{\bullet}$ radicals (Seinfeld & Pandis, 1998). The formation of $HO^{\bullet}$ radicals in the free troposphere is therefore dependent on the availability of water vapour. This reaction initiates the oxidation of most trace gases in the atmosphere (Levy, 1971).

$$O(^1D) + H_2O \rightarrow 2HO^{\bullet} \qquad \text{R4}$$

This is the only gas-phase reaction in the troposphere that is able to break the H-O bond in H_2O (Seinfeld & Pandis, 1998) to form $HO^{\bullet}$. Although the photolysis of O_3 is seen as the principle

source of $HO^{\bullet}$ in the lower troposphere, it can also be formed through other reactions. These reactions include the photolysis of nitrous acid, formaldehyde and carbonyls, as well as the night time reactions of O_3 with alkenes (Adkinson, 2000). The $HO^{\bullet}$ radical reacts with almost all the atmospheric gaseous species present in the troposphere. The gaseous species that do not react with the $HO^{\bullet}$, such as chlorofluorocarbons (CFCs) and other non-H containing haloalkanes, have longer lifetimes and are transported into the stratosphere, where they are photochemically destroyed (Seinfeld & Pandis, 1998; Adkinson, 2000).The $HO^{\bullet}$ radical also does not react with any major constituents of the atmosphere, such as N_2, O_2, CO_2 or H_2O.

It has been suggested that approximately 75% of the $HO^{\bullet}$ react with CO to produce CO_2 and $H^{\bullet}$, while that remaining in the atmosphere react with CH_4 to produce H_2O and the methyl radical (CH_3^{*}) in a clean and "natural" atmosphere (Valentin, 1991; Pienaar & Helas, 1996). According to Crutzen & Zimmerman (1991) $HO^{\bullet}$ radicals react readily with CO and CH_4 in the background troposphere, but are not necessarily the reactions that leads to the removal of $HO^{\bullet}$. They are the starting point of various, often lengthy, chain reactions that lead to the loss of atmospheric $HO^{\bullet}$.

$CO + HO^{\bullet} \rightarrow CO_2 + H^{\bullet}$ R5

$CH_4 + HO^{\bullet} \rightarrow CH_3^{\bullet} + H_2O$ R6

The $H^{\bullet}$ and $CH_3^{\bullet}$ radicals formed combines rapidly with O_2 to form the hydroperoxyl radical $HO_2^{\bullet}$ and methylperoxyl ($CH_3O_2^{\bullet}$) radical

$H^{\bullet} + O_2 + M \rightarrow HO_2^{\bullet} + M$ (M = N_2 or O_2) R7

$CH_3^{\bullet} + O_2 + M \rightarrow CH_3O_2^{\bullet} + M$ R8

2.2.3.2. NO_x chemistry

Once NO is released into the atmosphere from natural or anthropogenic sources, it is rapidly oxidised to NO_2 that undergoes a series of chemical reactions (Fellenberg, 1997; Atkinson, 2000). The photolysis of NO_2 is an important reaction in tropospheric chemistry (Blacet, 1995). It is the only reaction though which O_3 is formed in the troposphere. In a clean and "natural" atmosphere the O_3 formed will react with NO to regenerate NO_2.

$NO_2 + h\upsilon \rightarrow NO + O(^3P)$ R9

$O(^3P) + O_2 + M \rightarrow O_3 + M$ (M = N_2 or O_2) R10

$NO + O_3 \rightarrow NO_2 + O_2$ R11

$NO_2 + HO^{\bullet}$ (+M) $\rightarrow HNO_3$ + (M) R12

NO_2 reacts with O_3 to produce the $NO_3^{\bullet}$ radical during night-time in the absence of sunlight. The $NO_3^{\bullet}$ radical formed during night reacts rapidly with sunlight in the morning to form NO and NO_2.

$NO_2 + O_3 \rightarrow NO_3^{\bullet} + O_2$ R13a

$NO_3^{\bullet} + h\upsilon \rightarrow NO + O_2$

R13b

$NO_3^{\bullet} + h\upsilon \rightarrow NO_2 + O(^3P)$ R13c

During the following relative rapid equilibrium dinitrogenpentoxide (N_2O_5) acts as a reservoir for the $NO_3^{\bullet}$ radical, which enhances the role of $NO_3^{\bullet}$ during night-time oxidation processes

$NO_2 + NO_3^{\bullet} \longleftrightarrow N_2O_5$ R14

$N_2O_5 + h\upsilon \rightarrow NO_3 + NO_2$ (<406 nm) R15

$HO^{\bullet} + NO \xrightarrow{M} HONO$ R16

$HO^{\bullet} + NO_2 \xrightarrow{M} HNO_3$, where M = N_2 or O_2 R12

According to the reactions and processes presented in Sections 2.2.3.1 and 2.2.3.2, tropospheric O_3 ultimately 'controls' the chemical oxidation potential of the troposphere.

2.2.3.3. Oxidation of CO

The oxidation of CO begins with CO reacting with $HO^{\bullet}$ to form an $H^{\bullet}$ atom and CO_2 (R5). The $H^{\bullet}$ radical then combines with O_2 to form $HO_2^{\bullet}$ (R7).

$CO + HO^{\bullet} \rightarrow CO_2 + H^{\bullet}$ R5

$H^{\bullet} + O_2 + M \rightarrow HO_2^{\bullet} + M$ (M = N_2 or O_2) R7

These $HO_2^{\bullet}$ molecules (R7) can react with NO or, in the case of an NO poor environment, with either O_3 or another $HO_2^{\bullet}$ radical. The net result is different for all of these reactions. If $HO_2^{\bullet}$ reacts with NO, NO_2 will be formed that almost immediately reacts with uv radiation to form NO and O. The O atom combines with an O_2 molecule to form O_3. The net result therefore is the oxidation of CO to CO_2 and the formation of O_3 with NO and NO_2 acting as catalysts. In the presence of NO, CO is considered to be an important precursor for O_3 formation.

$HO_2^{\bullet} + NO \rightarrow NO_2 + HO^{\bullet}$ R17

$NO_2 + h\upsilon \rightarrow NO + O(^3P)$ R9

$O(^3P) + O_2 + M \rightarrow O_3 + M$ R10

$CO + 2O_2 + h\upsilon \rightarrow CO_2 + O_3$ (net reaction)

In NO-poor environments there is a competing chain of reactions, leading to the destruction of O_3 due to the reaction of $HO_2^{\bullet}$ radicals with O_3 instead of NO. CO is still oxidized to CO_2, but in the process O_3 is removed.

$CO + HO^{\bullet} \rightarrow CO_2 + H^{\bullet}$ R5

$H^{\bullet} + O_2 + M \rightarrow HO_2^{\bullet} + M$ (M = N_2 or O_2) R7

$HO_2^{\bullet} + O_3 \rightarrow HO^{\bullet} + 2O_2$ R18

$CO + O_3 \rightarrow CO_2 + O_2$ (net reaction)

Besides the reaction of $HO_2^{\bullet}$ with NO and O_3 (in reactions R17 and R18), it can also react with other $HO_2^{\bullet}$ radicals to produce hydrogen peroxide (H_2O_2), which is a strong oxidising agent in aqueous solutions. H_2O_2 has a high solubility in water. Therefore it can be removed efficiently by uptakes in clouds and through precipitation. H_2O_2 plays an important role in aqueous oxidation chemistry, especially through the oxidation of SO_2 to sulphuric acid (H_2SO_4) (see 2.2.3.5). The reaction leading to the formation of H_2O_2 is

$HO_2^{\bullet} + HO_2^{\bullet} \rightarrow H_2O_2 + O_2$ R19

H_2O_2 can also undergo photolysis within a time scale of a week to regenerate $HO^{\bullet}$ or it can react with an additional $HO^{\bullet}$ to form $HO_2^{\bullet}$.

$H_2O_2 + h\upsilon \rightarrow HO^{\bullet} + HO^{\bullet}$ (≤ 350 nm) R20

$H_2O_2 + HO^{\bullet} \rightarrow HO_2^{\bullet} + H_2O$ R21

Al the reactions associated with the oxidation of atmospheric CO and the products that are formed are summarised in Figure 2.4.

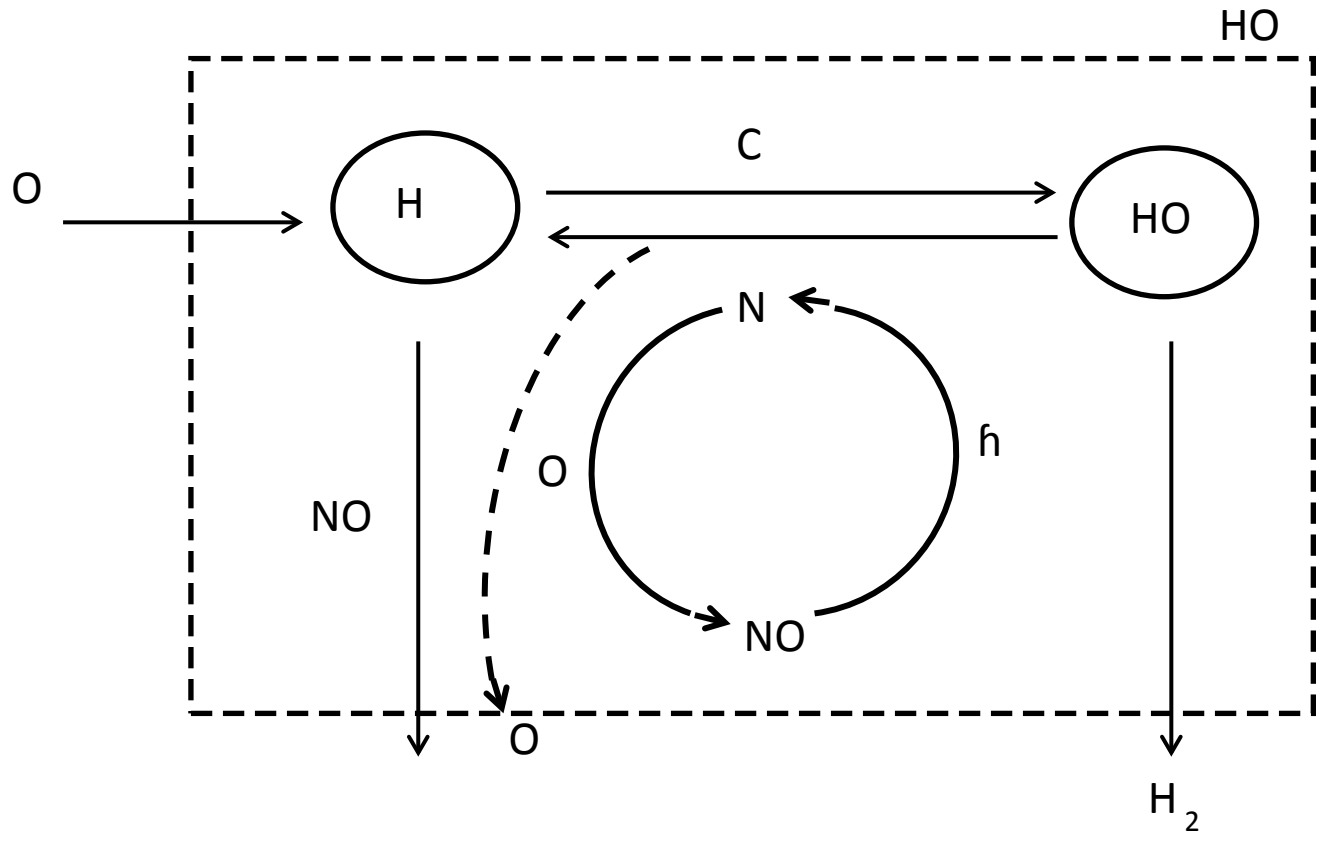

Figure 2.4: Reactions including the HO_X ($OH^{\bullet}$ and $HO_2^{\bullet}$) in CO oxidation (adopted from Seinfeld & Pandis, 1998) where P_{HOX} is the rate of $OH^{\bullet}$ generation from O_3 photolysis.

2.2.3.4. CH_4 Chemistry

Similarly to the oxidation of CO, the oxidation of CH_4 is also important in the troposphere, since approximately a quarter of the atmospheric $HO^{\bullet}$ radicals react with CH_4. Again, the availability of NO plays an important role in determining the oxidation pathways (Crutzen & Zimmermann, 1991). Different pathways can be followed that lead to the formation of formaldehyde (CH_2O) and O_3.

$CH_4 + HO^{\bullet} \rightarrow CH_3^{\bullet} + H_2O$ R6

$CH_3^{\bullet} + O_2 + M \rightarrow CH_3O_2^{\bullet} + M$ methylperoxy radical R8

$CH_3O_2^{\bullet} + NO \rightarrow NO_2 + CH_3O^{\bullet}$ methoxy radical R21

$CH_3O^{\bullet} + O_2 \rightarrow CH_2O + HO_2$ formaldehyde R22

$HO_2^{\bullet} + NO \rightarrow NO_2 + HO^{\bullet}$ R17

$NO_2 + h\upsilon \rightarrow NO + O(^3P)$ R13c

$O(^3P) + O_2 + M \rightarrow O_3 + M$ R10

$2CH_4 + 4O_2 \rightarrow CH_2O + H_2O + 2O_3$ (net reaction)

Sections 2.2.3.3 and 2.2.3.4 also shows the influence of CO and CH_4 on the formation of tropospheric O_3. Through the oxidation reactions of CO and CH_4 with $HO^{\bullet}$, O_3 is formed in the presence of NO.

2.2.3.5. Chemistry of volatile organic compounds

In general the oxidation of all atmospheric VOCs can also result in the formation of O_3. The net result, however, strongly depends on the relative ratio and reactivity of species involved in the processes. O_3 formation in the remote troposphere is dominated by the oxidation of the long-lived CH_4 and CO. The atmospheric lifetime of CO and CH_4 are approximately 2 months and 9 years, respectively (Atkinson, 2000). In urban and regional areas atmospheric VOCs, which includes alkenes, aromatics and oxygenated organic species are considered to be the most import precursor species for O_3 formation (Seinfeld & Pandis, 1998). Although reactions of VOCs do not directly produce O_3, they participate in the formation of radicals through R23 and R24 indicated below, where R denotes an alkyl radical (C_nH_{2n+1}). The reactions listed lead to the formation of intermediate radicals, i.e. $RO_2^{\bullet}$ and $HO_2^{\bullet}$. These radicals react with NO in urban atmospheres, converting NO to NO_2 which is then photolysed to O_3 through R9 and R10 (Atkinson, 2000).

$HO^{\bullet} + RH \rightarrow R^{\bullet} + H_2O$ R23

$R^{\bullet} + O_2 \rightarrow RO_2^{\bullet}$ R24

$RO_2^{\bullet} + NO \rightarrow NO_2 + RO^{\bullet}$ R25

$RO_2^{\bullet} + O_2 \rightarrow R'CHO + HO_2^{\bullet}$ R26

VOCs and NO_x are in constant competition to react with the $HO^{\bullet}$ radical, which is the key reactive species in the chemistry of tropospheric O_3 formation (Seinfeld & Pandis, 1998). The relation between O_3, NO_x and VOCs can be illustrated by means of O_3 isopleths presented in Figure 2.6. The isopleths plot gives the dependency of O_3 production as a function of VOC and NO_x concentrations. These isopleths indicate that O_3 formation is a highly nonlinear process in relation to NO_x and VOC tropospheric concentrations.

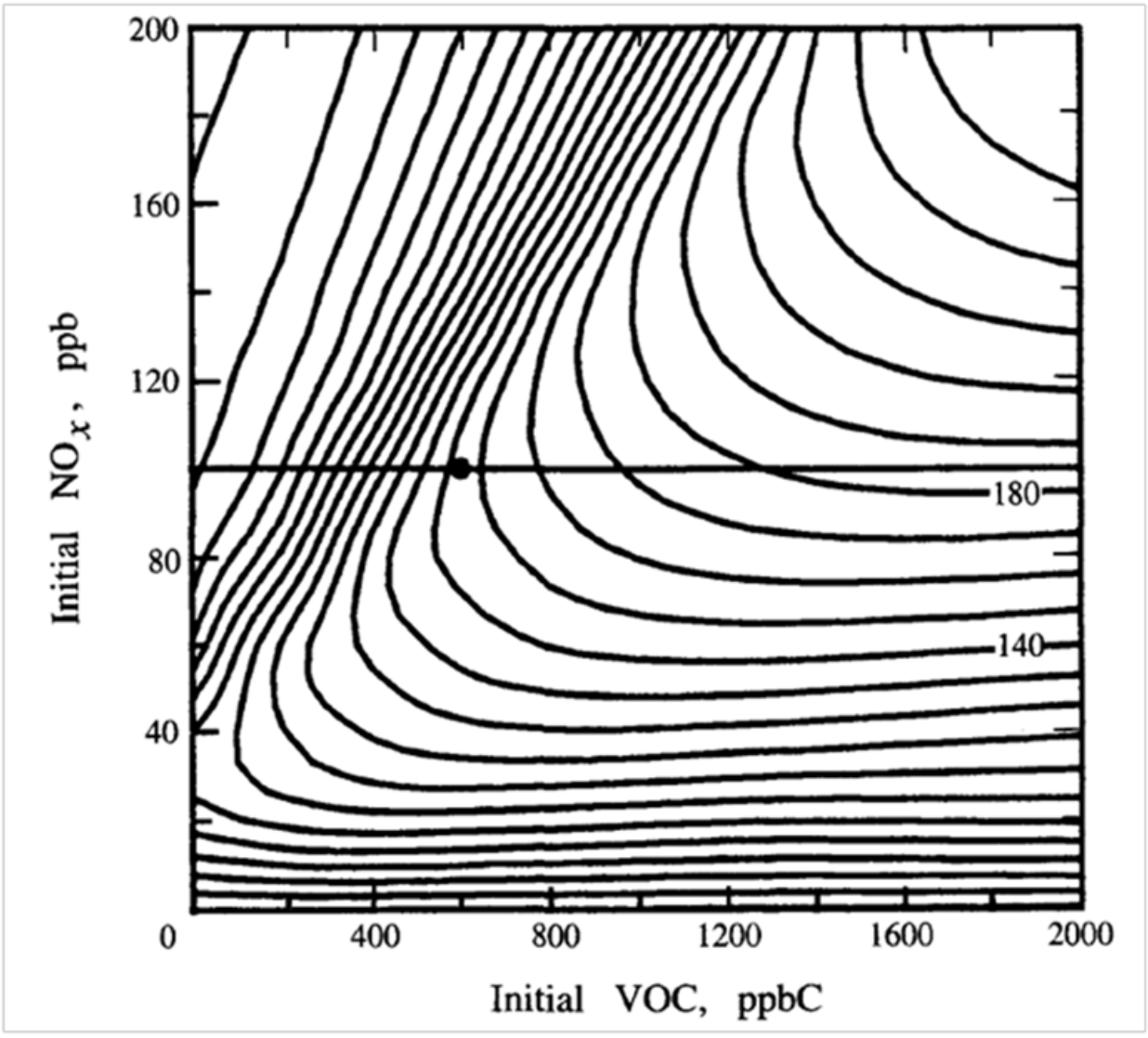

Figure 2.5: Generic O_3 isopleths indicating the dependency of O_3 formation on the initial VOC and NO_x concentrations (adopted from Seinfeld & Pandis, 1998).

When NO_x levels are low the rate of O_3 formation increases with increasing NO_x concentrations in a non-linear fashion. As NO_x concentrations increases the rate of increase in O_3 formation slows down and eventually reach a local maximum. In a NO_x -sensitive regime O_3 increases with increasing NO_x and shows relatively little change in response to increased VOC levels. Less NO_x reduces the titration of O_3 with NO that allows O_3 to accumulate in the troposphere, while higher NO_x levels causes a decrease in O_3 formation. However, in VOC-limited regions O_3 concentrations depend on the amount of VOCs in the atmosphere. Reduction of VOC emissions will only lead to lower O_3 concentrations in the VOC-sensitive region.

O_3 concentration generally shows a diurnal cycle, since sunlight is essential for O_3 formation. At night, O_3 levels are low, since no photochemical formation takes place, and these levels are further reduced due to the oxidation of NO to NO_2 by O_3 (R11). The seasonal trends show higher levels of tropospheric O_3 across a large region in the north of South Africa during spring (Diab *et al.*, 2003). This can be attributed to increased NO_x and CO emissions from biomass burning, which occurs at a high frequency during this time of year (Lourens *et al.*, 2011).

VOCs are not only important in the formation of O_3. It also participates in other atmospheric chemical reactions. The oxidation of RH and intermediate products with NO can also lead to the formation of peroxyacyl nitrites $R'C(O)O_2NO_2$ (Sillman, 1999; Duncan & Chameides, 1998; Staggelbach *et al.*, 1997; Kleinman, 2005).

$HO^{\bullet} + RH \rightarrow R^{\bullet} + H_2O$ R23

$R^{\bullet} + O_2 \rightarrow RO_2^{\bullet}$ R24

$RO_2^{\bullet} + NO \rightarrow NO_2 + RO^{\bullet}$ R25

$RO_2^{\bullet} + O_2 \rightarrow R'CHO + HO_2^{\bullet}$ R26

$HO_2^{\bullet} + NO \rightarrow NO_2 + HO^{\bullet}$ R27

$R'CHO + HO^{\bullet} \rightarrow R'CO + H_2O$ R28

$R'C^{\bullet}O + O_2 \rightarrow R'C(O)O_2^{\bullet}$ R29

$R'C(O)O_2^{\bullet} + NO_2 (+ M) \Leftrightarrow R'C(O)O_2NO_2 (+ M)$ R30

The degradation and transformation processes of VOCs (i.e. R23 - R30) in the troposphere in general can be illustrated by Figure 2.6.

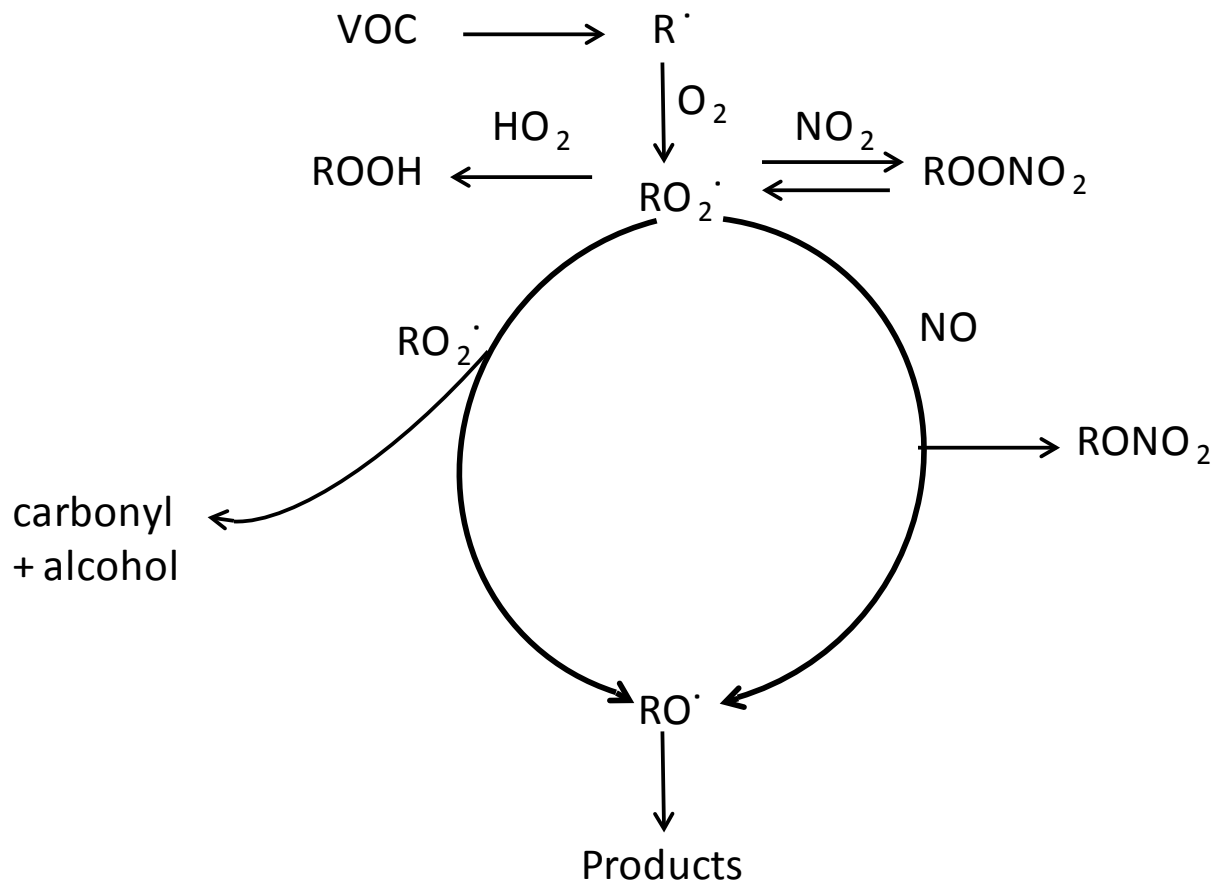

Figure 2.6: Tropospheric degradation and transformation reactions of volatile organic compounds (Atkinson, 2000).

2.2.3.6. SO_2 chemistry

SO_2 participates in various transformation reactions in the atmosphere, with the most important reactions involving oxidation that leads to acid formation (Fellenberg, 1997). The residence time of SO_2 in the atmosphere ranges between 12h and six days (Kellogg *et al.*, 1972). During oxidation reactions, excited oxygen atoms react with water vapour to form the hydroxyl radical

$O(^1D) + H_2O \rightarrow 2(HO^{\bullet})$

R4

The reactive $HO^{\bullet}$-radicals react with SO_2 and form sulphuric acid (H_2SO_4)

$SO_2 + 2HO^{\bullet} \rightarrow H_2SO_4$ R30

H_2SO_4 is also formed through the reaction of H_2O and SO_2, H_2SO_4 is captured by water droplets in clouds and removed from the atmosphere as acid rain.

$SO_2 + H_2O \leftrightarrow H^+ + HSO_3^- \leftrightarrow 2H^+ + SO_3^{2-}$ R41

$HSO_3^- + O_3 \rightarrow SO_4^{2-} + H^+ + O_2$ R42

$HSO_3^- + H_2SO_2 \rightarrow SO_4^{2-} + H^+ + H_2O$ R43

In Figure 2.7 the tropospheric cycle of SO_2 is presented, with the most important reactions and products indicated.

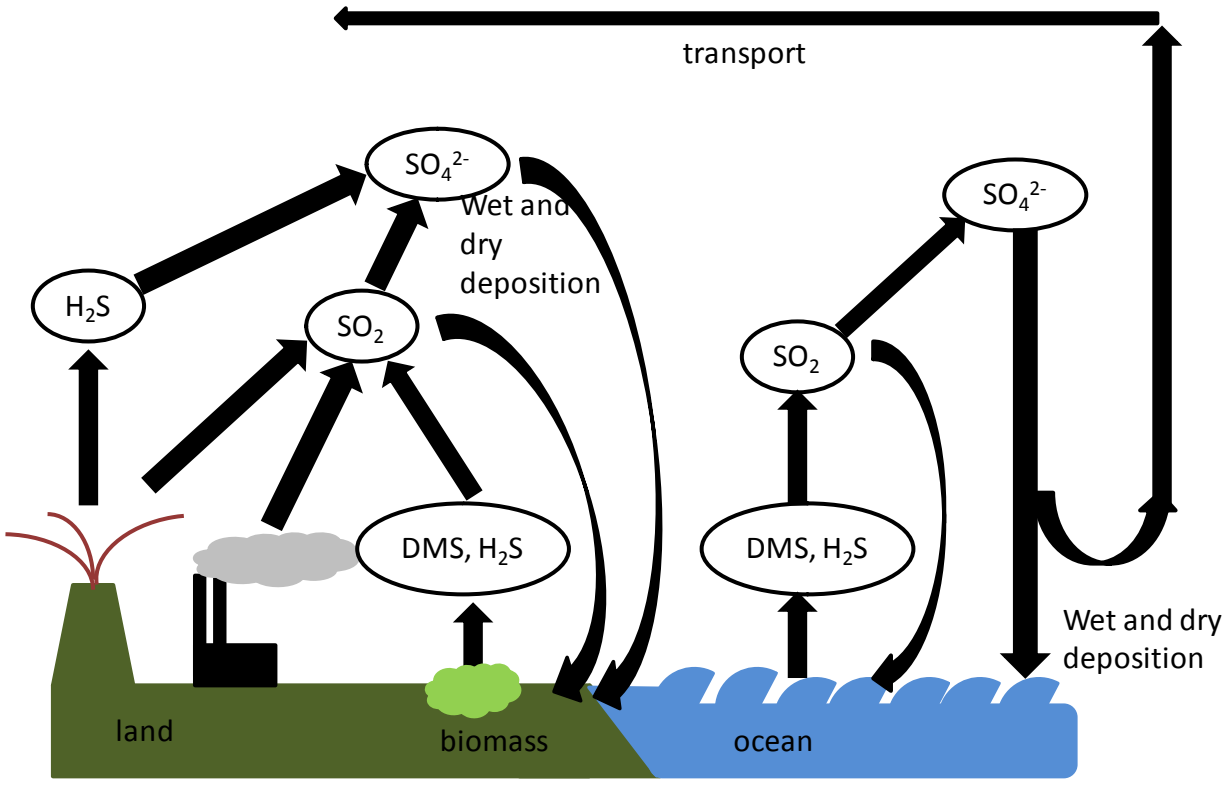

Figure 2.7:Tropospheric SO_2 cycle (Smith, 2011).

2.2.4. South African legislation

South Africa is a fast developing country that faces the challenges associated with economic growth, e.g. impacts on the environment. The South African Constitution is the primary legislation governing air quality management within the country. Currently the *National Environment Management: Air Quality Act (Act No. 39 of 2004) (NEMA:AQA)* is being enforced to regulate air quality in "order to protect the environment by providing reasonable measures for the prevention of pollution and ecological degradation and for securing ecologically sustainable development while promoting justifiable economic and social development; to provide for national norms and standards regulating air quality monitoring, management and control by all spheres of government; for specific air quality measures" (NEMA, 2004).

NEMA:AQA of 2004 (Act No 29 of 2004) contains specific provision to identify problem regions in terms of air quality and term these region "Priority Areas". In terms of section 18 (1) of the AQA, the Minister of Environmental Affairs and Tourism (at the time the declaration was made, currently the portfolio changed to Department of Environmental Affairs) may, by notice in the Gazette, declare an area as a priority area if the Minister reasonably believes that:

- ambient air quality standards are being, or may be, exceeded in the area, or any other situation exists that is causing, or may cause, a significant negative impact on air quality in the area; and
- the area requires specific air quality management action to rectify the situation.

The Department of Environmental Affairs (DEA) functions as the lead agent in the management of the priority area and is required in terms of Section 19(1) of the NEMA:AQA of 2004 (Act No 29 of 2004) to develop an Air Quality Management Plan (AQMP) for the priority area (Zunckel *et al.*, 2010). In South Africa three priority areas have been declared i.e. the Vaal Triangle Air-shed Priority Area, The Mpumalanga Highveld Priority Area and the Waterberg Bojanala Priority Area.

2.2.5. Air Quality priority areas in South Africa

Two priority areas which are considered to have significant impacts on air quality in the Jhb-Pta megacity will be discussed in this section.

2.2.5.1. Vaal Triangle Air-shed Priority Area

The Vaal Triangle has several industrial activities, which include several large petrochemical and associated chemical industries, several large pyrometallurgical steel and alloy smelters, and two coal-fired power stations. It is also a commercial centre, with millions of people using motor vehicles. There are also many informal settlements where coal, wood and paraffin are commonly used as energy sources (as mentioned in Section 2.2.2). Several studies have been conducted in this area indicating that air quality in the area is poor, which has a direct negative impact on the health and the well-being of people living in this area (Mathee & Von Schirnding, 2003). This includes respiratory ailments and diseases, early morning coughing; wheezing, and asthma (Mathee & Von Schirnding, 2003).

Due to the above-mentioned problems the first national air pollution hotspot, viz. the Vaal Triangle Air-shed Priority Area, was declared by the Minster of Environmental Affairs and Tourism in terms of Section 18(1) of the NEMA:AQA (Act No. 29 of 2004) on 21 April 2006. This priority area is presented in Figure 2.8. The boundaries of this Priority area go across provincial boundaries and include the following municipal areas (as seen in Figure 2.8) (AQMP, 2006):

- the Emfuleni Local Municipality (Sedibeng) in Gauteng Province;
- the Midvaal Local Municipality (Sedibeng) in Gauteng Province;
- the administrative regions of Doornkop and Soweto, Diepkoof and Meadowlands and Ennerdale and Orange Farm within the boundaries of the Jhb-Pta megacity in Gauteng;
- the Metsimaholo Municipality in the North Free State, Free State Province.

The study area is shown on Figure 2.8. The green line defines the Vaal Triangle Air-shed priority area. The southern part of the Jhb-Pta megacity is incorporated into Vaal Triangle Air-shed priority area and it is therefore relevant to this study.

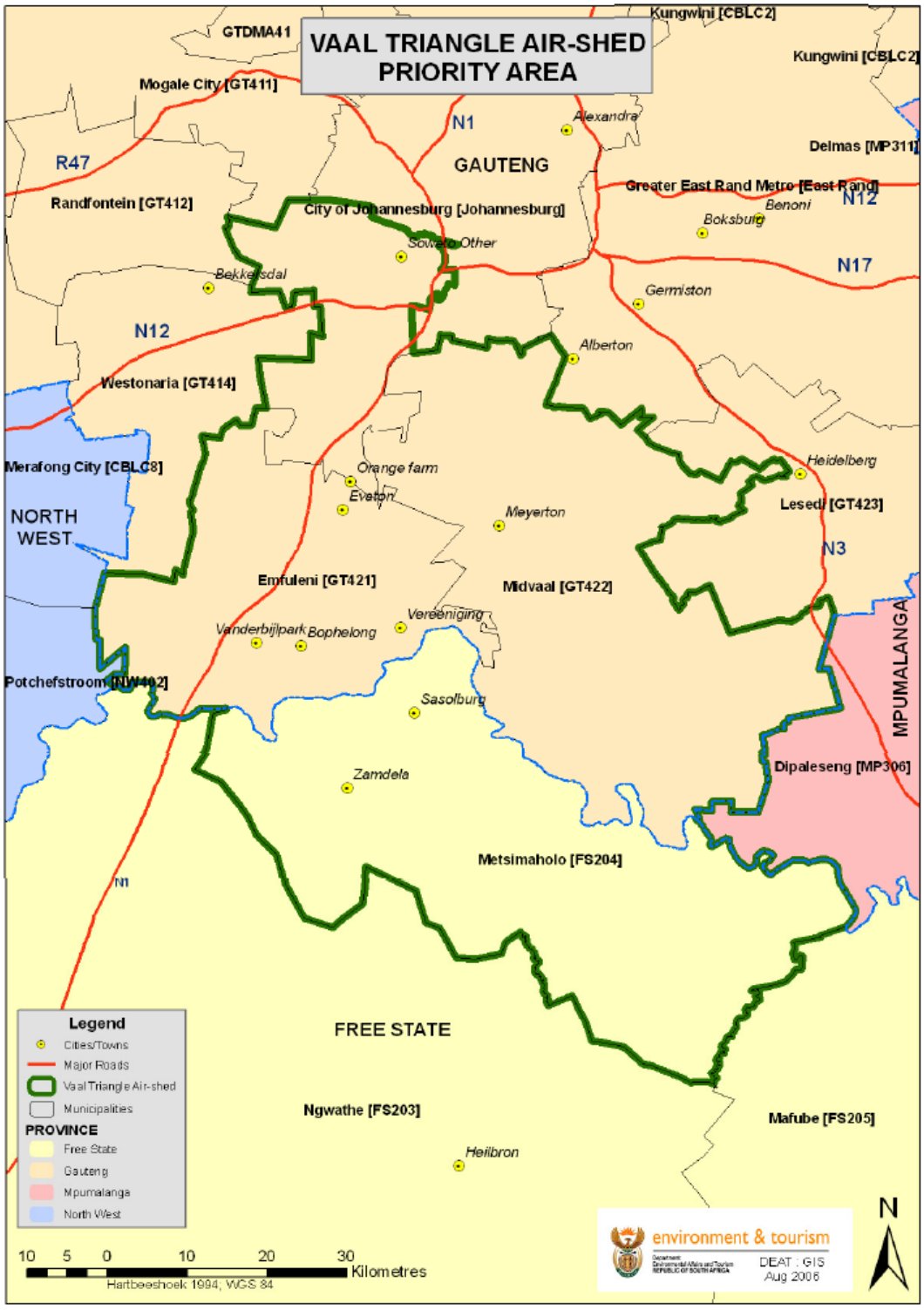

Figure 2.8: The Vaal Triangle Air-shed priority area (adopted from AQMP, 2006).

2.2.5.2. Mpumalanga Highveld Priority Area

Air quality in the Mpumalanga Highveld region is of major concern for both government and industry. Due to poor air quality in this region a second priority area, termed the Mpumalanga Highveld Priority Area, which encompasses the eastern Gauteng and western Mpumalanga, was declared by the Minster of Environmental Affairs and Tourism in terms of Section 18(1) of the NEMA: AQA (Act No. 29 of 2004) on the 4 May 2007.

The geographical expanse of this priority area is shown in Figure 2.9. The total area of the declared priority area is 31,106 km^2 with approximately 3,6 million people living in the region. The area extends from the eastern parts of Gauteng, up to Middelburg in the north and to the edge of the escarpment in the south and the east. The area incorporates parts of the Gauteng and Mpumalanga Provinces (Zunckel *et al.*, 2010). Major towns present in this region include Witbank, Middelburg, Secunda, Standerton, Edenvale, Boksburg, Benoni and Balfour. It is also clear from this map that industrial activity in this area not only influence the Jhb-Pta megacity, but that this priority area also incorporates the eastern parts of the Jhb-Pta megacity.

Figure 2.9: Mpumalanga Highveld priority area (Government Gazette, 2007).

Industrial sources are by far the largest contributor of emissions in the Highveld area, accounting for 89% of PM_{10}, 90% of NO_x and 99% of SO_2 (Zunckel *et al.*, 2010). During a recent study major industrial sources in the Mpumalanga Highveld were grouped into several categories, i.e. power generation, coal mining, primary metallurgical operations, secondary metallurgical operations, brick manufacturers, petrochemical industry and Ekurhuleni industrial sources (Zunckel *et al.*, 2010).

The Mpumalanga Province is rich in coal reserves, with a large coal-to-petroleum industry situated in Secunda. Coal-fired power stations are the main source of electricity in South Africa with approximately 80% of the power production generated in the Mpumalanga Highveld. There are also other minerals deposited in this area. There are chromite, magnetite, silicon and iron deposits in the northern and western sides, gold deposits in the western side, while nickel, gold, asbestos, copper, cobalt and antimony are mined in the east (Freight transport data bank, 2004). The largest manufacturer of stainless steel and second largest producer of steel in South Africa are also in the Mpumalanga province, as well as the world's biggest producer of vanadium.

2.2.6. Previous studies in the Jhb-Pta megacity

Burger & Thomas (2002) conducted a study in the greater Johannesburg area as part of the national standard setting process. The objective of this study was to determine the impact of heavy traffic density on VOC emissions. This study indicated high benzene and toluene concentrations, with maximum levels of 21.6 ppbv and 19.8 ppbv, respectively and average concentrations of 9.8 ppbv and 9.2 ppbv respectively. The ratio between benzene and toluene was shown to be 1.07. In another study in this area the fuel consumption for Johannesburg was modelled (Goyns, 2008), with estimated total emissions calculated to be 4.13 Mt CO_2, 82.77 kt CO, 9.15 kt HC, and 24.49 kt NO_x for Johannesburg. Therefore high NO_x, SO_2 and VOC emissions can be expected for the Jhb-Pta megacity.

A recent study by Beukes et al. (2012) indicated that air mass plumes passing over the Jhb-Pta megacity arriving at a relatively new comprehensively equipped site for atmospheric measurements at Welgegund (70 km west of the Jhb-Pta megacity) (www.welgegund.org) have

much higher concentrations of NO, NO_2, O_3, SO_2, CO and VOCs, as well as total organic aerosol content compared to regional background concentrations.

Various local authorities within the Jhb-Pta megacity and the DEA have established measurement stations in the Jhb-Pta megacity. Some of these stations supply data to the South African Air Quality Information System (SAAQIS). It is difficult to extract data from SAAQIS in order to summarise and evaluate the dataset. Internal DEA and local authority reports are also not available in the peer reviewed published public domain. It can therefore be stated that many measurements have been and are currently conducted in the Jhb-Pta megacity, but in contrast to developed countries, limited information is currently available in the peer reviewed published public domain.

2.3. EXPERIMENTAL AND METHODS

2.3.1. Site description

A high-resolution (0.25 degrees) gridded archived forecast of the population density data of 2010, which was adjusted to match United Nations totals, were used (CIESIN, 2010) to compile a realistic illustration of the population density of southern Africa. In this figure the colorbar indicates the number of people per km^2 (http://sedac.ciesin.columbia.edu/gpw). National roads in South Africa are also indicated in Figure 2.10. The Jhb-Pta megacity is located in the Gauteng province which is the smallest province shown in Figure 2.10 and where the highest population density is indicated. It shows the importance of the Jhb-Pta megacity in South Africa and clearly illustrates that most of the national roads lead to or cross within the Jhb-Pta megacity.

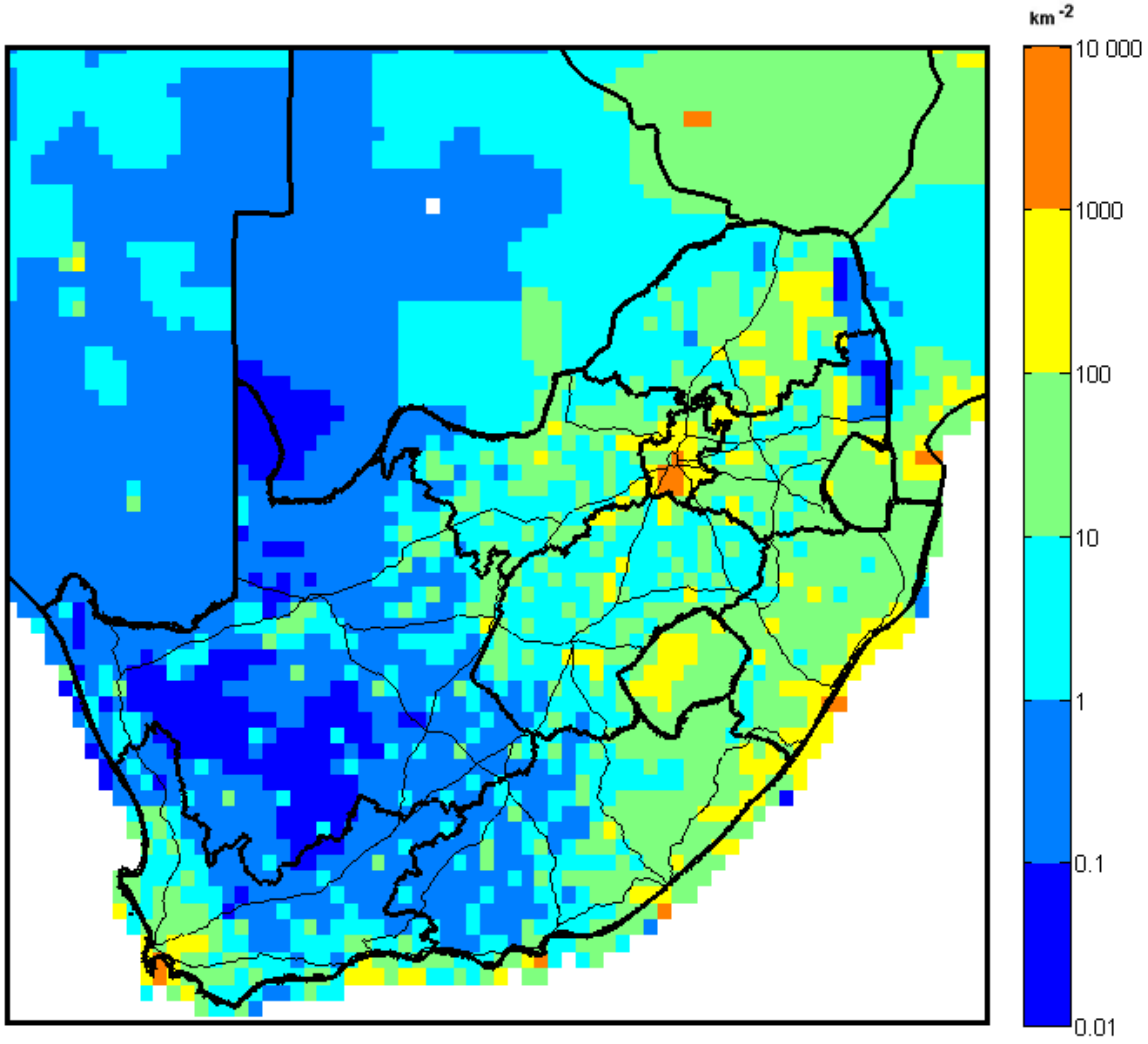

Figure 2.10: Population density and national highways (CIESIN, 2010; Laakso *et al.*, 2012).

The main objective of the measurements conducted in the Jhb-Pta megacity was to obtain data that would be representative of air quality in this area in order to use the data for modelling purposes. A prerequisite for a modelling study of this nature is to utilise data that represents typical air quality that the general population are exposed to in an area. To set up new measurement stations would not have been time or cost effective for this particular study. Permission was therefore obtained from local authorities to use data collected at air quality monitoring sites that was operated by local municipalities, as well as provincial and governmental departments (DEA). Permission was also granted to conduct additional sampling at these stations. The locations of these sites are shown in Figure 2.11. These sites were situated at relevant locations to measure the direct influences of urban air pollution e.g. traffic emissions, biomass burning and residential pollution. Seven sites were located within the

boundaries of the Jhb-Pta megacity (sites M1, M2, M3, M4, M6, M7, M8) with one site (M5) outside the domain of the model. This site (M5) was used to collect rural background data in close proximity to the Jhb-Pta megacity.

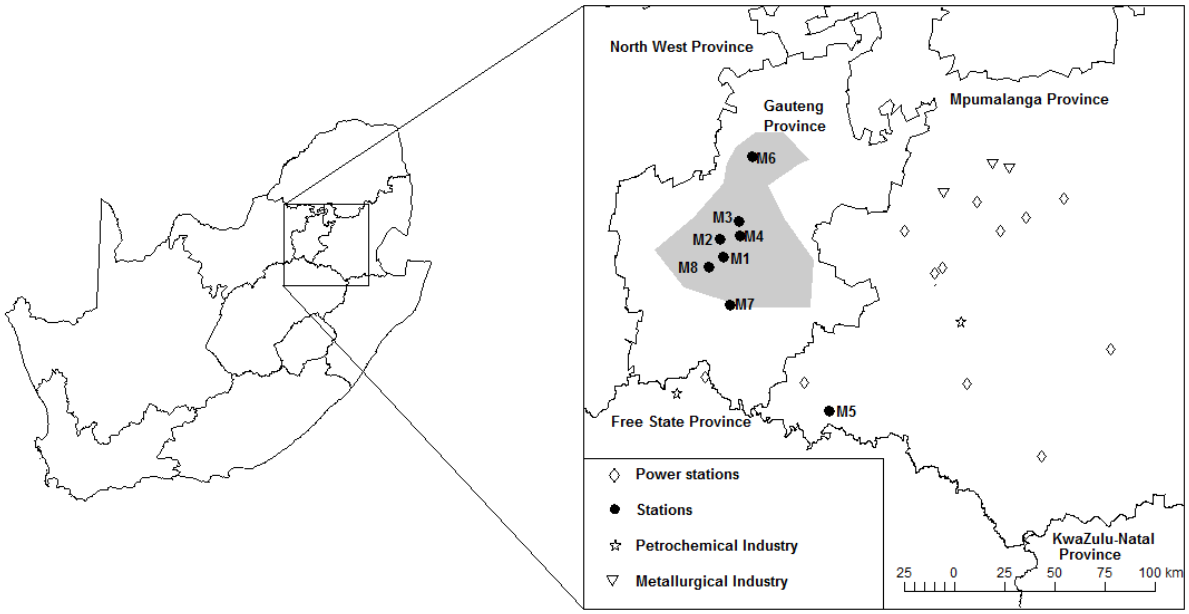

Figure 2.11: Measurement sampling sites in the Jhb-Pta megacity is denoted with "M". The grey indicates the Jhb-Pta megacity. Major point sources in the Mpumalanga Highveld are also indicated.

M1 (26.20°, 28.03°) was positioned within the central business district to measure urban commercial and industrial emissions, whereas M2 (26.12°, 28.00°) was situated in a park to measure urban background concentrations. The primary emission source of M3 (-26.04°, 28.09°) was vehicular emissions, since it is at the intersection of the N1 national and M1 secondary highways. M4 (-26.11°, 28.10°) was located on a roof of a medical facility in an informal settlement and was positioned to be indicative of a site influenced by household combustion. M6 (-25.75°, 28.14°) was located in the northern part of the Jhb-Pta megacity within an industrial region. M7 (-26.41°,28.08°) is located between a residential area and highways where both traffic and domestic burning emissions are measured. M8 (-26.25°, 27.95°) is located in close proximity to an interchange in one of the major settlements. This station mostly measured industrial activity with some influences from traffic emissions. The rural site, M5 (-26.89°, 28.63°) is located in Mpumalanga on a farm and is relatively isolated from any

direct pollution sources. All the air quality stations measured the priority pollutants NO_x, SO_2 and O_3. Benzene, tolene, ethylbenzene and xylene (BTEX) were not routinely measured at these stations and were therefore additionally measured at some of the stations for a period of two months. BTEX are good indicators for HC related chemistry (Singh *et al.*, 1985). Meteorological parameters such as temperature, pressure and relative humidity were also measured at the stations. In Table 2.1 a summary of parameters measured at all the monitoring sites are presented.

Table 2.1: Summary of monitoring sites and parameters measured.

Station	Species measured	Meteorology parameters measured	Average period	Possible sources
M1	PM_{10}, NO_x, NO_2, NO, O_3, CO	Wind speed and wind direction	5-10 min	Residential and industrial
M2	NO_X, NO_2, NO_X	Wind speed and direction	5-10 min	Residential
M3	PM_{10}, $PM_{2.5}$, SO_2, NO_x, O_3, CO, NO_2	Wind speed and direction, relative humidity, pressure	5-10 min	Vehicle emissions
M4	PM_{10}, SO_2, NO_2, O_3, CO	Wind speed and direction, temperature, rain fall, relative humidity, solar radiation, pressure	5-10 min	Domestic fuel burning
M5	PM_{10}, SO_2, NO_x, O_3,	Wind speed, Wind direction, Rain fall, relative humidity, solar radiation	5-10 min	Background

M6	PM_{10}, SO_2, NO_x, O_3	Wind speed, Wind direction, Rain fall, relative humidity, solar radiation	5-10 min	Industrial
M7	PM_{10}, $PM_{2.5}$, SO_2, NO_x, O_3. CO	Wind speed, Wind direction, Rain fall, relative humidity, solar radiation	5-10 min	Vehicular emissions and domestic fuel burning
M8	NO_X, O_3. CO, SO_2	Wind speed, Wind direction, Rain fall, relative humidity, solar radiation	5-10 min	industrial with some influences from vehicle emissions

2.3.2. Sampling methods

Different techniques exist for measuring pollutant species in ambient air. One approach is active sampling where near real-time instruments (or active sampling), such as infra-red spectrometers or portable gas chromatographs are utilised (Harper, 2000). These measurements provide valuable information regarding the temporal characteristics of atmospheric pollutants and their interactions with one another. However, most of these instruments are expensive and require maintenance, field calibrations and constant power supply, which make it difficult to measure at remote sites and to conduct long-term measurements programs if cost and/or expertise are limited. An alternative method to perform measurements is passive (or diffusive) sampling. The samplers are cost-effective, lightweight, small, silent and requires no electricity or field calibrations (Martins *et al.*, 2007). Although this approach solves some of the problems, the integrity of the sample must be ensured through the collection, transportation and analysis stages (Harper, 1992). Additionally, the detail with regard to temporal characteristics is lost, since the results of passives samplers are usually time weighted averages. Both active and passive sampling were used during this study and are therefore discussed in detail in Annex A.

2.3.2.1. NO_x monitoring

Passive (diffusive) sampling

The Atmospheric Chemistry Research Group (ACRG) at the North-West University (NWU) has demonstrated the effectiveness of monitoring tropospheric inorganic gas pollutants (NO_2, SO_2 and O_3) with passive sampling since 1995 (Dhammapala, 1996; Martins *et al.*, 2007). Passive samplers are based on chemical and physical processes, i.e. chemical reactions and laminar diffusion, respectively. The rate at which gases in ambient air diffuses into the sampler is governed by Fick's Law of diffusion, which is influenced by physical parameters, such as gaseous diffusion through a static layer or porous material that is controlled by the diffusion coefficient of the respective gases (Brown, 1999). A detailed description of the passive sampling technique is discussed in Appendix A.

NO_2 analyses were performed on a Varian Cary 50 ultraviolet/-visible (UV/vis) spectrophotometer shown in Figure 2.12. The NO_2 samples were leached in 5 cm^3 of de-ionised water and then treated with 5 cm^3 of the diazotising agent before their absorbance was scanned at 540 nm. This analytical method has a detection limit of ca. 0.02 ppb (Dhammapala, 1996). The diazotising agent consists of sulphanilamide, naphthylethylenediamine dihydrochloride (NEDA) and H_2PO_4. A five-point calibration curve was determined for NO_2 analyses by preparing standards at 0.1, 1, 2.5, 5, and 12.5 ppm of $NaNO_2$ and NaI. The NaI is added to ensure the same I concentration in the standards and the samples (Dhammapala, 1996).

Figure 2.12: Varian Cary 50 UV-visible spectrophotometer.

Active sampling

Different techniques and instruments currently exist to measure in situ NO and NO_2 concentrations. Some of the most well-known instruments include the standard chemiluminescence monitors equipped with molybdenum oxide converters, the tuneable infrared laser differential absorption spectrometers (TILDAS) and the differential optical absorption spectrometers (DOAS). Of these techniques the most commonly used and also designated by the US EPA, are the chemiluminescence instruments (CL NO_x monitors) (Demerjian, 2000; Dunlea *et al.*, 2007). All ground-based NO_2 measurements in this investigation were conducted with standard chemiluminescence instruments using molybdenum oxide converters. For a more detailed description of these instruments see Fontjin et al. (1970); Ridley & Howlett, (1974).

Within the instrument NO_2 is first transformed into NO before it is measured using the chemiluminescent reaction, where NO_2 is converted to NO by a molybdenum NO_2-to-NO converter heated to about 325°C. The instrument operates on the principle of luminescence where NO and O_3 reacts to produce a characteristic luminescence with an intensity that is linearly proportional to the NO concentrations. Infrared light emission results when electronically excited NO_2^* molecules decay to lower energy states (Dunlea *et al.*, 2007). O_3 was selected as the reactant since the reaction between NO and O_3 had been investigated extensively (Fontjin *et al.*, 1970). The chemiluminescence is due to the following reactions

$NO + O_3 \rightarrow NO_2^* + O_2$ R13a

$NO_2^* \rightarrow NO_3 + h\upsilon$ R45

The final measurement obtained with the instrument is the total NO_x concentration. The technique is uncomplicated and relatively reliable. Dunlea et al. (2007) and Steinbacher et al. (2007) pointed out that this method not only converts the NO_2 to NO, but also partially converts other oxidized nitrogen compounds such as nitric acid (HNO_3), alkyl nitrates ($C_nH_{n+2}NO_3$) and peroxacetyl nitrate (PAN), which can therefore measure overestimates between 17-30% of NO_2. However, this technique is still widely applied and currently represents the only actively monitored available near-surface data for the regions investigated in this study.

2.3.2.2. O_3 monitoring

Passive sampling

The same passive samplers and methods described in Annex A were used for O_3 measurements The absorbent solution used was nitrate, since atmospheric O_3 concentrations are measured indirectly by determining the amount of nitrate that is formed during the reaction:

$$O_3(g) + NO_2^- \rightarrow NO_3^- + O_2 \qquad \text{R46}$$

The absorbing solution consisted of 1 % (w/v) $NaNO_2$, 1% (w/v) K_2CO_3 and 2 cm^3 glycerol that was dissolved in a 100 mL of a 70 % water/30 % methanol mixture. K_2CO_3 kept the solution at a pH of 12, since oxidation of NO_2^- does not occur above pH 12. Collection efficiency tests have shown that O_3 reacts optimally with NO_2^- when the NO_2^- and carbonate species are from salts of different metals. This can be due to the higher hydroscopy of crystals that are formed when the mixed sodium (Na) and potassium (K) crystals are formed (Martins *et al.*, 2007; Dhammapala, 1996). O_3 samples were analysed on a suppressed Dionex Ion Chromatography (IC) system (ICS-300) fitted with an Ionpac AS18 (2x50mm) analytical column, an Ionpac AG18 (2x50mm) guard column and an ASRS Ultra 11 2 mm self-regulating suppressor shown in Figure 2.13.

Figure 2.13: Ion Dionex Chromatography module/SP system.

Samples were prepared for IC analysis by removing the Whatman filter from the sampler and placing it in a clean vial. Since ambient O_3 concentrations are usually higher than SO_2 and NO_2, O_3 samples were dissolved in 25 cm^3 de-ionised water (5 cm^3 de-ionised water was added to SO_2 and NO_2 samples). The samples were then de-ionised for 15 minutes before they were analysed on the IC. A five-point calibration curve was determined for O_3 at 0.1, 1, 2, 5, and 10 ppm.

Active sampling

Various techniques have been developed to measure O_3 *in situ*. These methods include UV absorption, Differential Optical Absorption Spectroscopy (DOAS), chemiluminescence and chemical titration methods (Parrish & Fehsendeld, 2000). The UV absorption technique used in various high quality reliable and commercially available instruments was used for O_3 measurements in this study (Parrish & Fehsendeld, 2000). These instruments operate on the principle that O_3 molecules absorb UV light at a wavelength of 254 nm that is emitted from a low pressure mercury discharge lamp (Parrish & Fehsendeld, 2000). The degree to which the UV

light is absorbed is directly related to the O_3 concentration as described by the Beer-Lambert Law:

$$\frac{I}{I_o}A = e^{-KLC} \qquad 2.1$$

K = molecular absorption coefficient, 308 cm^{-1} (at 0°C and 1 atm),

L = length of cell, 38 cm,

C = ozone concentration in parts per million (ppm),

I = UV light intensity of sample with ozone (sample gas) and

I_0 = UV light intensity of sample without ozone (reference gas).

2.3.2.3. VOC monitoring

Adsorbent tubes

Adsorbent tubes are an effective method to conduct VOC sampling due to the accurate and reliable results (Zabiegala et al., 2002). They can be used for both active (air forced through the tube by a pump) and passive (air flows through the tube by means of diffusion) sampling. The samplers consist of tubes packed with an adsorbent. These tubes can either be stainless steel or glass tubes packed with 0.1 to 2 g solid sorbent material that is either a porous polymer or charcoal (EPA, 1997) depending on the NMHCs to be collected. In Figure 2.14 an example of a stainless steel absorbent tube is shown, which was also used in this investigation.

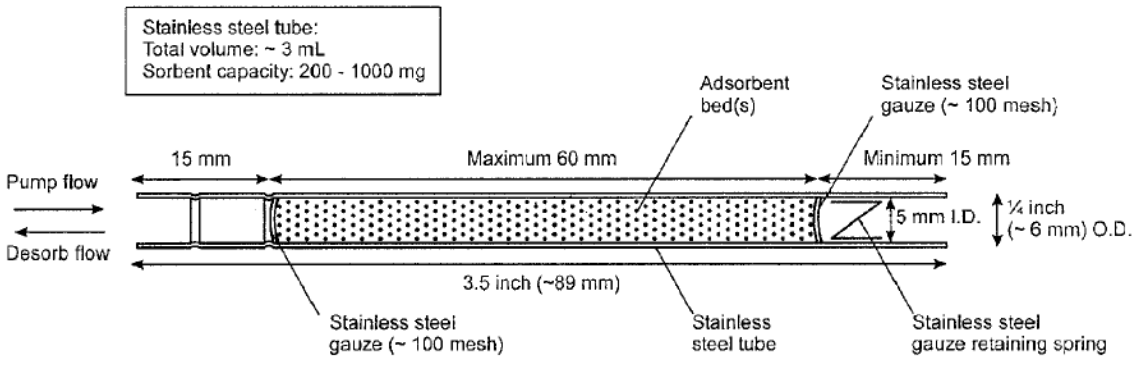

Figure 2.14: Stainless steel adsorbent tube used for VOC measurements in this study (EPA, 1997).

The efficiency of the sorbent is determined by the adsorbent capacity of the sorbent material, with larger loadability of the sorbent leading to larger possible sampling volumes. Tenax TA and Carbotrap 106 porous polymeric material are the most frequently used sorbent materials, particularly for VOC sampling (McClenny *et al.*, 2002). However, multi-bed tubes, such as Carbotrap 300, have become more popular in recent years, especially for active sampling. Adsorbents are arranged in such a manner that the least volatile compounds are trapped on the weakest sorbent at the front end of the tube, while the more volatile compounds are trapped by stronger sorbents at the back of the tube. As recommended by the EPA, Tenax TA adsorbent tubes were used for passive sampling of VOCs, whereas Carbotrap 300 tubes were utilised for active measurements in this study.

The adsorbent tubes were tested for leaks and preconditioned with helium for 30 min at 350°C at a flow of 50 $cm^3.min^{-1}$ before they were used. After treatment, the tubes were sealed with Swagelok® brass ¼" caps (P/N 0990-8851) and stored in a fridge at temperatures below 18°C prior to sampling. After sampling, the exposed tubes were wrapped individually in aluminium foil and stored below 18ºC before they were analysed. Samples were analysed with a Marks International Unity Thermal Desorber, Agilent Technologies 7890A gas chromatograph (GC) connected to an Agilent Technologies 5975C VL Micromass Autospec mass spectrometer (MS) in compliance with the EPA TO-17 compendium and NIOSH 2549 method.

The tubes were analysed by using a two-stage thermal desorption method. The samples were first tested for leaks and then purged with zero air to reduce the risk of adsorbent oxidation during desorption. Thereafter, the samples were heated for five minutes. The volatiles on the adsorbent were removed with nitrogen gas into a cold trap (-30°C) where they were reconcentrated for four minutes. At the end of this period, the cold trap was heated rapidly for five minutes. Thermal desorption was then used to transfer the concentrated VOCs from the cold trap to the gas chromatograph for separation and detection with the MS.

Passive sampling

Passive (diffusive) sampling is governed by the rate of diffusion that is determined by Fick's first law of diffusion. Uptake rates for compounds can either be theoretically derived from Fick's first law (Equation A.1) or experimentally determined. The ideal theoretical uptake rate (U) is determined by

$$U = \frac{D \times A}{I} \qquad 2.2$$

where

A = cross-sectional area of the diffusive path, or the equivalent sorption surface (cm^3),

I = length of static layer of sample (cm),

D= diffusion coefficient (cm^2. min^{-1}) and

U = ideal theoretical update rate (cm^3.min^{-1}).

With the known ideal uptake rate, the atmospheric concentrations of the compound can then be determined

$$C = \frac{X}{U_p \times t} \qquad 2.3$$

where

C= atmospheric concentration (cm^3/min),

U_p = Ideal uptake rate (cm^3.min^{-1}),

X = amount of the analyte which is absorbed on the tube (ng) and

T = time of exposure (min).

The experimental uptake rates are usually presented in units of either, ng.ppm^{-1}.min^{-1} or pg.ppb^{-1}.min^{-1}, in order to give atmospheric concentrations in ppm or ppb. U_p is the uptake rate at ambient conditions. The conversion of U (cm^3.min^{-1}) to U_p (ng.ppm^{-1}.min^{-1}) is

$$U_p = \frac{U * M * 293 * P}{24.5 * T * 101.1} \qquad 2.4$$

U_p= ideal diffusive uptake rate (ng.ppm^{-1}.min^{-1}),

M= molecular mass of analyte (g/mol),

P = pressure of sampled atmosphere during sampling (kPa),
T = temperature of ambient air sampled (K) and
24.5 l/mol = molar gas volume at 760 mm Hg and 25 ºC at 298K.

Table 2.2 presents the theoretical uptake rate calculated with equation 2.9 and the experimental uptake rates from literature determined for each one of the compounds measured in this study.

Table 2.2: Theoretical and experimental uptake rates (adopted from Lourens, 2008).

Component	Diffusion Coefficient (cm^2/s)	Molecular Weight (g/mol)	Uptake Rate (cm^3/min)	Theoretical Uptake Rate (ng/ppm.min)	Experimental Uptake Rate (ng/ppm.min)
Benzene	9.32E-02	78.10	0.59	1.90	0.70±0.09[a]
Toluene	8.49E-02	92.10	0.54	2.04	1.03±0.26[a]
Ethylbenzene	7.55E-02	106.20	0.48	2.09	1.50±0.40[c]
o Xylene	6.88E-02	106.20	0.44	1.90	1.46±0.67[a]
m,p Xylene	7.27E-02	106.20	0.46	2.01	1.46±0.67[a]

[a] Uptake rates obtained from Markes International Limited (2006).

[b] Uptake rates obtained from the Diffusive Monitor Issue 12 (2001).

[c] Uptake rate obtained from Potter (2008).

The theoretical uptake rate is only an indication of the ideal uptake rate for each component for the specific tube and packing material. It does not include other variables, such as exposure time and wind speed. Ethylbenzene is the only compound studied for which the experimentally determined uptake rate, for an exposure time of four weeks with Tenax TA absorbed, could not be found in literature. Therefore an extrapolated value relative to the other compounds was used as calculated by Potter (2008). Since the value was extrapolated, a relative large error of 0.4 ng/ppm.min was assumed.

Two tubes were exposed at each site for a month. The tubes were fitted onto the same aluminium stands used for the passive sampling of inorganic gaseous species (Figure 2.14) into a special fitting. The Swagelok caps were removed from the tubes before exposure in the field and replaced with diffusive caps for effective air diffusion into the tubes. The tubes were placed faced down in the special fitting onto the shaft of the stand. After the sampling period, the diffusive caps were removed and the tubes were sealed-off with the Swagelok caps.

Active sampling

Active sampling at flow rates between 5 and 200 ml/min for short sampling periods between 1 and 8 hours are commonly applied (Skov *et al.*, 2001; Duan *et al.*, 2008). Active VOC sampling was achieved by using a pump that forced air though the stainless steel adsorbent tubes at a set flow rate. Supelco air sampler Model 1067 pumps presented in Figure 2.15 were used for active VOC sampling. The instrument was loaded with Carbotrap 300 absorbent tubes that were used during the 8-hour sampling periods that were conducted consecutively for two days. The sampling was performed twice during each month for a period of two months between March and May 2010. Sampling started in the second week of March, while the last sampling was conducted in the first week of May. The sampling schedule is shown in Figure 2.16. The flow rate for each sampler was measured before and after each measurement and was mostly at 10.6 +- 0.2 mL/min. The sampling times were 06:00 - 14:00, 14:00 - 22:00, 22:00 - 06:00. These times were selected due to logistics and safety reasons.

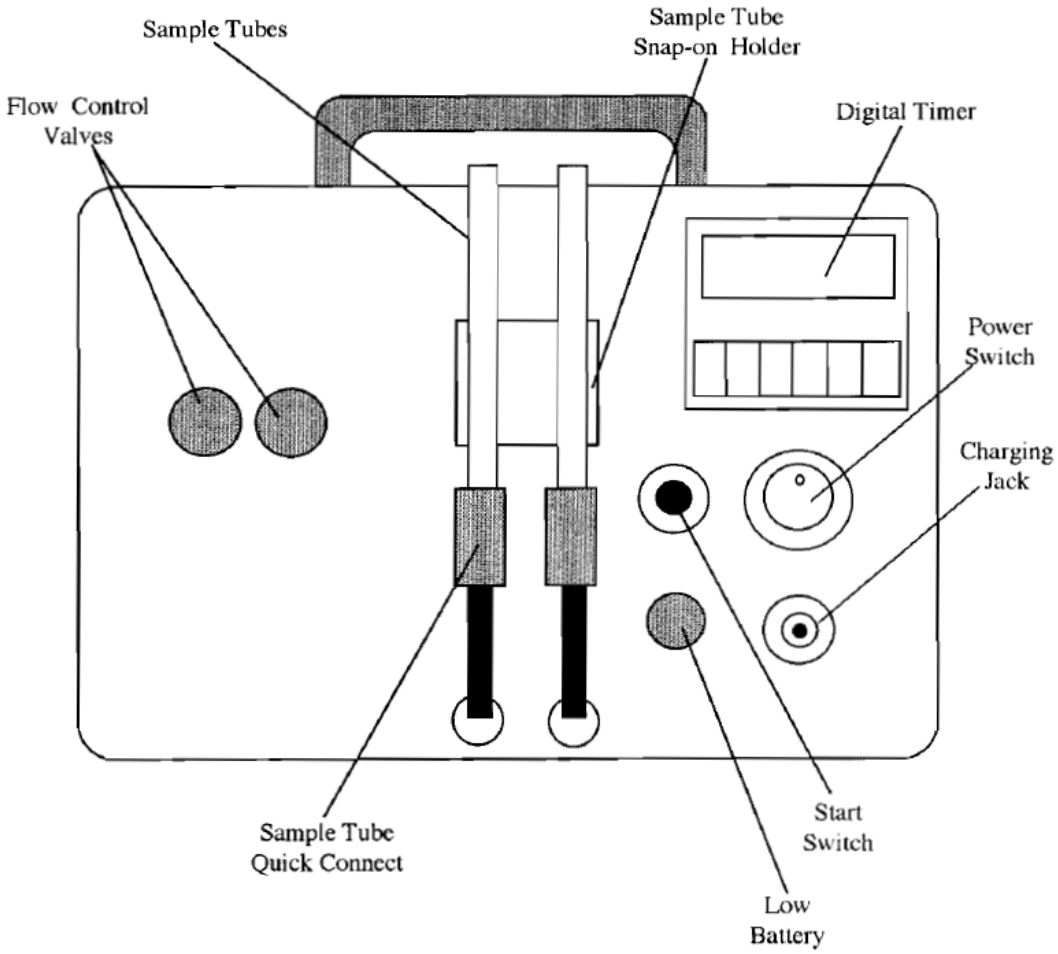

Figure 2.15: Supelco Air Sampler Model 1067 used during the active VOC sampling study.

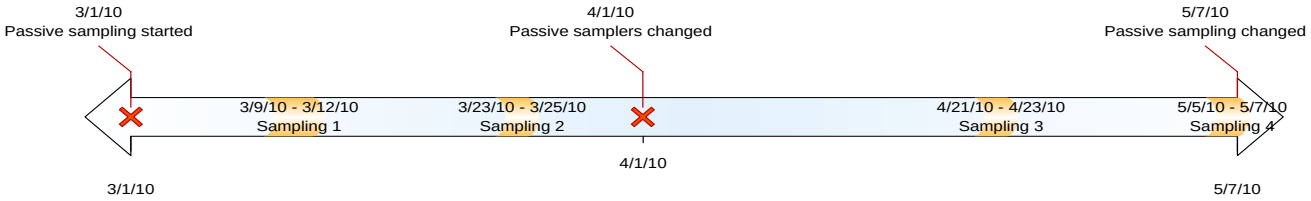

Figure 2.16: Graphical illustration of the active VOC sampling schedule.

2.3.2.4. SO_2 monitoring

Passive sampling

The same samplers and methods described in Section 2.3.2.1 were used for passive sampling of SO_2. The absorbing solution was prepared by dissolving 1 g NaOH in less than 15 cm^3 de-ionised water and diluting it in a 100 mL methanol solution. NaOH was used to trap and collect SO_2 which oxidised to sulphate (SO_4^{2-}) during sampling on the filter.

$$2SO_2(g) + 4OH^- + O_2 \rightarrow 2H_2O + 2SO_4^{2-} \qquad \text{R47}$$

The concentration of the sulphate is determined with a suppressed ICS-300 fitted with the same column, guard column and suppressor setup as described in Section 2.3.2.1 (O_3 passive sampling). The samples were leached in 5 cm^3 de-ionised water and sonicated for 15 minutes, after which the extracted sample was injected into the IC. SO_4^{2-} standards of 0, 1, 5, 10 and 25 $\mu mol.dm^{-3}$ were prepared.

Active sampling

Commercial pulsed fluorescence (PF) detectors for SO_2 measurements are inexpensive and are widely used in urban, rural and regional monitoring (Luke, 1997). The PF technology operates on the principle that SO_2 molecules are excited by absorption of UV light at a specific wavelength, followed by the decay to a lower energy state to emit UV light at a different wavelength. This reaction is shown in R48. The amount of fluorescence measured is proportional to the SO_2 concentration. This method is designed by Thermo Environmental Instruments (Luke, 1997).

$$SO_2 + h\upsilon_1 \rightarrow SO_2^* \rightarrow SO_2 + h\upsilon_2 \qquad \text{R48}$$

2.4. RESULTS

Results from the datasets acquired with passive and active sampling are presented in this section. As mentioned previously, the main objective of the sampling campaign was to obtain representative input data for modelling purposes and to obtain background information on the current air quality levels of the Jhb-Pta megacity. All measured data are also compared to other megacities world-wide.

The passive sampling dataset was obtained in a sampling campaign conducted during March to May 2010, during which monthly mixing ratios of O_3, SO_2, NO_2 and BTEX was determined at six of the eight sites. Sites M1-M6 was used for passive sampling whereas M7 and M8 was used for active BTEX measurement. Concentrations of O_3, SO_2 and NO_2 measured with active samplers were also obtained from the air quality monitoring sites where the passive measurements were conducted in order to also assess diurnal variation of the gaseous species measured. Unfortunately, due to various power failures and maintenance problems with some of the instruments, the active sampling results for 2010 were not representative of the region and could not be used in this study. Therefore, the active sampling measurements for the period March 2009 to May 2009 were utilised. Although the concentrations measured with passive samplers in 2010 cannot be directly compared to the active sampling measurement, the results could still be used to be indicative of typical concentration levels and diurnal variations during that specific time of year. Active BTEX sampling was also conducted for 8-hour periods at four of the eight sites during the passive sampling campaign as described in Section 2.3.2.3.

Generally a minimum of 80% data availability is required to achieve minimum data quality assurance (SANAS, 2000). Although there were data losses at the stations due to logistical reasons the percentage verifiable data was >91%. From the 32 passive samplers used for the inorganic gaseous species monitored, 100% of the samplers were recovered and 97% of the data were used. From the total number of 96 tubes used for BTEX monitoring during the 2 months sampling campaign, data from only 8 tubes could not be recovered.

2.4.1. NO_2

The monthly mixing ratios measured for NO_2 with passive and active samplers at the different sites are presented in Table 2.3. No active data was obtained for M4. The mixing ratios measured for NO_2 at the different sites for the two months ranged from a minimum of 3.3 ppb

(rural background site) to maximum of 19.4 ppb (residential and industrial). The concentrations of NO_2 at the sites impacted by industry, vehicular emissions and residential sources were in the same order of magnitude and much higher than the NO_2 levels measured at the background site. A good correlation was found between the two months at the background site with concentrations of 3.6 and 3.3 ppb. These values were also in agreement with a previous study conducted at site M5 for a full year (Lourens, 2008). Concentrations measured in this study were also compared to other measurement sites in South Africa, i.e. Amersfoort and Louise Trichardt, which are influenced by biomass burning and industrial sources. The monthly average concentrations for March and April during 2009 and 2010 at these sites were below 1 ppb. The large difference between these sites and Jhb-Pta megacity indicate that Jhb-Pta megacity is closer to the emissions sources.

Table 2.3: Monthly NO_2 mixing ratios (ppb) at all the sites for the two months of passive sampling in 2010 and two months of active sampling in 2009.

	M1	M2	M3	M4	M5	M6
Possible sources	**Residential and industrial**	**Residential**	**Vehicle emissions**	**Domestic fuel burning**	**Background**	**Industrial**
March 2010	19.4	14.4	18.8	16.6	3.6	18.8
April 2010	19.1	13.3	17.9	14.7	3.3	12.8
March 2009	14.7	25.0	11.7	-	7.2	21.4
April 2009	14.5	29.8	29.0	-	8.1	20.9

The average diurnal cycle for three months measured with active samplers for NO_2 in the Jhb-Pta megacity is presented in Figure 2.17. A strong diurnal cycle is observed at all the stations. M2 exhibits the highest averaged mixing ratio, while M5 had the lowest values.

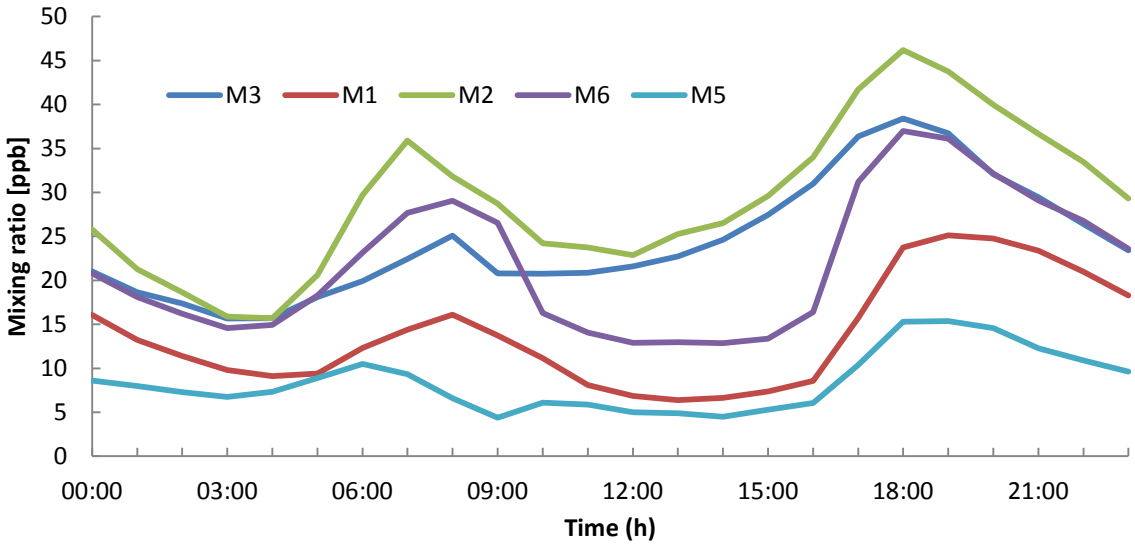

Figure 2.17: Three month (March to May 2009) averaged diurnal cycle for NO_2.

Two distinct peaks are observed at all the stations. These peaks are characteristic of cities and coincided with peak traffic hour emissions of NO_2 (Lourens *et al.*, 2011). The early morning peak between 6:00 - 9:00 coincide with the time commuters travel to work whereas the evening peak between 18:00 - 21:00 are during the period when people return to their homes from work. The more pronounced second peak can most-likely be attributed to the decrease in photochemistry during evenings that leads to higher NO_2 concentrations that are not rapidly removed from the atmosphere. In a previous investigation in an industrialised area in South Africa these two diurnal NO_2 peaks were also observed (Venter *et al.*, 2012). In this study the emissions from household combustion for space heating and cooking was determined to also contribute to atmospheric NO_2 concentrations in that area. Household combustion within in the suburbs of the Jhb-Pta megacity and other emissions can also contribute to the NO_2 peaks observed. (Venter *et al.*, 2012). In this study traffic emissions were considered to be the main source in the Jhb-Pta megacity.

A previous study indicated that the annual average for NO_2 within the Jhb-Pta megacity for 2006 were 30 ppb (State of the air Report, 2006). In this study the average NO_2 concentration measured for two months at all the sites (excluding M5) with passive samplers was 16 ppb, while active measurements indicated a three months average of 19 ppb. Table 2.4 present a comparison of the measured Jhb-Pta megacity ambient NO_2 concentration with other megacities published in previous studies (Ranjeet & Molina, 2011; Gurjar *et al.*, 2008;

Baldasano & Jiménez, 2002; APMA, 2002). Data obtained from Ranjeet & Molina (2011) ranged from 1990-2002, data obtained from Gurjar et al. (2008) ranged from 1990 – 2001 and APMA (2002) data ranged from 1995 – 2000. The data obtained from Baldasano et al. (2002) is more recent and is for the period 1999 – 2010. The comparison of NO_2 levels of the Jhb-Pta megacity measured in this study with other megacities indicate that NO_2 concentrations in the Jhb-Pta megacity are comparable to NO_2 levels in Chicago, Guadalajara, Buenos Aires and Santiago. NO_2 concentrations in Berlin were lower, if compared to NO_2 levels measured in other cities.

Table 2.4: NO_2 concentrations in megacities world-wide.

City	concentrations (ug/m^3) *ppb	Reference
Jhb-Pta megacity	16* and 19*	This study
Chicago	10.1-20	Ranjeet & Molina (2011)
Guadalajara	10.1-20	Ranjeet & Molina (2011)
Lima	85	Baldasano et al. (2002)
Sao Paulo	50-60	Gurjar et al. (2008)
Buenos Aires	20	Gurjar et al. (2008)
Cairo	>50	Ranjeet & Molina (2011)
Santiago	10.1-20	Ranjeet & Molina (2011)
St Petersburg	>82	Baldasano et al. (2002)
Berlin	5.1-10	Ranjeet & Molina (2011)
Madrid	>60	Baldasano et al. (2002)
Athens	50-60	Baldasano et al. (2002)
Shanghai	73	Gurjar et al. (2008)
Delhi	36	Gurjar et al. (2008)

Mumbai	43	Gurjar et al. (2008)
Bangkok	49	APMA, (2002)
Kolkata	37	Gurjar et al. (2008)
Tokyo	55	Gurjar et al. (2008)
Rio de Janeiro	60	Gurjar et al. (2008)

2.4.2. O_3

The monthly mixing ratios measured for O_3 with passive samplers at the sampling sites are presented in Table 2.5. The highest O_3 levels were measured at the background site (M5), which also correlates with a previous study conducted at site M5 for a full seasonal cycle (Lourens, 2008). The average O_3 levels for M5 were 25 ppb for the two months. The average O_3 concentrations measured at sites in the Jhb-Pta megacity were in the same order with average values for the two months ranging between 16 and 18 ppb. High pollutant concentrations in the city lead to titration of O_3. This is usually observed for regions with large point sources in South Africa. Lourens et al. (2011) who conducted a study in the Mpumalanga Highveld also indicated that sites with low O_3 had high NO_2 and VOCs concentrations, while the opposite was observed for sites with low NO_2 and VOC levels. Aging of the megacity plume can also result in O_3 formation from precursor species measured at the background site (M5).

Table 2.5: Monthly O_3 mixing ratios (ppb) at all the sites for the two months of sampling.

	M1	M2	M3	M4	M5	M6
Possible sources	**Residential and industrial**	**Residential**	**Vehicle emissions**	**Domestic fuel burning**	**Background**	**Industrial**
March	18.6	15.8	14.2	18.3	28.8	22.5
April	15.8	18.6	14.2	18.3	21.6	10.4

In Figure 2.18 the diurnal trends of O_3 based on the 2009 active sampling measurements during the same time of year that passive sampling was conducted in 2010 are presented. A different trend is observed compared to the patterns observed for NO_2. O_3 is characterized by high

mixing ratios between 13:00 – 15:00 and low mixing ratios during morning and evenings. This is expected due to the chemistry of tropospheric O_3 that is primarily formed through the reaction of NO_2 with sunlight as discussed previously (Section 2.2.3.4).

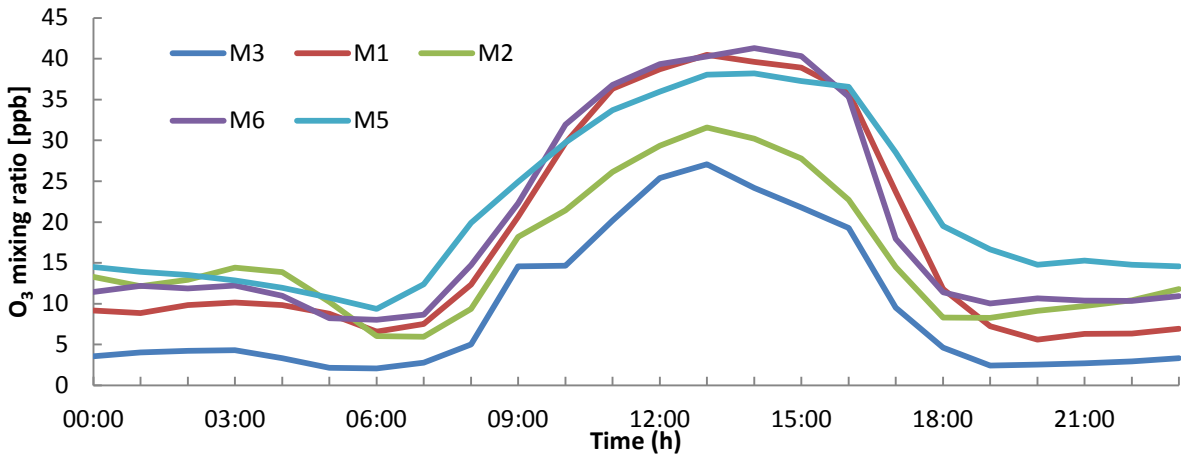

Figure 2.18: Three months (March to May 2009) averaged diurnal cycle of O_3 for all the stations.

During night-time the earth surface is cooled promoting the stratification of the lower atmospheric layers near the surface as well as the formation of a nocturnal stable ML (Stull, 1997). In the early morning solar radiation starts to warm the surface of the earth and destroys the stable ML. This leads to the formation of a convective mixing layer with turbulent vortexes responsible for the vertical movements in the lower atmosphere, thus increasing the ML height (Xu *et al.*, 2011). With the increase in sunlight photochemical reactions start to take place and precursor species of O_3 trapped in the stable ML decrease as O_3 concentration increases in the troposphere (Adkinson, 2000; Xu *et al.*, 2011). Minimum values for atmospheric NO_2 are observed around 14:00 when O_3 levels peak. This similar diurnal variation is observed in many urban areas around the world and in the rest of the interior in South Africa (Lal *et al.,* 2000; Dueñas *et al.,* 2002; Zhang & Oanh, 2002; Mazzeo *et al.,* 2005; Xu *et al.,* 2011, Venter *et al.,* 2012, Laasko *et al.,* 2010, Josipoiv *et al.,* 2010).

The averaged O_3 concentration determined with passive samplers were 18 ppb, while active measurements also had an average of 18 ppb (M5 excluded). Table 2.6 compares the ambient O_3 concentration measured in this study in the Jhb-Pta megacity with other megacities obtained during previous studies (NETCEN, 2001; Baldasano *et al.*, 2002, CEPIS, 2001; WRI – AirBase, 2001; Ayto Madrid, 2001). The data obtained from Baldasano et al. (2002) is for the period

1999 – 2001, data obtained from NETCEN (2001) is from 2000. Data used from WRI- AirBase (2001) ranged from 1995 – 1999 and APMA (2002) data ranged from 1995 – 2000. Data obtained from Ayto. Madrid (2001) while data from CEPIS (2001) was between 1999 – 2000. The comparison of O_3 levels in the Jhb-Pta megacity with other megacities indicate that O_3 concentrations in the Jhb-Pta megacity are comparable to O_3 levels in London, Santiago, Hong Kong and Lisbon. Lower O_3 levels are measured in Guatemala, O_3 concentrations for other cities listed in the table are much higher.

Table 2.6: O_3 concentrations in megacities world-wide.

City	concentrations (ug/m^3)	Reference
Jhb-Pta megacity	35	This study
London	30	NETCEN(2001); Baldasano et al. (2002)
Liverpool	51	NETCEN(2001); Baldasano et al. (2002)
Montreal	40	NAPS C.U.M. (2001); Baldasano et al. (2002)
Mexico City	72	CEPIS (2001); Baldasano et al. (2002)
Guadalajara	44	CEPIS (2001); Baldasano et al. (2002)
Melbourne	51	NSW-EPA (2001); Baldasano et al. (2002)
Leeds	40	NETCEN (2001); Baldasano et al. (2002)
Santiago	31	CEPIS (2001); CONAMA (2001); Baldasano et al. (2002)
Hong Kong	32	APMA, 2002
Guatemala	23	CEPIS (2001); Baldasano et al. (2002)
Lisbon	30	WRI –AirBase (2001); Baldasano et al. (2002)
Rome	37	Airbase (2001); Baldasano et al. (2002)
Madrid	32	Ayto. Madrid (2001); Baldasano et al. (2002)

2.4.3. VOCs (BTEX)

The complete dataset obtained with diffusive measurement of BTEX species with adsorbent tubes in March and April 2010 are listed in Table 2.7. From this data it is evident that toluene levels are predominantly higher than benzene. Benzene mixing ratios ranged between 0.7 ppb and 3.06 ppb at the different sites, while toluene levels were between 0.2 ppb and 7.8 ppb. Low levels of ethylbenzene were measured at all the sites during the sampling period. The mixing ratios of ethylbenzene ranged from 0.04 ppb to 0.96 ppb. Xylene concentrations were between 0.09 ppb and 4.47 ppb, which compared to benzene levels measured at all the different sites. BTEX mixing ratios were the lowest at the background site (M5) for both months.

Table 2.7: BTEX mixing ratios (ppb) measured in March and April 2010.

		M1	M2	M3	M4	M5	M6
	Possible sources	**Residential and industrial**	**Resident-ial**	**Vehicle emissions**	**Domestic fuel burning**	**Back-ground**	**Industrial**
Benzene	**March**	1.23	1.93	2.12	2.38	0.7	2.71
	April	2.66	-	3.06	3.04	0.75	2.7
Toluene	**March**	1.55	3.8	3.12	3.3	0.2	3.46
	April	5.32	7.08	6.94	4.61	0.65	4.56
Ethyl-benzene	**March**	0.37	0.52	0.45	0.46	0.04	0.45
	April	0.78	0.31	0.96	0.69	-	0.71
Xylene	**March**	0.97	2.54	2.2	2.13	0.09	2.25
	April	3.69	1.38	4.47	3.06	0.3	3.43

Higher BTEX levels corresponded with higher NO_2 and SO_2 levels measured at sites situated in industrialised areas, which was also observed in the study of Lourens et al. (2011). The BTEX mixing ratios measured for the Jhb-Pta megacity can be compared to BTEX levels measured by Lourens et al. (2011) at Witbank, which is a city associated with a large number of industrial activities. Benzene mixing ratios at Witbank measured for March and April 2008 were 1.23 ppb and 1.80 ppb, respectively. Toluene mixing ratios for the two months were 1.36 ppb and 1.67

ppb, ethylbenzene concentrations were 0.21 ppb and 0.33 ppb, while level of 0.23 ppb and 0.18 ppb were measured for xylene. BTEX concentrations were higher in the Jhb-Pta megacity compared to the results obtained in Witbank. This can probably be attributed to more emission sources in the much larger Jhb-Pta megacity.

The BTEX levels in the Jhb-Pta megacity can be mainly be attributed to the fuel combustion from traffic emissions. South Africa is still enforcing Euro 2 regulations and need to improve to Euro 5 in 2020 (GN, 2003). This will decrease the benzene content in petrol resulting in a reduction in benzene emissions from traffic sources. Other sources of BTEX in the Jhb-Pta megacity are household combustion and industrial activities within the Jhb-Pta megacity, while biomass burning and industrial activities in the Mpumalanga Highveld and Vaal Triangle industrial area can also contribute to VOC levels in the megacity.

In Table 2.8 BTEX mixing ratios measured in this investigation are compared to BTEX levels measured in other cities in the world (Derwent *et al.,* 2000; Monod *et al.*, 2001; Na & Kim, 2001; Ozkaynak & Spengler, 2001; Yamamoto *et al.,* 2000). Toluene levels are predominantly higher in all the cities listed. Higher toluene concentrations have also been observed in other studies conducted in urban areas (e.g. Brocco et al., 1997; Kourtidis et al., 2002). This can be ascribed to the higher toluene content in fuels used in vehicles, as well as industrial activities utilising toluene as a solvent (Nelson & Quigley, 1983). It is also seems that benzene en xylene concentrations measured in most of the cities are comparable. BTEX levels measured in this study compares well with BTEX concentrations in London. The highest BTEX concentrations were measured in Sao Paulo, Berlin and Santiago, while the lowest BTEX levels were obtained in Yokohama and Edinburgh indicated from results in Table 2.7. BTEX concentrations in the Jhb-Pta megacity were well below levels measured in cities with the highest BTEX levels. It is, however, difficult to directly compare BTEX concentrations of different cities, since each city has unique conditions e.g. meteorological conditions and different sources. Data obtained from Derwent et al. (2000) was measured in 1999 and data obtained from Monod et al. (2001) was measured in 2000.

Table 2.8: Comparison of BTEX mixing ratios (ppb) measured in the Jhb-Pta megacity with other cities in the world.

City	Benzene	Toluene	Ethylbenzene	Xylene	Reference
Jhb-Pta megacity	2.03	3.21	0.45	2.07	This study
Liverpool	0.89	2.08	0.87	2.68	Derwent et al. (2000)
Yokohama	0.38-1.13	1.23 - 8.95	0.12-0.88	0.23-0.46	Yamamoto et al. (2000)
London	1.87	3.62	0.73	2.14	Derwent et al. (2000)
Edinburgh	0.7	1.28	0.31	0.82	Derwent et al. (2000)
Bristol	1.22	2.66	0.5	1.47	Derwent et al. (2000)
London	2.7	7.2	1.4	3.7	Monod et al. (2001)
São Paulo	5.2	7.4	1.4	4.2	Colón et al. (2001)
Berlin	6.9	13.8	2.8	7.5	Monod et al. (2001)
Seoul	1	6.4	0.7	2.3	Na & Kim (2001)
Santiago	6.11	22.17	—	10.81	Ozkaynak & Spengler (2001)

The diurnal variation of BTEX for the Jhb-Pta megacity is presented in Figures 2.20 to 2.23. The 8-hour average BTEX concentrations were calculated from active sampling measurements conducted between 06:00 - 14:00, 14:00 - 22:00 and 22:00 - 06:00 for two consecutive days. These measurements were conducted at the sites M3, M5, M7 and M8. The averaged BTEX mixing ratio for the entire sampling period for each site is given in Table 2.9.

Table 2.9: Averaged BTEX mixing ratios (ppb) for the sampling period measured at the sites.

	Possible sources	M3 Vehicle emissions	M5 Back-ground	M7 Domestic burning / vehicle emissions	M8 Industrial/ Vehicle emissions
Benzene		1.7	1.1	1.8	1.7
Toluene		2.8	1.5	2.4	3.4
Ethyl-benzene		0.4	0.6	0.4	0.7
Xylene		1.3	0.9	1.4	2.6

From Table 2.9 and Figures 2.19 to 2.22 showed toluene was again higher than benzene in most of these measurements. The BTEX concentrations of each species measured at all these sites were in the same order. The sites within in the Jhb-Pta megacity, however, had a few instances where higher BTEX concentrations were measured compared to the average BTEX levels determined at each site during the measurement campaign.

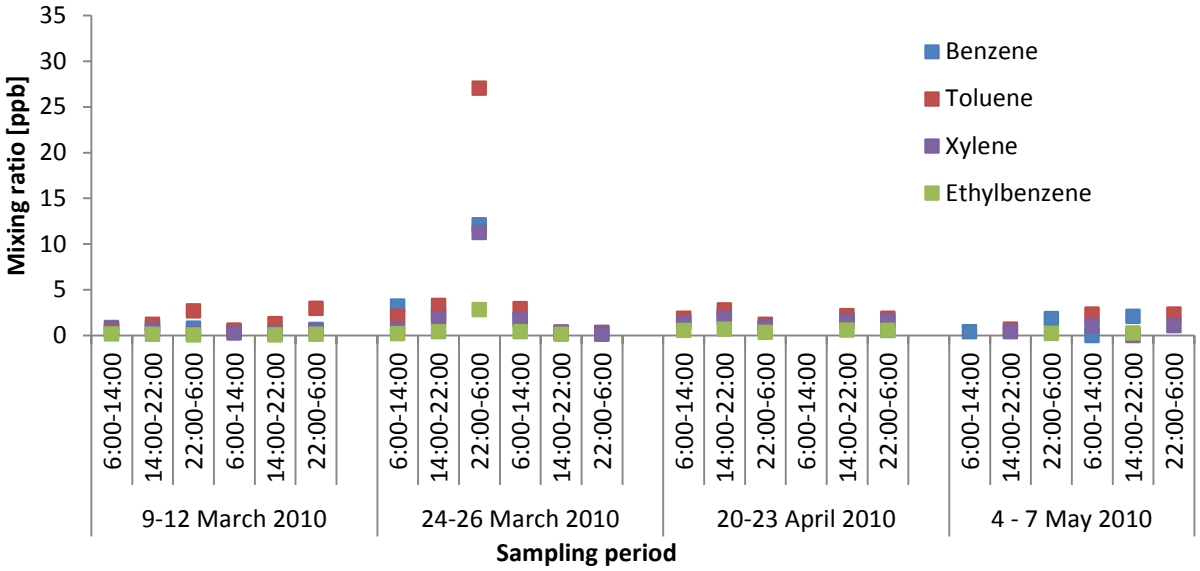

Figure 2.19: BTEX mixing ratios for the total sampling period at station M3.

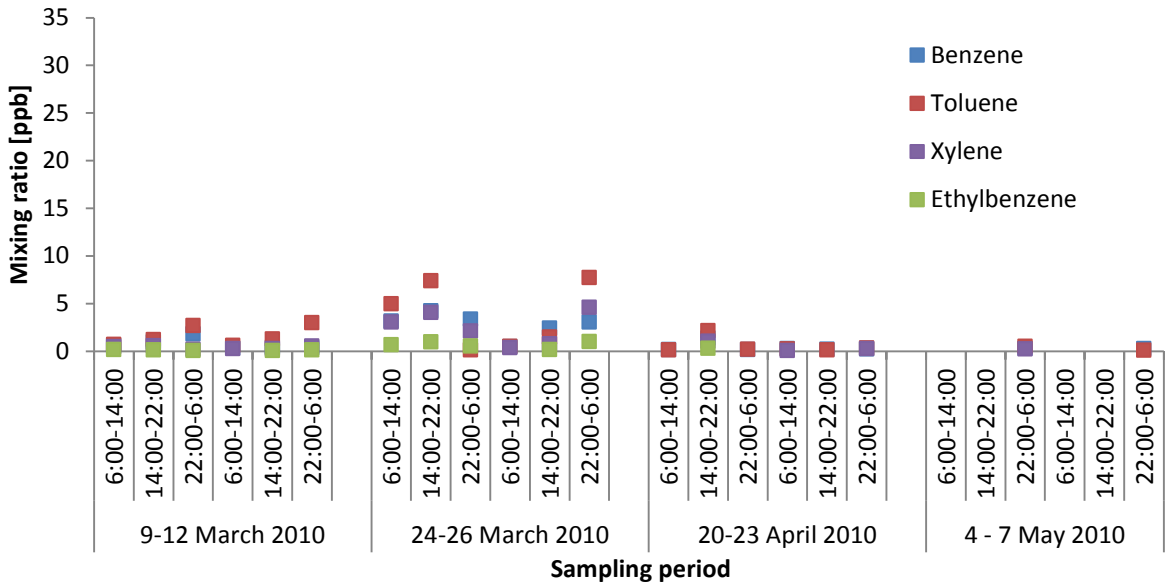

Figure 2.20: BTEX mixing ratios for the total sampling period at station M5.

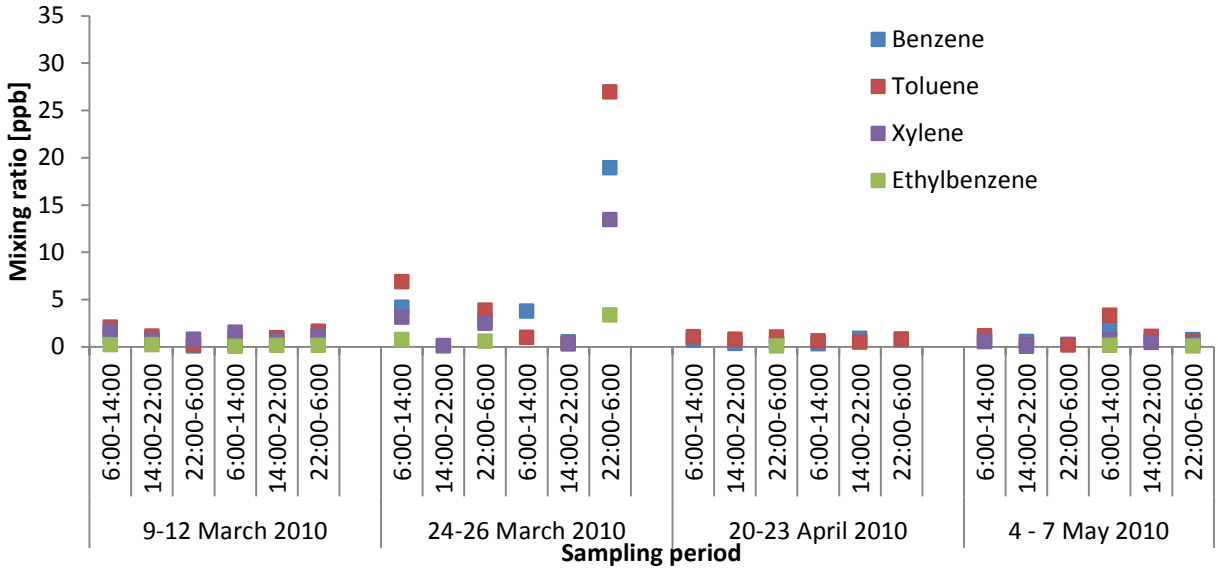

Figure 2.21: BTEX mixing ratios for the total sampling period at station M7.

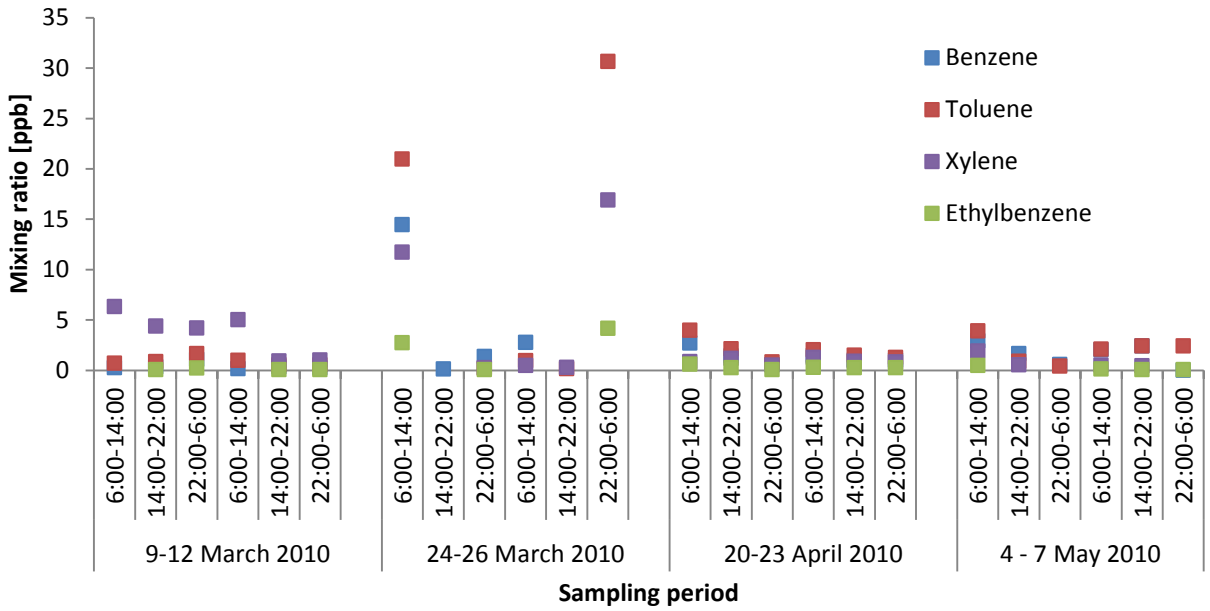

Figure 2.22: BTEX mixing ratios for the total sampling period at station M8.

Figure 2.23 to Figure 2.26 presents the diurnal variation of BTEX at the different sites. All the sites showed similar trends with higher BTEX mixing ratios during night-time and lower mixing ratios are observed during day-time. Previous studies have also shown higher values of BTEX at nighttimes (Tiwari *et al.*, 2010), which was also attributed to the calm conditions prevalent during night-times and no photochemistry taking place in the atmosphere. $HO^{\bullet}$ radicals that are formed through photochemical reactions are a major sink of aromatic VOCs (Seinfeld & Pandis, 1998). During day-time VOCs are removed by photochemical reactions with $OH^{\bullet}$ and the formation of $RO_2^{\bullet}$ radicals that produce NO_2 and subsequently O_3.

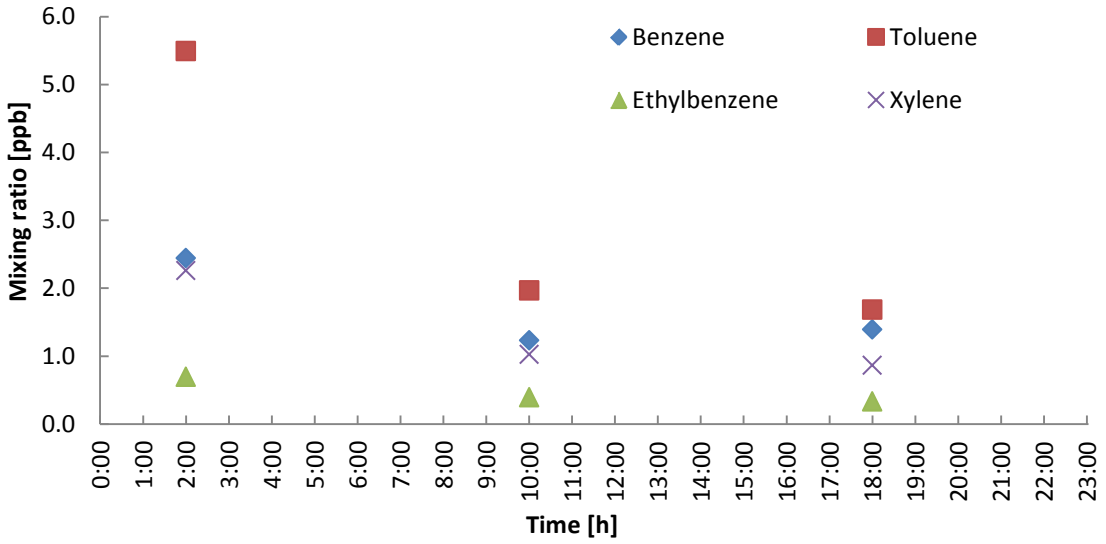

Figure 2.23: Diurnal average BTEX mixing ratios for the total sampling period at station M3

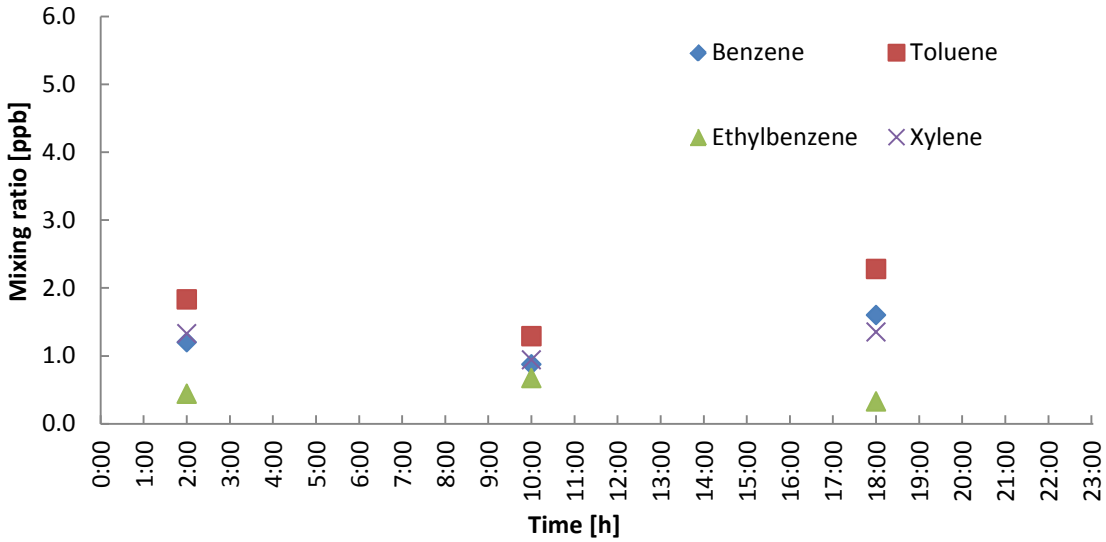

Figure 2.24: Diurnal average BTEX mixing ratios for the total sampling period at station M5.

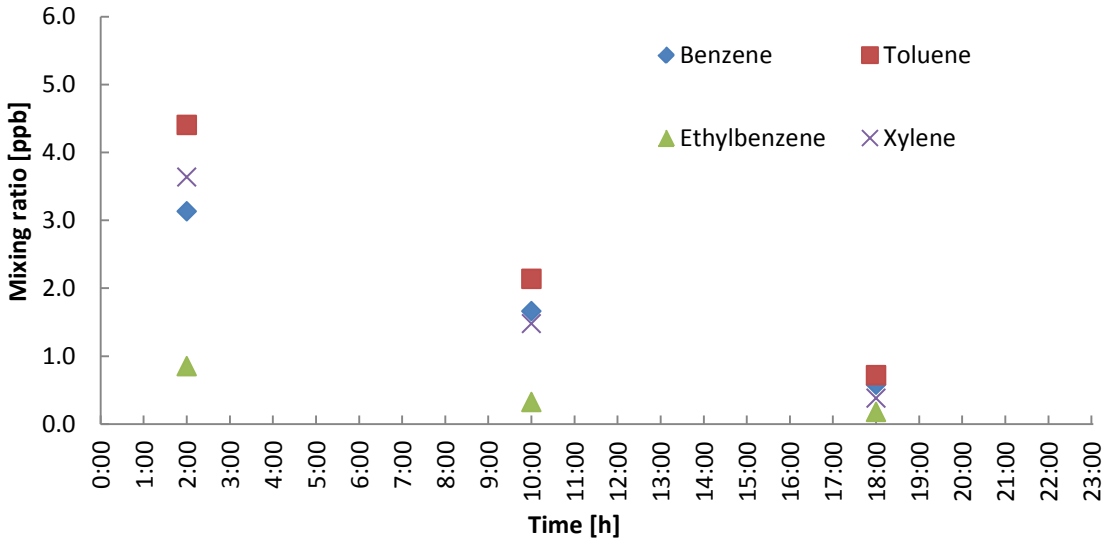

Figure 2.25: Diurnal average BTEX mixing ratios for the total sampling period at station M7.

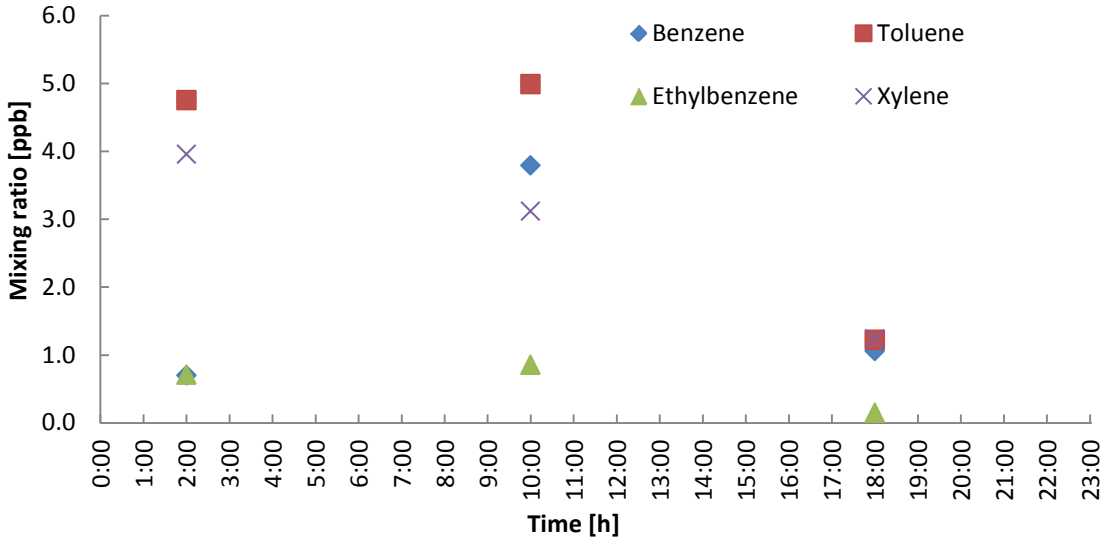

Figure 2.26: Diurnal average BTEX mixing ratios for the total sampling period at station M8.

Emission sources of BTEX species can be indicated by calculating their interspecific ratios. Due to the difference in reaction rates of BTEX species with $HO^{\bullet}$, these ratios provide information on the age of the air mass, which could be indicative of the source and distances from the source of these species in the atmosphere. Using the ratios removes dialy variations, meteorological factors and different emissions strents between species (Roberts *et al.*, 1984). Benzene and toluene have lifetime of 9.4 and 1.9 days, respectively (Atkinson, 1990), while the lifetime of xylenes and ethylbenzene are in the order of hours i.e. 7.8 hours and 11 hours (Tiwari *et al.*,

2010; Khoder, 2007). The ratio of a more reactive BTEX to a less reactive BTEX the lifetime against $HO^{\bullet}$ was used. Ratios of toluene/benzene (T/B), xylene/ benzene (X/B) and xylene/ ethylbenzene (X/EB) are listed in Table 2.10.

Table 2.10: Toluene/benzene (T/B), xylene/benzene (X/B) and xylene/ ethylbenzene (X/EB) mixing ratio (ppb) ratio at different sampling locations.

	T/B	X/B	X/EB
M3	1.47	1.47	3.17
M7	2.29	1.89	4.44
M8	1.37	1.12	4.51
M5	1.01	0.83	3.20

A higher ratio indicates relatively little photochemical processing of the air mass and major impact from primary emissions, whereas a lower ratio is reflective of more aged air mass and thus that the VOCs most probably were emitted from more distant sources (Guo *et al.,* 2007). The ratio of T/B can act as in indicator for traffic emissions when the ratio is within the range of 1.5-4.3, when the ratio > 4.3, solvent source is higher as reported by Hoque et al. (2008). The X/B and X/EB can be used as indication of aged air masses. A lower X/B and X/EB ratio implies and aged air parcel (Guo *et al.*, 2007).

Benzene, toluene and xylenes are emitted predominantly by motor vehicle-related sources. Previous studies have shown that high T/B ratios approaching 1 are most likely from traffic emissions in the city, with the value increases with the closeness of the pollution source (Gelenscer *et al.*, 1997).. Highest T/B ratio was observed at site M7 (2.29) followed by site M3 (1.47) and site M8 (1.37). The lowest T/B ratio was measured at M5. Lower X/B and X/EB ratios were also measured at this site which indicates aged air masses. This is in agreement since the site is located as background away from direct emissions sources. High T/B ratios measured at M7 indicate vehicle emissions might be a pollution source. High ratios of both X/B and X/EB at M7 indicate relative closeness to the pollution source. These ratios indicate the site might be influenced by close urban-roadside emissions sources. The T/B ratios at M3 and M8 are higher than M5 but lower than M7 which indicates traffic sources might not be the main source. Lower of X/B and X/EB ratios at these sites also indicate an aged air masses (Hsieh & Tsai, 2003).

These differences in ratios at these site in the megacity indicate the complexicity of mixed traffic, industrial and household combustion sources, as well as the impact of the two adjoining declared air pollution hotspots (Section 2.2.5.1. and 2.2.5.2.), that are unique to the Jhb-Pta megacity.

2.4.4. SO_2

The monthly average SO_2 mixing ratios measured with passive samplers for March and April 2010 are presented in Table 2.11. SO_2 levels ranged between 1.6 ppb and 6.6 ppb at the different sites. Most of the sites within the Jhb-Pta megacity with residential, vehicular emissions and industrial sources exhibited higher levels of SO_2 for the month of March as seen in Table 2.6, while lower mixing ratios were measured during April. The highest mixing ratio was measured at M6. This site measured predominately industrial emissions and is also in close proximity to a power station. The measurement site is upwind from the power station, which could have had an influence on SO_2 measured. Although the background site M5 are relatively high in comparison with the other stations, the mixing ratios at this site are in agreement with a previous study conducted at the same site (Lourens *et al.*, 2011). The high SO_2 mixing ratios at the background site can be attributed to a combination of emissions from a local major source in the surrounding area and the longer lifetime of SO_2 in the atmosphere. Previous studies in South Africa indicated that SO_2 mixing ratios over the Highveld are between 3- 10 ppb with > 10 ppb concentration measured close to sources (Zunckel *et al.*, 2000). SO_2 in the megacity is comparable to those sites in the Highveld that are influenced by industrial sources (Lourens *et al.*, 2011). No active SO_2 data were obtained from the monitoring stations. Therefore, no diurnal cycle for SO_2 was determined.

Table 2.11: Monthly SO_2 mixing ratios (ppb) at all the sites for March and April.

	M1	M2	M3	M4	M5	M6
Possible sources	**Residential and industrial**	**Residential**	**Vehicle emissions**	**Domestic fuel burning**	**Background**	**Industrial**
March	5.9	3.5	5.9	4.5	5.0	6.6
April	3.6	1.6	3.9	2.3	2.3	1.8

Since these SO_2 concentrations were only determined for two months, these results are only an indication of SO_2 in the Jhb-Pta area used to compare SO_2 levels to other cities in the world.

Table 2.12 compares SO_2 concentrations measured at other megacities around the world with levels measured in the Jhb-Pta megacity. Previous studies (e.g. Ranjeet & Molina, 2011; Gurjar *et al.*, 2008; Baldasano & Jiménez, 2002; APMA, 2002; De leeuw *et al.,* 2001; Molina & Molina, 2002) indicated the concentrations in different large or megacities world-wide is comparable to measurement in Jhb-Pta megacity. From the comparison of SO_2 concentrations measured in the Jhb-Pta megacity with other megacities in Table 2.11 it is noticeable that Jhb-Pta megacity were at the higher end of values reported for other megacities. SO_2 concentrations in the Jhb-Pta megacity are comparable to SO_2 levels in other large cities such as Chicago, London, Montreal and Paris. SO_2 concentrations in Moscow is much lower than in Jhb-Pta megacity with SO_2 levels for other cities listed in the table are much higher. These high SO_2 concentrations in the Jhb-Pta megacity can possibly be attributed to the high level of household combustion of high sulphur containing coals and the impact of the Mpumalanga Highveld and Vaal Triangle Air-shed priority areas, which are well known for relatively high SO_2 levels.

Table 2.12: SO_2 annual concentrations of megacities world-wide.

City	Concentration (ug/m^3) * ppb	Reference
Jhb-Pta megacity	3.9*	This study
Chicago	10.1-20	Ranjeet & Molina (2011)
Los Angeles	3.4	Gurjar et al. (2008)
Montreal	10.1-20	Ranjeet & Molina (2011)
New York	8.4	Gurjar et al. (2008)
Mexico city	17.9	Molina & Molina (2004); Ranjeet & Molina (2011)
Guadalajara	20.1-50	Ranjeet & Molina (2011)
Lima	20.1-50	Ranjeet & Molina (2011)
Sao Paulo	6.9	Gurjar et al. (2008)
Buenos Aires	7.6	Gurjar et al. (2008)
Santiago	10.1-20	Ranjeet & Molina (2011)
London	10.1-20	Ranjeet & Molina (2011)
Paris	10.1-20	Baldasano et al. (2002)
Madrid	20.1-50	Ranjeet & Molina (2011)
Rome	10.1-20	Baldasano et al. (2002)
Athens	10.1-20	Ranjeet & Molina (2011)
Bratislava	10.1-20	Baldasano et al. (2002)
Moscow	5.7	Gurjar et al. (2008)
Cairo	14.1	Khoder (2009)
Delhi	6.9	Gurjar et al. (2008)
Mumbai	7.3	Gurjar et al. (2008)
Bangkok	10.1-20	APMA, 2002;Ranjeet & Molina (2011)

City	Concentration (ug/m^3) * ppb	Reference
Kolkata	7.3	Gurjar et al. (2008)
Tianjin	>50	Ranjeet & Molina (2011)
Beijing	34.3	APMA, 2002;Gurjar et al. (2008)
Shenyang	>50	Baldasano et al. (2002)
Seoul	10.1-20	APMA, 2002; Baldasano et al. (2002)
Tokyo	7.3	Gurjar et al. (2008)

2.5. CONCLUSION

Results presented in this chapter clearly indicate that inorganic gases (i.e. NO_2, SO_2, O_3) and VOCs (i.e. BTEX) contribute largely to urban air pollution within the Jhb-Pta megacity and the related tropospheric chemical reactions. . The main objective for the measurements conducted in the Jhb-Pta megacity was to obtain data that is representative of air quality within this area to use in a modelling study. The measurements obtained gave a good reflection of the actual air quality within the Jhb-Pta megacity and the influences of the Mpumalanga Highveld and Vaal Triangle Air-shed Priority.

All the sites were situated at strategically chosen locations to measure the direct influences of urban air pollution e.g. traffic emissions, biomass burning and residential pollution. The highest level for NO_2 was measured at M1 (Residential and industrial site). A strong diurnal cycle for NO_2 was observed at most of the stations. The early morning peak observed between 6:00-9:00 coincided with the time commuters travel to work, whereas the evening peak 18:00-21:00 can be attributed to both traffic emissions and biomass fuel burning for space heating and cooking. NO_2 levels measured in the Jhb-Pta megacity are comparable to certain megacities around the world.

The highest O_3 concentrations were measured at the background site M5. Lower concentrations measured in the Jhb-Pta megacity indicate that O_3 is titrated in the megacity due to relative high pollution levels. All the results obtained from site M5 is in good agreement with a previous study conducted at the site over a period of one year.

Toluene was predominantly higher than other BTEX species measured. The lowest BTEX values were measured at the background site M5 However, the highest mixing ratios were measured at M7 and M8, both which are mostly influenced by urban-roadside emissions or urban-residential emissions. BTEX ratios were conducted to determine the pollution source. High T/B ratios measured at M7 indicate vehicle emissions might be a pollution source. High ratios of both X/B and X/EB at M7 indicate relative closeness to the pollution source. These ratios indicate the site might be influenced by close urban-roadside emissions sources. . The lowest T/B ratio was measured at M5. Lower X/B and X/EB ratios were also measured at this site which indicates aged air masses. M5 is the background site therefore a distance from primary sources. Although X/B ratios are low and implies aging of the air masses, high X/EB ratios were measured at site M3 and M8 which indicate there are other sources contributing, not only traffic or aging of air masses. These mixed results indicate the complexicity of mixed traffic, industrial and household combustion sources, as well as the impact of the two adjoining declared air pollution hotspots that are quite unique to the Jhb-Pta megacity.

References

ADKINSON, R. 2000. Atmospheric chemistry of VOCs and NOx. *Atmospheric Environment*, 34:2063-2101.

AGENCY, EEA (European Environment. 2009. EMEP/EEA air pollutant emission inventory guidebook. APMA. 2002. *Benchmarking Urban Air Quality Management and Practice in Major and Mega Cities o Asia*. Seoul.

AQMP. 2006. *Air Quality Management Plan Vaal Airshed Priority Area*.

ATKINSON, R. 2000. Atmospheric chemistry of VOCs and NOx. *Atmospheric Environment*, 24:2063-2101.

BALDASANO, J.M., VALERA, E. & JIMENEZ, P. 2002. Air quality data from large cities. *The Science of the Total Environment*

BAYA, M.P. & SISKOS, P.A. 1996. Evaluation of Anasorb CMS and Comparison With Tenax TA for the Sampling of Volatile Organic Compounds in Indoor and Outdoor Air by Breakthrough Measurements. *Analyst*, 5:303-307.

BEUKES, J.P., VAKKARI, V., VAN ZYL, P.G., VENTER, A.D., JOSIPOVIC, M., JAARS, K., TIITA, P., LAAKSO, H., KULMALA, D., WORSNOP, D., PIENAAR, J.J., JARVINEN, E., CHELLAPERMAL, R., IGNATIUS, K., MAALICK, Z., CESNULYTE, V., RIPAMONTI, G., LABAN, T.L., SKRABALOVA, L., DU TOIT, M., VIRKKULA, A. & LAAKSO, L. 2013. Source region plume characterisation of the interior of South Africa, as measured at Welgegund. In preparation for submission to Atmospheric Chemistry and Physics.

BLASTING, T.J. 2012. Recent Greenhouse Gas Concentrations. http://cdiac.oml.gov/pns/current_ghg.html Date of access: 15 May 2012.

BLIGNAUT, J.N., CHITTIGA-MABUGU, M.R. & MABUGU, R.M. 2005. Constructing a greenhouse gas emissino inventory using energy balances: the case of South Africa for 998. *Journal of Energy in Southern Africa*, 16(3)

BOUBEL, R.W., FOX, D.L., TURNER, D.B. & STERN, C. 1994. Air Quality. *In*: *Fundaments of Air Pollution*, 3rd ed. Academic Press. 46 p.

BROCCO, D., FRATARCANGELI, R., LEPORE, L., PETRICCA, M. & VENTRONE, I. 1997. Determination of aromatic hydrocarbons in urban air of Rome. *Atmospheric Environment*, 31(4):557-566.

BROWN, R.H. 1999. Monitoring the ambient environment with diffusive samplers: theory and practical considerations. *Journal of Environmental Monitoring*, 1:1-9.

BURGER, J.W. 2006. *Identification and comparison of the volatile organic compound concentrations in ambient air in the Cape Town Metropolis and the Vaal Triangle.* Potchefstroom.

BURGER, W.L. & THOMAS, R.G. 2002. *Ambient Air Sampling Campaign: Selected vehicle activity sites*. Wieder Park.

BUTLER, T.M., LAWRENCE, M.G., TARABORRELLI, D. & LELIEVELD, J. 2011. Tagged Ozone Production Potential (TOPP) of Volatile Organic Compounds. *Atmospheric Environment*, 45:4082-4090.

CAO, Z-L. & HEWITT, N. 1994. Build-up of artifacts on adsorbents during storage and its effect on passive sampling and gas chromatography-flame ionization detection of low concentrations of volatile organic compounds in air. *Journal of Chromatography A*, 688(1-2): 368-374.

CARDELINO, C.A. & CHAMEIDES, W.L. 1990. Natural hydrocarbons, urbanization, and urban ozone. *Journal of Geophysical Research Atmosphere*, 95:13971-13979.

CARSLAW, D.C. & BEEVERS, S.D. 2005. Estimations of road vechile primary NO2 exhaust emission fraction using monitoring data in London. *Atmopsheric Environment*, 29:167-177.

CIESIN. 2010. Gridded Population of the World Future Estimates (GPWFE). http://sedac.ciesin.columbia.edu/gpw

CLEMENT, K. & FOSTER, S. 2000. *An investigation into mining as an energy and water using sector and its environmental impacts*.

COSIJN, C. & TYSON, P.D. 1996. Stable discontinuities in the atmopshere over South Africa. *South African Journal of Science*, 92:281-286.

CRUTZEN, P.J. & ZIMMERMANN, P.H. 1991. The changing photochemistry of the troposphere. *Tellus*, 43(A/B):136-151.

DE LEEUW, F.A.A.M., MOUSSIOPOULOS, N., SAHM, P. & BARTONAVA, A. 2001. Urban air quality in larger conurbation in the European Union. *Environmental Modelling and Software*, 16(4):399-414.

DEA. 2006. Draft-final Initial State of the Air Report. Date of access: 12 March 2012. <www.saaqis.co.za>

DEMERJIAN, K.L. 2000. A review of national monitoring networks in North America. *Atmospheric Environment*, 34:1861-1884.

DERWENT, R.G., DAVIES, T.J., DELANEY, M., DOLLARD, G.J., FIELD, R.A., DUMITREAN, P., NASON, P.D., JONES, B.M.R. & PEPLER, S.A. 2000. Analysis and interpretation of the continuous hourly monitoring data for 26 C2-C6 hydrocarbons at 12 United Kingdom sites during 1996. *Atmospheric Environment*, 41:297-312.

DERWENT, R.G., DAVIES, T.J., DELANEY, M., DOLLARD, G.J., FIELD, R.A., DUMITREAN, P., NASON, P.D., JONES, B.M.R. & PEPLER, S.A. 2002. Analysis and interpretation of the continuous hourly monitoring data for 26 C2-C6 hydrocarbons at 12 United Kindgom sites during 1996.. *Atmospheric Environment*, 34:297-312.

DERWENT, R., JENKIN, M. & SAUNDERS, S. 1996. Photochemical ozone creation potentials for a large number of reactive hydrocarbons under European conditions. *Atmospheric Environment*, 30:181-199.

DHAMMAPALA, R.S. 1996. Use of Diffusive Samplers for the sampling of atmospheric pollutants. Potchefstroom: North-West University: Dissertation-Msc.

DIAB, R.D., RAGHUNANDAN, A., THOMPSON, A.M. & THOURET, V. 2003. Classification of tropospheric ozone profile over Johannesburg based on mozaic aircraft data. *Atmospheric Chemistry and Physics*, 3:713-723.

DUAN, J., TAN, J., YANG, L., WU, S. & HAO, J. 2008. Concentration, sources and ozone formation potential of volatile organic compounds (VOCs) during ozone episode in Beijing. *Atmospheric Research*, 88:25-25.

DUENAS, C., FERNANDEZ, M.C., CARRETERO, S. & LIGER, E. 2002. Assessment of Ozone Variations and Meteorological Effects in an Urban Area in the Mediterranean-Coast. *Science of Total Environment*, 299:97-113.

DUNCAN, B. & CHAMEIDES, W. 1998. Effects of urban emission control strategies on the export of oone and ozone precursors from the urban atmosphere to the troposphere. *Journal of Geophysical Research*, 103:28159-28179.

DUNLEA, E.J., S.C., Hherndon, NELSON, D.D. & VOLKAMER, R.M. et al. 2007. Evalution of nitorgen dioxide chemiluminescence monitors in a polluted urban environment. *Atmospheric Chemistry and Physics Discussion*, 7:569-604.

ENYA, T., SUZUKI, H., WATANABE, T., HIRAYAMA, T. & HISAMATSU, Y. 1997. 3-Nitrobenzanthone, a powerful bacterial mutagen and suspected human carcinogen foud in diesel exhaust and airborne particles. *Environmental Science and Technology*, 21:2772-2776.

EPA, (UNITED STATES ENVIRONMENTAL PROTECTION AGENCY). 1997. Part 51: requirements for preparation, adoption and submittal of implementation plans.

FELLENBERG, G. 1997. The chemistry of pollution. Chichester: Wiley.

FONTJIN, A., SABADELL, A.J. & RONCO, R.J. 1970. Homogeneous chemiluminescence measurements of nitric oxide with ozone. *Analytical Chemistry*, 42:575-579.

FREEMAN, P.N.W., NAUDE, C.M., PRETORIUS, J., COOVADIA, T. & MATJILA, S.M. 2000. *The transport Sector-Energy use and Environmental Impacts*.

FREIMAN, M.T. & PIKETH, S.J. 2003. Air transport into and out of the industrial Highveld region of South Africa. *Journal of Applied Meteorology*, 42:994-1002.

GAFFEN, M., NAUDE, C., LOMBAARD, P., MASSDORP, G., TAYLOR, A. & PRETORUIS, J. 2000. *A Quantitive analysis of full cost associated with motor vehicle use in South Africa*.

GARSTANG, M., TYSON, P.D., SWAP, R., EDWARDS, M., KALLBERG, P. & LINDESAY, J.A. 1996. Horizontal and vertical transport of air over southern Africa. *Journal of Geophysical Research*, 101(D19):23721-23736.

GELENSCER, A., SISZLER, K. & HLAVAY, J. 1997. Toluene-benzene concentration ratio as a tool for characterizing the distance from vehicular emission sources. *Environmental Science and Technology*, 7:235-240.

GJMC/IVL/CSIR. 1999. *Mapping of Air Pollution levels in Johannesburg*. Johannesburg.

GN. 2003. *Final draft joint implementation strategy for the control of exhaust emissions from road-going vehicles in the Republic South Africa*. Notice 3324 of 2003: Staatskoerant.

GODISH, T. 2004. Air Quality. *In*: *Chapter 2: Atmospheric Pollution and Pollutants*, 4th ed. Washington, D.C: Lewis Publishers. 57-77 p.

GONZALEZ ABAD, G., ALLEN, N.D.C., BERNATH, P.F., BOONE, C.D., MCLEOD, S.D., MANNEY, G.L., TOON, G.C., CAROUGE, C., WANG, Y., WU, S., BARKLEY, M.P., PALMER, P.I., XIAO, Y. & FU, T.M. 2011. Ethane, ethyne and carbon monoxide concentrations in the upper troposphere and lower stratosphere from ACE and GEOS-ChemPa comparison study. *Atmopsheric Chemistry an Physics*, 11:9927-9941.

GORCHAKOV, G., SEMOUTNIKOVA, E., KARPOV, A. & LEZINA, E. Air pollution in Moscow Megacity. *Advanced Topics in Environmental Health and Air Pollution Case studies*

GOYNS, P.H. 2008. *Modelling real-world driving, fuel consumption and emissions of passenger vehicles: a case study in Johannesburg*. Johannesburg.

GUENIER, J.P. & MULLER, J. 1984. Sampling of gaseous pollutants on actived charcoal with 900 mg tubes. *The Annals of Occupational Hygiene*, 28(1):61-75.

GUO, H., SO, K.L., SIMPSON, I.J., BARLETTA, B., MEINARDI, S. & BLAKE, D.R. 2007. C1-C8 volatile organic compounds in the atmosphere of Hong Kong: Overview of atmospheric processing and source apportionment. *Atmospheric Environment*, 41:1456-1472.

HAN, X. & NAEHER, L.P. 2005. A review of traffic-related air pollution exposure assessment studies in the developing world. *Environment International*, 32:106-120.

HARPER, M. 1992. Methods of characterizing sorbents for air sampling purposes. (*In* Findamentals of Adsorption: Proc. IVth International Conference on Fundamentals of Adsorption. Kyoto: Kodansha Press, Japan. p. 267.)

HARPER, M. 2000. Sorbent trapping of volatile organic compounds from air. *Journal of Chromotography*, 885:129-151.

HO, K.F., LEE, S.C., GUO, H. & TSAI, W.Y. 2004. Seasonal and diurnal variations of volatile organic compounds (VOCs) in the atmosphere of Hong Kong. *Science Total Environment*, 322:155-166.
HOQUE, R.R., KHILLARE, P.S., AGARWAL, T., SHRIDHAR, V. & BALACHANDRAN, S. 2008. Spatial and temporal variation of BTEX in the urban atmosphere of Delhi, India. *Science of the Total Environment*, 1(392):30-40.

HSIEH, C.C. & TSAI, J.H. 2003. VOC concentration characteristics in Southern Taiwan. *Chemosphere*, 50:545-556.

HURLEY, P. 2002. *The Air Pollution Model (TAPM) Version 2. Part 1: Technical Description*.
JORQUERA, H. 2002. Air quality at Santiago, Chile: a box modeling apporach I. Carbon monoxide, nitrogen oxides and sulfur dioxide.. *Atmospheric Environment*, 36:315-330.

JOSIPOVIC, M., ANNEGRARN, H.J., KNEEN, M.A., PIENAAR, J.J & PIKETH, S.J. 2010. Concentrations, distributions and critical level exceedance assessment of SO2, NO2 and O3 in South Africa. *Environmental Monitoring Assessment*, 171:181-196.

KAMPA, M. & CASTANAS, E. 2008. Human health effects of air pollution. *Environmental Pollution*, 151(2):362-7. 23 Jul.

KELLOGG, W.W., CADLE, R.D., ALLEN, E.R., LAZRUS, A.L. & MARTELL, E.A. 1972. The Sulfur Cycle. *Science*, 175(4022):587-596.

KHODER, M.I. 2007. Ambient levels of volatile organic compounds in the atmosphere of Greater Cairo. *Atmospheric Environment*, 41:554-566.

KLEINMAN, L.I. 2005. The dependence of tropospheric ozone production rate on ozone precursors. *Atmospheric Enivornment*, 39:575-586.

KLEINMAN, L., DAUM, P., LEE, J., LEE, Y., NUNNERMACKER, L., SPRINGSTON, S., NEWMAN, L., WEINSTEINLLOYD, J. & SILLMAN, S. 1997. Dependence of ozone production on NO and hydrocarbons in the troposphere. *Geophysical Research Letters*, 39:575-586.

KOURTIDIS, K.A., ZIOMAS, I., ZEREFOS, C., KOSMIDIS, E., SYMEONIDIS, P. & CHRISTOPHILOPOULOS, E. 2002. Benzene, toluene, ozone, NO2 and SO2 measurements in an urban street canyon in Thessaloniki. *Atmospheric Environment*, 36:5355-5364.

KOURTIDIS, K., ZIOMAS, I., ZEREFOS, C., KOSMIDIS, E., SYMEONIDIS, P., CHRISTOPHILOPOULOS, E., KARATHANASSIS, S. & MPLOUTSOS, A. 2002. Benzene, toluene, O3, NO2 and SO2 measurements in an urban street canyon in Thessaloniki, Greece. *Atmospheric Environment*, 36:5355-5364.

KRISHNAMURTI, T.N., FUELBERG, H.E., SINHA, C., OOSTERHOF, D., BENSMAN, L. & KUMAI, V.B. 1993. The meteorological environment of the tropospheric ozone maximum over the tropical South Atlantic Ocean. *Journal Geophysical Research*, 98:10621-10641.

LAAKSO, L. & PIENAAR, J.J. 2012. Air pollution and the interactions between atmosphere, biosphere and the anthroposphere in. *In*: PAUW, Dr. J., VAN JAARSVELD, A., WESSELS, K. & ZIETSMAN, L., eds. *Earth Observation and Environmental Change in South Africa*, in press, 2011. 8 p.

LAAKSO, L., VAKKARI, V., LAAKSO, H., VIRKKULA, A., KULMALA, M., BEUKES, J.P., VAN ZYL, P.G., PIENAAR, J.J., CHILOANE, K., GILARDONI, S., VIGNATI, E., WIEDENSOHLER, A., TUCH, T., BIRMILI, W., PIKETH, S., COLETTE, K., FOURIE, G.D., KOMPPLA, M., LIHAVAINEN, H., DE LEEUW, G. & KERMINEN, V.M. 2010. South African EUCAARI-measurements: a site with high atmospheric variability. *Atmospheric Chemistry and Physics Discussions*, 10(12):30691-30729.

LAL, S., NAJA, M. & SUBBARAYA, B.H. 2000. Seasonal variations in surface ozone and its precursors over an urban site in India. *Atmospheric Environment*, 24:2713-2724.

LIU, C., XU, Z., DU, Y. & GUO, H. 2000. Analyses of volatile organic compounds concentrations and variation trends in the air of Changchun, the norteast of China. *Atmospheric Environment*, 34:4459-4466.

LOGAN, J.A., PRATHER, M.J., WOFSY, S.C. & MCELROY, M.B. 1981. Tropospheric chemistry: A global perspective. *Journal of Geophysical Research*, 86:7210-7254.

LOURENS, A.S.M. 2008. *Spatial and Temoporal Assessment of pollutants in the Highveld Priority Area, South Africa*. Potchefstroom.

LOURENS, A.S.M., BEUKES, J.P., VAN ZYL, P.G., FOURIE, G.D., BURGER, J.W., PIENAAR, J.J., READ, C.E. & JORDAAN, J.H. 2011. Spatial and temporal assessment of gaseous pollutants in the Highveld of South Africa. *South African Journal of Science*, 107(1/2):1-8.

LOURENS, A.S.M., BUTLER, T.M., BEUKES, J.P., VAN ZYL, P.G., BEIRLE, S., WAGNER, T., HEUE, K.-P., PIENAAR, J.J., FOURIE, G.D. & LAWRENCE, M.G. 2012. Re-evaluating the NO2 hotspot over the South African Highveld. *South African Journal of Science*:Submitted.

LUKE, W.T. 1997. Evaluation of a commercial pulsed fluorescence detector for the measurement of low-level SO2 concentrations during the gas-phase sulfur intercomparison Experiment. *Journal of geophysical research*, 102(D13):16,355-16,265.

MA, R., KREWSKI, D. & BURNETT, R.T. 2003. Random effects Cox models: a Poisson modelling approac. *Biometrika*, 90:157-169.

MARKOVIC, D.M. & MARKOVIC, D.A. 2005. The relationship between some meteorological parameters and the tropospheric concentrations of ozone in the urban area of Belgrade. *Journal of Serbian Chemical Society*, 70(12):1487-1495.

MARTINS, J.J., DHAMMAPALA, R.S., LACHMANN, G., GALY-LACAUZ, C. & PIENAAR, J.J. 2007. Long-term measuremnets of sulphur dioxide, nitrogen dioxide, ammonia, nitric acid and ozone in southern Africa using passive samplers. *South African Journal of Science*, 103:336-342.

MATHEE, A. & VON SCHIRNDING, Y. 2003. Air Quality and Health in the Greater Johannesburg. *In*: MCGRANAHAN, G. & MURRY, F., eds. *Air Pollution and Health in Rapid Developing Countries*, 1st ed. UK: Eartscan Publications Ltd. 206-216 p.

MAZZEO, N.A., VENEGAS, L.E. & CHOREN, H. 2005. Analaysis of NO, NO2, O3 and NOx concentrations measured at a green area of Buenos Aires City during wintertime. *Atmospheric Environment*, 39:3055-3068.

MCCLENNY, WA., OLIVER, K.D., JACUMIN, H.H. Jr. & DAUGTREY, E.H. Jr. 2002. Ambient level volatile organic compound (VOC) monitoring using solid adsorbents - recent US EPA studies. *Journal of Environmental Monitoring*, 4(5):695-705.

MCRAE, G.J. & SEINFELD, J.H. 1983. Development of a second-generation mathematical model for urban air pollution - II Evaluation of model perfomrance. *Atmopsheric Environment*, 17:501-522.

MEASUREMENT, National Research Council (U.S.). Committee on Tropospheric Ozone Formation and. 1991. Atmopsheric Chemistry of Ozone and its precursors. *In*: *Rethinking the ozone problem in urban and regional air pollution*, Washington D.C.: National Academic Press. 109-210 p.

MOLINA, L.T. & MOLINA, M.J. 2002. Air Quality in the Mexico Megacity: An Integrated Assessment. Kluwer: Academic Publishers.

MONOD, A., SIVE, C.S., AVINO, P., CHEN, T., BLAKE, D.R. & ROWLAND, S. 2001. Monoaromatic compounds in ambient air of various sites: a focus on correlations between the xylenes and ethylbenzene. *Atmospheric Environment*, 35:135-149.

MOSCHONAS, M., GLAVAS, S. & KOUIMTZIS, T. 2001. C3 to C9 hydrocarbon measurements in the two largest cities of Greece, Athens and Thessaloniki. Calculations of hydrocarbon emissions by species.Derivation of hydroxyl radical concentrations. *The Science of the Total Environment*, 271:117-133.

NA, K. & KIM, Y.P. 2001. Seasonal characteristics of ambient volatile organic compounds in Seoul, Korea. *Atmospheric Environment*, 25:2603-2614.

NELSON, P.F. & QUIGLEY, S.M. 1983. The m, p-xylenes: ethylbenzene ratio, a technique for estimating hydrocarbon age in ambient atmospheres. *Atmospheric Environment*, 17:659-662.

NELSON, P.F. & QUIGLEY, S.M. 1984. The hydrocarbon composition of exhaust emitted from gasoline fueled vehicles. *Atmospheric Environment*, 18:79-87.

NEMA. 2004. *National Environment Management: Air Quality Act*.

NOTICE, General. 12 December 2003. *Final draft joint implementation strategy for the control of exhaust emissions from road-going vehicles in, the Republic South Africa*. Notice 3324 of 2003: Staatskoerant.
OZCAN, H.K. 2012. Long term variations of the Atmospheric Air Pollutants in Istanbul City. *International Journal of Environmental Research*, 9:781-790.

PANKOW, J.F., LUO, W., BENDER, D.A., ISABELLE, L.M., HOLLINGSWORTH, J.S., CHEN, C., ASHER, W.E. & ZOGORSKI, J.S. 2003. Concentrations and co-occurrence correlations of 88 volatile organic compounds (VOCs) in the ambient air of 13 semi-rural to urban locations in the United States. , 37:5023-5046.

PARRA, M.A., GONZALEZ, L., ELUSTONDO, D., GARRIGO, J., BERMEJO, R. & SANTAMARIA, J.M. 2006. Spatial and temporal trends of volatile organic compounds (VOC) in a rural area of northen Spain. *Science Total Environment*, 370(1):157-67.

PARRISH, D.D. & FEHSENDELD, F.C. 2000. Methods for gas-phase measurements of ozone, ozone precursors and aerosol precursors. *Atmopsheric Environment*, 34:1921-1957.

PIENAAR, J.J & HELAS, G. 1996. The kinetivs of chemical processes affecting acidity in the atmosphere. *South African Journal of Science*, 92:128-131.

PIKETH, S.J. & WALTON, N. 2004. Vol.4 vols. Characteristics of atmospheric transport of air pollution for Africa. *In*: *The Handbook of Environmental Chemistry*, 173-195 p.

POTTER, A. 2008. *Passive sampling: uptake rates for ethylbenzene*. Email to: Lourens, ASM (13097628@nwu.ac.za)

PRESTON-WHYTE, R.A & DIAB, R.D. 1977. Towards an inversion climatology of southern Africa: Part II, non-surface inversions in the lower atmosphere. *South African Geopgraphical Journal*, 59(1):45-59.
RANJEET, S.S. & MOLINA, M., *eds*. 2011. World atlas of atmospheric air pollution. Anthem: Anthem Press.

RIDLEY, B.A. & HOWLETT, L.C. 1974. An instruments for nitric oxide measurements in the stratosphere. *Review Scientific Instruments*, 45:742-746.

ROBERTS, J.M., FEHSENFELD, F.C., LIU, S.C., BOLLINGER, M.J., HAHN, C., ALBRITTON, D.L. & SIEVERS, R.E. 1984. Measurement of aromatic hydrocarbon ratio and NOx concentrations in the rural troposphere: observations of air mass photochemical ageing and NOx removal. *Atmospheric Environment*, 18:2421-2432.

ROECKNER, E., BROKOPF, R., ESCH, M., GIORGETTA, M., HAGEMANN, S., KORNBLUEH, L., MANZINI, E., SCHLESE, U. & SCHULZWEIDA, U. 2006. Sensitivity of simulated climate to horizontal and vertical resolution in the ECHAM5 atmosphere model. *Journal of Climate*, 19:3771-3791.

RUDOLPH, J. 1995. The tropospheric distribution and budget of ethane. *Journal of Geophysical Research*, 100:11369-11381.

RUSSEL, A.G., MCCUE, K.F. & CASS, G.R. 1988. Mathematical modeling of the formation of nitrogen-containing air pollutants I. Evaluation of an eulerian photochemical model. *Environmental Science and Technology*, 22:263-271.

SALBY, M.L. 1996. Fundaments of Atmospheric Physics. Academic Press.

SANAS, R07-01. 2000. *Supplementary Requirements for the accreditation of continuous ambient air pollution monitoring stations.*

SCHERE, K.L. & DEMERJIAN, K.L. 1984. *User's guide for the photochemical box model (PBM)*.
SCORGIE, Y., ANNEGARN, H.J. & BURGER, L.W. 2004. *Fund for research into industrial development growth and equity (FRIDGE).Study to examine the potential socio-economic impact of measures to reduce air pollution from combustion*. Pretoria South Africa.

SCORGIE, Y., ANNEGARN, H. & RANDELL, L. 2003. *Air quality mangement plan for the city of Johannesburg*. Johannesburg.

SEINFELD, J.H. & PANDIS, S.N. 1998. Atmospheric Chemistry and Physics: from air pollution to climate change. New York: Wiley.

SILLMAN, S. 1999. The relation between ozone, NOx and hydrobarbons in urban and polluted rural environments. *Atmospheric Environment*, 33:1821-1845.

SILLMAN, S. & SAMSON, P.J. 1995. Impact of temperature on oxidant photochemistry in urban, polluted rural and remote environments. *Journal of Geophysical Reserach*, 100:11497-11508.

SINGH, H.B., SALAS, L.J., CANTRELL, B.K. & REDMOND, R.M. 1985. Distribution of aromatic hydrocarbons in the ambient air. *Atmospheric Environment*, 19:1911-1919.

SKOV, H., LINDSKOG, A., PALMGREN, F. & CHRISTENSEN, C.S. 2001. An overview of commonly used metods for measuring benzene in ambient air. *Atmospherif Environment*, 1:S141-S148.

SMITH, J. 2011. *Atmopsheric chemistry: Lecture 2: Tropospheric Chemistry and Aerosol*s.

SOWDEN, M. 2007. *Evaluating the Ozone Potential for the Highveld*. Pretirua.
SPALDING-FECHER, R., OKESE, D., EBERHART, R. & DAVIS, M. 2000. *Electricity production and the environment*.

STAGGELBACH, T., NEFTEL, A. & HOROWITZ, L.W. 1997. Photochemical oxidant formation over soutern Switzerland 2. Model results. *Journal of Geophysical Research*, 102:23363-23373.

STEINBACHER, M., ZELLWEGER, C., SCHWARZENBACH, B., BUGMANN, S., BUCHMANN, B., ORDONES, C., PREVOT, A.S.H. & HUEGLIN, C. 2007. Nitrogen oxide measurements at rural sites in Switzerland: Bias of conventional measurement techniques. *Journal of Geophysical Research*, 112(D11307)

STULL, R. 1997. An Introduction to Boundary Layer Meteorology. Boston: Kluwer Academic Publishers.
SWAP, R., GARSTANG, M., MACKO, S.A., TYSON, P.D., MAENHAUT, W., ARTAXO, P., KALLBERG, P. & TALBOT, R. 1996. The long range transport of southern African aerosols to the tropical South Atlantic. *Journal of Geophysical Research*, 101:23777-23791.

TANG, J.H., CHAN, L.Y., LI, Y.S., CHANG, C.C. & LIU, S.C. 2007. Characteristics and diurnal variations of NMHCs at urban, suburban and rural sites in the Pearl River elta and a remote site in South China. *Atmopsheric Environment*, 41(38):8620-8632.

THOMPSON, A.M., DIAB, R.D., BODEKER, G.E., ZUNCKEL, M., COETZEE, G.J.R., ARHER, C.B., MCNAMARA, D.P., PICKERING, K.E., COMBRINK, J., FISHMAN, J. & NGANGA, D. 1996. Ozone over southern Africa during SAFARI-92/TRACE A. *Journal of Geophysical Research*, D19(101):23793-23807.

TIWARI, V., HANAI, Y. & MASUNAGA, S. 2010. Ambient levels of volatile organic compounds in the vincity of petrochemical industrial area of Yokohama, Japan. *Air Quality and Health*, 3(2):65-75.

TSENG, K-H., WANG, J-L., CHENG, M-T. & TSUANG, B-J. 2009. Assesing the Relationship between Air Mass Age and Summer Ozone Episodes Based on Photochemical Indices. *Aerosol and Air Quality Research*, 9(2):148-171.

TYSON, P.D. 1997. Atmospheric transport of aerosols and trace gases over southern Africa. *Progress in Physical Geography*, 21(1):79-101.

TYSON, P.D. & D'ABRETON, P.C. 1998. Transport and recirculation of aerosol off southern Africa-Macroscale plume structure. *Atmospheric Environment*, 32(9):1511-1524.

TYSON, P.D., GARSTANG, M., SWAP, R.J., EDWARDS, M. & KALLBERG, M. 1996. An air transport climatology for subtropical southern Africa. *International Journal of Climatology*, 16(2):151-163.

TYSON, P.D. & PRESTON-WHYTE, R.A. 2000. The weather and climate of southern Africa. Oxford: Oxford University Press.

TYSON, P.D., PRESTON-WHYTE, R.A. & DIAB, R.D. 1976. Towards an invesion climatology of Southern Africa: Part1, Surface inversions. *South African Geographical Journal*, 58(2):151-163.

VENTER, A.D., VAKKARI, V., BEUKES, J.P., VAN ZYL, P.G., LAAKSO, H., MABASO, D., TIITTA, P., JOSIPOVIC, M., KULMALA, M., PIENAAR, J.J. & LAAKSO, L. 2012. An air quality assessment in the industrialized western Bushveld Igneous Complex, South Africa. *South African Journal of Science*, submitted

VOGEL, B., FIEDLER, F. & VOGEL, H. 1995. Influence of topography and biogenic volatile organic compounds emissions in the state of Baen-Wurttemberg on ozone concentrations during episodes of high air temperatures. *Journal of Geophysical Research*, 100:22907-22928.

XU, J., ZHANG, X., XU, X., ZHAO, X., MENG, W. & PU, W. 2011. Measurements of surface ozone and its precursors in urban and rural sites in Beijing. *Procedia Earth and Planetary Science*, 2:255-261.
YAMAMOTO, N., OKAYASU, H.T., MURAYAMA, S., MORI, S., HUNAHASHI, K. & SUZUKI, K. 2000. Measurement of volatile organic compounds in the urban atmosphere of Yokohama, Japan by an automated gas chromatographic system. *Atmospheric Environment*, 34:4441-4446.

ZAVALA, M., HERNDON, S.C., WOOD, E.C., ONASCH, T.B., KNIGHTON, W.B., MARR, L.C., KOLB, C.E. & MOLINA, L.T. 2009. Evaluation of mobile emissions contributions to Mexico City's emission inventory using on-road and cross-road emission measurements and ambient data. *Atmosperic Chemistry and Physics*, 9:6035-6317.

ZHANG, B.N. & OANH, N.T.K. 2002. Photochemcal smog pollution in the Bangkok Metropolitain Region of Thailand in relation to O3 precursor concentrations and meteorological conditions. *Atmospheric Environment*, 36:4211-4222.

ZUNCKEL, M., HELD, G., PRESTON-WHYTE, R.A & JOUBERT, A. 1996. Low-level wind maxima and transport of pyrogenic products over southern Africa. *Journal of Geophysical Research*, 101(D19):23745-23755.

ZUNCKEL, M., NAIKER, Y. & RAGHUNANDAN, A. 2010. *Air Quality mangement Plan for the Highveld Priority Area: Air Quality Baseline assessment for the Highveld Priority Area*.

ZUNCKEL, M., ROBERTSON, L., TYSON, P.D. & RODHE, H. 2000. Modelled transport and deposition of sulphur over Southern Africa. *Atmospheric Environment*, 32:2797-2808.

ZUNKCKEL, M., KOOSAILEE, A., YARWOOD, G., MAURE, G., VENJONOKA, K., VAN TIENHOVEN, A.M. & OTTER, L. 2005. Modelled surface ozone over southern African during the cross Border Air Pollution Impact Assessment Project. *Environmental Modelling and Software*, 21:911-924. June.

Graphical layout of Chapter 3

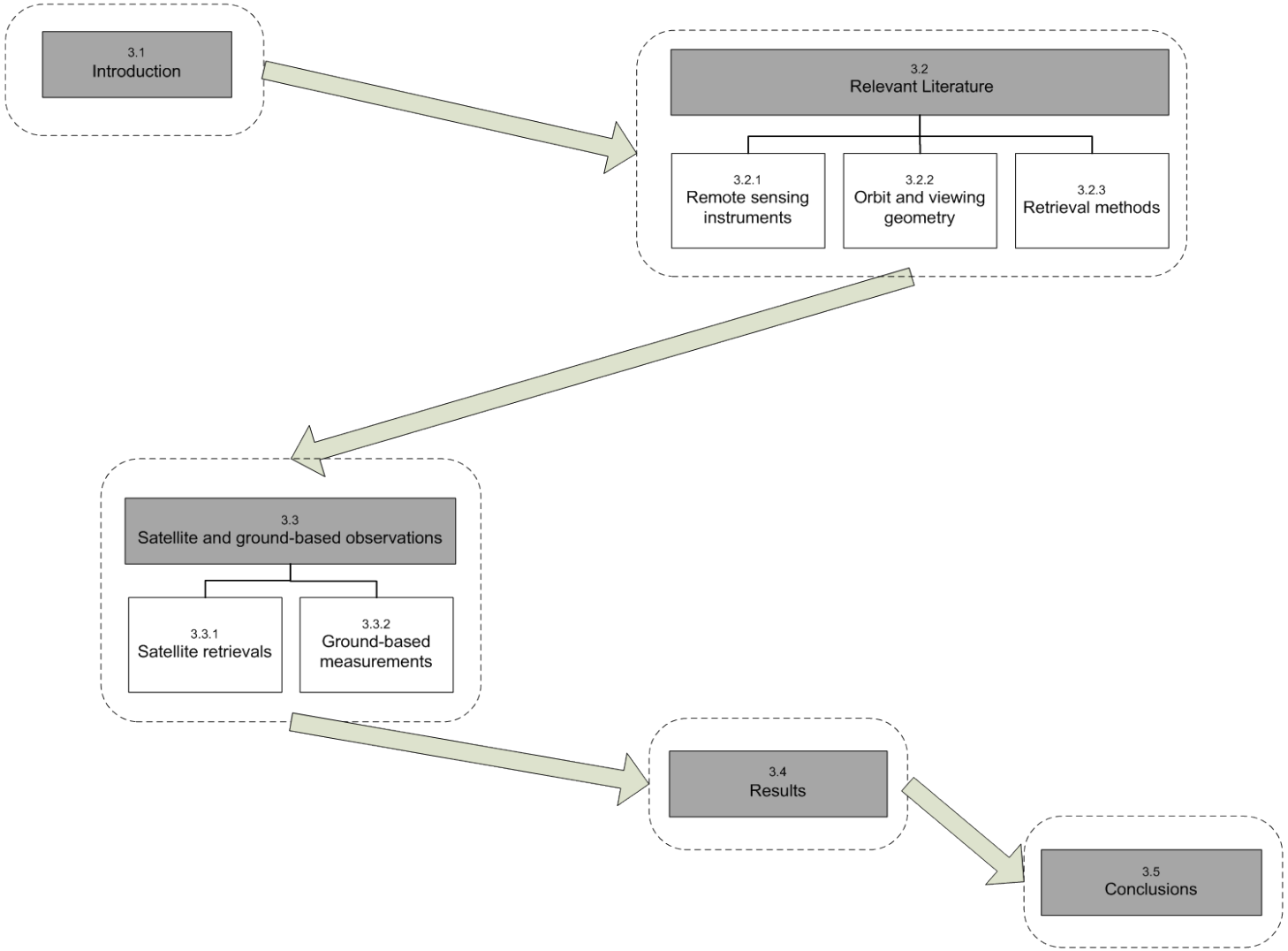

Chapter 3

Contextualising the NO_2 hotspot over South Africa

3.1 INTRODUCTION

Satellite-based instruments such as the Global Ozone Monitoring Experiment (GOME 1 & 2) (Burrows *et al.*, 1999), the SCanning Imaging Absorption spectroMeter for Atmospheric CHartographY (SCIAMACHY) (Bovensmann *et al.*, 1999) and the Ozone Monitoring Instrument (OMI) (Levelt *et al.*, 2006) have effectively been used over the past number of decades to quantify trends of various atmospheric trace gas concentrations, e.g. nitrogen dioxide (NO_2), sulphur dioxide (SO_2), water (H_2O), bromine monoxide (BrO) and formaldehyde (HCHO) on a global scale (Martin, 2008; Wagner *et al.*, 2011). One of the prominent NO_2 hotspots seen on global maps from satellite retrievals is over the South African Highveld (Highveld hotspot). The tropospheric NO_2 column density of this area is comparable to that observed for central and northern Europe, eastern North-America and south-east Asia (Beirle *et al.*, 2004), as shown in Figure 3.1. In addition to the well-known source from eleven (total 19.98 GW generation capacity) coal-fired power stations (see Section 2.2.5.2), there are also wide-spread regional sources, such as road transport, biomass burning and human settlements, as well as other large point sources including metallurgical, mining and petrochemical operations (Freiman & Piketh, 2003) resulting in high emission densities in this region. Power generation contributes 73% of the total estimated nitrogen oxide (NO_x) emissions of 978 781 tons per annum and 82% of the total estimated SO_2 emissions of 1 622 233 tons per annum (Zunckel *et al.*, 2011). According to Wells *et al*. (1996), as well as Held and Mphepya (2000), 90% of the industrial NO_x emissions in South Africa originate from the Highveld hotspot. In the recent assessment of global emissions by Lamarque *et al*. (2010), emissions from South Africa amounted to 420kt (N)/yr for the year 2000, which constituted 1.6% of the global anthropogenic NO_2 emissions.

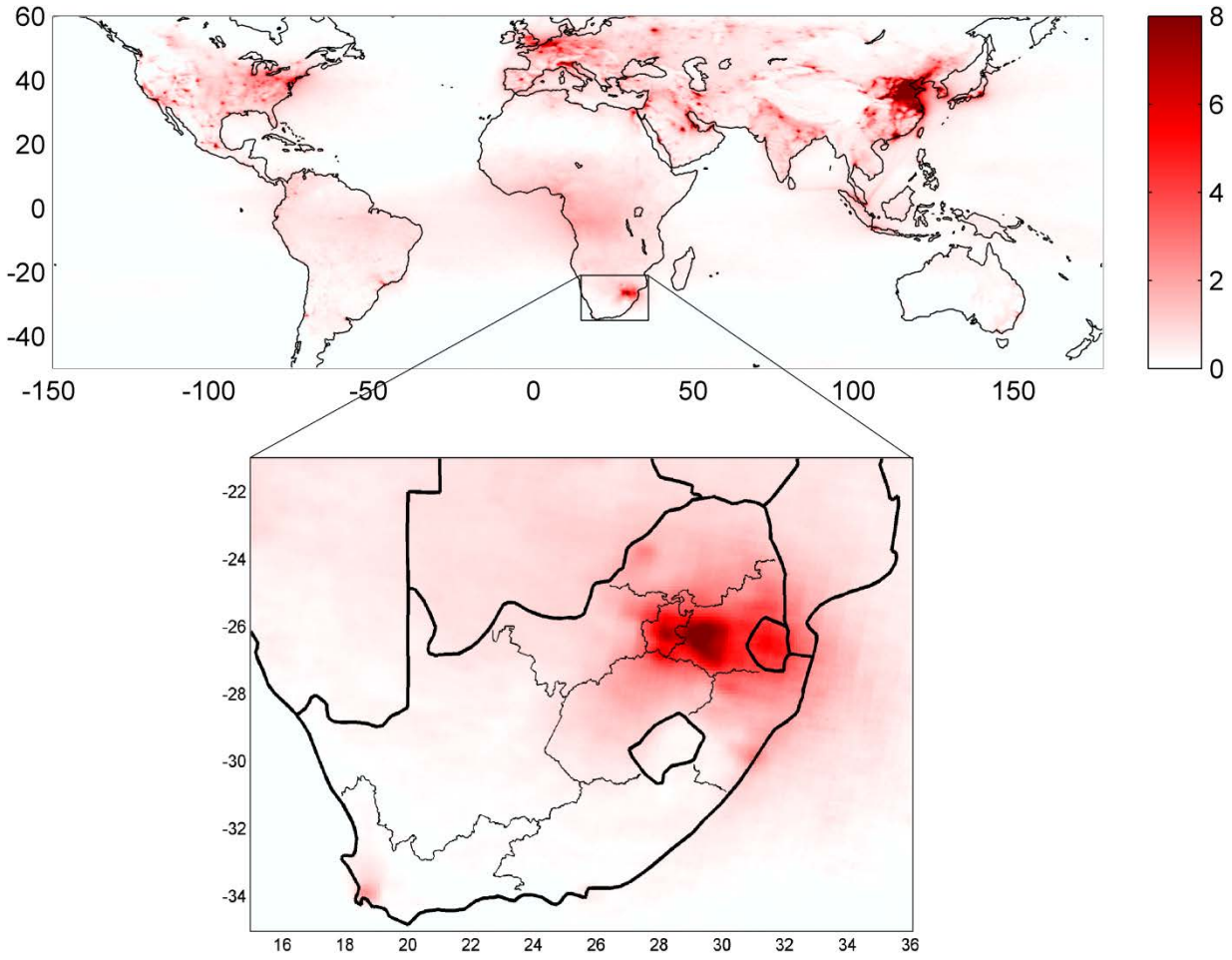

Figure 3.1: Mean tropospheric vertical NO_2 column in 10*15 molecules/cm^2 from SCIAMACHY measurements for 2003-2010, courtesy of Steffen Beirle, MPI Mainz, Germany

In Figure 3.1, a smaller area, with a seemingly less substantial NO_2 column density, can be seen approximately 100km west of the Highveld hotspot. This corresponds with the geographical location of the Jhb-Pta megacity. Ground-based measurements conducted in this study indicate that satellite observations may underestimate the importance of this conurbation for local NO_x pollution due to specific diurnal cycles of emissions. It is realised that ground-based measurements of local concentrations cannot be compared directly to satellite-based column measurements. However, the aim of this chapter is to emphasise the potential contribution of the emissions from the Jhb-Pta megacity to the NO_2 hotspot observed from space. The diurnal cycles of ground-based measurements of NO_x are evaluated for the two areas of interest, i.e. the Jhb-Pta megacity and the Highveld hotspot and compared to the satellite-based NO_2 observations.

3.2 RELEVENT LITERATURE

3.2.1 Remote sensing instruments

Remote sensing refers to the use of electromagnetic radiation to acquire information without being in physical contact of the object (Martin, 2008). For the past decade, remote sensing instruments have provided valuable information with regard to spatial patterns, emissions and seasonal variation of atmospheric trace gases (e.g. Boersma *et al.*, 2007; Richter *et al.*, 2005; Beirle *et al.*, 2004; Beirle *et al.*, 2011). These data are essential for the assessment of regional and global air quality, acid deposition and climate change.

Remote sensing instruments, such as GOME (and GOME2), OMI and SCIAMACHY, are all passive remote sensing spectrometers equipped on satellites. These instruments observe backscattered, reflected, transmitted or emitted radiation from the atmosphere and the surface of the earth at different wavelengths (Burrows *et al.*, 1999). These are also the main instruments currently utilised to measure vertical tropospheric NO_2 column densities. Their specifications and physical properties are listed in Table 3.1.

Table 3.1: Specifications and properties of the major remote sensing instruments measuring NO_2 column densities

Instrument	On-board satellite	Satellite launched (global coverage)	Trace gas measurements	Wavelengths	Spatial resolution	Data available	Local overpass time
GOME	ERS-2 (European Remote Sensing Satellite-2)	April 1995 (3 days)	O_3, NO_2, SO_2, HCHO, H_2O, BrO, OClO	V-NIR: 0.24-0.79µm (resolution 0.2-0.4nm)	320 x 40km^2	1996-2003	10:30
GOME-2	ERS-2	June 2006 (1 day)	O_3, NO_2, related cloud information, SO_2, aerosol	V-NIR: 0.24-0.79µm (resolution 0.2-0.4nm)	80 x 40km^2	2007-2011	9:30
OMI	EOS Aura ERS-2	June, 2004 (1 day)	O_3, NO_2, SO_2, aerosol, HCHO,CHOCHO and BrO	350-500nm	13km x 24km^2 for nadir view	2004-present	13:38
SCIAMACHY	ENVISAT	1 March 2002 (6 days)	O_3, NO_2, BrO, SO_2, HCHO, OClO, HDO, CH_4, CO, CO_2,	Resolution (0.2nm to 1.5nm) Range (240 and 2380nm)	60x 30km^2 occasionally 30 x30km^2	2002-present	10:00

Different remote sensing instruments exist to measure specific species, as indicated in Table 3.1 above. In this study, the NO_2 column densities measured with only two of these instruments, i.e. SCHIAMACHY and OMI, were employed and will therefore be discussed in more detail in the following sections.

3.2.2 Orbit and viewing geometry

The primary satellites, SCIAMACHY and OMI, used to obtain information on lower tropospheric trace gas concentrations, orbit the earth in a polar, sun-synchronous way. A typical orbit altitude is 705km, which results in an orbiting speed of 100 minutes per orbit, i.e. approximately 14 complete orbits per day (Martin, 2008). The equator is crossed twice by the satellites during an orbit, once in the southward or descending direction and once in the northward or ascending direction (Martin, 2008). At low and mid latitudes, the resultant observations occur at a near-constant local time. SCIAMACHY crosses the equator at approximately 10:00 local time (Beirle *et al.*, 2010), while OMI crosses the equator at 13:30 local time, everyday.

Viewing geometry refers to the method of observation from satellites to the surface of the earth. Both SCIAMACHY and OMI are UV/Vis spectrometers that measure direct sunlight and backscattered light from the earth's atmosphere (Boersma *et al.*, 2007). SCIAMACHY measures the solar radiation between 220nm and 2380nm, while OMI measures between 270nm and 500nm (Boersma *et al.*, 2007).

SCIAMACHY measures in three viewing geometries, i.e. nadir, limb and occultation, as indicated in Figure 3.2, while OMI only measures in the nadir viewing geometry. The nadir mode observes the atmospheric volume directly under the instrument (i.e. spacecraft) and can scan an area of up to 960km^2 of the surface of the earth with a maximum resolution of 30km x 30km obtaining a global coverage within approximately six days (Boersma *et al.*, 2007). The OMI nadir viewing mode has a 114° field of view, which corresponds to an approximately 2600km wide scan of the earth's atmosphere, leading to a global coverage within approximately one day (Anon, 2009). In the limb mode, which is exclusive to SCIAMACHY, the instrument looks at the edge of the atmosphere and scans at different tangent altitudes over a range of up to 960km in the horizontal direction and a vertical range of approximately 2.6km, as indicated in Figure 3.2 (b) (Bovensmann *et al.*, 1999). The same geometry as mentioned for the limb and nadir is used during occultation measurements, except that the sun or the moon is in the field of view of the

instrument. One of the unique properties of SCIAMACHY is the option to measure in both limb and nadir viewing geometries obtaining three-dimensional information of the atmosphere. The method applied is to first observe the atmospheric column in limb and then, after seven minutes, the same atmospheric volume is observed in the nadir viewing geometry (Bovensmann *et al.*, 1999). From the combination of the alternating limb and nadir measurements, the stratospheric column of NO_2 can be derived and removed from the total column measurements of NO_2 (Beirle *et al.*, 2010). Tropospheric specie information is only available from a nadir spectrum, and therefore the nadir and limb viewing modes are mostly used (Wagner *et al.*, 2008).

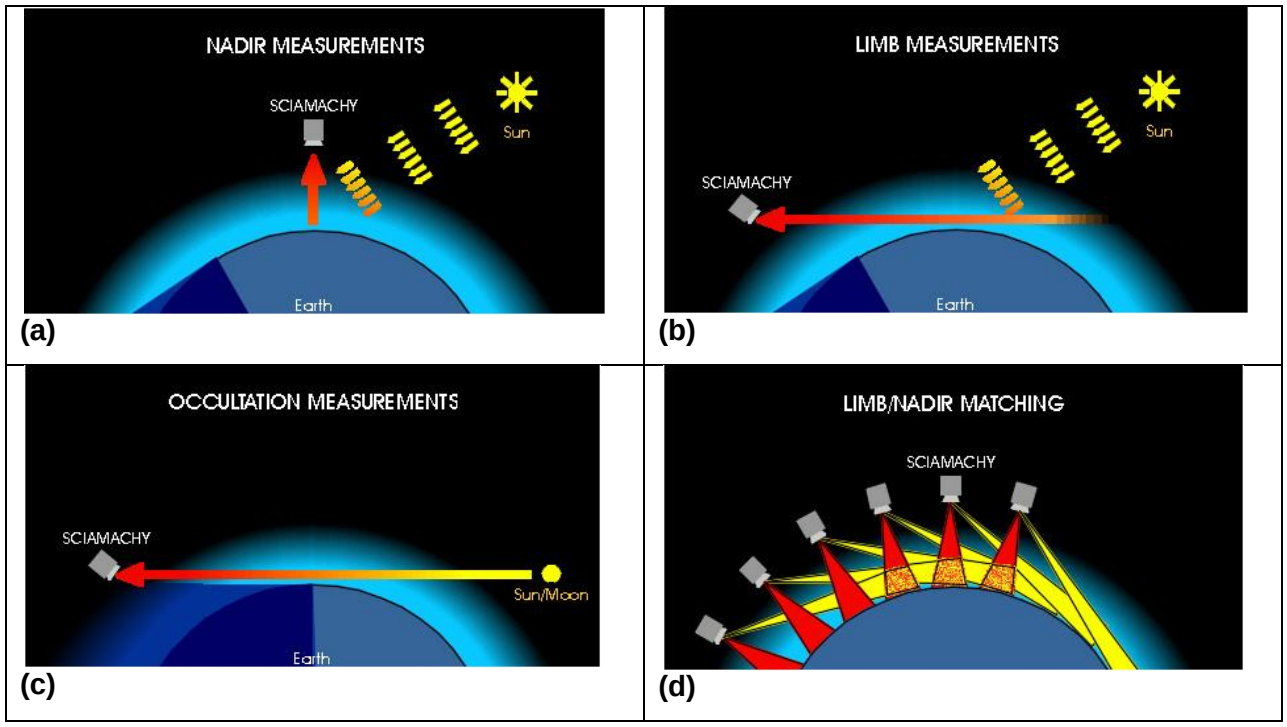

Figure 3.2: Different geometric modes for SCIAMACHY (a) nadir mode (b) limb mode (c) occultation mode; (d) first in limb and then, after about seven minutes, in nadir geometry (adopted from www.iup.uni-bremen.de/eng/)

3.2.3 Retrieval methods

There are different techniques for satellites to retrieve information of atmospheric trace gases from the lower troposphere. Most of the instruments use passive techniques, which observe either solar backscatter (<4um) or thermal infrared emissions (4-50um) (Martin, 2008). Remote sensing instruments do not directly measure atmospheric composition. A retrieval is obtained by calculating the atmospheric composition that best produces the observed radiation (Martin,

2008). These retrievals often require external information on a number of geophysical fields, such as surface reflectivity or emissivity, cloud coverage, the viewing geometry and the retrieval wavelength that makes these retrievals complex.

A variety of algorithms to extract physical parameters by accounting for atmospheric radiative transfer have in recent years been developed in numerous studies, with several scientific applications and are integral to the success of modern-day remote sensing (Martin, 2008; Martin *et al.*, 2003; Bucsela *et al.*, 2006; Boersma *et al.*, 2009; Wagner *et al.*, 2008). Vertical column densities of atmospheric trace gas species involve two steps; firstly, the slant column densities are determined by fitting the modelled atmospheric spectra to the observed absorption spectra, and secondly, an air mass factor (AMF) is used to convert the slant column densities from space into total vertical columns (Palmer *et al.,* 2001).

Tropospheric NO_2 column densities from GOME have been retrieved by various atmospheric research groups (Beirle *et al.*, 2003; Boersma *et al.*, 2004; Martin *et al.*, 2002; Richter & Burrows, 2002). For SCIAMACHY and OMI, the retrieval algorithms are similar to those for GOME-1. Tropospheric NO_2 column densities are retrieved from OMI by two groups (Bucsela *et al.*, 2006; Boersma *et al.*, 2007). Some of the retrievals involve a spectral fit, determination of the stratospheric NO_2 column density using observations over remote regions and oceans, as well as an AMF calculation to convert slant column density into vertical columns (Martin, 2008; Richter & Burrows, 2002), whereas other groups obtain the stratospheric column from a model. Tropospheric NO_2 columns are closely related to surface NO_2 concentrations. Petritolli *et al*. (2004), Ordonez *et al.* (2006) and Boersma *et al*. (2009) have applied tropospheric NO_2 columns to reveal significant correlations with *in situ* NO_2 measurements.

3.3 SATELLITE AND GROUND-BASED OBSERVATIONS

3.3.1 Satellite retrievals

Multi-year NO_2 retrievals were utilised from SCIAMACHY (MPI retrieval, (Beirle *et al.*, 2010) for the years 2003 to 2010) (www.temis.nl) and OMI (Dutch OMI NO_2 product DOMINO (v1.02), (Boersma *et al.*, 2007), which were available from the Tropospheric Emission Monitoring Internet Service (www.temis.nl) for the years 2005 to 2009. Both instruments orbit the earth in a polar, sun-synchronous orbit, with local South African overpass times of 10:00 (SCIAMACHY)

and 13:30 (OMI). Therefore, the comparison of NO_2 measurements from SCIAMACHY and OMI holds some, but limited, information on diurnal cycles (Boersma *et al.*, 2009).

From the spectral measurements of the satellite instruments, slant column densities (SCDs), i.e. integrated concentrations along the effective light path, of NO_2 are derived. The stratospheric slant column is subtracted from the total slant column, yielding the tropospheric slant column density (TSCD). For details about these procedures, see Beirle *et al*. (2010) (for SCIAMACHY) and Boersma *et al*. (2007) (for OMI). For the translation of the TSCD into a tropospheric vertical column density, general tropospheric air mass factors (AMF) were needed. This requires prior assumptions on the ground albedo, as well as the vertical profiles of aerosol, clouds and NO_2, which makes it the most uncertain step within satellite retrievals.

To make the comparison of the SCIAMACHY and OMI datasets meaningful (since they differ in viewing geometry, local time, ground pixel size, and the way AMF has been calculated), we focus on a) TSCDs (which are far less uncertain than TVCDs) and b) investigate relative patterns, i.e. ratios of TSCDs for the Jhb-Pta megacity versus the Highveld hotspot. This approach mostly eliminates potential systematic biases due to the use of different satellite instruments and retrievals.

3.3.2 Ground-based measurements

Hourly near-surface concentrations of NO_2 were obtained from four air quality monitoring stations within the Jhb-Pta megacity (for more detail see Chapter 2) and at five stations in the Highveld hotspot for a period of three months in autumn 2009 (March to May). These stations were strategically chosen since they were regarded to be representative of the ambient concentrations of these two areas. Figure 3.3 indicates the positioning of these measurement stations within the Jhb-Pta megacity (indicated by the grey area) and in the Highveld hotspot. The afore-mentioned atmospheric monitoring stations were operated in the Jhb-Pta megacity by the City of Johannesburg, while those in the Highveld hotspot were operated by industries. Apart from the strategic positioning within the context of this chapter, these stations also complied with the South African Air Quality Information System (SAAQIS) requirements for quality control. Data received from these stations were also manually checked to identify possible errors and outliers. All ground-based NO_2 measurements were taken in the same manner as described in Section 2.3.2.

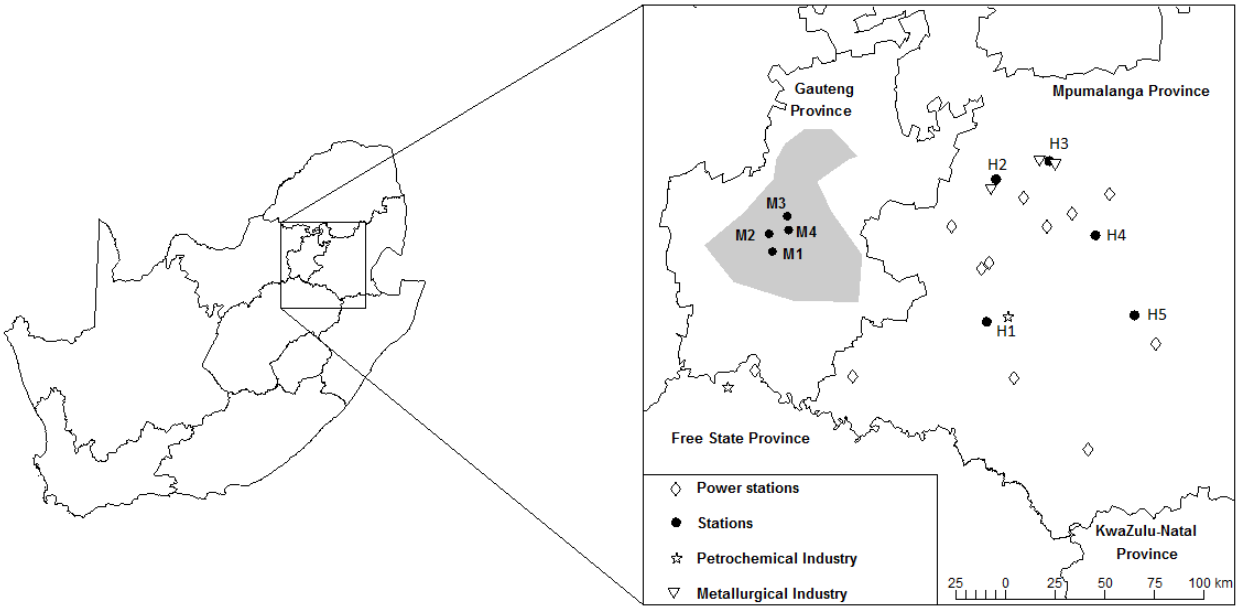

Figure 3.3: Sampling sites showing major point sources, with 'M' denoting the Jhb-Pta megacity and 'H' the 'Highveld hotspot'; the grey indicates the Jhb-Pta megacity

3.4 RESULTS

Figure 3.4 shows the average NO_2 diurnal cycles for each of the ground-based stations in the Jhb-Pta megacity and the Highveld hotspot for a three-month period (March to May 2009). It is evident from Figure 3.4 that the NO_2 mixing ratios of the Jhb-Pta megacity and the Highveld hotspot were mostly in the same order of magnitude. The Jhb-Pta megacity diurnal cycles were characteristic of urban areas dominated by traffic emissions of NO_2, with maximum atmospheric NO_2 levels observed during peak traffic periods in the early morning and late afternoon (Han *et al.*, 2011). In contrast, the NO_2 diurnal cycles measured at the monitoring stations in the Highveld hotspot were less pronounced, which can be ascribed to the industrial activities mainly responsible for NO_2 emissions in this area, which operate 24 hours per day (Collett *et al.*, 2010). Measurement station H2 was the exception, since it was relatively close to a city in the Highveld hotspot, i.e. Witbank, with a distinct diurnal cycle due to the influence of traffic emissions and/or household combustion for space heating and cooking. Additionally, this site might also be influenced by the trapping of industrial plumes in the nocturnal boundary layer.

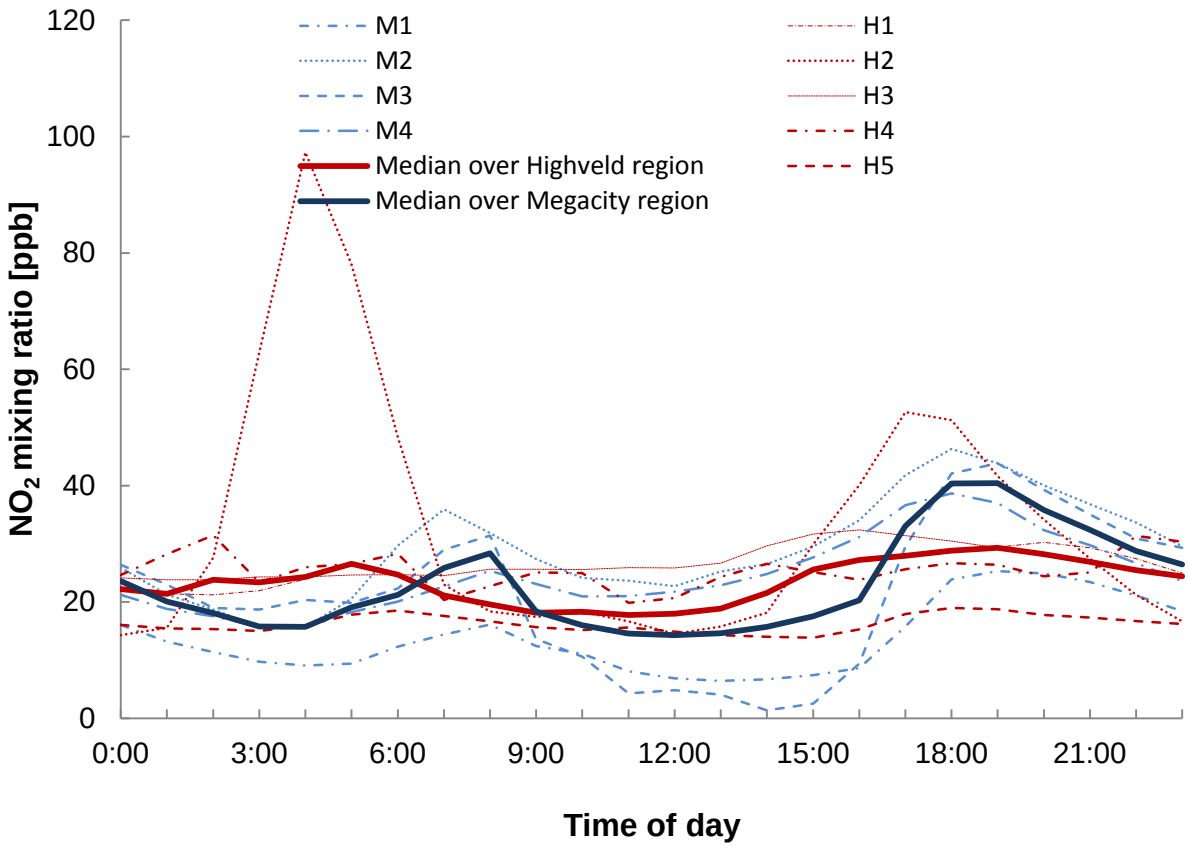

Figure 3.4: Median diurnal NO_2 mixing ratios for each of the ground-based stations, for the period March to May 2009 and median over each region; M denotes a Jhb-Pta megacity station and H a Highveld hotspot station, with numbers corresponding to the locations indicated in Figure 3.3

In order to facilitate the comparison of the NO_2 levels of the two areas with each other, the ratio of the median of the four Jhb-Pta megacity measurement stations versus the median of the five Highveld stations was computed and is plotted in Figure 3.5 as a function of the time of day. From this average diurnal cycle ratio, it is apparent that there are two distinct periods, i.e. between 06:00 and 09:00 in the morning and 17:00 and 21:00 in the evening when the near-surface NO_2 mixing ratios of the Jhb-Pta megacity are higher than that of the Highveld hotspot. These time periods coincide with peak traffic hours in the Jhb-Pta megacity. Traffic emissions in the Jhb-Pta megacity are compounded by the poor public transport system and an aging vehicular fleet, if compared to Megacities in more industrially developed countries.

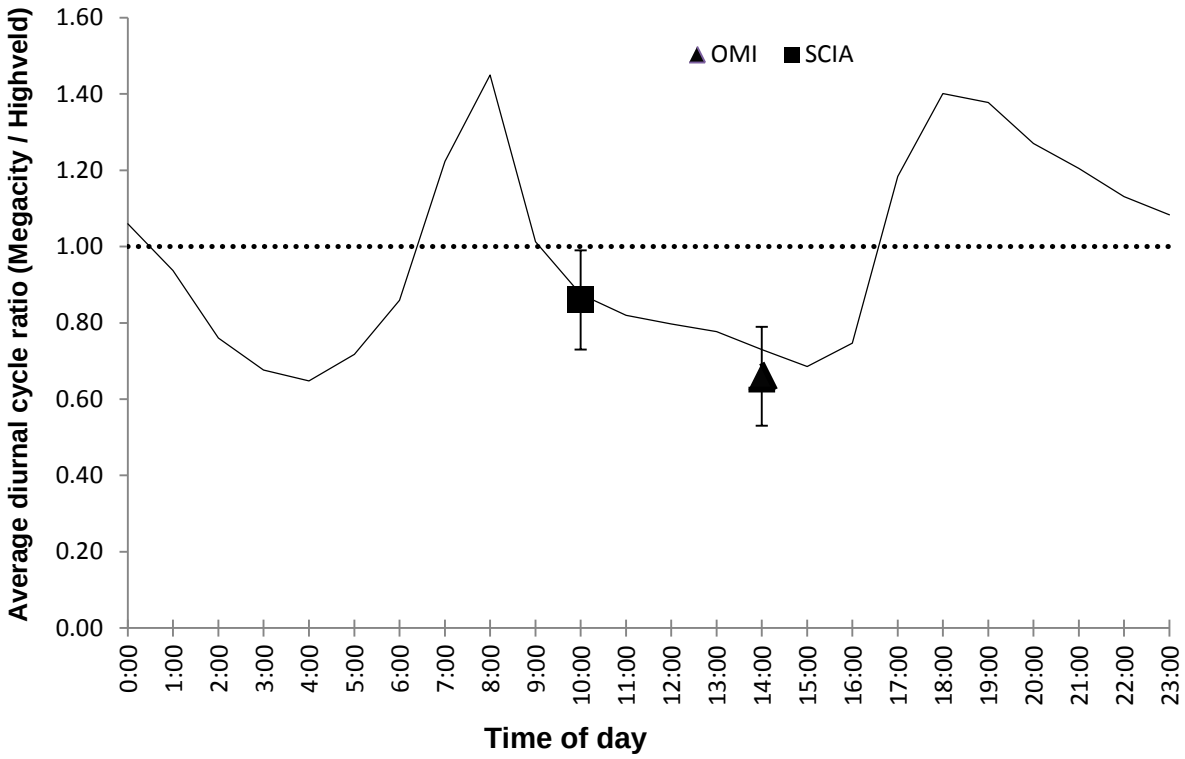

Figure 3.5: Average diurnal cycle ratio, defined as the averaged NO_2 diurnal mixing ratio of the four Jhb-Pta megacity measurement stations divided by the averaged NO_2 diurnal mixing ratio of the five monitoring stations in the Highveld hotspot for a three-month period (March to May 2009); the square and triangle are the ratios of the TSCD for the Jhb-Pta megacity divided by the TSCD for the Highveld hotspot for SCIAMACHY and OMI measurements

The ratio for the TSCD for the megacity divided by the TSCD for the Highveld hotspot is also shown in Figure 3.5 for SCIAMACHY (averaged over 2003 to 2009) and OMI (2005 to 2009). The ratios were calculated from mean maps on a 0.35°×0.35° grid. The actual numbers depend on the choice of the areas used for averaging. For the Highveld, 3×3 pixels (i.e. ≈ 1°×1°) were taken that contained all H-stations. For the megacity, two different areas were considered, i.e. 1 pixel (containing all M-stations), as well as 3×3 pixels (the same area as the Highveld). The upper ends of the error bars reflect the first choice, the lower end the second and the square/triangle the average of both ratios. The ratios of TSCDs could generally be biased if AMFs would be different for the Highveld hotspot and Jhb-Pta megacity. However, terrain

height, aerosol load (MODIS AOD), and mean cloud fraction (from OMI) are quite similar for both regions.

From Figure 3.5, it is evident that the satellite-observed NO_2 TSCDs over the Highveld hotspot are generally higher than that over the Jhb-Pta megacity, i.e. ratios of the TSCD in Figure 3.6 are always below one. However, the 24-hour average ratio of the ground-based observations is close to one (0.90), indicating that at ground level, the overall NO_2 pollution levels in the Jhb-Pta megacity are comparable to the more well-known Highveld hotspot. Although the geographical area covered by the Highveld hotspot is larger than the area of the Jhb-Pta megacity pollution, the latter clearly deserves more attention than it received in the past, due to the large urban population that is affected by this pollution.

3.5 CONCLUSION

We have shown that the NO_2 Highveld hotspot – which has become well known over the last decade in the international science community due to its prominence in satellite images – is accompanied by a second hotspot over the Jhb-Pta megacity, with peak NO_2 pollution levels exceeding the maximum daily Highveld values during the morning and evening rush hours. Arguably, it can be stated that the Jhb-Pta megacity pollution is of considerably greater importance due to the more than 10 million people living in the Jhb-Pta megacity, compared to the relatively low population density of the Highveld hotspot. Although satellite instruments have been extremely valuable in pointing out hotspots such as these worldwide, an example of the limitations due to their specific overpass times has been presented here. Satellite observations do not measure NO_2 TSCD during times when NO_2 levels peak in the Jhb-Pta megacity, as indicated by ground-based measurements. During these peak times, near-surface NO_2 mixing ratios of the Jhb-Pta megacity exceeded that of the Highveld hotspot.

A further assessment of this issue will require more ground-based and aircraft profile measurements of the region; In particular, a direct observation of tropospheric NO_2 vertical column densities with ground-based MAX-DOAS measurements (e.g. Wagner *et al.,* 2011) or airborne instruments might especially be valuable. Heue *et al*. (2008) proved that airborne (aircraft fitted) DOAS measurements can be used for this type of application over the Highveld of South Africa. However, a more comprehensive study of this nature is required over both the Highveld hotspot and the Jhb-Pta megacity to have a better understanding of the true extent of

the NO_2 hotspot over the interior of South Africa. An improved understanding, as well as greater public and political awareness of this pollution hotspot will be valuable, especially in light of eventually determining the consequences of this additional hotspot for O_3 production, impacts on health and agriculture and effective mitigation measures.

ACKNOWLEDGEMENTS

The free use of tropospheric NO_2 column data from the OMI sensor from www.temis.nl is acknowledged.

REFERENCES

ANON. 2009. *Ozone Monitoring Instrument (OMI): data user's guide*.

BEIRLE, S., BOERSMA, K.F., PLATT, U., LAWRENCE, M.G. & WAGNER, T. 2011. Megacity emisison and lifetimes of nitrogen oxides probed from space. *Science*, 333(6050):1737-1739.

BEIRLE, S., KUHL, S., PUKITE, J. & WAGNER, T. 2010. Retrieval of tropospheric column denisties of NO_2 from combined SCIAMACHY nidar/limb measurements. *Atmospheric Measurements and Technical discussion*, 3:283-299.

BEIRLE, S., PLATT, U., VON GLASOW, R., WENIG, M. & WAGNER, T. 2004. Estimate of nitrogen oxide emissions from shipping by satellite remote sensing. *Geophysical Research Letter*, 31(18):18102.

BEIRLE, S., PLATT, U., WENIG, M. & WAGNER, T. 2003. Weekly cycle of NO_2 by GOME measurements: A signature of anthropogenic sources. *Atmospheric Chemistry and Physics*, 3:2225-2232.

BEIRLE, S., U., Platt, WENIG, M. & WAGNER, T. 2004. Highly resolved global distribution of tropospheric NO_2 using GOME narrow swath mode data. *Atmospheric Chemistry and Physics*, 4(7):1913-1924.

BOERSMA, K.F., ESKES, H.J. & BRINKSMA, E.J. 2004. Error analysis for tropospheric NO_2 retrieval from space. *Journal of Geophysical Research*, 109:D04311.

BOERSMA, K. F., ESKES, H. J., VEEFKIND, J. P., BRINKSMA, E. J., VAN DER AARDE, R. J., SNEEP, M., VAN DEN OORD, G.H.J., LEVELT, P.F., STAMMES, P., GLEASON, J.F. & BUSCELA, E.J. 2007. Near-real time retrieval of tropospheric NO_2 from OMI. *Atmospheric Chemistry and Physics*, 7:2013-2128.

BOERSMA, K.F., JACOBS, D.J., TRANIC, M., RUDICH, Y., DESMEDT, L., DIRKSEN, R. & ESKES, H.J. 2009. Validation of urban NO_2 concentrations and their diurnal and seasonal variations observed from the SCIAMACHY and OMI sensors using in situ surface measurements in Israeli cities. *Atmospheric Chemistry and Physics*, 9:2867-2879.

BOVENSMANN, H., BUROOWS, H., BUCHWITZ, J., FRERICK, M., NOEL, J., ROZANOV, S., CHANCE, K. & GOEDE, A. 1999. Mission objectives and measurements modes. *Journal of Atmospheric Sciences*, 56(2):127-150.

BUCSELA, E.J., CELARIER, E.A., WENIG, M.O., GLEASON, J.F., VEEFKIND, J.P., BOERSMA, K.F. & BRINKSMA, E.J. 2006. Algorithm for NO_2 vertical column retrieval from the ozone monitoring instrument. *IEEE Transactions on Geoscience and Remote Sensing*, 44:1245-1258.

BURROWS, J., WEBER, M., BUCHWITZ, M. & ROZANOV, V., *et al*. 1999. The global ozone monitoring experiment (GOME): Mission concept and first scientific results. *Journal of Atmospheric Sciences*, 56:151-175.

COLLETT, K.S., PIKETH, S.J. & ROSS, K.E. 2010. An assessment of the atmospheric nitrogen budget on the Highveld. *South African Journal of Science*, 106(5):1-9.

FREIMAN, M.T. & PIKETH, S.J. 2003. Air transport into and out of the industrial Highveld region of South Africa. *Journal of Applied Meteorology*, 42:994-1002.

HAN, S., BIAN, H., LIU, A., LI, X. & ZHANG, X. 2011. Analysis of the relationshop between O_3, NO and NO_2 in Tianjin China. *Air Quality Research*, 11:128-139.

LEVELT, P., VAN DEN OORD, G., DOBBER, M., MALKKI, A., VISSER, H., DE VRIES, J., STAMMERS, P., LUNDELL, J. & SAARI, H. 2006. The ozone monitoring instrument. *IEEE Trans Geoscience Remote Sensing*, 10:1093-1101.

MARTIN, R.V. 2008. Satellite remote sensing of surface air quality. *Atmospheric Environment*, 42:7823-784.July.

MARTIN, R.V. 2008. Satellite remote sensing of surface air quality. *Atmospheric Environment*, 42:7823-7843.

MARTIN, R.V., CHANCE, K., JACOB, D.J., KUROSU, T.P., SPURR, R.J.D., BUCSELA, E., GLEASON, J.F., PALMER, P.I., BEY, I., FIORE, A.M., LI, Q., YANTOSCA, R.M. & KOELEMEIJER, R.B.A. 2002. An improved retrieval of tropospheric nitrogen dioxide from GOME. *Journal of Geophysical Research*, 107:D20.

MARTIN, R.V., JACOB, D.J., CHANCE, K.V., KUROSU, T.P., PALMER, P.I. & EVANS, M.J. 2003. Global inventory of nitrogen oxide emissions constrained by space-based observations of NO_2 columns. *Journal of Geophysical Research*, 108:4537.

ORDONEZ, C., RICHTER, A., STEINBACHER, M., ZELLWEGER, C., NUSS, H., BURROWS, J.P. & PREVOT, A.S.H. 2006. Comparison of 7 years of satellite-borne and ground-based tropospheric NO2 measurements around MIlan, Italy. *Journal of Geophysical Research*, 111:D05310.

PALMER, P., JACOB, D., CHANCE, K., MARTIN, R., SPURR, R.D., KUROSU, T.P., BEY, I., YANTOSCA, R., FIORE, A. & LI, O. 2001. Air mass factor formulation for spectroscopic measurements from satelites: Application to formaldehyde retrievals from the Global Ozone Monitoring Experiment. *Journal of Geophysical Research*, 106(D13):14539-14550. July.

PETRITOLI, A., BONASONI, P., GIOVANELLI, G., RAVEGNANI, F., KOSTADINOV, I., BORTOLI, D., WEISS, A., SCHAUB, D., RICHTER, A. & FORTEZZA, F. 2004. First comparison between ground-based and satellite-borne measurements of tropospheric nitrogen dioxide in the Po basin. *Journal of Geophysical Research*, 109:D15307.

RICHTER, A. & BURROWS, J.P. 2002. Tropospheric NO_2 from GOME measurements. *Advances in Space Research*, 29:1673-1683.

RICHTER, A., BURROWS, J.P., NUSZ, H., GRANIER, C. & NIEMEIER, U. 2005. Increase in tropospheric nitrogen dioxide over China observed from space. *Nature*, 437(7055):129-132.

WAGNER, T., BEIRLE, S., BRAUERS, T., SEUTSCHMANN, T., FRIESS, U., HAK, C., HALLA, J.D., HEUE, K-P., JUNKERMANN, W., LI, X., PLATT, U. & PUNDT-GRUBER, I. 2011. Inversion of tropospheric profiles of aerosol extinction and HCHO and NO_2 mixing ratios from MAX-DOAS observations in Milano during the summer of 2003 and comparison with independent data sets. *Atmopsheric Measurements and Technical Discussion*, 4(3):3891-3964.

WAGNER, T., BEIRLE, S., DEUTSCHMANN, T., EIGEMEIER, E., FRANKENBERG, C., GRZEGORSKI, M., LIU, C., MARBACH, T., PLATT, U. & PENNING DE VRIES, M. 2008. Monitoring of atmospheric trace gases, clouds, aerosols and surface properties from UV/vis/NIR satellite instruments. *Journal of Optics A: Pure and Applied Optics*, 10:1464-4258.

ZUNCKEL, M., NAIKER, Y. & RAGHUNANDAN, A. 2011. *THE HIGHVELD PRIORITY AREA AIR QUALITY MANAGEMENT PLAN*.

Graphical layout of Chapter 4

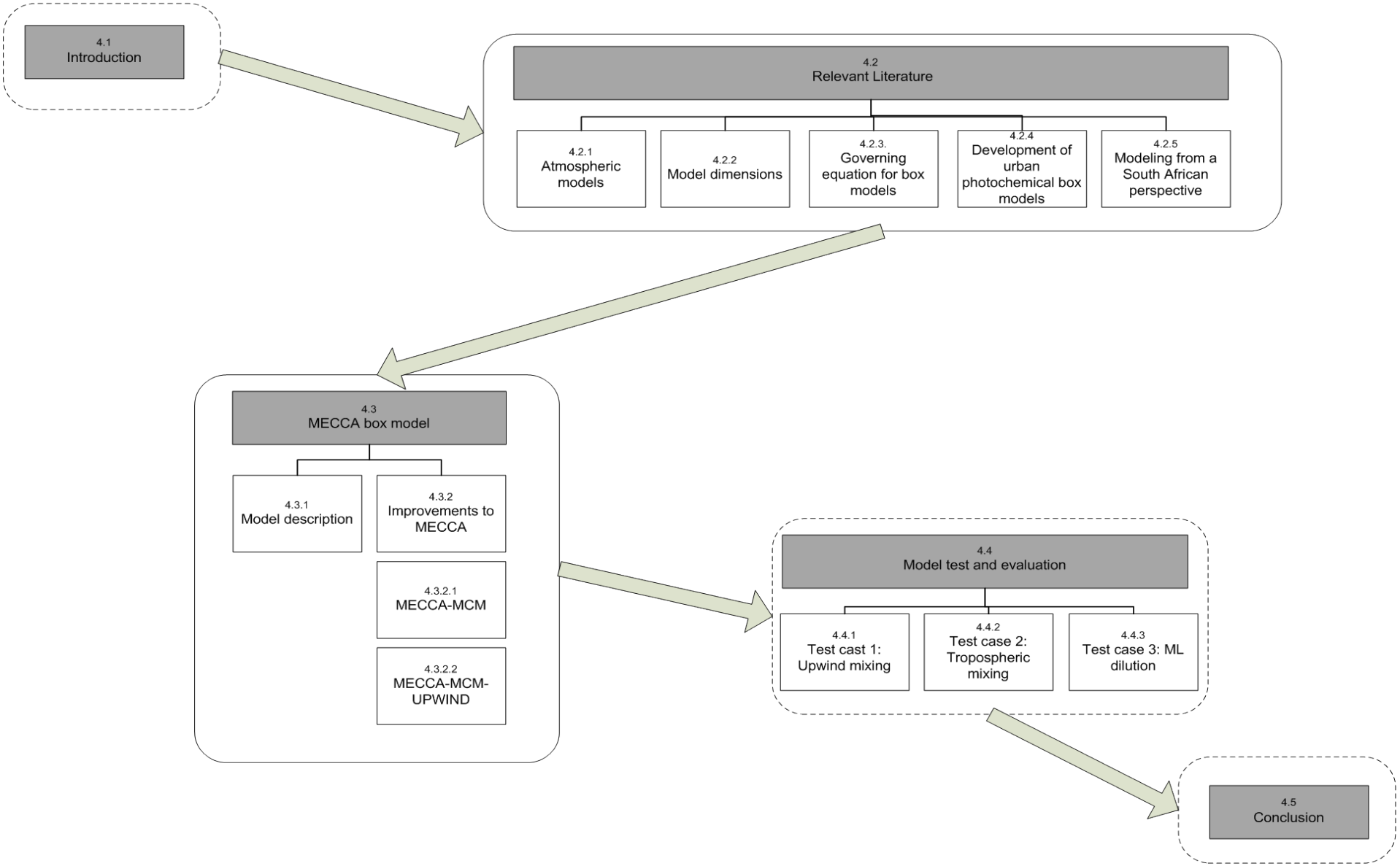

Chapter 4:

Model Development

4.1. INTRODUCTION

In the preceding chapter field measurements conducted to obtain realistic information on the current state of air quality within the Jhb-Pta megacity were presented. However, such monitoring studies can be spatially and temporally restricted. Numerical models of atmospheric processes in conjunction with field measurements and laboratory studies present a good methodology to study the chemistry of the atmosphere. Field work provides information on the current state of the atmosphere, whereas laboratory studies focus on a single atmospheric process (Jin & Demerjian, 1993; Jacobson, 1999). A close relation exists between these three approaches, since models of atmospheric processes are a mathematical representation of physical, chemical and radiative processes in the atmosphere (Jacobson, 1999), while data obtained from field measurements and laboratory experiments are required to apply and evaluate these models. Air quality models are applied to a wide range of domains – from short-range transport inside a building, up to long-range transport of pollutants over several thousands of kilometres. Models are valuable tools in environmental sciences and air quality management (Jin & Demerjian, 1993), which are used to improve the understanding of atmospheric processes and their interactions, as well as assist in projecting the success of legislative air quality goals resulting from the implementation of emission control plans.

In this chapter relevant literature to understand atmospheric models and principles will be presented, the MECCA model used in this study with developments employed to improve the model will be described and in the last section the model will be evaluated.

4.2. RELEVANT LITERATURE

4.2.1. Atmospheric models

Physical and chemical processes associated with urban air pollution does not only affect the local atmosphere, but range over wide temporal and spatial scales, which can have an effect on global tropospheric chemistry and climate (Srivastava & Padma S. Rao, 2011) . A wide variety of air quality models have been developed over the past decades. Although these models vary in complexity and efficiency, they provide valuable insights into the photochemical system of the atmosphere (Venkatram *et al.*, 1998).

Atmospheric models are computer programs that are developed to represent the actual atmospheric system. In respect to time scales, air pollution events occur over periods of hours to days, regional acid deposition over periods of days to weeks, and climate change events occur over periods of months to hundreds of years and longer (Jacobson, 1999; Spalding-Fecher *et al.*, 2000). Atmospheric and climate models are developed to fit within these time frames. With the improvement of knowledge and technology in recent decades, the resolution of atmospheric models have also improved. Table 4.1 gives a summary of typical model scales and their current resolutions.

Table 4.1: Typical domain length for different scales of numerical models

Model scale	Typical Domain	Typical resolution	Example of parameters calculated	Example of model
Local	4 km	1-50 m	Vehicular emissions, influences of buildings and obstacles	• Computational Fluid Dynamics (CDF)
City - meso	10 km	0.5-3 km	Air pollution, wind fluxes	• High Resolution Limited Area Model (HIRLAM) • The Fifth Generation Penn State/NCAR Mesoscale Model (MM5)
Regional	2 – 2,000	3-10 km	Gravity waves, thunderstorms	• Weather Research and Forecasting model (WRF)

Model scale	Typical Domain	Typical resolution	Example of parameters calculated	Example of model
	km		tornados, cloud clusters, local winds, urban air pollution	• Regional Atmospheric Modelling System (RAMS)
Global	>> 10 000 km	1° x 1°	Global circulation, stratospheric O_3 reduction global warming	• ECHAM/MESSy Atmospheric Chemistry model (EMAC) • Global Forecast System (GFS)

Models can generally be divided into two types, i.e. physical and mathematical models. Physical models are used to simulate atmospheric processes by means of a small-scale representation of the actual system, e.g. the simulation of wind tunnels (Jacobson, 1999; Srivastava & Padma S. Rao, 2011; Seinfeld, 1998). However, for areas with complex terrain, stack down wash, complex flow conditions or large buildings, physical models are not appropriate and therefore mathematical models are generally preferred. Gaussian mathematical models were first developed during the sixties (Builtjes, 2001) and are still widely used to measure the impact of pollutants being regarded as non-reactive (such as CO and SO_2) or pollutants. Two different mathematical approaches developed are the Eulerian and Lagrangian approaches (Zannetti, 1990), which are still the most commonly used models for photochemical modelling. Gaussian models can be nested within these approaches. All the models listed in Table 4.1 are mathematical models. In Figure 4.1 a schematic representation of Eulerian and Lagrangian model approaches are presented.

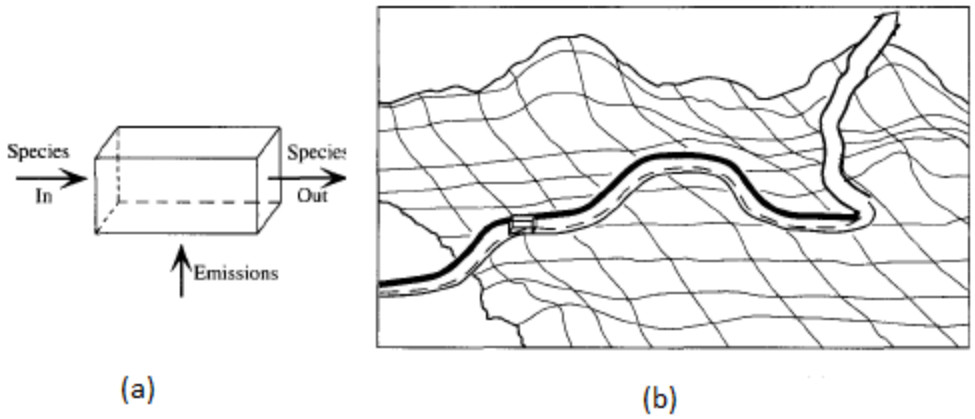

Figure 4.1: Schematic depiction of (a) an Eulerian model and (b) a Lagrangian model adopted from Seinfeld and Pandis (1996).

Eulerian models simulate atmospheric chemical species concentrations in an array of fixed grid cells as shown in Figure 1 (a). In Eulerian photochemical models, a grid is superimposed to cover the entire computational domain and the equations governing the relevant physical and chemical processes are solved in each grid cell. Alternatively to Eulerian models, the Lagrangian approach consists of air parcels that move with the local wind resulting in no frequent (depending on the specific Lagrangian model applied) mass exchange between the parcel and the surroundings, with the exception of species emissions (Boubel *et al.*, 1994; van Leeuwen & Iermens, 1995; Steinbacher *et al.*, 2007). Since the air parcel moves continuously as shown in Figure 4.1, the model simulates species concentrations for each time step at a different location along the trajectory path.

4.2.2. Model dimensions

Atmospheric models are also characterised based on the dimensions they represent. In Figure 4.2 these different dimensions are presented according to Jacobson (1999), i.e. zero (box)-, one-, two- or three dimensional representations, which are discussed in subsequent paragraphs.

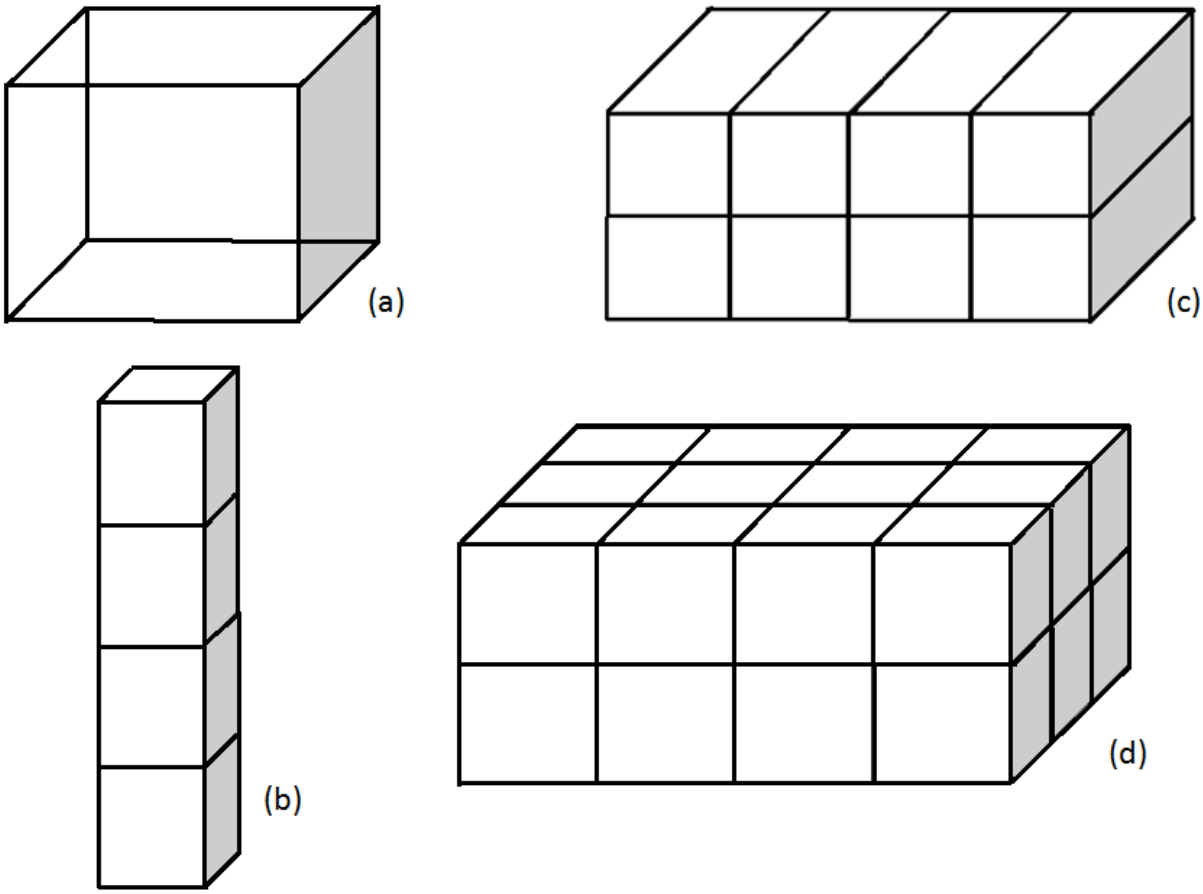

Figure 4.2: Model dimensions with (a) representing a box model, (b) a 1-D model, (c) a 2-D and (d) a 3-D model.

Zero-dimensional (O-D) or box models are the simplest model in which chemical and/or physical transformations occur. This box represents a selected atmospheric domain, which could be an urban area, a country or the global atmosphere. It is assumed that all emissions within the box are mixed instantaneously, while the gas and particle concentrations are distributed uniformly throughout the box. The processes determining the concentration within

the box e.g. emissions, deposition and chemistry, are not calculated spatially, but only temporally. Therefore the processes and calculated concentrations are a function of time (t), $c_i(t)$ only. Box models are commonly used to improve the understanding of atmospheric photochemical interactions. Some examples of the applications of photochemical box models were presented by Gerasopoulos et al. (2006) and Huang et al. (2001). Another example where box models are useful is the investigation of the air quality in street canyons, e.g. the Street Canyon Plume Box model used by Gualtieri, (2010) that computed street level 1-h CO concentrations. Box models have been applied in cities and in larger geographic regions (e.g. Kono & Ito, 1990; Yamartino & Wiegand, 1986; Gifford & Hanna, 1973; Robeson & Steyn, 1990). Box models can also be used to generate information that can be used in more advanced models. 0-D models capture the complexity of the photochemistry, but are constrained by not having transport processes through the box.

One-dimensional (1-D) models are a set of boxes stacked vertically on top of each other to simulate vertical mixing and transport between the boxes. Since the model domain consists of homogeneous layers in the horizontal level, the concentrations are calculated as a function of time, $c_i(t,z)$ and height, (z). The 1-D model captures the effect of vertical transport in addition to photochemical reactions that takes place. An example of where this model was applied was a study conducted by Wang et al. (2000; 2001) where a 1-D model was used to determine nitrogen oxide (NO_x) emissions from snow, based on surface measurements over the South Pole.

Two-dimensional (2-D) models can lie in the *x-y*, *x-z* or *y-z* Cartesian coordinate planes. The advantage of these models compared to 1-D models is that transport can be treated more realistically and larger spatial regions can be simulated utilising a 2-D model (Jacobson, 1999). The species concentrations are also uniform along the third dimension and depend on the remaining dimensions and time, $c_i(x,z,t)$. These models have often been used to describe global atmospheric chemistry assuming that concentrations are a function of latitude and altitude, but not longitude. They can be used to simulate dynamics, transport, gas chemistry and aerosol evolution. An example where a 2-D atmospheric transport equation model was used is Ma (2010) that simulated the long range transport of semi volatile organic compounds from the tropical latitudes to the Arctic.

Three-dimensional (3-D) models are a set of horizontal 2-D models layered on top of one another. The full concentration field is simulated within the 3-D models i.e. concentrations of species as a function of three dimensions, x, y and z, and time, $c_i(x,y,z,t)$. A disadvantage of 3-D models is that they require large amounts of computer-time and central memory resources. 3-D models are used for global, hemispheric or nested simulations. Global climate models can consist of a base model coupled to different sub models describing climate, atmospheric chemistry and economic development processes. Examples of these models are MATCH-MPIC (Lawrence *et al.*, 1999), MESSy (Jockel *et al.*, 2005) andSTOCHEM-HadAM3 (Collins *et al.*, 1997; Stevenson *et al.*, 2004).

The models described above can also be used in conjunction with one another to better understand atmospheric chemistry. Wang et al. (2000; 2007) investigated the observation of large amounts of reactive nitrogen (N) over the Antarctic plateau during a campaign by utilizing a 1-D and 3-D model. The high NO_x emissions resulting from nitrate (NO_3^-) photolysis in snow packs together with active photochemistry lead to significant ozone (O_3) production. The 1-D chemistry-diffusion model was applied to capture the effect of vertical transport and also parameterise the daytime NO_x emissions from snow as a function of wind and temperature. A relative good comparison was found between the modelled emissions and the emission flux aircraft measurements (Wang *et al.*, 2003; Fried *et al.*, 2003; Kondo *et al.*, 2004). The NO_x emissions parameterisation was then employed in the 3-D chemical transport model to study the advection and photochemistry of NO_x snow emissions over the Antarctic Plateau (Wang *et al.*, 2007). The 3-D model simulated the surface NO emissions better than the 1-D model, although it was still under predicted compared to field measurements.

As the model dimension increases the complexity and computational time increase. A specific model needs to be selected depending on the objective of the study. Box models can aid in calculating the material balance over an entire region, to determine the relative contributions of sources, initial conditions and inflow on a region's air quality. A photochemical box model was chosen as the most appropriate investigative tool for this investigation. In the following section the mathematical equations governing a typical box model will be explained. The box model used during this study will also be discussed, as well as improvements that was made to the existing model as part of this study.

4.2.3. Mathematical equations governing box models

As described previously, the box model is seen as one cell within an entire area enclosed in a specific volume as indicated in Figure 4.3. First, it is assumed that air with i species is within a fixed volume with the axis defined as X, Y and H, where H is the box height, while X and Y represents the length and width of the box, respectively. H remains constant, while X and Y are varied ($\Delta X \Delta Y H$). By convention wind with a uniform velocity of u flowing along the X-direction can transport background species into the box. Emissions are emitted in the XY plane of the box.

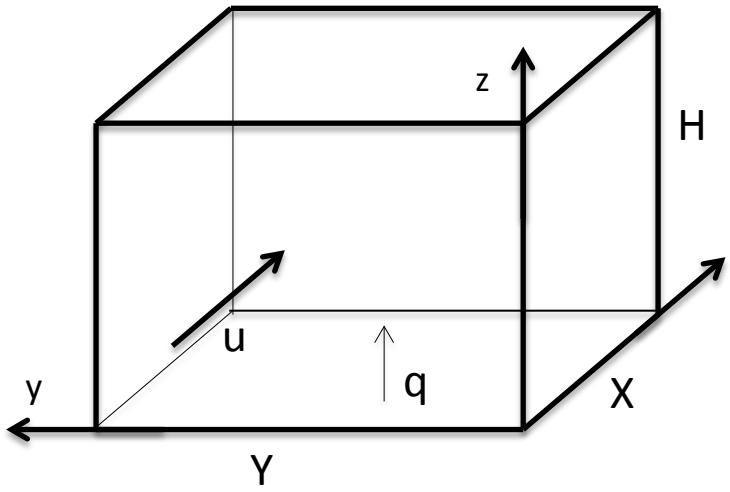

Figure 4.3: Illustration of a typical box model.

The air in the box is instantaneously mixed and therefore the concentration of the species within the box remains uniform. A material balance can then be taken in the box and the concentrations of the species in the box must at any instance satisfy the material balance. The concentration of the species within the box are defined as c_i.

$$\frac{dc_i}{dt} = \frac{q_i}{H} + R_i - \frac{v_{d,i}}{H} c_i + \frac{u}{x}(c_i^o - c_i) \qquad 4.1$$

where

q_i is the mass emission rate of i per area,

R_i is the chemical production rate,

$v_{d,i}$ the dry deposition velocity of specie i,

c_i^o the background concentration,
u the wind speed with a constant direction,
x is the length of the box.

The unsteady accumulation of pollutants are therefore equal to the amount of species advected into the box by the wind; the amount of species advected out of the box; the emissions released in the box and the amount of c_i generated by chemical reactions, as indicated by Equation 4.1.

4.2.4. Development of urban photochemical box models

The first box model successfully developed and used to assess air quality in urban areas was the urban scale photochemical box model (PBM) developed by Schere (1984). The model was a single-cell domain that was applied over the urban area of interest. It had a variable volume and well-mixed reacting cell within which the physical and chemical processes participating in the formation of O_3 could be simulated (Schere, 1984). This model was, however, a simplification of the dispersion processes in a city, since it exhibited limitations in simulating the vertical entrainment and the photolytic rate constants. Therefore it was improved by Jin & Demerjian (1993) who incorporated a 1-D high resolution mixing layer (ML) model to consider the effects of urban heat islands. This improved PBM model proved to be able to predict urban air quality and to provide an improved tool for assessing air quality strategies (Jin & Demerjian, 1993). This PBM model was also effective for the study of rapid physical-chemical processes associated with urban air quality (Uno & Wakamatsu, 1992; Huang *et al.*, 2001).

Since then various other photochemical models have been developed to study the production of O_3 in urban and rural areas (Butler *et al.*, 2011; Kleinman, 1991; Sillman, 1995). Young *et al.* (1997) effectively developed and used a photochemical box model to investigate the best emission control strategy to reduce O_3 levels in Mexico City. O_3 isopleths that illustrates O_3 production as a function of its precursors NO_x and volatile organic compounds (VOCs) can be used to determine whether O_3 formation in the megacity is either NO_x- or VOC-limited. In urban areas with high NO_x concentrations the production of O_3 is limited by the presence of atmospheric VOCs, while the production of O_3 is limited by the availability of NO_x when high levels of atmospheric VOC are present (Sillman, 1999; Kleinman *et al.*, 1997; Butler *et al.*, 2011). Furthermore, Sillman, (1999) and Kleinman et al. (1997) showed that the formation of O_3 from VOC oxidation is related to the number of transformations of NO to NO_2 by peroxy

radicals. Different idealised methods have been applied in models to determine the O_3 production potentials from VOCs (Butler *et al.*, 2011; Capps *et al.*, 2010; Carter, 1994; Derwent *et al.*, 1996).

4.2.5. Modelling from a South African perspective

According to the National Environmental Management: Air Quality Act, 2004 (Act No. 39 of 2004) it is a requirement to use air quality models in decision-making processes and impact studies in South Africa. Although South Africa is still in the early stages of implementing local measures to reduce air pollution in urban areas, good advances in the understanding of air pollution and knowledge of local sources contributing to poor air quality have been made. According to the afore-mentioned act, dispersion modelling is required by governmental and local authorities, as well as industries to ensure that emissions are within allowable limits. Therefore, the main focus from a South African perspective has been on dispersion modelling and not on improvement of processes within these models. However, these models are seldom developed and modified for the unique South African conditions (Fourie, 2006). Most of the dispersion modelling conducted in South Africa is performed with models obtained from America and/or Europe. The chemical mechanisms for most of the dispersion models are limited to the main reactions that participate in O_3 formation.

In order to investigate the interaction of O_3 precursor species in the Jhb-Pta megacity and to determine the possible contribution of areas surrounding the Jhb-Pta megacity, an existing photochemical box model, MECCA (Module Efficiently Calculating the Chemistry of the Atmosphere), was further developed and modified in this investigation. MECCA was modified in other studies to include the Master Chemical Mechanism (MCM) (Bloss *et al.*, 2005; Jenkin *et al.*, 2003), as described in Butler (2009) and Butler et al. (2011). This version is termed MECCA-MCM. Based on the MECCA-MCM model, the new MECCA-MCM-UPWIND version was developed and used in this investigation. In the next paragraphs the MECCA and MECCA-MCM models are described in detail, after which the specifics of the MECCA-MCM-UPWIND version will be presented.

4.3. MECCA BOX MODEL

4.3.1. Model description

MECCA was originally developed by Sander et al. 2005 at the Max-Planck Institute for Chemistry (MPIC) in Mainz, Germany. MECCA is a multi-purpose atmospheric chemistry model that contains chemical mechanisms describing tropospheric and stratospheric chemistry in both the gaseous and aqueous phases (Sander *et al.*, 2005). The MECCA version developed by Sander et al. (2005) includes the basic hydrogen oxides (HO_x), NO_x, O_3 and methane (CH_4) chemistry, as well as the chemistry of non-methane hydrocarbons (NMHCs), halogens (Cl, Br, I), sulphur (S) and mercury (Hg). The model has the flexibility to add chemical mechanisms and is freely available to be used in the scientific community. The programming code that the model is written in is FORTRAN and the model runs on UNIX/Linux platforms. The structure of the MECCA model is showed in Figure 4.4. The model consists of different sub routines that run in sequence with one another during each time step. The sub model MECCA box model which contains all the subroutines within it, the initialization, chemistry-MIM and physics modules rus in in sequence. The physics subroutine update at each time step the model time and physical parameters such temperature, pressure etc. The JVAL routine is for the calculations of the photolysis rate coefficients.

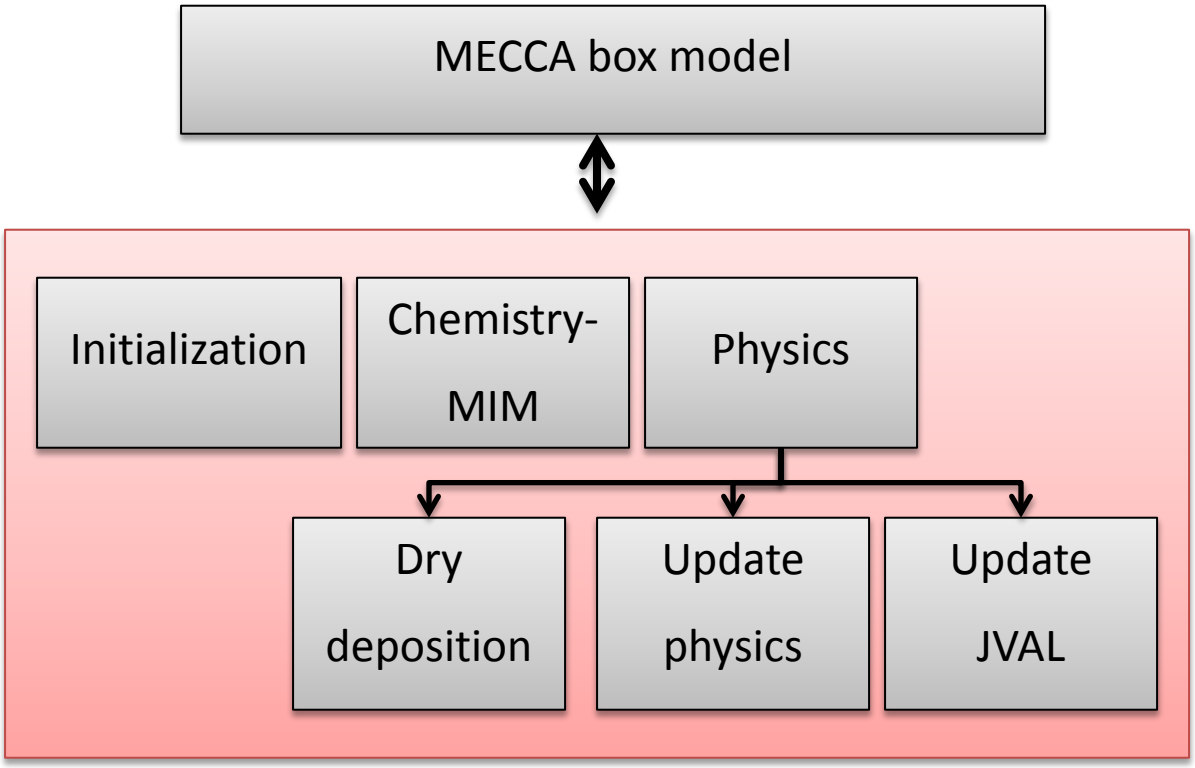

Figure 4.4: Structure of MECCA as a standalone box model.

A model with a comprehensive chemical mechanism requires efficient tools for the computational and simulation of chemical kinetics systems. A major computational challenge is the coexistence of very stable (e.g. CH_4) and very reactive (e.g. exited oxygen O (1D)) species and their impacts on the step size selection in the solvers in the resulting systems of ordinary differential equations (ODEs). The step size is determined by the slope of the differential equation that represents the change in concentration over time. If the slope is flat then the step size is big, while the step size is small if the slope is steep. This complicates the selection in the step size since stable species have a less steep slope than the reactive species. The solution of the differential equations is the modelled answer. Since the concentration of a chemical system evolves in time according to the differential law of mass action kinetics, a computer simulation is required to implement the differential system and its numerical integration in time (Damian *et al.*, 2002). Several software packages have been developed over the past years to integrate these sets of ODEs e.g.

- Facsimile (Curtis & Sweetenham, 1987),
- AutoChem (http://pdfcentral.shriver.umbc.edu/AutoChem/),
- Spack (DJOUAD *et al.*, 2003),
- Chemkin (http://www.reactiondesign.com/products/open/chemkin.html),
- Odepack (http://www.llnl.gov/CASC/odepack/) and
- KPP (the Kinetic PreProcessor) (SANDU & SANDER, 2006).

KPP was chosen as the numerical integrator for MECCA due to the following reasons (Sander *et al.*, 2005);

- the generated chemistry code is suitable for integration into larger models,
- KPP is capable of producing a Fortran 95 code,
- KPP allows a choice of several integrators,
- the code is free.

KPP translates a specification of the chemical mechanism into the computer programming languages Fortran 77, Fortran 90, C or MATLAB simulation codes that implements the concentration time derivative function and its Jacobian matrix, together with a suitable numerical integration scheme. KPP incorporates a library with several widely used chemical integrators, while new integrators can also be added to the library.

4.3.2. Improvements to MECCA

4.3.2.1. MECCA-MCM

MCM was added to the MECCA box model and the MECCA-MCM model was used as described by Butler (2009) and Butler et al. (2011). The chemistry in the original version of MECCA only included limited chemistry of hydrocarbons. The need to investigate the chemical interactions of hydrocarbon species with atmospheric processes required the implementation of the full MCM. The MCM v3.1 (Bloss *et al.*, 2005; Jenkin *et al.*, 2003), obtained via website: http://mcm.leeds.ac.uk/MCM is a near-explicit chemical mechanism that describes the detailed gas-phase chemical processes involved in the atmospheric degradation of a series of primary emitted VOCs. These include a large number of the major species emitted form

anthropogenic activities (hydrocarbons and oxygenated VOCs), based primarily on the speciation defined by the UK National Atmospheric Emissions Inventory (NAEI) (Passant, 2002). It also includes the following primarily emitted biogenic species: isoprene, three monoterpenes (α-pinene, β-pinene, limonene), one sesquiterpene (β-caryophyllene), one oxygenated VOC (2-methyl-but-3-ene-2-ol) and one organosulphur species (dimethyl sulphide, DMS). The resultant mechanism contains about 17000 elementary reactions of 6700 primary, secondary and radical chemical species.

MCM was originally developed to provide accurate, robust and up-to-date information concerning the role of specific organic compounds on ground-level O_3 formation in relation to air quality policy development in Europe. However, it also provides a research tool for investigating other atmospheric processes where a detailed representation of the chemistry is required, e.g. the generation and distributions of speciated radical and stable intermediates formed during VOC degradation. A series of versions of MCM i.e. v1, v2, v3, v3.1 have been updated and improved according to Jenkin et al. (1997); Kenkin et al. (2003); Saunders et al. (2003) and Bloss et al. (2005). MCM also acts as a reference benchmark mechanism to assist the development and/or evaluation of reduced mechanisms that are required for many applications (e.g. Bonn *et al.,* 2004; Jenkin *et al.,* 2008; Poschl *et al.,* 2000; Taraborrelli *et al.,* 2009; Whitehouse *et al.,* 2004). These applications include simulation of chamber (laboratory) and field measurement studies.

The inclusion of the MCM led to a number of coding changes within the MECCA model. KPP had to be adjusted to deal with the size of the chemical mechanisms. An interface was created using input name list files to give the user flexibility to change the species input into the model. A schematic diagram of the MECCA-MCM box model structure is given in Figure 4.5. The model consists of different sub routines that run in sequence with one another during each time step. Two sub models e.g. MECCA box model and MECCA-MCM contains all the subroutines within it, the initialization, chemistry-MCM and physics modules. The physics subroutine update at each time step the model time and physical parameters. All these sub routines run within the MECCA box model sub modules. The chemistry happens within MECCA-MCM and KPP generated routines which uses the species data from the input name list files and includes the species concentration at each time step back into MECCA box model.

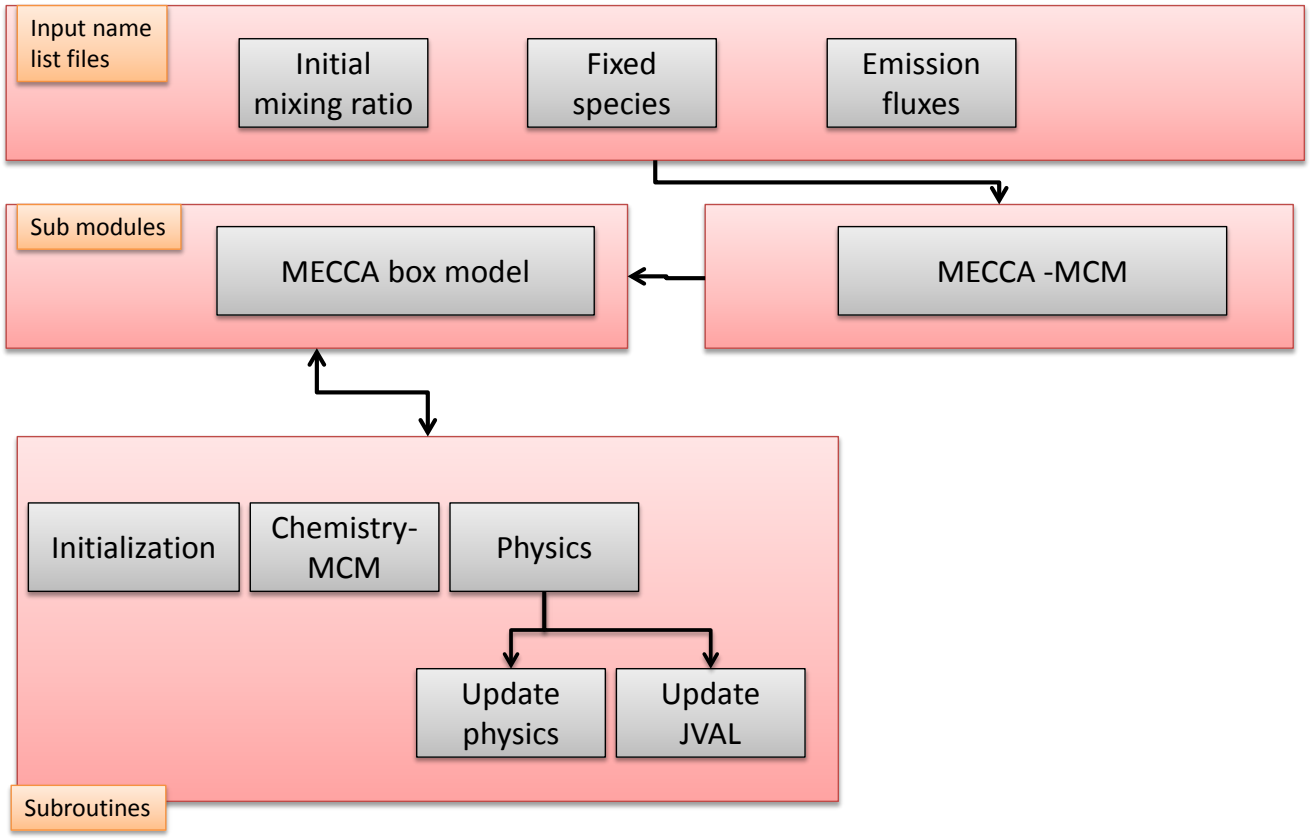

Figure 4.5: MECCA-MCM structure as standalone box model with sub modules and subroutines.

4.3.2.2. MECCA-MCM-UPWIND

MECCA and MECCA-MCM were designed to simulate the photochemical reactions within an idealised, isolated system. In order to accurately study the air quality within a specific urban area, the representation of the model and the ability to simulate the actual environment (Boubel *et al.*, 1994) are very important factors. In this study, the MECCA-MCM model was further improved and modified to better represent the Jhb-Pta megacity and influences of surrounding areas. This updated version is termed the MECCA-MCM-UPWIND model. The improvements made to the MECCA-MCM model in this study included mixing processes such as horizontal

mixing from upwind sources and vertical mixing from the free troposphere. The processes were included as subroutines within MECCA-MCM as indicated in Figure 4.6.

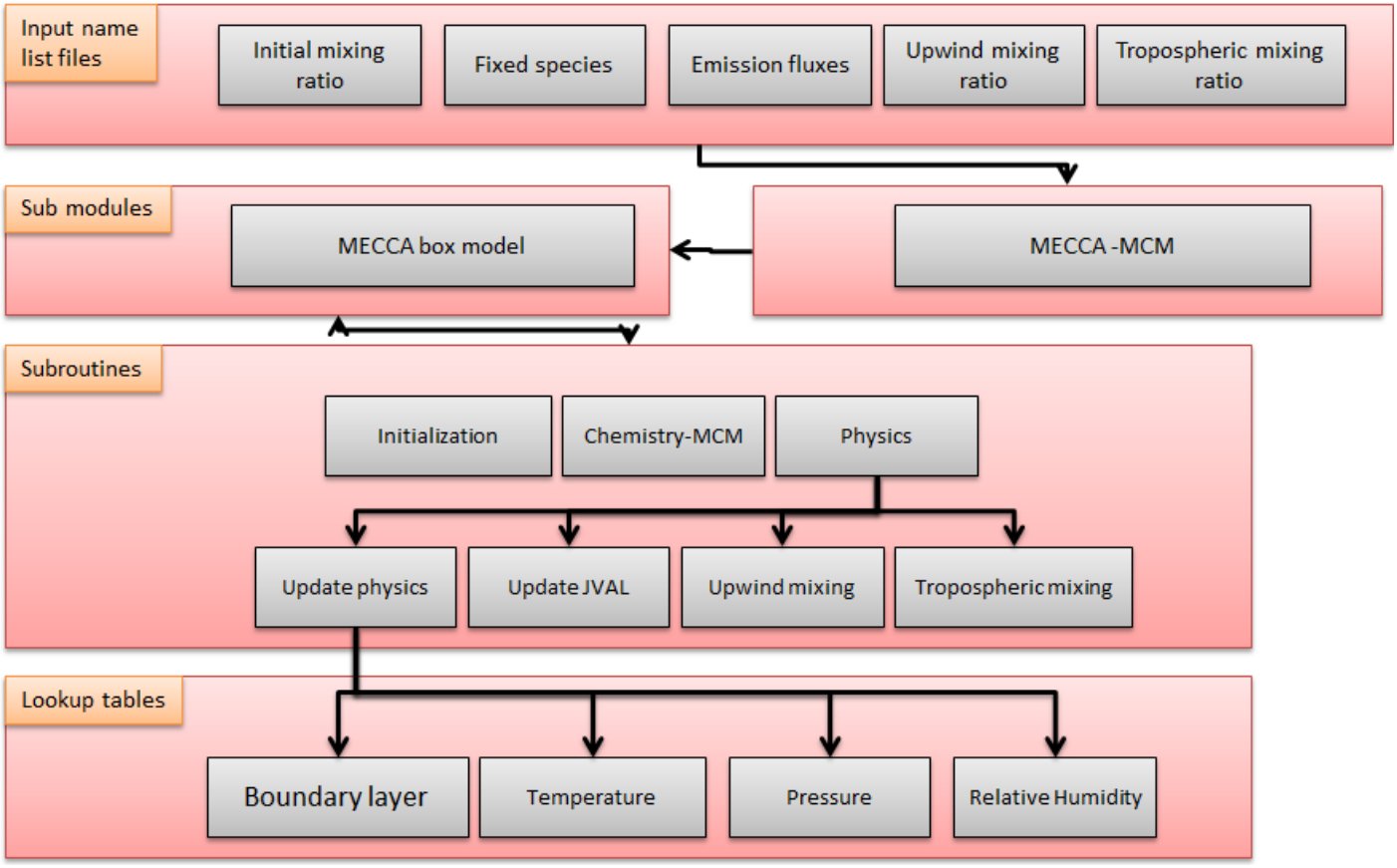

Figure 4.6: MECCA-MCM-UPWIND structure as a standalone box model with sub modules and subroutines.

All the improvements made to MECCA-MCM in the MECCA-MCM-UPWIND model are illustrated in Figure 4.6. The changes were made in the physics subroutine of MECCA-MCM. Meteorological parameters such as pressure, temperature, relative humidity and ML height varies diurnally and seasonally. Therefore a new addition to the model includes lookup tables created for the user to change the input as required for a specific time of day or year. Name list files were also created wherein the concentrations of the species from upwind sources and the free troposphere could be read into, which are included in the model as the Tropospheric mixing ratio and Upwind mixing ratio. These concentrations can be defined and changed by the user.

The model domain is assumed to be well mixed and emissions sources are homogeneously distributed across the bottom surface of the domain. It is therefore assumed that entrainment of air outside the modelling domain occurs laterally by advective transport and vertically by the growth in the mixing layer (Jin & Demerjian, 1993). The horizontal and vertical mixing processes implemented in MECCA-MCM-UPWIND will be explained in subsequent paragraphs. The advection term presented in Equation 4.1 (Section 4.2.3) will also be discussed in more detail within the context of the MECCA-MCM-UPWIND model developed in this study.

Horizontal transport

In Figure 4.7 a schematic illustration of the horizontal mixing scheme is presented. The length of the box is defined as x. Wind transports the upwind species into the box domain, which provides an entrainment of species from the upwind side. It is assumed that wind speed $\boldsymbol{u}$, remains constant throughout the simulations. The x-axis defines the distance of the box. The time step is defined in the third dimension (z-axis) which is not displayed on Figure 4.7 and therefore only illustrated on the x-axis. With each time step the concentration within the box changes and can be defined as the sum of the fraction of the concentration of species advected into the box by the wind plus the fraction of the concentration of species remaining inside the box indicated in Figure 4.7. The fraction of the total box displaced by the advected air mass that change at each time step is $\frac{\mathbf{u\Delta t}}{\mathbf{x}}$, where $\Delta\mathbf{t}$ is the incremental time step and $\Delta\mathbf{x}$ the total length of the box. As the wind transports the species into the box, the fraction of the box with the upwind concentration $\mathbf{C_u}$ increases as the fraction of the box with the initial concentration in the box $\mathbf{C_i}$ decreases up to a stage where all the upwind concentrations is advected through the box providing a dilution rate. The concentration of the species within the box at time step n+1 due to upwind mixing can be expressed as:

$$C_i^{n+1} = \left(\frac{x-u\Delta t}{x}\right) C_i^n + \frac{u\Delta t}{x} C_i^{u,n} \qquad 4.2$$

where

C_i^n is the concentration of the species within the box, e.g. C_{box} in Figure 4.7,

C_{ini} is the initial concentration of the species that is equal to C_{box},

$C_i^{u,n}$ is the concentration of the upwind species transported into the box at time step n,

Δx is the total length of the box,

u is the wind speed and

Δt is the time step $t_{n+1} - t_n$ and is constant.

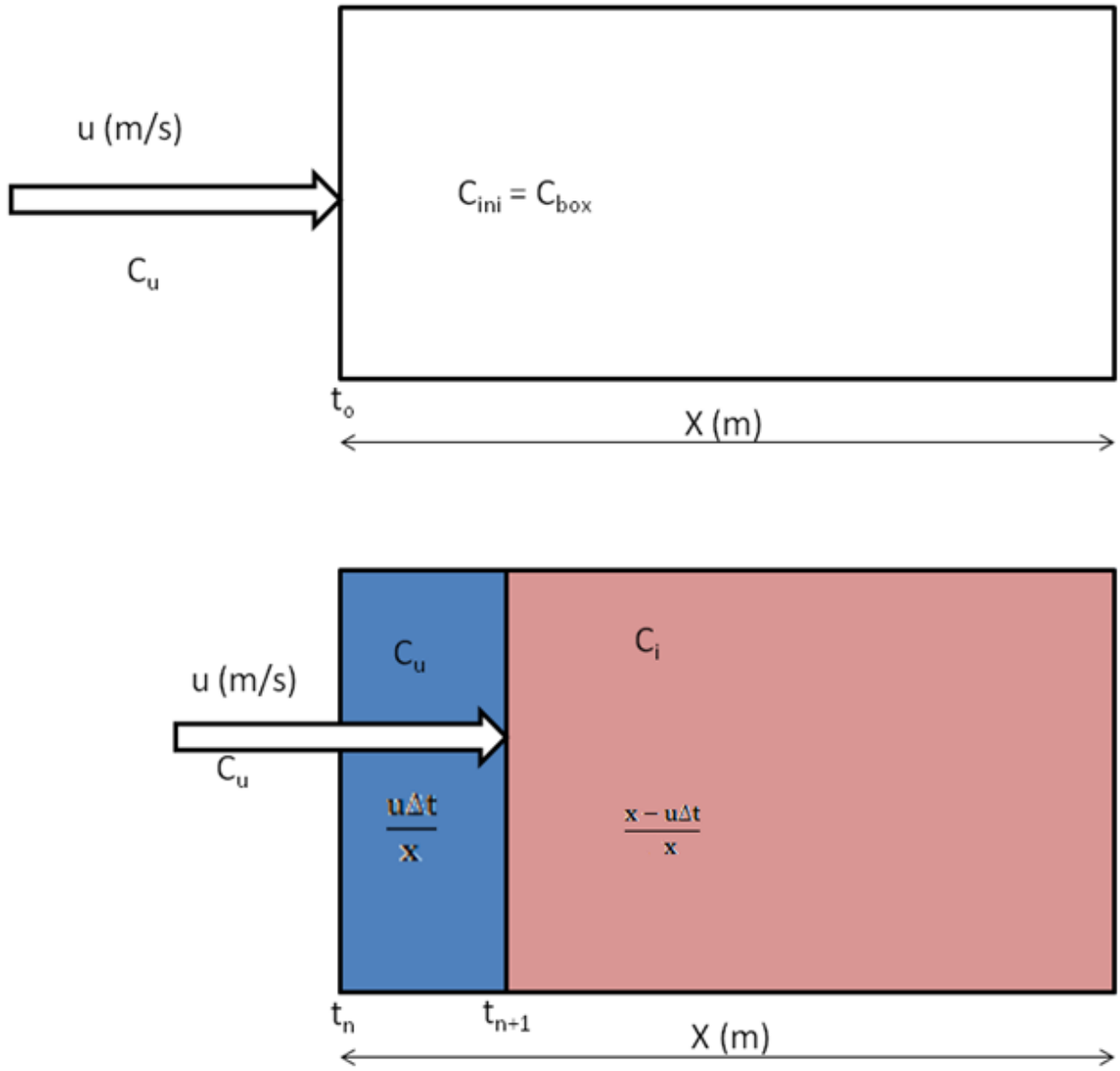

Figure 4.7: Schematic illustration of the horizontal mixing scheme.

Vertical transport

Previous photochemical box model studies have indicated the importance of including vertical entrainment in the model (Jin & Demerjian, 1993). O_3 is often trapped above tropospheric inversion layers present in urban areas at night, which is mixed down to the surface the next morning with the breakup of these layers (Demerjian & Schere, 1979). The atmospheric boundary layer (ABL) is a fundamental parameter characterising the structure of the lower troposphere. With respect to environmental applications and photochemical modelling, the ABL is often referred to as the mixed layer (Beyrich, 1997). This is the height up to which pollutants can be expected to readily mix in the atmosphere. It is also one of the most important parameters governing the horizontal and vertical dispersion of atmospheric pollutants and consequently the concentrations of atmospheric species. Within this study the term mixed layer or mixing layer (ML) will be used. The ML is usually in the order of 1 km, but can vary from a few hundred meters to 3 km (Jacobson, 1999) above the surface of the earth.

The growth rate of the ML controls the vertical entrainment, which have an impact on the concentrations within the modelling domain. It is therefore important to accurately specify the growth rate of the ML within the model. In order to represent the diurnal variability of the ML height in the model, a simplified representation was constructed with monthly measurement data from Preston-Whyte & Diab (1977). For purposes of this study it was sufficient that the ML height was representative of the modelled area and not specific for a particular incident. Therefore the ML for ideal conditions was used as illustrated in Figure 4.8. The ML height was assumed to be constant at an altitude of 400 m during the night-time up until sunrise, after which it increases to 2160 m between 12h-18h during the day.

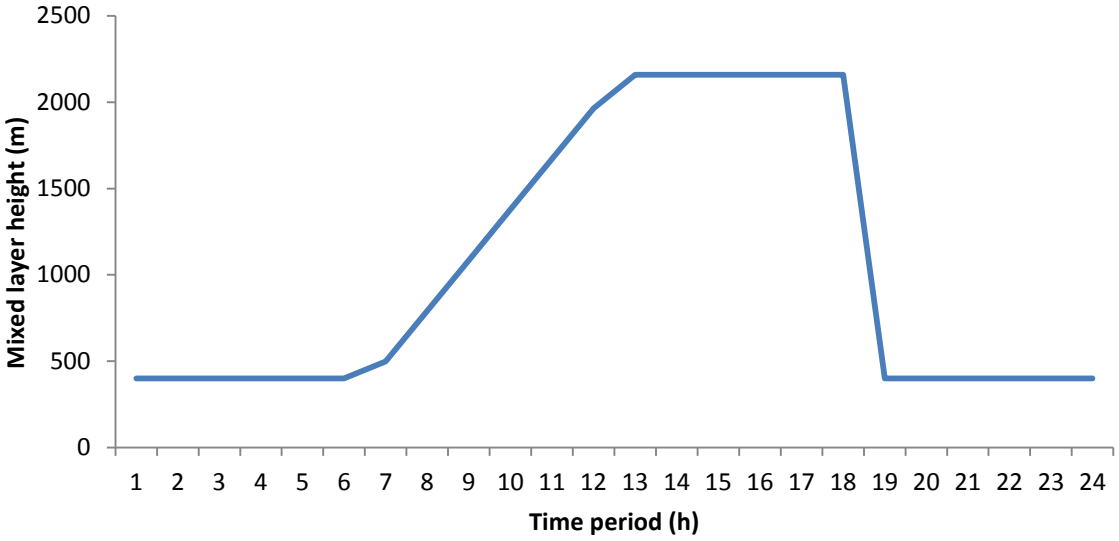

Figure 4.8: Simplified illustration of diurnal growth of the ML.

During the times when the ML is stable there will be no entrainment or dilution from the troposphere and the concentration inside the box should not change between time steps. When the ML increases, the box entrains air from the atmosphere above the layer. The dilution caused by the entrainment will change the concentration C_i, and therefore this process should be included in the model. The concentration within the box will either increase or decrease depending on the concentration of the species in the free troposphere above the ML. The vertical mixing scheme is illustrated in Figure 4.9 below. The area beneath the ML is split into smaller steps illustrating the mixing height (MH) in the box model at each time step. The grey area above the ML represents the concentration of species in the free troposphere. The growth of the MH is specified by the user for each hour and then interpolated for each time step. MECCA-MCM-UPWIND reads the data in from the name list file.

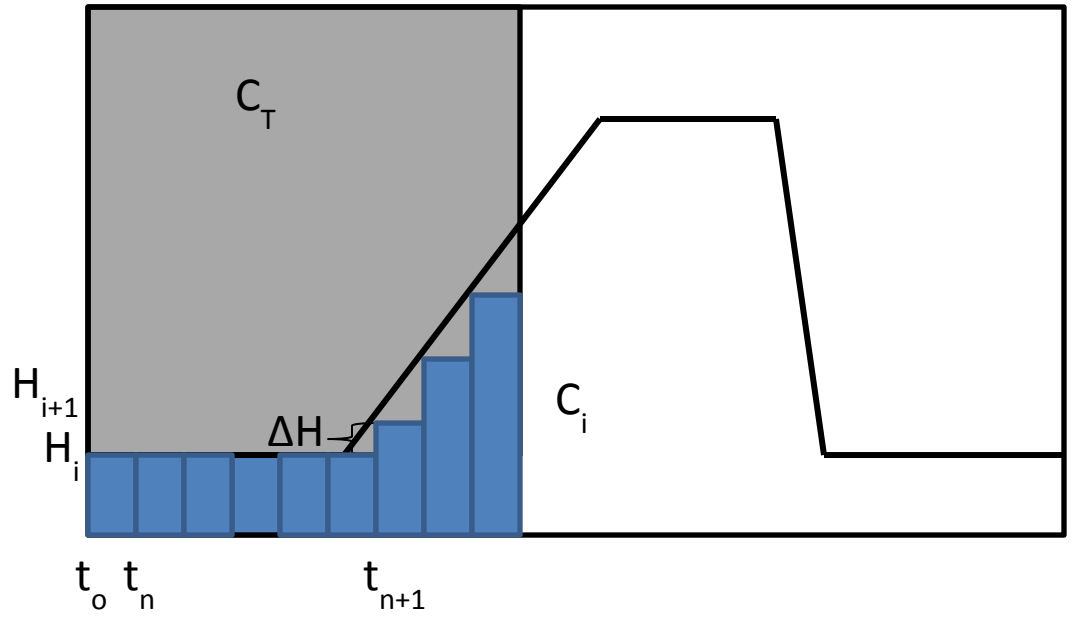

Figure 4.9: Schematic illustration of the vertical mixing scheme.

At time step n the box has a height H, the concentration inside the box is,C_i^n and the concentration above the MH is $\mathrm{C_i^{T,n}}$. After time Δt at time step n+1, the box height H increases to $\mathrm{H} + \Delta\mathrm{H}$. The concentration of species i at time step n+1 can be given by:

$$c_i^{n+1} = \left(\frac{C_i^n * H + C_i^T * \Delta H}{H + \Delta H}\right) \qquad 4.3$$

Where ΔH>=0

When the ML decreases, there is no direct change in the concentration $\mathrm{C_i}$ inside the ML therefore no mixing occurs and the concentration within the box stays the same.

4.4. MODEL TEST AND EVALUATION

Model tests were designed to evaluate the changes made to the model for the purposes of this investigation. The model domain is assumed to be a city with a horizontal dimension of 100 km. The meteorological parameters for atmospheric temperature, pressure and relative humidity, were set at constant values of 284K, 854 Pa and 68%, respectively. Since the modifications made to the model were related to transport and mixing, a relatively chemically inert species, CH_4, was chosen to indicate the responses of the model in order to minimise the effects of chemical reactions on test results. CH_4 has an atmospheric lifetime of approximately 8 years. In order to eliminate any possible reactions with O_3, the chemistry within the model was switched off by setting initial, upwind and tropospheric mixing ratios of O_3 to zero.

The three aspects of the model that were tested were the horizontal upwind mixing, vertical tropospheric mixing and the ML dilution. Although these processes were running in sequence within the model during the tests, they were evaluated separately. The names given to each of the test case studies were:

Test case 1: Upwind mixing
Test case 2: Tropospheric mixing
Test case 3: ML dilution

4.4.1. Test case 1: Upwind mixing

In this test case the impact of changes of wind speed on the time it takes to reach the steady-state concentration was tested. When pollutants are transported horizontally into a city experiencing a constant MH, and the effects of emissions, chemistry, and entrainment or dilution from above are excluded, the species within the city are characterised by the turnover timescale due to upwind mixing. The wind blows in the x direction with speed $\boldsymbol{u}$ (see Figure 4.3). This velocity is constant and independent of time, location and elevation above the surface. In this test case, no additional emissions within the city were added. When higher pollutant concentration enters the city, mixing within the city will occurs as the wind blows the pollutants through the city. After a certain period the pollutant concentration inside the city will approach the pollutant concentration upwind of the city. The change in concentration of a chemical

species over time within the city is equal to the volumetric flow into the city minus the volumetric flow out of the city, which can be presented by the equation

$$\frac{dC}{dt}V = F_{in} - F_{out} \quad (4.4)$$

where

F_{in} and F_{in} = Molar flow rate (mol/s) that is

$$F_{in=}C_{upwind}\left(\frac{mol}{m^3}\right) \times u\ \left(\frac{m}{s}\right) \times Area(m^2)$$

$$F_{out=}C_{box}\left(\frac{mol}{m^3}\right) \times u\ \left(\frac{m}{s}\right) \times Area(m^2)$$

The volumetric flow rate, Q, (m^3/s) is defined as:

$$Q = u\ \left(\frac{m}{s}\right) \times Area(m^2)$$

where

V = volume of the box (m^3)

t = time (s)

Area = the area of the incoming air mass (m^2), which can be solved, yielding the solution

$$C_{box} = C_{initial}e^{-\frac{Q}{V}t} + C_{upwind}(1 - e^{-\frac{Q}{V}t}) \quad (4.5)$$

According to equation 4.5 when the wind speed (u) increases (e.g. Q increase) the exponential term $e^{-\frac{Q}{V}t}$ will decrease causing the C_{upwind} to increase. Therefore the time it takes for the concentration of the pollutant inside the box to reach the upwind pollutant concentration will decrease. Equation 4.5 was used with the input data as chosen in Table 4.2 to mathematically calculate the time it will take to reach C_{upwind} .

Table 4.2: Input data used for test case 1.

Upwind mixing ratio for CH_4 (ppm)	2
Initial mixing ratio for CH_4 (ppm) in box	1.8
Tropospheric mixing ratio for CH_4 (ppm)	-
ML height (m)	1000
Emission flux (molec/cm^2/s)	-
Wind speed (m/s)	0.6, 2, 5

Low (0.6 m/s), medium (2 m/s) and high wind speeds (5 m/s) were used to determine the steady state concentrations of the CH_4 pollutant. The steady-state concentrations calculated from Equation 4.5 are illustrated in Figure 4.10. As indicated in Figure 4.10, the total time for the concentration in the box to approach the upwind concentration due to dilution and mixing within the box calculated with Equation 4.5 for the wind speeds 0.6, 2 and 5 m/s were 171, 51 and 21 hours, respectively, for a city of 100 km in length. For high wind speeds such as 5 m/s the upwind concentration will be reached in less than a day, whereas for low wind speeds the upwind concentration can take up to 8 days to be mixed through the city.

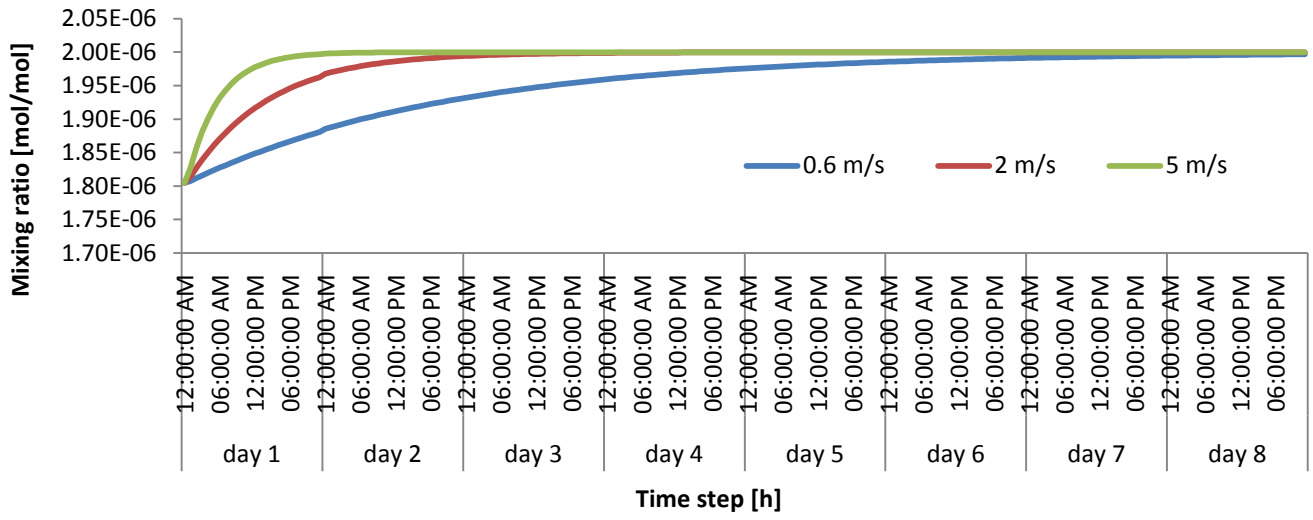

Figure 4.10: Steady state mixing ratio for CH_4 at different wind speeds as calculated with Equation 4.5.

The results obtained from the calculations above were compared to the model run. If the model functioned correctly, then the results presented in Figure 4.10 should be replicated. The results obtained with the improved model (MECCA-MCM-UPWIND) are presented in Figure 4.11. It is evident that similar steady state concentrations were obtained for the different wind speeds calculated with Equation 4. 5, which indicate that the model is behaving as expected. For a wind speed of 0.6 m/s the time to reach steady state (e.g. the upwind pollutant concentration) are at time step 513, which correlate to 7 days. For wind speed of 2 m/s the steady-state concentration was reached after time step 154, i.e. 2.125 days, and for a wind speed of 5 m/s the time step was 60, i.e. less than 1 day.

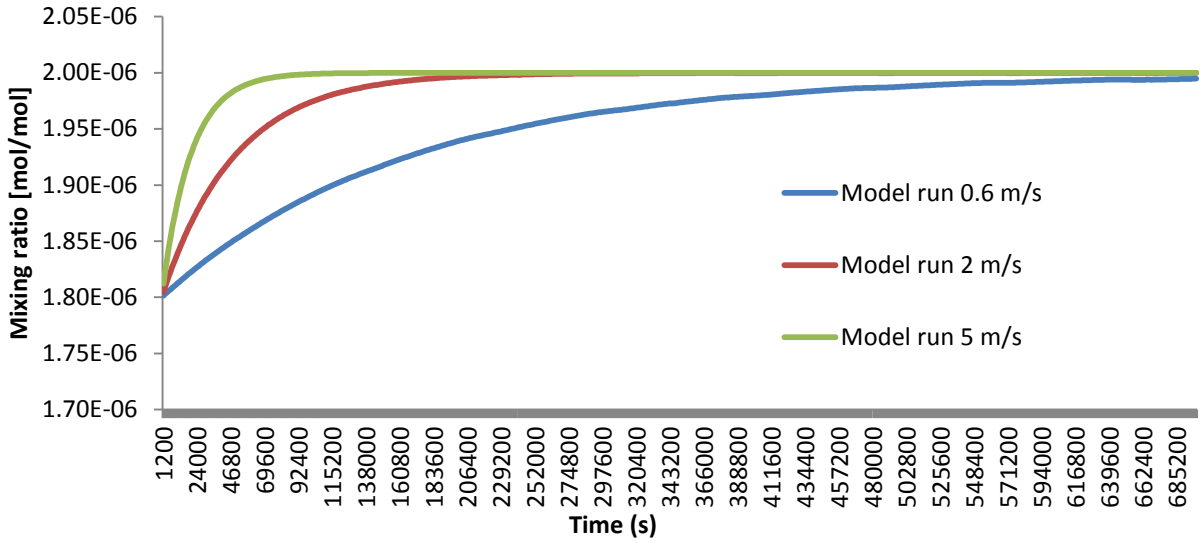

Figure 4.11: Mixing ratios of CH_4 for different wind speeds done by model run.

Test Case 1 shows that care should be taken to determine the wind speed for effective mixing from upwind sources that occurs outside the city. The steady state concentration for CH_4 is reached much faster at higher wind speeds than for the lower wind speeds. Photochemical models, for instance, will be more accurate when light winds occur, since most of the emissions will remain within the cell and species will react, rather than being rapidly transported through the downwind side of the cell (Boubel *et al.*, 1994).

4.4.2. Test case 2: Tropospheric mixing

Entrainment from the free troposphere into the boundary layer as described by Equation 4.2 was tested in this section. In the previous test case the MH height remained constant, while for this test case study the MH was varied in order to determine the effectiveness of the exchange between the ML and the upper troposphere. The MH was changed for each time of the day as indicated in Figure 4.9 and the horizontal upwind mixing was kept constant in this test case.

It was expected that if the mixing ratio of CH_4 above the ML was higher than the CH_4 mixing ratio below the ML, the CH_4 mixing ratio in the city will increase as the ML increases during daytime due to more polluted air being mixed into the city or box. The opposite was expected if the mixing ratio of CH_4 above the ML was set lower than the mixing ratio within the city, with the CH_4 mixing ratio within the city (box) decreasing as the ML height increases due to dilution of CH_4. If the mixing ratio of CH_4 within the ML and above the ML were the same then no change was expected. These three conditions were tested with three scenarios, where the

- mixing ratio of CH_4 above the ML was zero, CH_4 (above) = $C_i^n(0)$.
- the mixing ratio above the ML was equal to the mixing ratio of CH_4 within the box, CH_4 (above) = CH_4 (C_i^n).
- the mixing ratio of CH_4 above the ML was equal to twice the CH_4 mixing ratio in the box, CH_4 (above) = CH_4 (2x C_i^n).

In Table 4.3 the input date used for this test case is listed.

Table 4.3: Input data used for test case 2: tropospheric mixing.

	$C_i^n(0)$	(C_i^n)	(2x C_i^n)
Upwind mixing for CH_4 (ppm)	-	-	-
Initial mixing ratio for CH_4 (ppm)	1	1	1
Tropospheric mixing ratio for CH_4 (ppm)	0	1	2
ML height (m)	Change according to Figure 4.9	Change according to Figure 4.9	Change according to Figure 4.9
Emission flux (molec/cm^2/s)	-	-	--

Wind speed (m/s)	-	-	-

The concentration within the box can be determined if C_{ini}, C_{trop}, as well as V_{ini} and V_{trop} of the box are known. The total volume of the box V_{ss} can be calculated from the initial ML height. The concentration of air was determined from the natural gas law at the selected temperature and pressure. The steady-state concentration C_{ss} is therefore equal to the sum of the initial and tropospheric concentrations, while the steady-state volume V_{ss} is equal to the sum of the initial and tropospheric volumes after the ML increased to the final point.

$$C_{ss}V_{ss} = C_{ini}V_{ini} + C_{trop}V_{trop} \quad 4.6$$

From Equation 4.6 the following equation can be obtained:

$$C_{ss} = \frac{C_{ini}V_{ini}+C_{trop}V_{trop}}{V_{ss}} \quad 4.7$$

When the ML decreases after 18:00 as indicated in Figure 4.8 the air originally inside the box is excluded from the box therefore the total amount of mol in the box change as the volume decrease leaving the concentration C_i constant. The input data from Table 4.3 was used to calculate the steady-state concentrations of CH_4 with Equation 4.7. The results are listed in Table 4.4.

Table 4.4: Results of final concentration values determined with Equation 4.7.

	$\boldsymbol{C_i^n(0)}$	$\boldsymbol{(C_i^n)}$	$\boldsymbol{(2xC_i^n)}$
C_{ini} (molec/m^3)	218	218	218
C_{trop} (molec/m^3)	0	218	436
V_{ini} (m^3 x 10^{18})	4	4	4
V_{trop} (m^3 x 10^{18})	13.6	13.6	13.6
V_{ss} (m^3 x 10^{18})	17.6	17.6	17.6
C_{ss} (molec/m^3)	**49.5**	**218**	**387**
Steady state mixing	**0.23**	**1**	**1.8**

ratio (nmol/mol)

The results calculated for C_{ss} presented in Table 4.4 show the changes in the concentrations of CH_4 within the box that can be expected for the different scenarios. An increase in volume with lower CH_4 concentration above the mixing layer ($C_i^n(0)$ results in dilution within the box. No change in the box concentration is expected when the concentration within the box and above the ML is the same (C_i^n). When the concentration of CH_4 in the troposphere is higher than the mixing ratios inside the box, the CH_4 concentration within the box will increase$(2xC_i^n)$.

These same input data (Table 4.3) used to calculate the steady-state concentrations (C_{ss}) with Equation 4.7 were used in the MECCA-MCM-UPWIND model to test whether the expected mixing ratios were determined with the model. The model was run for one day (24 hours) starting at 00:00. The results obtained with the model are presented in Figure 4.12. The expected pattern for each of the scenarios was obtained with the MECCA-MCM-UPWIND model that indicates that the model was behaving as expected. The concentrations from the model run was calculated to be 48 molec/m^3, 218 molec/m^3 388 molec/m^3 for $C_i^n(0)$, (C_i^n), (2x C_i^n), respectively. These values compared well with the steady-state concentrations calculated with Equation 4.7 and presented in Table 4.4.

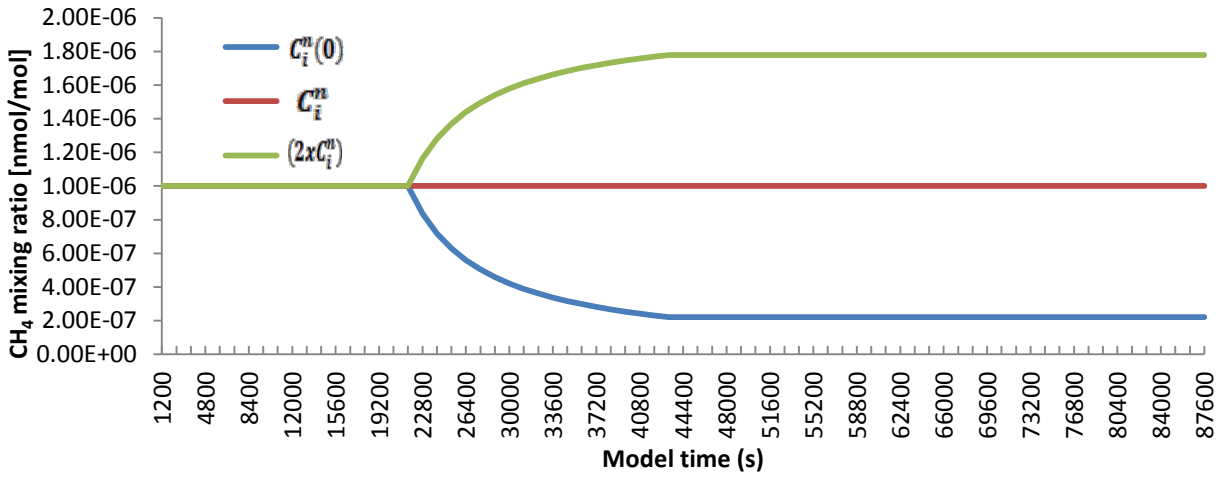

Figure 4.12: Change in modelled CH_4 mixing ratio due to vertical mixing.

4.4.3. Test case 3: ML dilution

The influence of the diurnal ML height variation was tested by investigating the dilution rate of emitted species as the volume of the box changes. In the third test case, the CH_4 emission flux emitted from the surface was kept constant. It was assumed that the concentration of CH_4 is zero within the city and upwind of the city. Therefore no upwind mixing will occur if the wind speed is set to zero. This test case assessed the expected behaviour of dilution of emissions into a changing volume. Input data used is presented in Table 4.5.

Table 4.5: Input data used for test case 3.

Upwind mixing ratio for CH_4 (ppm)	-
Initial mixing ratio for CH_4 (ppm)	-
Tropospheric mixing ratio for CH_4 (ppm)	-
ML height (m)	Change according to Figure 4.9
Emission flux (molec/cm^3/s)	1e9
Wind speed (m/s)	0

With the emission rate, volume and time steps known, the rate of dilution can be mathematically calculated. Initially the ML height stays constant resulting in a constant volume box. The change in concentration of CH_4 during a time step is calculated from

$$\Delta C_{CH4} = \frac{q \times \Delta t}{H} \qquad 4.8$$

where q is the emission flux, Δt is change in time step and H is the ML height at time t_n. Figure 4.14 present the model results from the predicted change in CH_4 concentration for each time step, as well as the volume change over the box, with the x-axis indicating the model time steps.

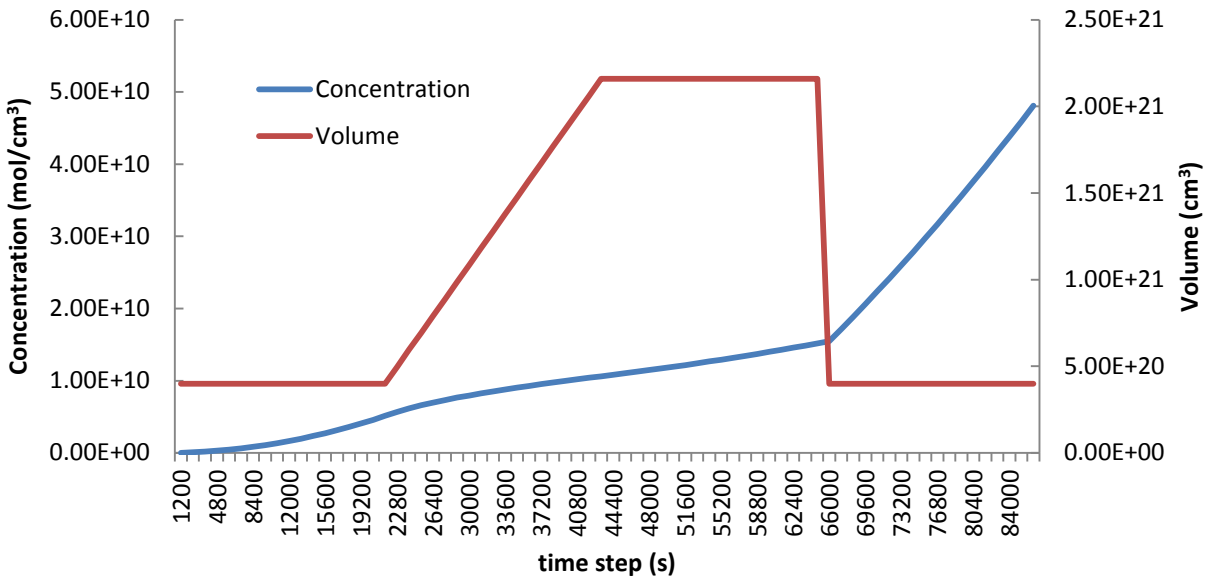

Figure 4.13: Calculations of CH_4 concentration as the volume change over the city with changes in ML height, according to Equation 4.8.

During the morning, when the mixing layer height is constant, the concentration of CH_4 will increase at a constant rate due to the emissions being evenly diluted throughout the box. When the volume of the box increases the rate of dilution will be slower and the atmospheric concentration will therefore increase at a slower rate due to the larger volume to be diluted into. After sunset the ML decreases sharply, decreasing the volume of the box and resulting in a steep increase of CH_4 concentrations with constant emission fluxes of CH_4. These calculations were verified with model runs presented in Figure 4.14. The modelled and results calculated with Equation 4.8 correlated precisely.

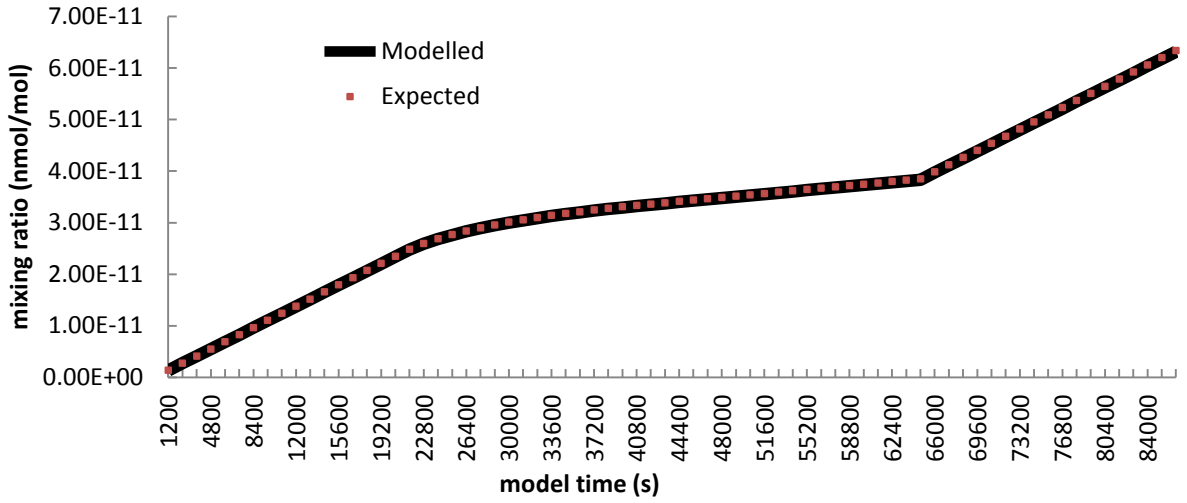

Figure 4.14: The modelled and expected results illustrate the dilution effect of CH_4 within the city with increase in ML height.

4.5. CONCLUSION

Atmospheric modelling in South Africa is still a developing science, with the current main focus being on dispersion modelling. Photochemical box models with a comprehensive chemical scheme are very useful tools to investigate air quality and the chemical processes within a region by investigating the main reactions that participate in O_3 formation.

The existing photochemical box model MECCA-MCM was further developed and improved in this study. This model was named MECCA-MCM-UPWIND, which included horizontal and vertical mixing processes. These processes were included to simulate the advection of upwind air masses into the modelling domain, as well as the entrainment from the troposphere through the diurnal ML height variation. These three processes, i.e. horizontal mixing, vertical mixing and ML height variation included in MECCA-MCM-UPWIND, were tested and evaluated to determine the efficiency of the model to represent atmospheric mixing processes. A chemical inert species, CH_4, was chosen as the test chemical. The chemistry of the model was switched off by setting O_3 to zero.

Horizontal (upwind) mixing was tested by determining the time that it takes atmospheric CH_4 to reach steady-state concentrations at different wind speeds. The calculated and model run estimated the time required to reach steady-state concentration were 171, 51, and 21 hours for 0.6, 2 and 5 m/s wind speeds, respectively. The model therefore simulated the horizontal mixing as expected. Vertical (tropospheric) mixing was tested through the use of three simplified scenarios to determine the dilution or entrainment of CH_4 from above the ML layer. The model run was found to be in good agreement with the results calculated mathematically for each scenario.

The diurnal ML height variation was tested by investigating the dilution rate as the volume of the box changes with constant emission fluxes. The model behaved as predicted and was in good agreement with calculations. Therefore the effect of dilution with changes in the ML height during a day is well determined with the model.

REFERENCE

BLASTING, T.J. 2012. Recent Greenhouse Gas Concentrations. http://cdiac.oml.gov/pns/current_ghg.html Date of access: 15 May 2012.

BLIGNAUT, J.N., CHITTIGA-MABUGU, M.R. & MABUGU, R.M. 2005. Constructing a greenhouse gas emissino inventory using energy balances: the case of South Africa for 998. *Journal of Energy in Southern Africa*, 16(3)

BLOSS, C., WAGNER, V., JENKIN, M.E., VOLKAMER, R., W.J., Bloss, LEE, J.D., HEARD, D.E., WIRTZ, K., MARTIN-REVIEJO, M., REA, G., WENGER, J.C. & PILLING, M.J. 2005. Development of a detailed chemical mechanism (MCM) for the atmospheric oxidation of aromatic hydrocarbons. *Atmospheric Chemistry and Physics*, 5:641-664. 1 March.

BONN, B., VON KUHLMANN, R. & LAWERENCE, M.G. 2004. High contribution of biogenic hydroperoxides to secondary organic aerosol formation. *Geophysical Research Letters*, 31(L10108):1-4.

BOUBEL, R.W., FOX, D.L., TURNER, D.B. & STERN, A.C. 1994. Air pollution Modeling and Prediction. *In*: *Fundamentals of Air Pollution*, 3rd ed. London: Academic Press. 333 p.

BUILTJES, P.J.H. 2001. Air pollution modelling and its applications XIV. New York: Kluwer Academic Publishers.

BUTLER, T. 2009. Automated sequence analysis of atmospheric oxidation pathways: SEQUENCE version 1.0. *Geoscience Model Development*, 2:145-152.

BUTLER, T.M., LAWRENCE, M.G., TARABORRELLI, D. & LELIEVELD, J. 2011. Tagged O3 Production Potential (TOPP) of Volatile Organic Compounds. *Atmospheric Environment*, 45:4082-4090.

CAPPS, S.L., HU, Y. & RUSSEL, A.G. 2010. Assessing Near-Field and Downwind Impacts of Reactivity-based Substututions. *Journal of Air and Waste Menagement Association*, 60:316-327.

CARSLAW, D.C. & BEEVERS, S.D. 2005. Estimations of road vechile primary NO2 exhaust emission fraction using monitoring data in London. *Atmopsheric Environment*, 29:167-177.

CARTER, W. 1994. Development of ozone reacticity scales for volatile organic compounds. *Journal of Air and Waste Mangement Association*, 44:881-899.

CLEMENT, K. & FOSTER, S. 2000. *An investigation into mining as an energy and water using sector and its environmental impacts*.

COLLINS, W.J., STEVENSON, D.S., JOHNSON, C.E. & DERWENT, R.G. 1997. Tropopsheric ozone in a global-scale three-dimesional Lagrangian model and iets response to NOx emission controls. *Journal of Atmospheric Chemistry*, 26:223-274.

CURTIS, A.R. & SWEETENHAM, W.P. 1987. Facsimile/Chekmat User's Manual. *Technical Rep*

DAMIAN, V., SANDU, A., DAMIAN, M., POTRA, F. & CARMICHAEL, G.R. 2002. The Kinetic PreProcessor KPP- A software Environment for Solving Chemical Kinetics. *Computers and Chemical Engineering*, 26:1567-1579.

DERWENT, R., JENKIN, M. & SAUNDERS, S. 1996. Photochemical ozone creation potentials for a large number of reactive hydrocarbons under European conditions. *Atmospheric Environment*, 30:181-199.

DJOUAD, R., SPORTISSE, B. & AUDIFFREN, N. 2003. Reduction of multiphase atmospheric chemistry. *Journal of Atmospheric Chemistry*, 46:131-157.

FOURIE, G.D. 2006. Modelling the long range transport and transformatin of air pollutants over the south african region. Potchefstroom: PhD thesis.

FREEMAN, P.N.W., NAUDE, C.M., PRETORIUS, J., COOVADIA, T. & MATJILA, S.M. 2000. *The transport Sector-Energy use and Environmental Impacts*.

FRIED, A., WANG, Y., WERT, B., WALEGA, J., RIDLEY, B., ATLAS, E., SHETTER, R., LEFER, B., COFFEY, M.T., HANNIGAN, J., BLAKE, D., BLAKE, N., MEINARDI, S., TALBT, B., DIBB, J., SCHEUER, E., WINGENTER, O., SNOW, J., HEIKES, B. & EHHALT, D. 2003. Tunable diode laser measuremets of formaldehyde during the TOPSE 2000 study: Distrubtions, trends, and model comparisons. *Journal of geophysical Research*, 108:8365-8387.

GAFFEN, M., NAUDE, C., LOMBAARD, P., MASSDORP, G., TAYLOR, A. & PRETORUIS, J. 2000. *A Quantitive analysis of full cost associated with motor vehicle use in South Africa*.

GIFFORD, F.A. & HANNA, S.R. 1973. Modelling urban air pollution. *Atmospheric Environment*, 7:131-136.

GONZALEZ ABAD, G., ALLEN, N.D.C., BERNATH, P.F., BOONE, C.D., MCLEOD, S.D., MANNEY, G.L., TOON, G.C., CAROUGE, C., WANG, Y., WU, S., BARKLEY, M.P., PALMER, P.I., XIAO, Y. & FU, T.M. 2011. Ethane, ethyne and carbon monoxide concentrations in the upper troposphere and lower stratosphere from ACE and GEOS-ChemPa comparison study. *Atmopsheric Chemistry an Physics*, 11:9927-9941.

GUALTIERI,. 2010. A street conyon model intercomparison in Florence, Italy. *Water air and soil pollution*, 212(1-4):461-482. Oct.

HONORE, C., VAUTARD, R. & BEEKMANN, M. 2000. Low and high NOx chemical regimes in an urban environment. *Environmental Modelling and Software*, 15:559-564.

HUANG, H., AKUSTU, Y., ARAI, M. & TAMURA, M. 2001. Analysis of photochemical pollution in summer and winter using a photochemical box model in the center of Tokyo, Japan. *Chemosphere*, 44:223-230.

HURLEY, P. 2002. *The Air Pollution Model (TAPM) Version 2. Part 1: Technical Description*.

ISAKSEN, I.S.A., HESSTVEDT, E. & HOV, O. 1987. A chemical model for urban plumes: Test for ozone and particulate sulphur formation in St. Louise urban plume. *Atmopsheric Environment*, 32:279-289.

JACOBSON, M.Z. 1999. Fundamentals of Atmospheric modeling. Cambridge University.

JENKIN, M.E., SAUNDERS, S.M. & PILLING, M.J. 1997. The tropospheric degradation of volatile organic compounds: a protocol for mechanism development. *Atmospheric Environment*, 31(1):81-104.

JENKIN, M.E., SAUNDERS, S.M., WAGNER, V. & PILLING, M.J. 2003. Protocol for the development of the Master Chemical Mechanism, MCM v3 (Part B): tropospheric degradation of aromatic volatile organic compounds. *Atmospheric Chemistry and Physics*, 3:181-193. 12 February.

JENKIN, M.E., WATSON, L.A., UTEMBE, S.R. & SHALLCROSS, D.E. 2008. A common Representative Intermediates (CRI) mechanism for VOC degradation. Part 1: Gas phase mechanism development. *Atmospheric Environment*, 42(31):7185-7195.

JIN, S. & DEMERJIAN, K. 1993. A photochemical box model for urban air quality study. *Atmospheric Environment*, 278(1):371-387. 3 July.

JIN, S. & DEMERJIAN, K. 1993. A photochemical box model for urban air quality study. *Atmospheric Environment*, 278(1):371-387. 3 July.

JOCKEL, P., SANDER, R., KERKWAG, A., TOST, H. & LELIEVELD, J. 2005. Technical Note: The Modular Earth Submodel System (MESSy):a new approach towards Earth System Modelling. *Atmospheric Chemistry and Physics*, 5:433-444.

KLEINMAN, L.I. 1991. Seasonal dependence of boundary layer peroxide concentration: the low and high NOx regimes. *Journal of Geophysical Research*, 96:20721-20733.

KLEINMAN, L.I. 2005. The dependence of tropospheric ozone production rate on ozone precursors. *Atmospheric Enivornment*, 39:575-586.

KLEINMAN, L., DAUM, P., LEE, J., LEE, Y., NUNNERMACKER, L., SPRINGSTON, S., NEWMAN, L., WEINSTEINLLOYD, J. & SILLMAN, S. 1997. Dependence of ozone production on NO and hydrocarbons in the troposphere. *Geophysical Research Letters*, 39:575-586.

KONDO, Y., NAKAMURA, K., CHEN, G., TAKEGAWA, N., KOIKE, M., MIYAZAKI, Y., KITA, K., CRAWFORD, J., KO, M., BLAKE, D.R., KAWAKAMI, S., SHIRAI, T., LILEY, B., WANG, Y. & OGAWA, T. 2004. Photochemistry of ozone over the western Pacific from winter to spring. *Journal of Geophysical Research Atmospheres*, 109:D23S02.

KONO, H. & ITO, S. 1990. A micro-scale dispersion model for motor vechile exhaust gas in urban area- OMG VOLUME-SOURCE model. *Atmospheric Environment*, 24B:243-251.

KU, J.Y., RAO, S.T. & RAO, K.S. 1987. Numerical simulations of air pollution in urban areas: Model development. *Atmospheric Environment*, 21:201-232.

KU, J.Y., RAO, S.T. & RAO, K.S. 1989. A comparison study of three urban air pollutoin models. *Atmospheric Environment*, 23:793-801.

LAMARQUE, J-F, BOND, T.C., EYRING, V., GRANIER, C., HEIL, A. & AL, et. 2010. Historical (1850-2000) gridded anthropogenic and biomass burning emissions of reactive gases and aerosols: methodology and application. *Atmospheric Chemistry and Physics*, 10:7017-7038.

LAWRENCE, M.G., CRUTZEN, P.J., RASH, P.J., EATON, B.E. & MAHOWALD, N.M. 1999. A model for studies of tropospheric photochemistry: Description, global distribution, and evaluations. *Journal of Geophysical Research*, 104:26,245-26,277.

LIEBENBERG-ENSLIN, H. 2008. *A review of existing Information on Air Quality issues related to vehicle emissions in South Africa*. Johannesburg.

LLOYD, P., RUKATO, H. & SWANEPOEL, R. *Liquied fuels prodcution*.

MA, J. 2010. Part1: 2-D modelling in the mean atmosphere. *Atmospherc Chemistry and Physics Discussion*, 10:453-489.

MCRAE, G.J., GOODIN, W.R. & SEINFELD, J.H. 1982. Development of a second-generation mathematical model for urban air pollution- I model formulation. *Atmospheric Environment*, 16:679-696.

MOSCHONAS, M., GLAVAS, S. & KOUIMTZIS, T. 2001. C3 to C9 hydrocarbon measurements in the two largest cities of Greece, Athens and Thessaloniki. Calculations of hydrocarbon emissions by species.Derivation of hydroxyl radical concentrations. *The Science of the Total Environment*, 271:117-133.

POSCHL, U., VON KUHLMANN, R., PIOSSON, N. & CRUTZEN, P.J. 2000. Development and Intercomparison of Condensed Isoprene Oxidation Mechanisms for Global Atmospheric Modeling. *Journal of Atmospheric Chemistry*, 37:29-52.

ROBESON, S.M. & STEYN, D.G. 1990. Evaluation and comparison of statistical forecast models for daily maximum ozone concentrations. *Atmospheric Environment*, 24B:303-312.

SALBY, M.L. 1996. Fundaments of Atmospheric Physics. Academic Press.

SANDER, R., A., Kerkweg, JOCKEL. & LELIEVELD, J. 2005. Technical note: The new comprehensive atmospheric chemistry module MECCA. *Atmospheric Chemistry and Physics*:445-450.

SANDER, R., BAUMGAERTNER, A., GROMOV, S., HARDER, H., JOCKEL, P, KERKWAG, A., KUBISTIN, D., REGELIN, E., RIEDE, H., SANDU, A., TARABORRELLI, D., TOST, H. & XIE, Z.-Q. 2011. The atmospheric chemistry box model CAABA/MECCA-3.0. *Geophysic model development*, 4:373-380. 19 January.

SANDER, R., KERKERG, A., TOST, H., LELIEVELD, J. & JÖCKEL, P. 2005. Techincal Note: The Modular Earth Submodel System (MESSy)-a new approach towards Earth System Modeling. *Atmospheric Chemistry and Physics*:433-444.

SANDU, A. & SANDER, R. 2006. Technical note: Simulating chemical systems in Fortran90 and Matlab with the Kinetic PreProcessor KPP-2.1. *Atmospheric Chemistry and Physics*, 6:187-195.

SAUNDERS, S.M., JENKIN, M.E., DERWENT, R.G. & PILLING, M.J. 2003. Protocol for the development of the Master Chemical Mechanism, MCM v3 (Part A): tropospheric degradation of non-aromatic volatile organic compounds. *Atmosheric Chemistry and Physics*:161-180.

SCHERE, K.L. & Demerjian, K.L. 1984. *User's Guide for the Photochemical Box Model (PBM)*. Triangle park, NC.

SCORGIE, Y., ANNEGARN, H.J. & BURGER, L.W. 2004a. *Fund for research into industrial development growth and equity(FRIDGE). Study to examine the potential socio-econmic impact of measures to reduce air pollution from combustion.* Pretoria.

SCORGIE, Y., ANNEGARN, H.J. & BURGER, L.W. 2004b. *Fund for research into industrial development growth and equity(FRIDGE). Study to examine the potential socio-economic impact on measures to reduce air pollution from combustion*. Pretoria.

SCORGY, Y., ANNEGARN, H.J. & BURGER, L.W. 2004c. *Fund for research into industrial development growth and equity(FRIDGE). Study to examine the potential socio-economic impact on measures to reduce air pollution from combustion*. Pretoria.

SEINFELD, J.H., Pandis, S.N. 1998. Atmospheric Chemistry and Physics: from air pollution to climate change. New York: Wiley.

SILLMAN, S. 1995. New developments in understanding the relation between ozone, NOx and hydrocarbons in urban atmosphere. *Advance series in physical chemistry*:145-171.

SILLMAN, S. 1999. The relation between ozone, NOx and hydrobarbons in urban and polluted rural environments. *Atmospheric Environment*, 33:1821-1845.

SPALDING-FECHER, R., OKESE, D., EBERHART, R. & DAVIS, M. 2000. *Electricity production and the environment*.

SPORTISSE, B. 2008. Fundamentals in Air Pollution: From Processes to Modelling. France: Springer.

SRIVASTAVA, A. & PADMA S. RAO, B. 2011. Urban air Pollution Modeling. *In*: MAZZEO, Nicolas, ed. *Air Quality- Models and Applications*, ISBN 978-953-307-307-1 ed. InTech.

STEINBACHER, M., ZELLWEGER, C., SCHWARZENBACH, B., BUGMANN, S., BUCHMANN, B., ORDONES, C., PREVOT, A.S.H. & HUEGLIN, C. 2007. Nitrogen oxide measurements at rural sites in Switzerland: Bias of conventional measurement techniques. *Journal of Geophysical Research*, 112(D11307)

STEVENSON, D.S., DOHERTY, R.M., SANDERSON, M.G., COLLINS, W.J., JOHNSON, C.E. & DERWENT, R.G. 2004. Radiative forcing from aircraft NOx emissions: mechanisms and seasonal dependence. *Journal of Geophysical Research*, 109:D17307.

STOHL, A. 2002. 1 vols. Computation, accuracy and applications of trajectories - A review and bibliography. *In*: AUSTIN, J., BRIMBLECHOMBE, P. & STURGES, W., eds. *Air pollution science for the 21st century*, Kidlington: Elsevier Sience Ltd. 615-620 p.

TARABORRELLI, D., LAWRENCE, M.G., BUTLER, T.M., SANDER, R. & LELIEVELD, J. 2009. Mainz Isoprene Mechanism 2 (MIM2): an isoprene oxidation mechanism for regional and global atmospheric modelling. *Atmospheric Chemistry and Physics*, 9:2851-2777.

TYSON, P.D., PRESTON-WHYTE, R.A. & DIAB, R.D. 1976. Towards an invesion climatology of Southern Africa: Part1, Surface inversions. *South African Geographical Journal*, 58(2):151-163.

UNO, I. & WAKAMATSU, S. 1992. Analysis of wintertime high concentration of NO2 using a photochemical box model. *Journal of Japanese Society Air Pollution*, 27:246-257.

VAN LEEUWEN, C.J. & IERMENS, M. 1995. Risk assessment of chemicals: an introduction. Springer.

VENKATRAM, A., SHUMING, D., HARIHARAN, R., CARTER, W. & GOLDSTEIN, R. 1998. The concept of species age in photochemical modeling. *Atmospheric Environment*:3403-3413.

WANG, Y., CHOI, Y., ZENG, T., DAVIS, D., BUHR, M., HUEY, L.G. & NEFF, W. 2007. Assessing the photochemical impact of snow NOx emissions over Antarctica during ANTCI 2003. *Atmospheric Environment*, 41:3944-3958.

WANG, Y., LIU, S.C., WINE, P.H., DAVIS, D.D., SANDHOLM, S.T., ATLAS, E.L., AVERY, M.A., BLAKE, D.R., BLAKE, N.J., BRUNE, W.H., HEIKES, B.G., SACHSE, G.W., SHETTER, R.E., SINGH, H.B., TALBOT, R.W. & TAN, D. 2001. Factoris controlling tropospheric O_3, OH, NOx and SO2 over the tropical Pacific during PEM-Tropics B. *Journal of Geophysical Research*, 106(D23):32733-32747.

WANG, Y., LIU, S.C., YU, H., SANDHOLM, S.T., CHEN, T.Y. & BLAKE, D.R. 2000. Influence of convection and biomass burning outflow on tropospheric chemistry over the tropical Pacific. *Journal of Geophysical Research Atmospheres*, 105(D7):9321-9333.

WANG, Y., RIDLEY, B., FRIED, A., CANTRELL, C., DAVIS, D., CHEN, G., SNOW, J., HEIKES, B., TALBOT, R., DIBB, J., FLOCKE, F., WEINHEIMER, A., BLAKE, N., BLAKE, D., SHETTER, R., LEFER, B., ATLAS, E., COFFEY, M., WALEGA, J. & WERT, B. 2003. Springtime photochemistry at northen mid and high latitudes. *Journal of Geophysical Research Atmospheres*, 108:8358-8390.

WHITEHOUSE, L.E., TOMLIN, A.S. & PILLING, M.J. 2004. Systematic reduction of complex tropospheric chemical mechanisms, Part I: sensitivity and time-scale analyses. *Atmospheric Chemistry and Physics*, 4:2025-2056.

WHITEHOUSE, L.E., TOMLIN, A.S. & PILLING, M.J. 2004. Sytematic reduction of complex tropospheric chemical mechanisms, Part II: Lumping using a time-scale based approach. *Atmospheric Chemistry and Physics*, 4:2057-2081.

YAMARTINO, R.J. & WIEGAND, G. 1986. Development and evaluation of simple models for the flow, turbulence and pollutant concentration fields within an urban street canyon. *Atmospheric Environment*, 20:2137-2156.

ZANNETTI, P. 1990. Air Pollution Modelling Theories, Computational Methods and Available Software. Southampton: Computational Mechanics Pulblication.

Graphical layout of Chapter 5

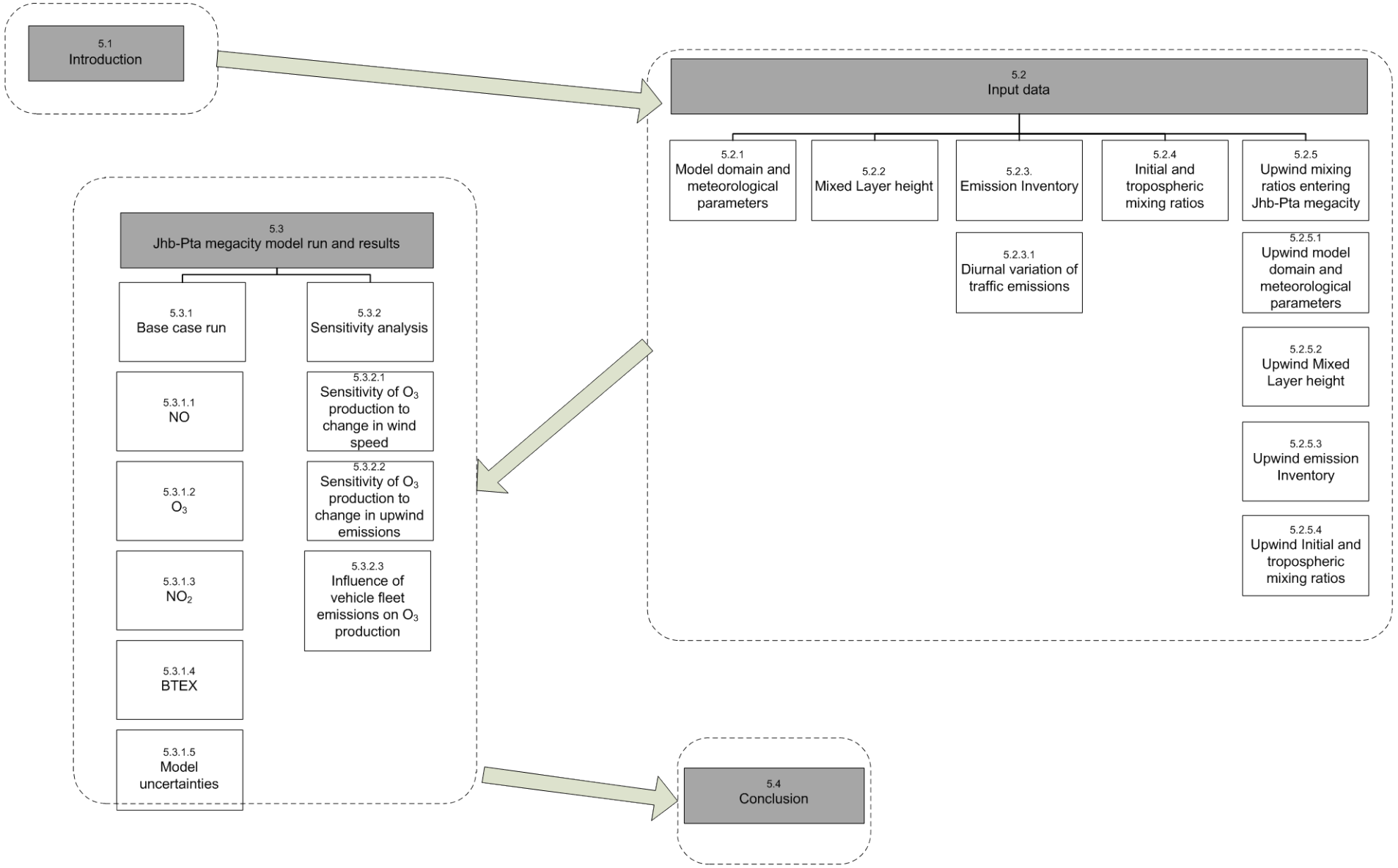

Chapter 5

Model results

5.1 INTRODUCTION

As discussed in the previous chapter, the MECCA-MCM-UPWIND model was developed based on the MECCA-MCM model. This improvement was done in order to facilitate the modelling of air quality in the Jhb-Pta megacity. In this chapter, the MECCA-MCM-UPWIND model will be used to calculate scenarios based on parameters that could potentially be altered in the future to mitigate air pollution in the Jhb-Pta megacity. This chapter is divided into two main sections, i.e. a description of the input data required for the model and the modelling results and sensitivity analyses.

The meteorological data, mixing layer (ML) growth, pollutant emissions and pollutant mixing ratios were required as input data for the model. The mixing ratio input data required were the initial, tropospheric and upwind mixing ratios. The initial and tropospheric mixing ratios could be obtained from ground-based measurements and published global model runs, while the composition of the upwind mixing ratios, i.e. the air mass advected into the Jhb-Pta megacity, were determined by running the MECCA-MCM-UPWIND model with representative data for the Mpumalanga Highveld.

5.2 INPUT DATA

5.2.1 Model domain and meteorological parameters

The model domain was selected to be 100km x 100km, which included the Jhb-Pta megacity, as well as the surrounding areas. The model domain is indicated by the rectangular block in the magnified area in Figure 5.1.

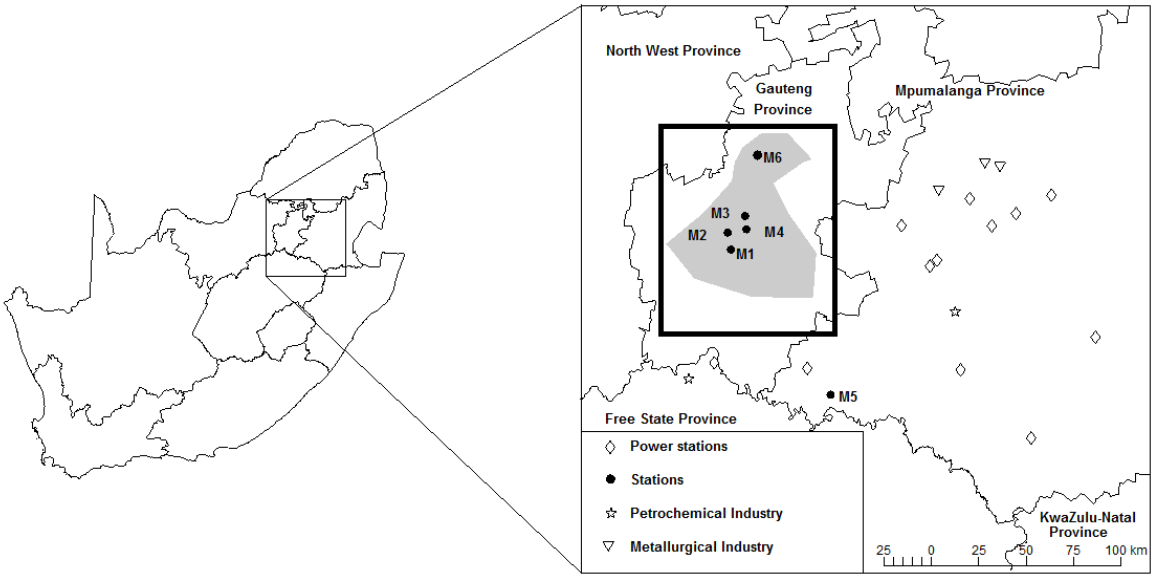

Figure 5.1: Model domain investigated, with the sampling stations in the Jhb-Pta megacity also shown; the Jhb-Pta megacity is indicated by the shaded grey area

From the five measurement stations located within the model domain, only three stations were conducting continuous meteorological measurements. Meteorological data from the other two stations, which only measure meteorological data, were unavailable due to maintenance. Meteorological data obtained from these three measurement stations were averaged over a three-month period (March-May) in 2009 to determine the diurnal variability of meteorological parameters in the Jhb-Pta megacity. According to this data, the average atmospheric pressure, temperature and relative humidity for autumn (March-May) in the Jhb-Pta megacity ranged between 285-295K, 84.3-84.6hPa and 40-80%, respectively. The diurnal patterns of this meteorological data are presented in Figures 5.2 and 5.3.

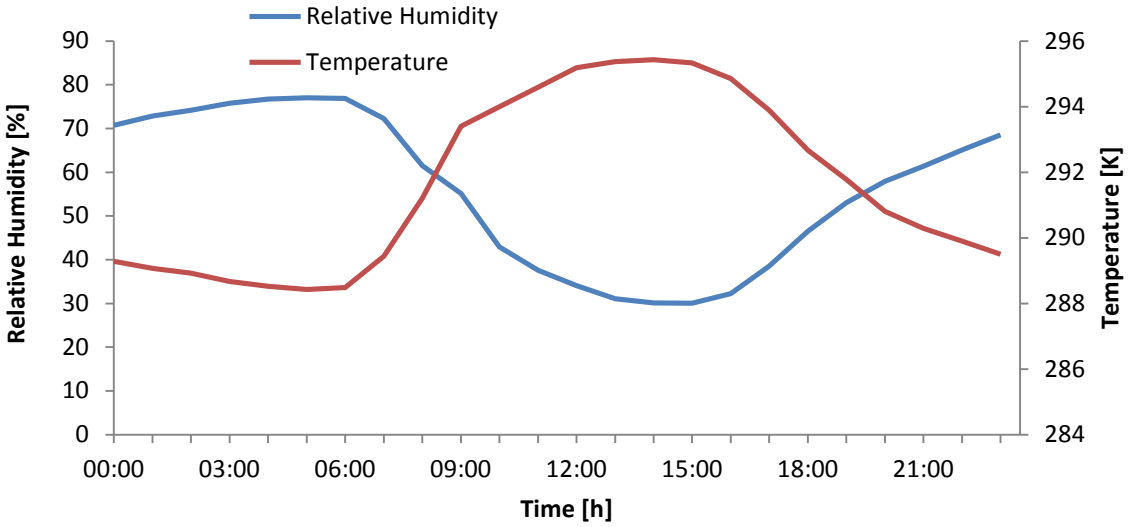

Figure 5.2: Average diurnal variation of the atmospheric temperature and relative humidity for the Jhb-Pta megacity during autumn (March-May)

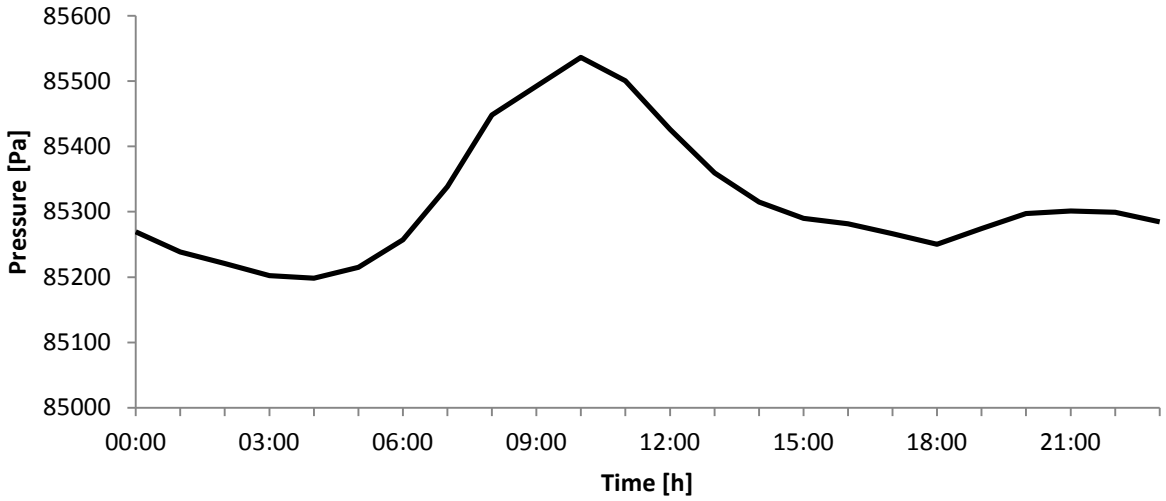

Figure 5.3: Average diurnal variation of atmospheric pressure for the Jhb-Pta megacity during autumn (March-May)

5.2.2 Mixing layer height

The atmospheric mixing layer (ML) can be determined from remote sensing instruments, upper atmospheric data or routinely measured meteorological data. In this study, none of the aforementioned data were available for the Jhb-Pta megacity to derive the ML. A validated meteorological model can also be used to estimate the ML if other types of measurement data are not available. Therefore, The Air Pollution Model (TAPM) (Hurley, 2002) was used to calculate the ML. TAPM is a prognostic dispersion model used to calculate pollutant species concentrations. The meteorological module in the model uses prognostic equations, which include momentum equations for horizontal wind components, scalar equations for potential virtual temperature and specific humidities of water vapour, cloud water and rain water, as well as values for turbulent kinetic energy and eddy dissipation rates (Hurley, 2002). TAPM was utilised to simulate surface and upper atmospheric meteorological data from 2004 to 2009 at a 2.5 x 2.5km resolution using synoptic scale meteorology (longitude/latitude grid at 1° grid spacing, for approximately 100km). Input data for TAPM was obtained from the US National Centre for Atmospheric Research (NCAR) (Fourie, 2009). The average diurnal ML for three months (March-May) for the Jhb-Pta megacity was determined over the five consecutive year period, which is presented in Figure 5.4.

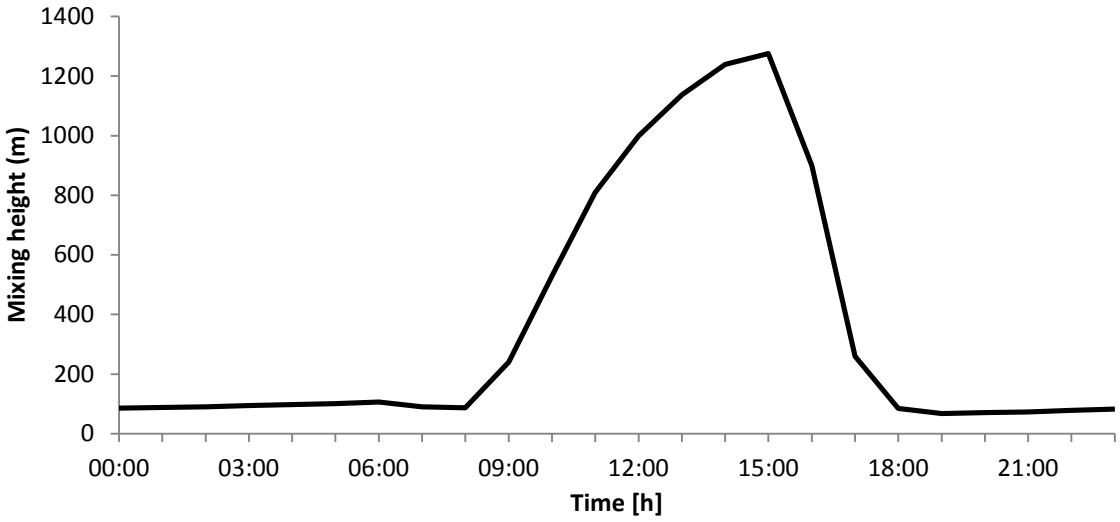

Figure 5.4: Average five-year (2004-2009) diurnal ML height obtained from TAPM for autumn (March-May) for the Jhb-Pta megacity

5.2.3 Emission inventory

South Africa does not currently have a comprehensive gridded national inventory for sources of atmospheric emissions, which complicated the acquisition of emission data to be used in the model. Detailed emission data does, however, exist for specific regions. These datasets were mostly obtained through research initiatives, e.g. SAFARI 2000, by metropolitan councils or by private companies on behalf of major industries. Although some data is held in open access databases (Sowden, 2007), data is often difficult to access. The disadvantages of these emission inventories available for South Africa are that these studies were all based on different methodologies, time periods and source literature, which make these datasets inconsistent with one another. South African legislation (see Section 2.2.4) is in the process of making emission inventory data publicly available.

An emission inventory was developed for the Mpumalanga Highveld region during the Fund for the Research into Industrial Development Growth and Equity (FRIDGE) campaign in 2004 (Scorgie *et al.*, 2004). Although this emission inventory was compiled for the Mpumalanga Highveld region, it also contained emissions sources for the Jhb-Pta megacity. These emission sources included residential vehicles, industry, residential activities and biomass combustion. The total emission per species determined during the FRIDGE study is presented in Table 5.1 below. Emissions for the species based on the FRIDGE study were used as estimated emissions in this investigation.

Table 5.1: Emission sources (ton/year) for the Jhb-Pta megacity based on the FRIDGE study

	Source types (ton/year)				
Species	**Vehicle sources**	**Industrial sources**	**Biomass burning**	**Residential/ Domestic fuel burning**	**Total**
CO_2	5 844 508		405 327	1 546 010	7 795 845
CO	272 579		10 33 122	90 232	362 811
CH_4	1 211		24 348	3 327	28 886
Other NMHC	33 103			4 117	37 220
Benzene	484	3		139	626
Formaldehyde	292				292
Acetaldehyde	149			164	313
1,3 Butadiene	451				451
NO_X	66 932	53 934		1 743	122 609
N_2O					

SO_2	10 103	20 811	7 877	38 791
Lead	242			242
N_2O	200		39	239

The full MCM chemistry scheme in MECCA-MCM-UPWIND (see Chapter 4) also included numerous non-methane hydrocarbon (NMHC) species. No data currently exists for detailed speciation of NMHCs in South Africa. Therefore, speciated emissions of NMHC, which included benzene, formaldehyde, acetaldehyde and 1,3 butadiene, as listed in Table 5.1, based on mass fractions for European conditions (Derwent *et al.*, 1996), were used as input data for NMHC emissions in the MECCA-MCM-UPWIND. These values are listed in Table 5.2. Since this speciation was based on European conditions, the estimated NMHC emissions could potentially be an under- or over-estimate.

Table 5.2: NMHC emissions (ton/year) based on mass fraction (adopted from Derwent *et al*., 1996)

Specie	Name	ton/year	Specie	Name	ton/year
Isobutene1-butene	C_4H_{10}	151	Butane	C_4H_{10}	1312
mp-Xylene	C_8H_{10}	939	trans-2-Butene	C_4H_8	288
o-Xylene	C_8H_{10}	813	cis-2-Butene	C_4H_8	288
1,2,3-Trimethyl-benzene	C_9H_{12}	166	1-Pentene	C_5H_{10}	99
Acetone	C_3H_6O	785	n-Pentane	C_5H_{12}	634
Ethanol	C_2H_6O	4474	Isoprene	C_5H_8	1
Ethylene	C_2H_4	1168	2-Methyl-2-butene	C_5H_{10}	83
Toluene	C_7H_8	2149	n-Hexane	C_6H_{14}	420
Propylene	C_3H_6	50	2-Methyl-heptane	C_8H_{18}	498
Propane	C_3H_8	164	Cyclohexane	C_6H_{12}	1
Isobutene	C_4H_{10}	1312	2-Methyl-hexane	C_7H_{16}	167
n-Octane	C_8H_{18}	89	n-Heptane	C_7H_{16}	108
Ethyl-benzene	C_8H_{10}	409			

5.2.3.1 Diurnal variation of traffic emissions

Vehicular emissions, which include nitrogen oxide (NO), nitrogen dioxide (NO_2), carbon monoxide (CO), carbon dioxide (CO_2), methane (CH_4), NMHCs, volatile organic compounds

(VOCs), acetaldehyde, formaldehyde, 1,3 butadiene and lead. In the Jhb-Pta megacity, traffic emissions are regarded as the major emission source contributing to approximately 80% of the total nitrogen oxide (NO_x) emissions (Jorquera, 2002). Vehicles also account for 60% of benzene, 100% of formaldehyde, 99% of acetaldehyde and 70% of NMHCs emissions (Liebenberg-Enslin, 2008). Since the focus of this study was not to develop an emission inventory, a generic emission inventory for traffic emissions was derived from previous studies.

Pollutant species from traffic emissions have a significant diurnal variability. Therefore, the species associated with traffic sources of emissions were varied on an hourly basis in the model. Goyns (2008) determined the real-world fuel consumption and emissions from passenger vehicles for Johannesburg. Traffic emissions of NO_x, hydrocarbons (HCs) and CO were based on petrol and diesel motor vehicles only, with heavy-duty vehicles, taxis and minibuses excluded from this study (Goyns, 2008). Although the study by Goyns (2008) was conducted only for Johannesburg, these results were used to represent the entire Jhb-Pta megacity. According to Goyns (2008), most of the traffic emissions are emitted during the periods 06:00 to 09:00 and 16:00 to 18:30, when people are commuting between their residence and work. In Figure 5.5, the fraction of total fuel consumption (FC) and the fraction of the total emissions of pollutant species during a working week are presented as a function of time period of the day, as determined by Goyns (2008).

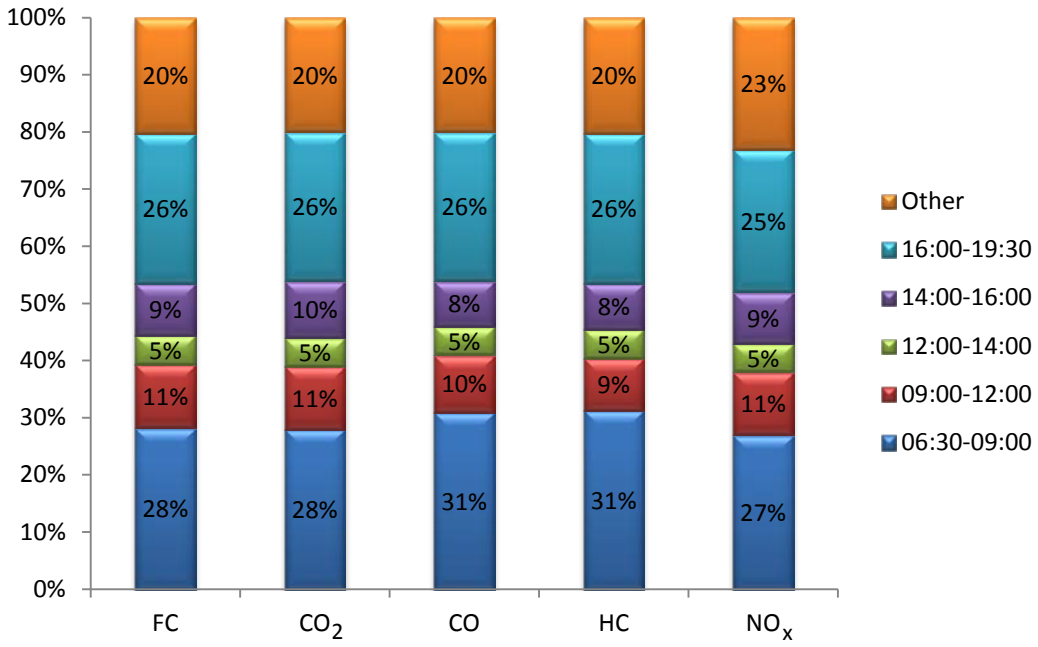

Figure 5.5: Fraction of total fuel consumption and emissions for weekdays for private passenger vehicles in the Jhb-Pta megacity as a function of period of the day (adopted from Goyns, 2008)

The above-mentioned diurnal variability is also in agreement with Menut *et al.* (2011), who derived hourly emission factors (Figure 5.6) based on pollutant concentrations in various cities in Europe by utilising a chemistry transport model, CHIMERE. Most of the emission values required for atmospheric modelling studies world-wide are generally only available on an annual basis, while hourly values are needed especially in photochemical box models. Hourly values were, however, needed for this study. Pollutant species were incorporated as hourly emissions in the model, based on the emission factors presented in Figure 5.6.

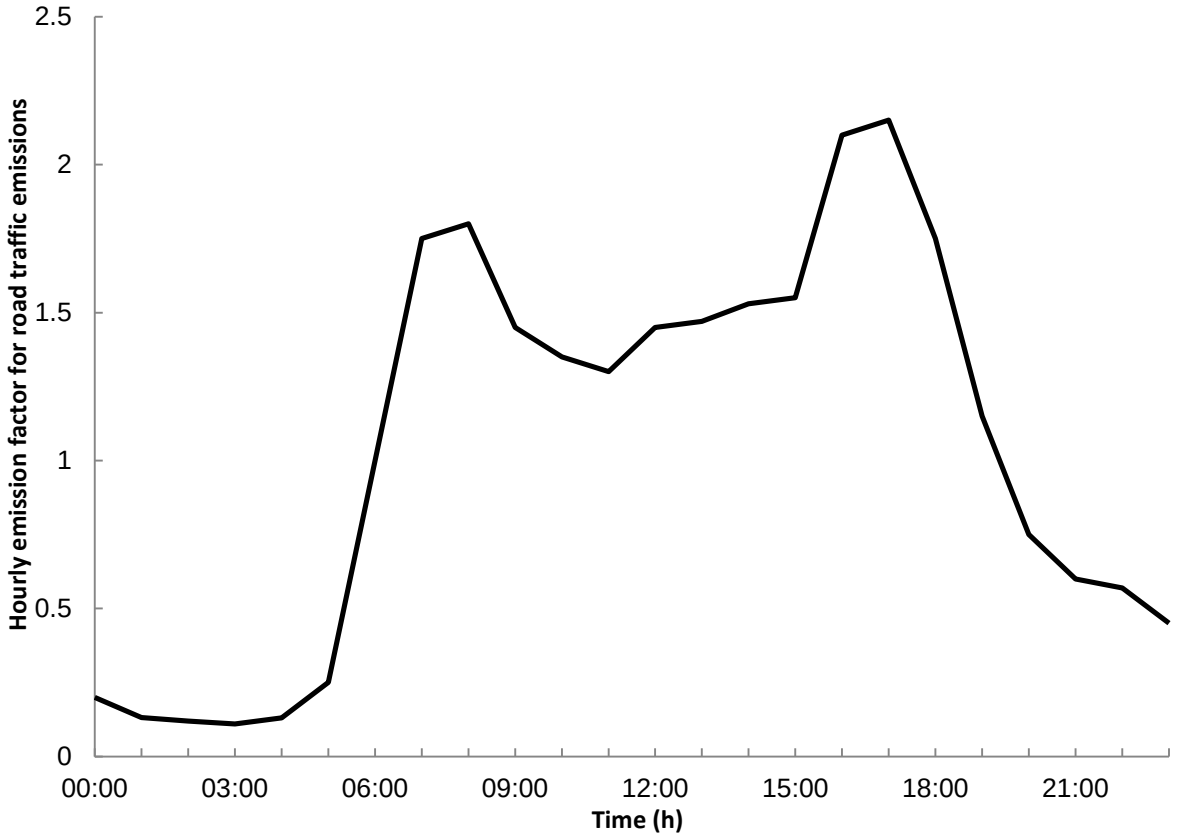

Figure 5.6: Diurnal variation of traffic emissions based on factor estimation (adopted from Menut *et al*., 2011)

Total atmospheric NO and NO_2 concentrations are commonly reported together as NO_x concentrations. For the model, however, it was required that the emissions of NO and NO_2 species were separated. Various factors influence the NO/NO_2 ratio, from raw exhaust gas, e.g. petrol or diesel engines, or exhaust gas from diesel engines after processing by a catalytic converter (Schaberg, 2012). A study conducted by Carslaw and Beevers (2005) indicated that the median primary NO_2 fraction from NO vehicle emissions from different roads in London's urban areas was 10.6 volume %. The European Monitoring and Evaluation Programme (EMEP) of the European Environmental Agency (EAA) compiled an air pollution emission inventory guidebook (EMEP/EEA), which provides guidance on estimating emissions from both anthropogenic or natural emission sources (Agency, 2009). Within the EMEP/EEA guidebook, the mass fraction of NO_2 in NO_x exhaust emissions for different passenger cars, light-duty trucks, heavy-duty vehicles (including buses) and motorcycles for various levels of vehicular

technologies based on Euro ratings for vehicular emissions was determined. The NO_2 in NO_x varied between 5-25 in mass %, depending on the type of vehicle and fuel (Schaberg, 2012). Based on the EMEP/EAA guidebook, it was assumed that the NO/NO_2 ratio for raw exhaust gas vehicle emissions in the model was 80% NO and 20% mass fraction NO_2.

The Euro fuel specification is defined as the acceptable limits for exhaust emissions of new vehicles in Europe in order to meet the stringent emission regulations. The 'criteria' atmospheric pollutants (See section 2.2.2) are regulated through these standards. South Africa has also adopted this standard classification reference method. The different Euro specifications are an indication of when they came into force, i.e. Euro-0 pre-1993; Euro-1 in 1993; Euro-2 in 1996; Euro-3 in 2000, Euro-4 in 2005 and Euro-6 in 2014. According to Goyns (2008), the private passenger vehicle fleet in the Jhb-Pta megacity consists of approximately 45% Euro-0 type petrol vehicles (pre Euro-1), 10% Euro-2 diesel vehicles, 30% Euro-2 petrol vehicles and 15% Euro-3 petrol vehicles. The percentages of each pollutant species emitted from the different Euro classified vehicles in Jhb-Pta are indicated in Table 5.3.

Table 5.3: Vehicle emissions for Jhb-Pta megacity according to the Euro classification (adopted from Goyns, 2008)

Euro-0 petrol (42% of total Jhb-Pta megacity passenger fleet)	Euro-2 diesel (10% of total Jhb-Pta megacity passenger fleet)	Euro-2 petrol (30% of total Jhb-Pta megacity passenger fleet)	Euro-3 petrol (15% of total Jhb-Pta megacity passenger fleet)
40% CO_2	19% CO_2	27% CO_2	15% CO_2
88% CO		10% CO	2% CO
93% HC		5% HC	0.5% HC
82% NO_x	14% NO_x	3% NO_x	0.4% NO_x

As indicated in Table 5.3, Euro-0 petrol vehicles have the highest emissions and produce 40% of CO_2, 88% of CO, 93% of HC and 82% of NO_x emissions. Euro-2 diesel vehicles produce 19% of the total CO_2 emissions and emit 14% of the NO_x emissions; whereas Euro-2 petrol vehicles produce 27% of CO_2 and only 10% of CO, 5% of HC emissions and 3% of NO_x emissions (Table 5.3). Euro-3 petrol vehicles contribute even less, with 15% of CO_2, 2% of CO,

0.5% of HC and 0.4% of NO_x emissions. These derived emissions excluded heavy-duty vehicles, taxis and minibuses, which also contribute significantly to vehicle emissions in the Jhb-Pta megacity.

In this study, the worst case scenario was assumed, i.e. that all vehicles in the Jhb-Pta megacity were Euro-0 types and the emission levels of these vehicles were used in the base case run. During the sensitivity analysis, the impact of the conversion of all vehicles to Euro-3 types on pollutant species in the atmosphere was also investigated.

5.2.4 Initial and tropospheric mixing ratios

The initial mixing ratios of most of the criteria pollutants representative of the Jhb-Pta megacity are presented in Chapter 2. The average mixing ratios for all the species (NO, NO_2, O_3 and BTEX) measured during the three-month (March-May) monitoring campaign are listed in Table 5.4. Measurements conducted at midnight (00:00) were used as the initial mixing ratio values in the MECCA-MCM-UPWIND model run, since the model's start time is 00:00.

No tropospheric data are available for most of the species in the Jhb-Pta megacity and therefore these mixing ratios were estimated either through model simulations or obtained from literature. Estimated tropospheric mixing ratios for other species were obtained from the global chemistry-climate model (EMAC) (Jöckel *et al.*, 2006). Output files from EMAC were generated for each day for all the major pollutant species (i.e. CO, CH_4, PAN, NO, NO_2, SO_2) and used as input into the MECCA-MCM-UPWIND model. Apart from CO and CH_4, the other most important tropospheric organic trace gases are ethane (C_2H_6) and ethyne (C_2H_2) (Gonzalez Abad *et al.*, 2011). C_2H_6 is the second most abundant HC in the atmosphere and has a lifetime of approximately two months (Rudolph, 1995), whereas C_2H_2 has an estimated lifetime of two to four weeks in the atmosphere (Logan *et al.*, 1981). Since no data are available for these species in the Jhb-Pta megacity, the global mixing ratios in the southern hemisphere of 0.04ppb and 0.044ppb for C_2H_6 and C_2H_2 were used, respectively (Blasting, 2012). The global mixing ratios for CO_2, CO and CH_4 were also used and are listed in Table 5.4 (Salby, 1996). Concentrations of species such as O_2, N_2 and CO_2 were fixed throughout the model runs. Tropospheric mixing ratios are also difficult to specify over the Jhb-Pta megacity region, due to limited vertical profile pollutant concentration data.

Table 5.4: Input data for the Jhb-Pta megacity for initial and tropospheric mixing ratios

Species	Chemical formula	Initial mixing ratio (ppb)	Tropospheric mixing ratio (ppb)	Emissions [d] (molec/cm^2/s)
nitrogen monoxide	NO	20[a]	0.1[c]	1.2x10^{11}*
nitrogen dioxide	NO_2	14[a]	1[c]	2.0x10^{10}*
sulphur dioxide	SO_2	23[a]	1	1.0x10^{10}
peroxyacetyl nitrate	PAN	2[b]	0.02[b]	-
ozone	O_3	7[a]	65[†]	-
carbon monoxide	CO	2700[a]	75[e]	9.1x10^{12}*
carbon dioxide	CO_2		345[c]**	6.7x10^{11}
methane	CH_4	1800[b]	175[c]**	1.2x10^{11}
ethane	C_2H_6		0.4[e]	12.1x10^{8}
ethylene	C_2H_4			1.7x10^{9}*
formaldehyde	CH_2O			6.6x10^{8}*
propylene	C_3H_6			1.4x10^{9}*
propane	C_3H_8			1.3x10^{9}*
isobutene1-butene	C_4H_{10}			5.4x10^{8}*
butane	C_4H_{10}			1.9x10^{9}*
trans-2-Butene	C_4H_8			4.3x10^{8}*
cis-2-Butene	C_4H_8			4.3x10^{8}*
1-Pentene	C_5H_{10}			1.2x10^{8}*
n-Pentane	C_5H_{12}			7.7x10^{8}*
2-Methyl-2-butene	C_5H_{10}			1.0x10^{8}*
n-Hexane	C_6H_{14}			5.8x10^{8}*
benzene	C_6H_6	3[a]	0.01*	5.5x10^{8}*
cyclohexane	C_6H_{12}			4.9x10^{5}*
2-Methyl-hexane	C_7H_{16}			1.4x10^{8}*
n-Heptane	C_7H_{16}			9.3x10^{7}*
toluene	C_7H_8	3[a]	0.01	9.8x10^{8}*
2-Methyl-heptane	C_8H_{18}			3.7x10^{8}*
n-Octane	C_8H_{18}			6.7x10^{7}*
ethyl-benzene	C_8H_{10}	4[a]	0.01	2.7x10^{8}*
mp-Xylenes	C_8H_{10}	4[a]	0.01	9.9x10^{7}*

o-Xylene	C_8H_{10}	4[a]	0.01	$2.4x10^{8}$*
1,2,3-Trimethyl-benzene	C_9H_{12}			$9.8x10^{8}$*
acetone	C_3H_6O			$7.0x10^{12}$*
acetylene	C_2H_2		0.04 [e]	$1.9x10^{10}$*
ethanol	C_2H_6O			$4.0x10^{9}$*
1,3-butaine	C_4H_6			$1.0x10^{8}$*

a- Monitoring data see Chapter 2
b- EMAC
c- Blasting, 2012
d- Emissions from this study
e- Gonzalez Abad *et al.*, 2011
f- Diab *et al.,* 2003; Bundi, 2006
g- Monitoring data see Chapter 3
** Mixing ratio in part per million (ppm)
* Emissions emitted hourly in the model. Listed values present the emission at the start of the model run.

One of the most important species in simulating boundary conditions of urban atmospheric processes is O_3 (Schere & Demerjian, 1984). Tropospheric O_3 over sub-equatorial and southern Africa has been an important research topic over the past decade (Swap *et al.*, 1996; Thompson *et al.*, 1996). These regions experience intensive biomass burning in spring, together with industrial and biogenic emissions (Swap *et al.*, 1996). All of these sources contribute to the elevated levels of tropospheric O_3 over this region (Thompson *et al.*, 1996). Most vertical tropospheric O_3 profiling studies in southern Africa have been conducted during sampling campaigns, such as SAFARI 2000. During SAFARI 2000, vertical tropospheric O_3 measured at Irene (Pretoria) was reported to be 60-65ppb, between 2 and 2.5km above ground level (Thompson *et al.*, 1996).

5.2.5 Upwind mixing ratios entering Jhb-Pta megacity

The Jhb-Pta megacity is not only influenced by emissions within the city, but also from air masses advected into the area. A recent study conducted by Beukes *et al*. (2012) indicated that the majority of air masses passing over the megacity arriving at an atmospheric research station at Welgegund (near Potchefstroom) (www.welgegund.co.za) also passed over the Mpumalanga Highveld. It can therefore be assumed that emissions from the Mpumalanga Highveld have a strong influence on the Jhb-Pta megacity. Primary pollutants emitted into the atmosphere within the Mpumalanga Highveld are transported into the Jhb-Pta megacity and also react in the atmosphere to form secondary pollutants. Secondary pollutants are usually an indication of the age of air mass (Tseng *et al.*, 2009). The chemistry of O_3, NO_x and VOCs is important in the photochemical aging of air masses (Sillman, 1999).

Since there are no air quality monitoring stations situated at the boundary region between the Jhb-Pta megacity and the Mpumalanga Highveld, the composition of air masses advected into the Jhb-Pta megacity from the Mpumalanga Highveld was determined with the MECCA-MCM-UPWIND model developed in this study. This required the model to be set up with new input data from the Mpumalanga Highveld, which will be discussed in the subsequent sections.

5.2.5.1 Upwind model domain and meteorological parameters

The setup for the MECCA-MCM-UPWIND model used to determine the composition of air masses advected into the megacity from the Mpumalanga Highveld was the same as presented in the previous sections. The input data required were meteorological data, mixing ratios and pollutant emissions. For this specific model run, these parameters had to be representative of the Mpumalanga Highveld region. The model domain for this simulation is illustrated in Figure 5.7 by a box drawn with a thinner line on the eastern side of the Jhb-Pta megacity modelling domain. The assumed direction of air mass transport is indicated by the arrow in Figure 5.7. The distance between the centre of the Mpumalanga Highveld modelling domain box and the boundary of Jhb-Pta megacity is approximately 70km.

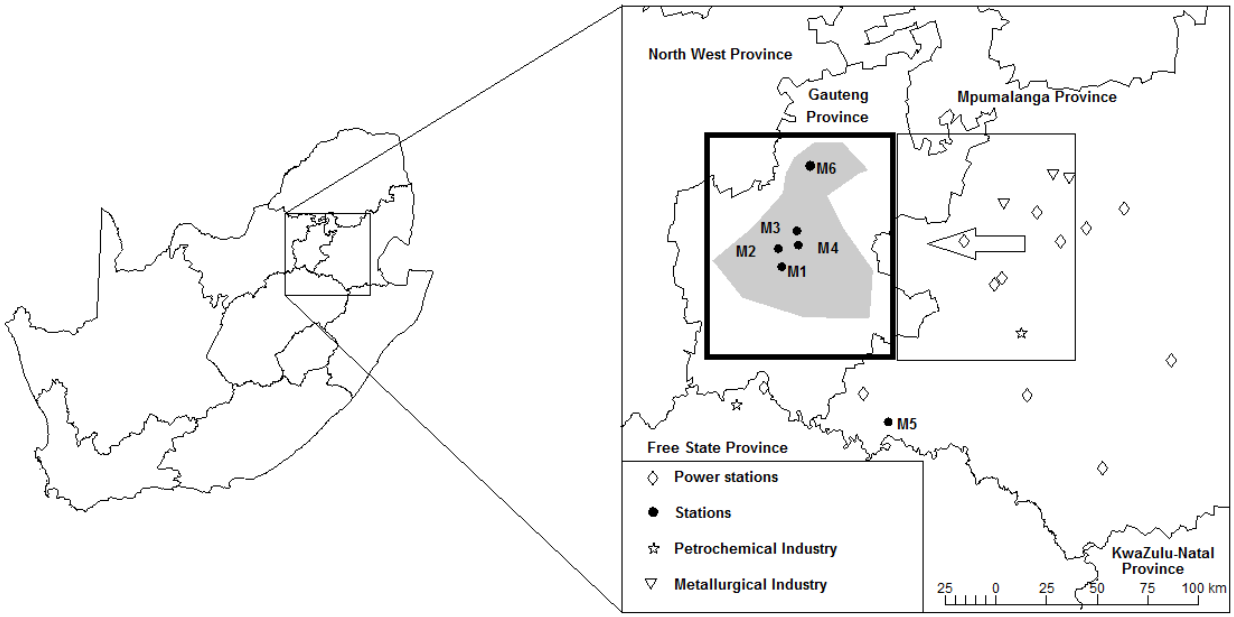

Figure 5.7: The Jhb-Pta megacity model domain is illustrated in the box drawn with the thick lines, while the Mpumalanga Highveld model domain is presented in the box drawn with the thin lines; the arrow indicates the direction of the air mass advected into the Jhb-Pta megacity

The same air quality monitoring stations in the Mpumalanga Highveld that were described in Chapter 3 were used to obtain initial mixing ratios for this model run. The average wind speed used was 1.7m/s, as determined from four of these air quality monitoring stations. A model spin-up time of 24 hours was performed in order to provide realistic initial concentrations. The model results averaged over a subsequent 24-hour period after the model spin-up time was used as the upwind mixing ratio input for the Jhb-Pta megacity base case and sensitivity runs. The diurnal variation of the pressure, temperature and relative humidity used at the model start time are presented in Figures 5.7 and 5.8 below.

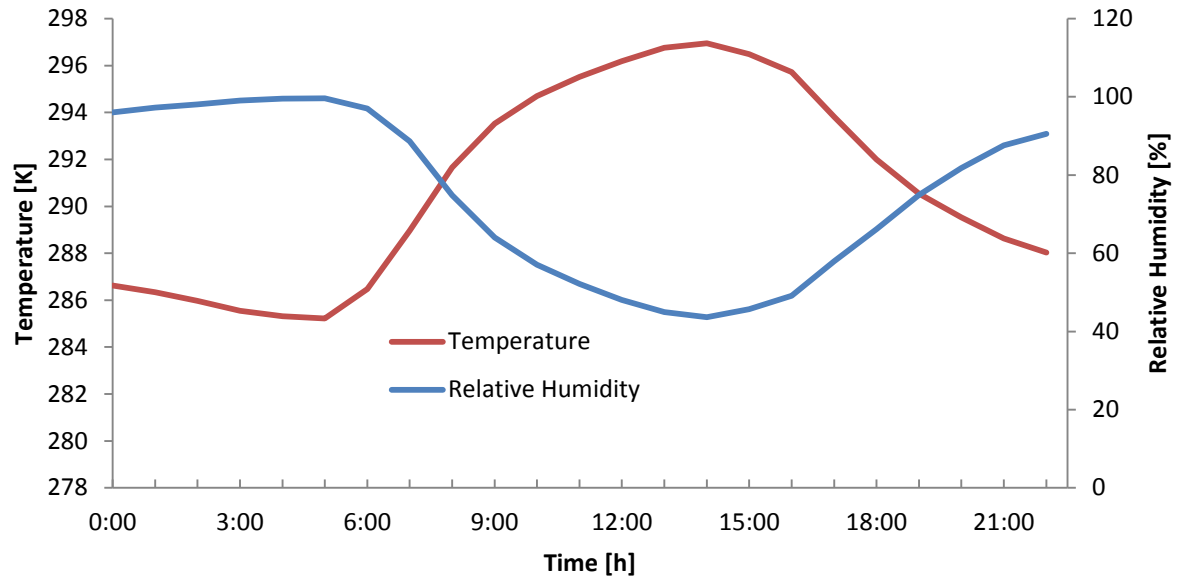

Figure 5.8: Diurnal variation of temperature and relative humidity in the Mpumalanga Highveld measured in autumn (March-May) at monitoring sites in Mpumalanga Highveld

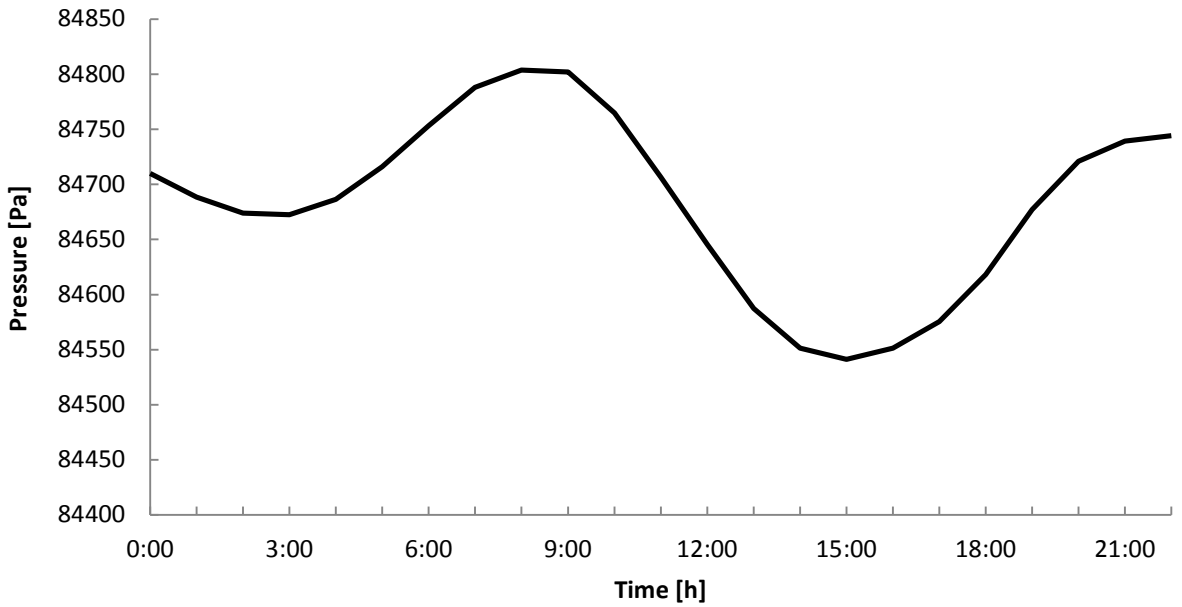

Figure 5.9: Diurnal variation of pressure in the Mpumalanga Highveld measured in autumn (March-May) at monitoring sites in Mpumalanga Highveld

5.2.5.2 Upwind mixing layer height

Since the Mpumalanga Highveld is situated at approximately the same height above sea level as the Jhb-Pta megacity, the ML height utilised for the Jhb-Pta megacity (Figure 5.4) was used for this model run.

5.2.5.3 Upwind emissions inventory

In contrast to the Jhb-Pta megacity, where traffic emissions and residential combustion are the major sources of pollutant emissions, industrial activities are the main emission sources in the Mpumalanga Highveld (see Section 2.2.5.2 for more detail). Since these industries mostly operate 24 hours per day, a less distinct diurnal variability of emissions in this region is observed compared to the Jhb-Pta megacity (Collett *et al.*, 2010). Therefore, it was not necessary to specify a temporal profile of emissions in the model run. Emission data for the Mpumalanga Highveld obtained from the FRIDGE study was utilised and is presented in Table 5.5. From Table 5.5, traffic emissions are lower than industrial emissions. According to literature, the initial NO/NO_2 ratio when released from a power station source into the atmosphere is approximately 95/5 mass %. In contrast, this ratio is 80% to 20% mass from vehicles. Therefore, an assumption was made to use the ratio of NO/NO_2 from the Highveld as 95% NO and 5% mass fraction NO_2 (Hewitt, 2001).

Table 5.5: Emission sources in the Mpumalanga Highveld based on the FRIDGE study

	Source types (ton/year)				
Species	**Vehicle sources**	**Industrial sources**	**Biomass burning**	**Residential/ Domestic fuel burning**	**Total**
CO_2	1 912 283	50 624 653	898 701	562 851	53 998 488
CO	49 579	658 113	35619	36 000	779 311
CH_4	292	96 523	1 315	1179	99 309
Other NMHC	6 517	368 647	1 699	443	377 306
Benzene	82			17	99
Formaldehyde	58				58
Acetaldehy	35			18	53

de					
1,3					
Butadiene	81				81
NO_X	24 065	869 993	1 699	352	896 109
N_2O	78		82	14	174
SO_2	5 781	1 826 236	329	3513	1 83 559
Lead	41				41

5.2.5.4 Upwind initial and tropospheric mixing ratios

The mixing ratios of all the pollutant species measured at the air quality monitoring stations in the Mpumalanga Highveld were used as initial mixing ratios. Average diurnal concentrations for the three months (March-May) were used. The input data for the model runs are summarised in Table 5.6. For this model run, the upwind mixing of species in the Mpumalanga Highveld is not included, since the simulation will focus on the aging of air mass transported between the Mpumalanga Highveld and the Jhb-Pta megacity. Therefore, the upwind mixing ratio of the species in the Mpumalanga Highveld is the same as the initial mixing ratios for all the simulations. The same tropospheric mixing ratios are used as indicated in Table 5.4. The results from this Mpumalanga Highveld model run, which are to be used as input for the Jhb-Pta megacity, are summarised in Table 5.7.

Table 5.6: Input data for the model run used to determine the composition of air mass entering Jhb-Pta megacity

Species	Chemical formula	Initial mixing ratio (ppb)	Tropospheric mixing ratio (ppb)	Emissions [d] (molec/cm^2/s)
nitrogen monoxide	NO	30	0.1[c]	1.42x10^{12} [d]
nitrogen dioxide	NO_2	29	1[c]	4.89x10^{10} [d]
sulphur dioxide	SO_2	11	1	2.8 x10^{11} [d]
ozone	O_3	13	45[f]	-
carbon monoxide	CO	0.33	7.5 [e*]	1.4 x10^{12} [d]

carbon dioxide	CO_2	-	345 [c*]	1.23 x10^{13} [d]
methane	CH_4		175 *	3.11x10^{11} [d]
ethane	C_2H_6		0.4 [e]	1.47x10^{7} [d]
benzene	C_6H_6	0.5 [h]	0.1	1.3x10^{7} [d]
toluene	C_7H_8	1 [h]	0.1	1.3x10^{9} [d]
ethyl-benzene	C_8H_{10}	0.2 [h]	0.1	1.89x10^{8} [d]
m/p-xylenes	C_8H_{10}	0.5 [h]	0.1	4.34x10^{8} [d]
o-xylene	C_8H_{10}	0.1 [h]	0.1	3.73x10^{8} [d]

a- Monitoring data see Chapter 2
b- EMAC
c- Blasting, 2012
d- Emissions from this study
e- Gonzalez Abad *et al.*, 2011
f- Diab *et al.,* 2003; Bundi, 2006
g- Monitoring data see Chapter 3
h- Lourens *et al.*, 2011, monthly averaged values
** Mixing ratio in part per million (ppm)
* Listed values present the emission at the start of the model run.

5.3 JHB-PTA MEGACITY MODEL RUNS

5.3.1 Base case model run

In Table 5.7, all of the input data used for the Jhb-Pta megacity base case run are listed. Pressure, temperature, relative humidity and the ML height were varied diurnally according to Figure 5.2 to Figure 5.4. The averaged wind speed of 1.7 m/s is representative of the air mass advected out of the Mpumalanga Highveld towards the Jhb-Pta megacity, and therefore used in the Jhb-Pta model runs. The model run for the base case simulation and sensitivity runs started at 00:00, with a model spin-up time of 24 hours. Results of the second 24-hour period, obtained after the model spin-up time, are presented.

Table 5.7: Input data for the Jhb-Pta megacity model run

Species	Formula	Initial mixing ratio (ppb)	Tropospheric mixing ratio (ppb)	Upwind mixing ratio (ppb) from Upwind model run	Emissions [d] (molec/cm^2/s)
nitrogen monoxide	NO	20[a]	0.1[c]	40	1.2×10^{11}*
nitrogen dioxide	NO_2	14[a]	1[c]	38	1.0×10^{10}*
peroxyacetyl nitrate	PAN	2[b]	0.02[b]	0.85	-
ozone	O_3	7[a]	65[f]	19	-
carbon monoxide	CO	2700[a]	75[e]	2982	9.1×10^{12}*
carbon dioxide	CO_2		345[c]**		6.7×10^{11}
methane	CH_4	1800[b]	175[c]**	6260	1.2×10^{11}
ethane	C_2H_6		0.4[e]	5.8	12.1×10^{8}
ethylene	C_2H_4				1.7×10^{9}*
formaldehyde	CH_2O				6.6×10^{8}*
propylene	C_3H_6				1.4×10^{9}*
propane	C_3H_8			0.64	1.3×10^{9}*
isobutene1-butene	C_4H_{10}				5.4×10^{8}*
butane	C_4H_{10}				1.9×10^{9}*
trans-2-Butene	C_4H_8				4.3×10^{8}*
cis-2-Butene	C_4H_8				4.3×10^{8}*
1-Pentene	C_5H_{10}				1.2×10^{8}*
n-Pentane	C_5H_{12}				7.7×10^{8}*

2-Methyl-2-butene	C_5H_{10}				$1.0x10^{8}$*
n-Hexane	C_6H_{14}				$5.8x10^{8}$*
benzene	C_6H_6	3[a]	0.01*	0.62	$5.5x10^{8}$*
cyclohexane	C_6H_{12}				$4.9x10^{5}$*
2-Methyl-hexane	C_7H_{16}				$1.4x10^{8}$*
n-Heptane	C_7H_{16}				$9.3x10^{7}$*
toluene	C_7H_8	3[a]	0.01	0.8	$9.8x10^{8}$*
2-Methyl-heptane	C_8H_{18}				$3.7x10^{8}$*
n-Octane	C_8H_{18}				$6.7x10^{7}$*
ethyl-benzene	C_8H_{10}	4[a]	0.01	0.23	$2.7x10^{8}$*
mp-Xylenes	C_8H_{10}	4[a]	0.01	0.42	$9.9x10^{7}$*
o-Xylene	C_8H_{10}	4[a]	0.01	0.41	$2.4x10^{8}$*
1,2,3-Trimethyl-benzene	C_9H_{12}				$9.8x10^{8}$*
acetone	C_3H_6O				$7.0x10^{12}$*
acetylene	C_2H_2		0.04[e]		$1.9x10^{10}$*
ethanol	C_2H_6O				$4.0x10^{9}$*
1,3-butaine	C_4H_6				$1.0x10^{8}$*

5.3.1.1 NO

In Figure 5.10, the modelled and measured diurnal profile for NO is presented. The diurnal variation in the modelled NO can be attributed to changes in emissions, transport, chemistry and the ML height in the box defined for the model. The modelled diurnal NO pattern is in good agreement with the measured NO trend. The peak of NO in the morning and evening is well produced by MECCA-MCM-UPWIND. The modelled NO increased rapidly in the early morning hours at approximately 05:00, with a peak at 06:00. This increased NO mixing ratio is due to increased emissions within the model. The measured data also shows the same tendency with NO usually peaking in the morning due to increases in emissions from vehicles and household combustion, together with a relatively low boundary layer height. The early morning peak between 6:00 and 9:00 coincides with the time that commuters travel to work (Lourens *et al.,* 2012). When the ML height starts to rise at 08:00, the modelled NO levels decrease rapidly due to both the break-up of the inversion layers, which results in more dilution of the atmosphere above the ML, and the reduction of emissions from the surface. Solar radiation increases in the morning and photochemistry starts to also affect the NO concentrations. The second peak

observed at 16:00 to 21:00 for both the measured and modelled data can be attributed to both traffic emissions and household combustion (space heating and cooking) (Venter *et al.*, 2012). A decrease in NO emissions is observed for the measured data after 19:00. This is due to a significant decrease in NO sources. However, the model results indicate an increase in NO mixing ratios. This can be explained due to emission and ML effects in the model. When the ML decreases within the model, it stops the vertical mixing from above the ML, which results in the accumulation of NO due to the decrease in volume and constant emissions emitted into the model.

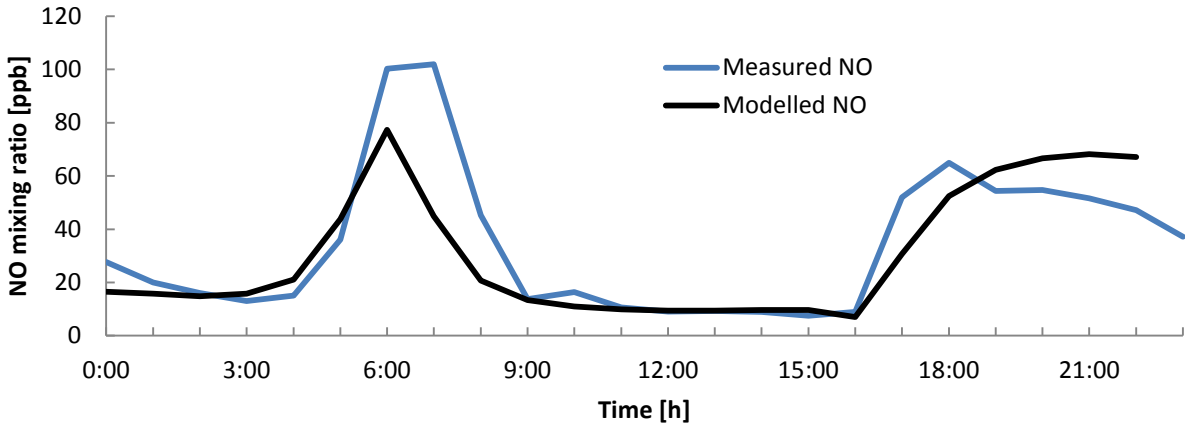

Figure 5.10: Modelled and measured diurnal NO mixing ratios

5.3.1.2 NO_2

It seems that the modelled NO_2 mixing ratios are over-predicted by MECCA-MCM-UPWIND, although they are in good agreement with the diurnal variability determined with the measured NO_2 concentrations, as presented in Figure 5.11. As the ML increases, NO and NO_2 mixing ratios decrease, which implies that less NO is available to chemically convert to NO_2 via Reaction 11 (Chapter 2). This leads to a decrease in NO_2 mixing ratios. Since 20% of NO_x emitted from vehicles are NO_2, diurnal changes of traffic emissions will also influence the trend observed. The second observed peak later in the day can be related to the slowed photolysis rate of NO_2, resulting in the accumulation of NO_2.

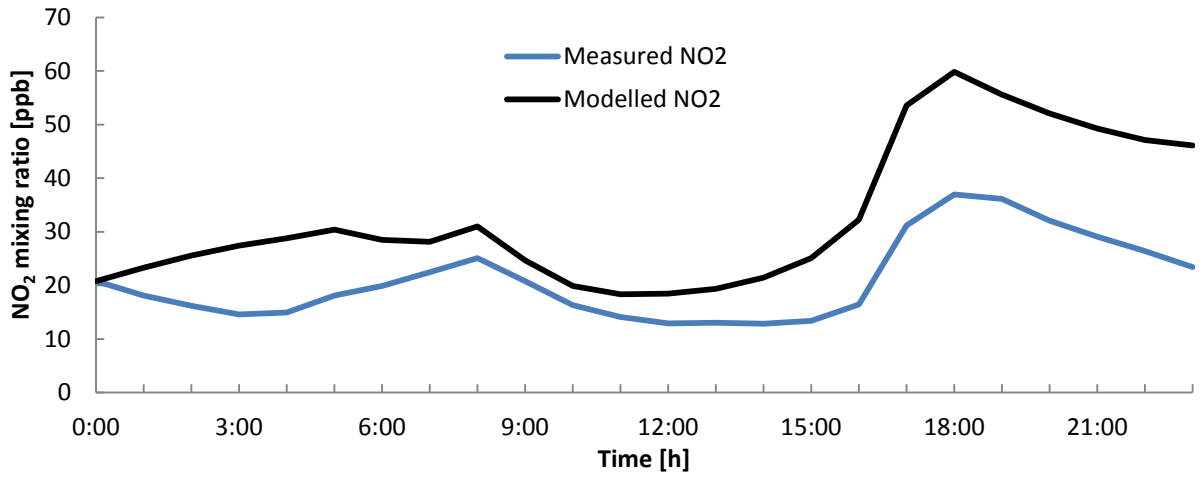

Figure 5.11: Modelled and measured diurnal NO_2 mixing ratios

5.3.1.3 O_3

The modelled and measured O_3 concentrations are presented in Figure 5.12. The diurnal cycle of O_3 is well predicted by MECCA-MCM-UPWIND and in good agreement with measured concentrations, although differences between the measured and modelled data were observed. MECCA-MCM-UPWIND simulated very low mixing ratios of O_3 during the early morning hours and evening hours with a slight over-prediction during the day-time mixing ratio of O_3. At night, O_3 is often lower in urban areas than in the surrounding areas due to titration reactions of O_3 and dry deposition (Sillman, 1999). During the daytime, increases in O_3 levels are observed, since it is produced through photochemical reactions as solar radiation increases. O_3 is produced during the day through the photochemistry of NO_x, VOC, and CO. Another factor

contributing to the increased O_3 concentrations during daytime is the growth of the ML with free tropospheric O_3 mixed into the ML. O_3 is accumulated through photochemical oxidation processes (see Section 2.2.3) throughout the day until dusk. At this time, the photochemical processes slow down due to the lower levels of solar radiation. The ML decrease also results in no entrainment from above.

Although lower O_3 mixing ratios for the model run for night-time concentrations are expected if compared to the measured data, the almost zero O_3 levels can be attributed to the NO_x-titration effect within the model. The model run in Figure 5.12 implies that there is enough NO in the model to completely convert all the O_3 to NO_2 through Reaction 11 (Chapter 2). NO_x titration can drive O_3 concentrations in urban areas to less than 1ppb (Sillman, 1999). The discrepancy between the measured and modelled results can be a possible limitation in models. Modelling studies, e.g. Stockwell *et al.* (2011), have emphasised the difficulty of correctly representing night-time chemistry in models. With NO_x-titration chemistry represented in MECCA-MCM-UPWIND, and the difficulty to represent the night-time chemistry in models, it could explain the low mixing ratios modelled for O_3. The day-time chemistry is well represented in MECCA-MCM-UPWIND.

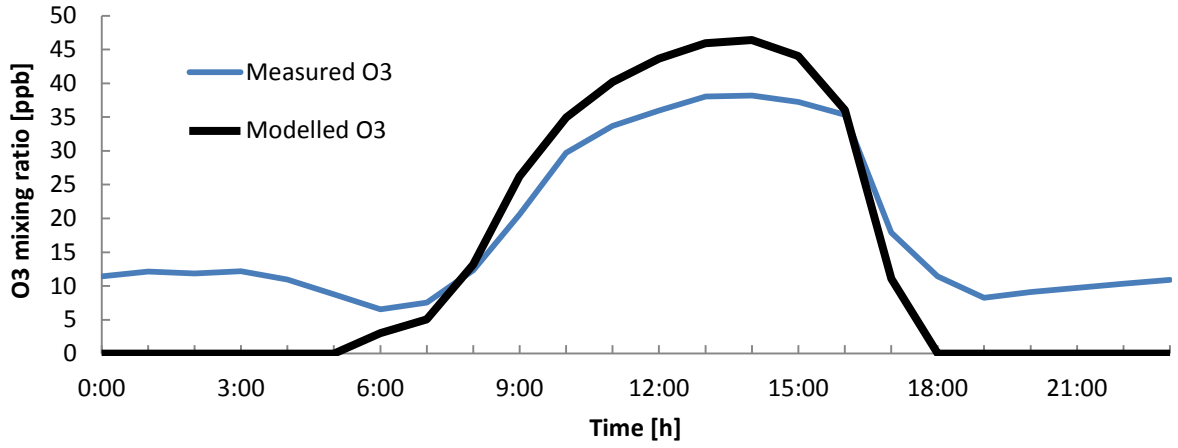

Figure 5.12: Modelled and measured diurnal O_3 mixing ratios

5.3.1.4 BTEX

Benzene, toluene, ethyl benzene and xylene (BTEX) are aromatic VOCs usually associated with anthropogenic activities. Figures 5.13(a) to 5.13(d) show the modelled BTEX concentrations

compared to observed data (see Chapter 2). Although no complete diurnal cycle can be presented for the measured BTEX concentrations, the three measured data points for all the BTEX species are in relatively good agreement with the modelled results. The modelled concentrations for all the BTEX species indicate the same pattern with mixing ratios decreasing steadily during early mornings. At 08:00, the species concentration decreases rapidly, which is also the same time that modelled O_3 increases. VOCs are removed by the photochemical reactions with $OH^{\bullet}$ and the formation of $RO_2^{\bullet}$ radicals that produce NO_2 and subsequently O_3 (2.2.3.4). Each different VOC species has a different effect on NO_2 and therefore also on O_3 formation (Butler *et al.,* 2011). In the presence of high NO_x concentrations, O_3 formation is limited by the availability of VOCs, while in the presence of low NO_x concentrations, O_3 formation is limited by the availability of VOCs (e.g. Kleinman *et al*., 1997, Sillman, 1999). $HO^{\bullet}$ radicals are a major sink of aromatic VOCs (Seinfeld & Pandis, 1998). A decrease in solar radiation leads to a reduction of photochemistry that causes lower $HO^{\bullet}$ radical concentrations, which are not available to react with VOCs to produce O_3. This leads to the accumulation of atmospheric VOCs, which explains the slight increase in BTEX concentrations observed during night time.

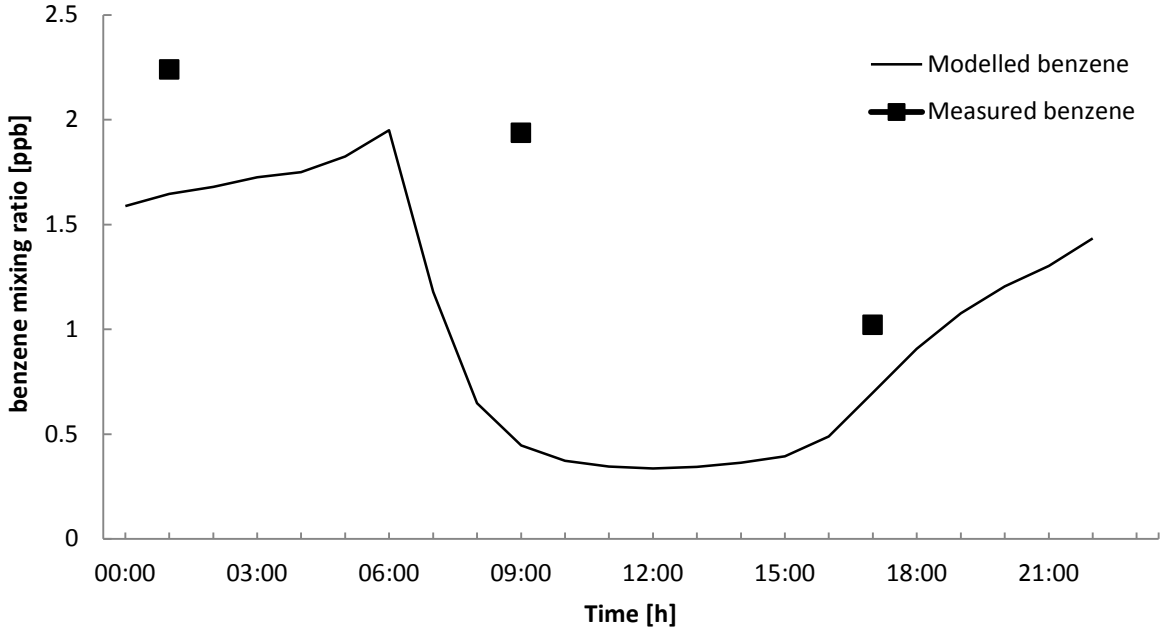

(a)

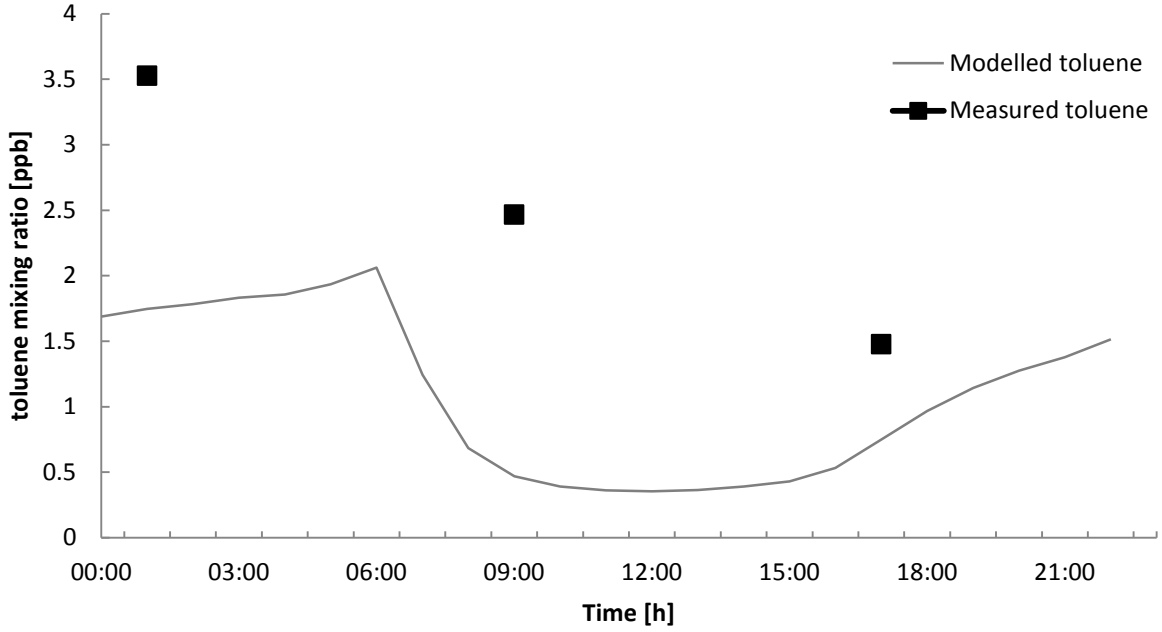
toluene mixing ratio [ppb]
4
3.5
3
2.5
2
1.5
1
0.5
0
00:00
03:00
06:00
09:00
12:00
15:00
18:00
21:00
Time [h]
Modelled toluene
Measured toluene

(b)

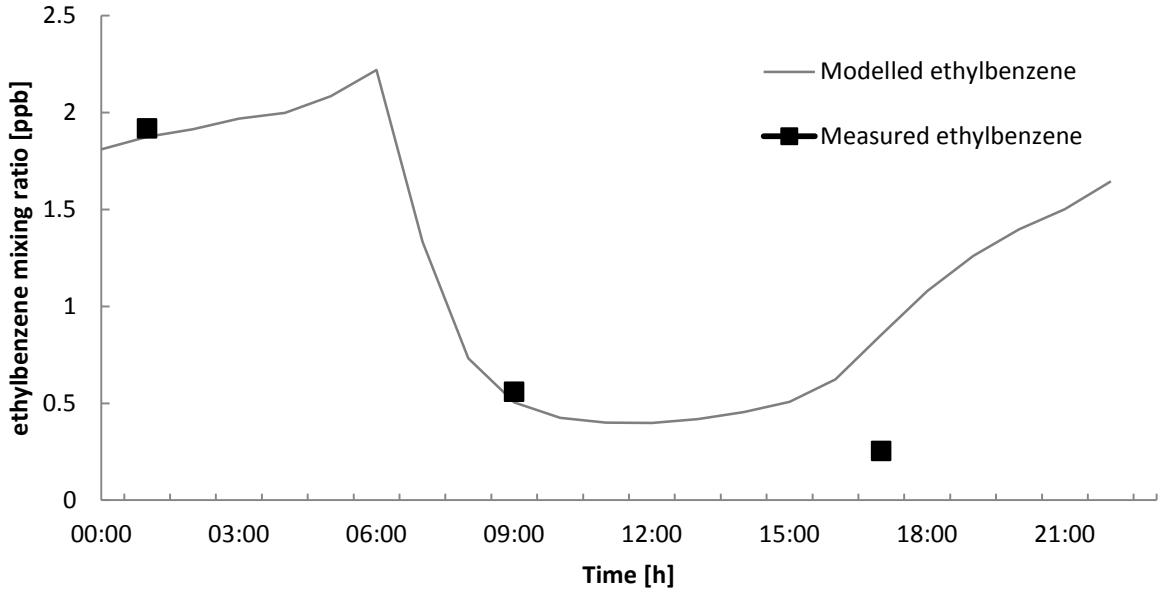
ethylbenzene mixing ratio [ppb]
2.5
2
1.5
1
0.5
0
00:00
03:00
06:00
09:00
12:00
15:00
18:00
21:00
Time [h]
Modelled ethylbenzene
Measured ethylbenzene

(c)

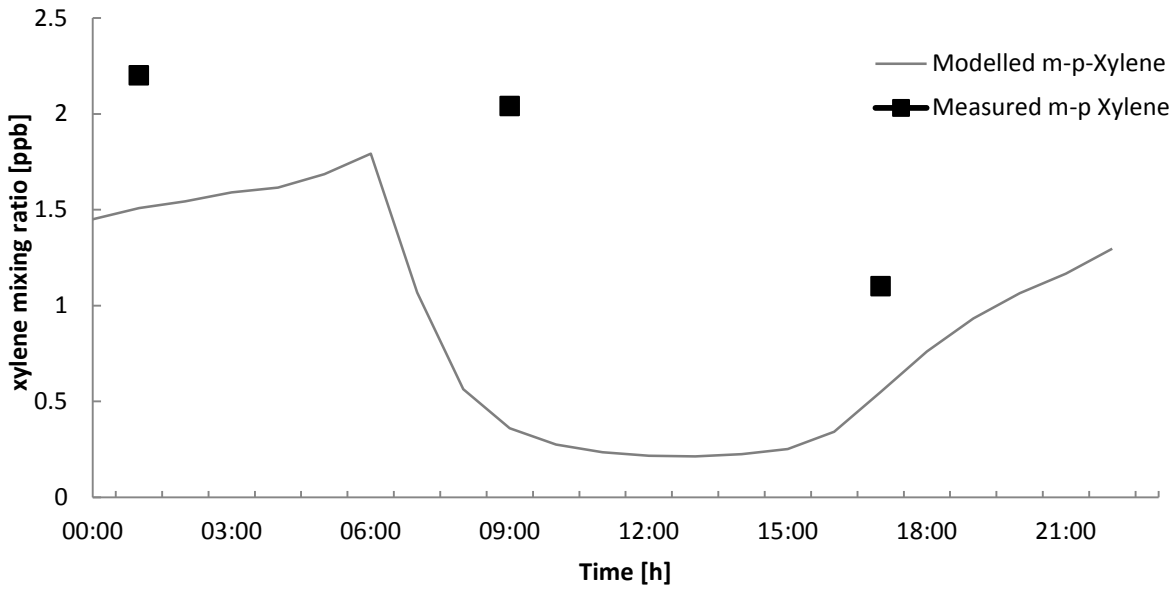

(d)

Figure 5.13: Comparison between modelled and measured diurnal BTEX species mixing ratios; (a) benzene, (b) toluene, (c) ethylbenzene and (d) p-xylene

5.3.1.5 Model uncertainties

Although the MECCA-MCM-UPWIND model has uncertainties, the model was able to predict the day-time chemistry relatively accurately, with modelled values comparing well with measured data. Box models are used with the implicit assumption that the air-shed pollutant concentrations are homogeneously distributed and that the meteorology is not complex, which is not the case for actual atmospheric conditions. Measurements of vertical profiles of pollutant concentrations would also assist in increasing the accuracy of the vertical transport estimates of the model. The largest uncertainty within the model is most likely the emission rates of pollutant species. A proper emission inventory would reduce the uncertainty related to emissions. A systemised monitoring network of NMHC concentrations around the Jhb-Pta megacity, for instance, will also increase the accuracy of the model. As studies of air pollution in Los Angeles indicate (Russel *et al.*, 1988; McRae & Seinfeld, 1983), accurate emission inventories and speciated HC concentrations are critical in determining O_3 reduction strategies. The lag in the NO mixing ratio peak and the higher NO_2 mixing ratios can also be attributed to the diurnal variability of emissions that is not taken into consideration in the model.

5.3.2 Sensitivity analysis

The MECCA-MCM-UPWIND model was further used to study the influence of different parameters on O_3 levels in the Jhb-Pta megacity and possible scenarios to alter or mitigate pollution were investigated. The sensitivity analyses performed here were designed to investigate the effects of both local and external factors on the production of O_3 in the Jhb-Pta megacity. Where necessary, the results from other modelled species are also provided. The first scenario investigated the response of O_3 levels to the variation of wind speed, and therefore the advection of polluted air masses from the Mpumalanga Highveld into the Jhb-Pta megacity. In the second scenario, the sensitivity of the atmospheric chemistry to changes in the local emissions within the Jhb-Pta megacity was investigated. A third sensitivity test investigated the influence of Euro specifications for vehicle emission on O_3 production. These sensitivity studies can identify parameters that could be altered in future to mitigate pollution in the Jhb-Pta megacity.

5.3.2.1 Sensitivity of O_3 production to changes in wind speed

In this model run, the sensitivity of Jhb-Pta megacity to the rate at which external pollution is advected into the megacity is examined. Although O_3 concentrations in the atmosphere are influenced by changes in meteorological conditions, such as ML height, temperature and wind speed, in this scenario, only wind speed was varied. The influence of no wind (0m/s), medium wind speed (1.7m/s) and high wind speed (3.4m/s) from the Mpumalanga Highveld was calculated with the MECCA-MCM-UPWIND model. The upwind model was run as explained in Section 5.2.5. The results are presented in Figure 5.14, and indicate that lower wind speeds lead to increases in O_3 mixing ratios in the Jhb-Pta megacity. The results show that wind speed plays an important role in the processes that control O_3 concentrations in the atmosphere. O_3 levels are 12ppb higher when there is no wind present compared to medium wind speed, while O_3 mixing ratios are 22ppb lower than medium wind speed conditions at higher wind speeds, according to the model.

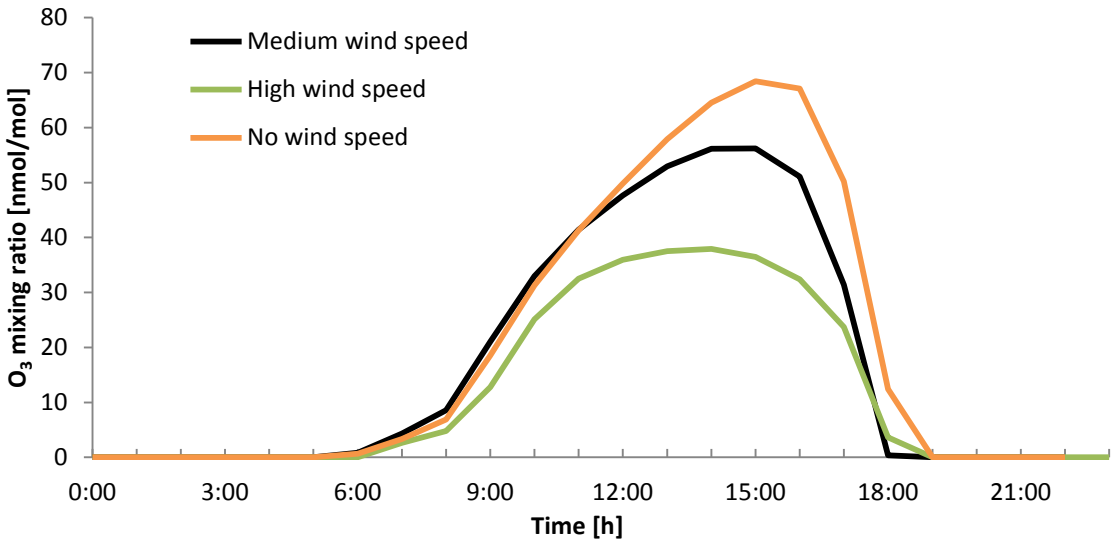

Figure 5.14: Sensitivity of the model to O_3 mixing ratios with changes in wind speed

When the upwind air mass enters the Jhb-Pta megacity it is instantaneously mixed, within the model, with the air in the Jhb-Pta megacity. This also means that if the wind speed doubles and other conditions remain equal, the upwind pollutants are effectively carried in at twice the rate. Therefore, more pollutant air mass, i.e. higher concentrations of NO_x, is transported from the Mpumalanga Highveld into the model, which can lead to the titration of O_3 within the Jhb-Pta megacity. In Figure 5.15, the NO mixing ratios are presented. It is evident that NO levels increase at higher wind speeds from the Mpumalanga Highveld. The same effect is observed for O_3 where a lower concentration of O_3 is advected into the Jhb-Pta megacity at twice the rate the concentrations of O_3 within the Jhb-Pta megacity will decrease. Increasing the O_3-titration effect, results in decreased O_3 levels in the Jhb-Pta megacity. It is therefore important to further investigate the influence of upwind mixing levels in the Mpumalanga Highveld on the Jhb-Pta megacity.

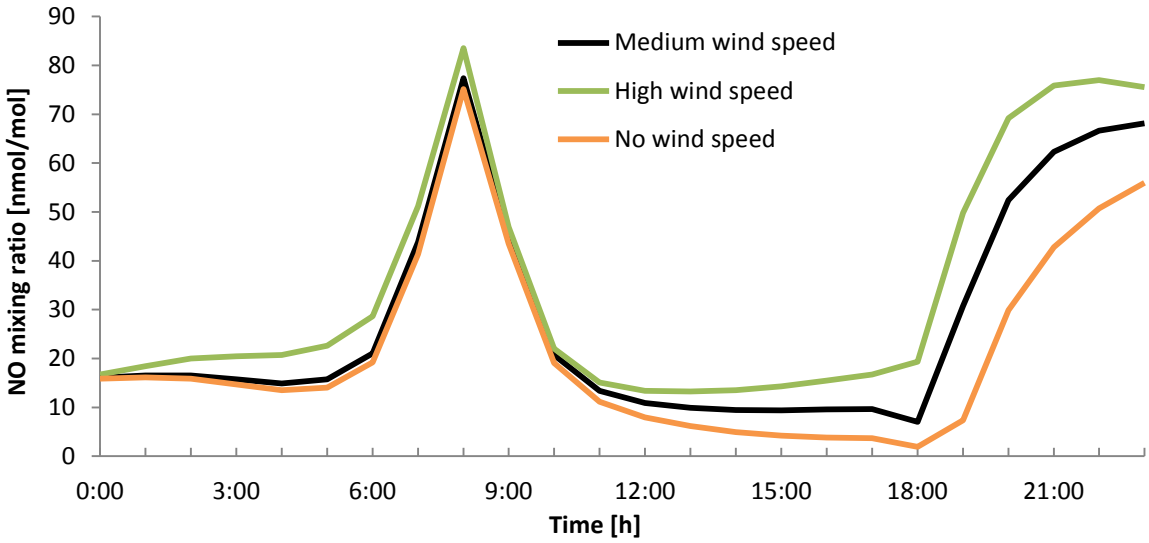

Figure 5.15: Sensitivity of the model to NO mixing ratios with changes in wind speed

In stagnant conditions where no upwind air is advected into the Jhb-Pta megacity, the concentration of the pollutants in the Jhb-Pta megacity is only influenced by the initial concentrations, emission levels, vertical mixing and chemistry within the Jhb-Pta megacity. Under these conditions, the local emissions and vertical mixing tend to contribute significantly to the photochemistry for the formation of O_3.

5.3.2.2 Sensitivity of O_3 production to change in Jhb-Pta megacity emissions

Table 5.8 lists the case studies used in this study to calculate the effect of emissions of VOCs and NO_x in the Jhb-Pta megacity on the photochemical production of O_3 occurring within the Jhb-Pta megacity. In this sensitivity analysis, NO_x is used as the collective term for both NO and NO_2. These case studies were conducted for the reduction and increase in VOC and NO_x concentrations individually, as well as in conjunction with each other. In order to avoid potential nonlinearities associated with changing the chemical regime (e.g. NO_x-limited or VOC- limited), increments of 10 to 50% were used.

Table 5.8: Summary of model runs for the prediction of the effect of increases and reductions of emission of VOCs and NO_x

Model runs	Cases	Increase / reduction incremental percentage of sources (%)
1-5	NO_x reduction only	10-50
6-10	NO_x increase only	10-50
11-15	VOC reduction only	10-50
16-20	VOC increase only	10-50
21-25	NO_x and VOC reduction	10-50
26-30	NO_x and VOC increase	10-50

Figures 5.16(a) and 5.16(b) show the results obtained for changes in NO_x and VOC emissions, respectively, while Figure 5.16(c) presents the results when changes in NO_x and VOC emissions are combined. Increases in the concentrations of NO_x and VOCs are indicated by the dashed lines, while reductions are indicated by the solid lines. It is evident that the reduction of NO_x emissions had a larger effect on O_3 levels than the increase of emissions thereof, while the opposite is observed for changes in VOC emissions. Significant changes in the production of O_3 were calculated for increased VOC emissions, while changes were less pronounced with the reduction of VOC concentrations. Lower NO_x and higher VOC mixing ratios resulted in higher O_3 levels. Interesting to note is the increase in O_3 production when both NO_x and VOC emissions are increased, while a slight decrease in O_3 production is observed when both NO_x and VOC emissions are reduced. The maximum change in O_3 concentrations in response to VOC emission increases was 126%, whereas it was only 27% for the VOC emission reduction. The maximum change in O_3 levels when NO_x emissions were reduced was 35%, while a maximum change of 2% was observed when NO_x emissions were increased. The maximum change in the O_3 concentration in response to the change in VOC and NO_x in combination with each other was 125% when levels of these species were increased. Although the same trend as for VOCs alone is seen, it seems that O_3 production in the Jhb-Pta megacity tends to be more affected by changes in VOC emissions than NO_x levels or both VOC and NO_x.

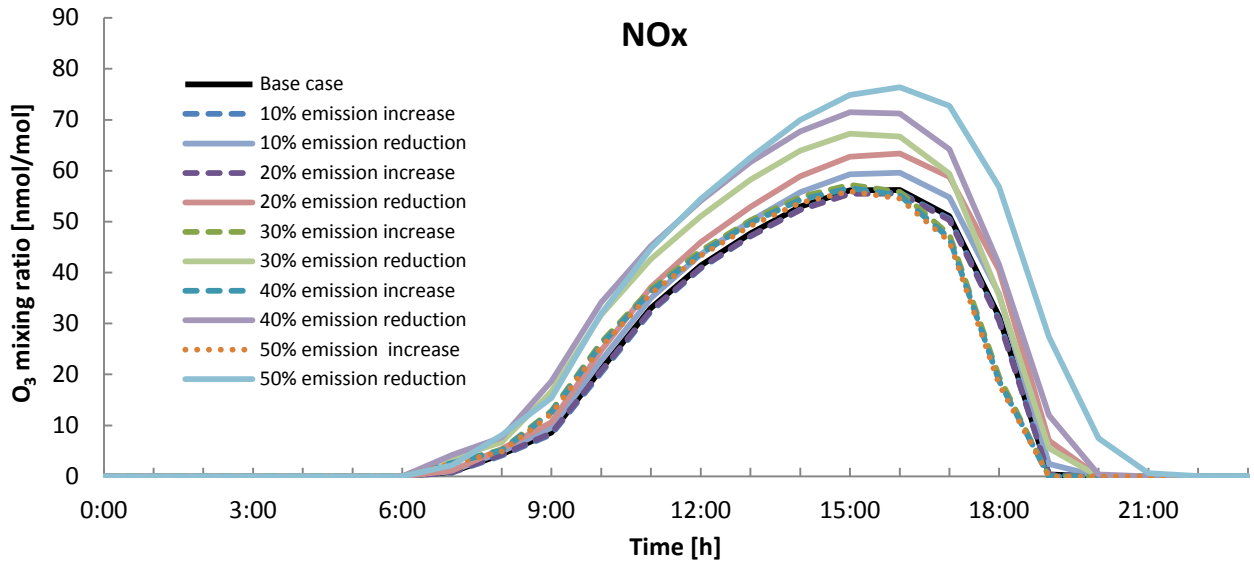
NOx
Base case
10% emission increase
10% emission reduction
20% emission increase
20% emission reduction
30% emission increase
30% emission reduction
40% emission increase
40% emission reduction
50% emission increase
50% emission reduction
O3 mixing ratio [nmol/mol]
Time [h]
0
10
20
30
40
50
60
70
80
90
0:00
3:00
6:00
9:00
12:00
15:00
18:00
21:00

(a)

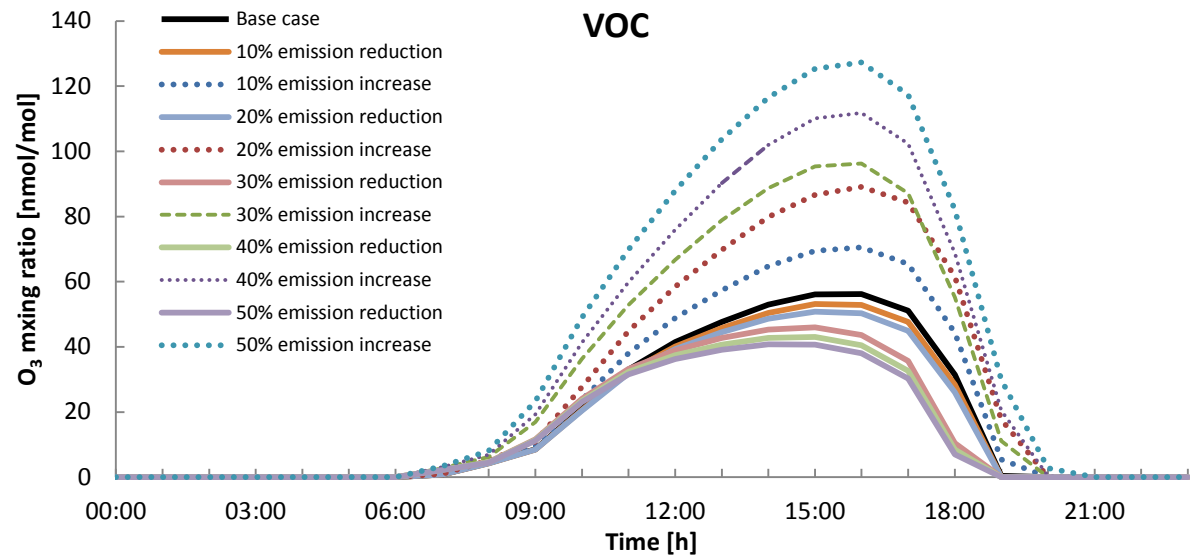
VOC
Base case
10% emission reduction
10% emission increase
20% emission reduction
20% emission increase
30% emission reduction
30% emission increase
40% emission reduction
40% emission increase
50% emission reduction
50% emission increase
O3 mxing ratio [nmol/mol]
Time [h]
0
20
40
60
80
100
120
140
00:00
03:00
06:00
09:00
12:00
15:00
18:00
21:00

(b)

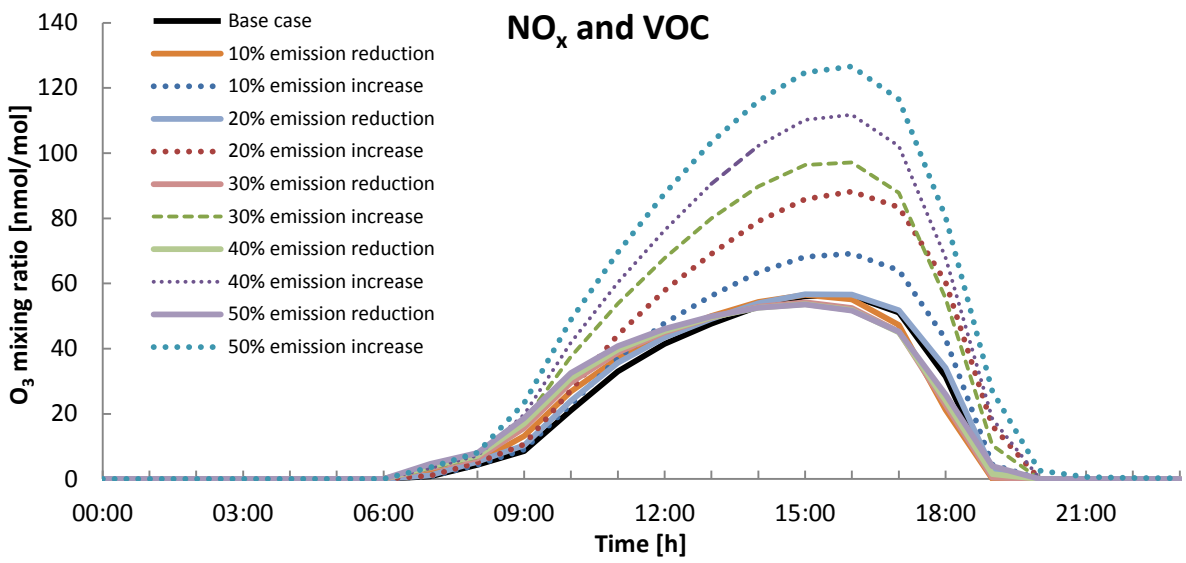

(c

Figure 5.16: O_3 mixing ratios for increases (dash lines) and reductions (solid lines) of NO_x (a), VOC (b) and VOC and NO_x (c) emissions

To better indicate the changes in atmospheric O_3 levels associated with changes in NO_x and VOC emissions individually, as well as in conjunction with one another, the maximum O_3 mixing ratio resulting from the percentage change for each case study was plotted in Figure 5.17. The O_3 base case concentration is indicated by the black cross at 56ppb.

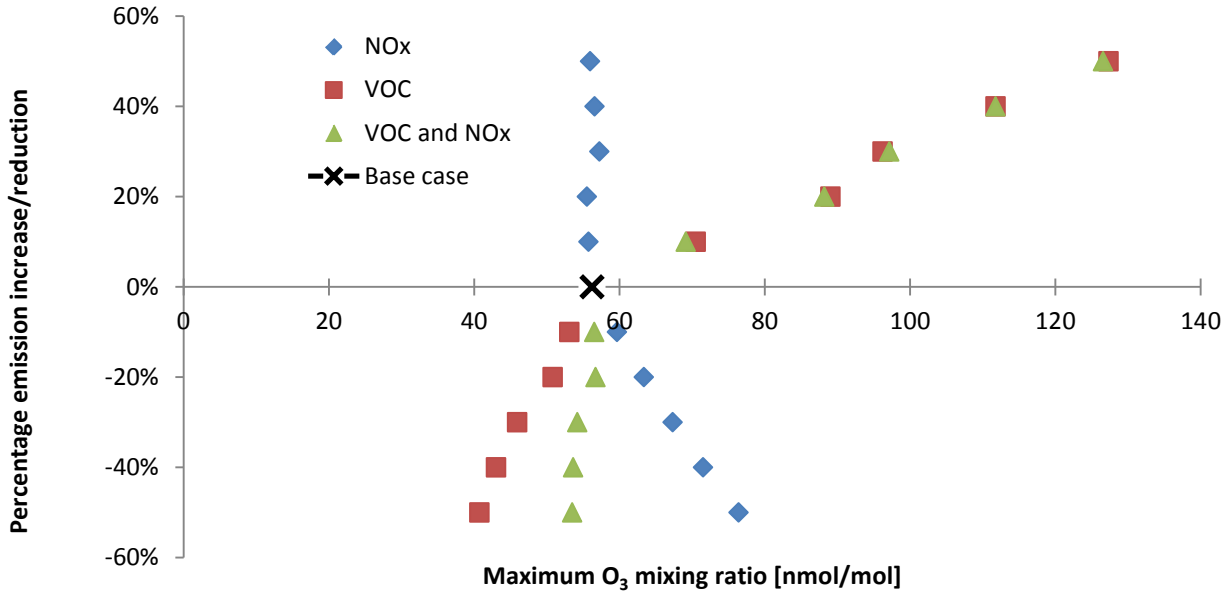

Figure 5.17: The change in the maximum O_3 mixing ratios associated with each percentage increase/decrease of NO_x and VOCs emissions

As discussed previously in Chapter 2, the relationship between NO_x and VOC concentrations for the production of O_3 can be illustrated by means of isopleth plots (Figure 2.6 in Chapter 2). On these isopleth plots, certain chemical regimes can be identified, i.e. areas where O_3 formation depends either on NO_x or VOC concentrations. The results obtained from the incremental changes in Figure 5.17 can be related to these O_3 isopleth plots. Figure 5.18 presents an idealised simplified representation of O_3 isopleths and is not calculated from actual data. Since the construction of isopleths was not part of this study simplified isopleths with representative trajectories will be used to explain the chemical regime, e.g. NO_x-limited or VOC-limited regions. The incremental emission changes in Figure 5.18 and associated changes in the O_3 production rate can indicate the chemical regime that is simulated in the Jhb-Pta megacity.

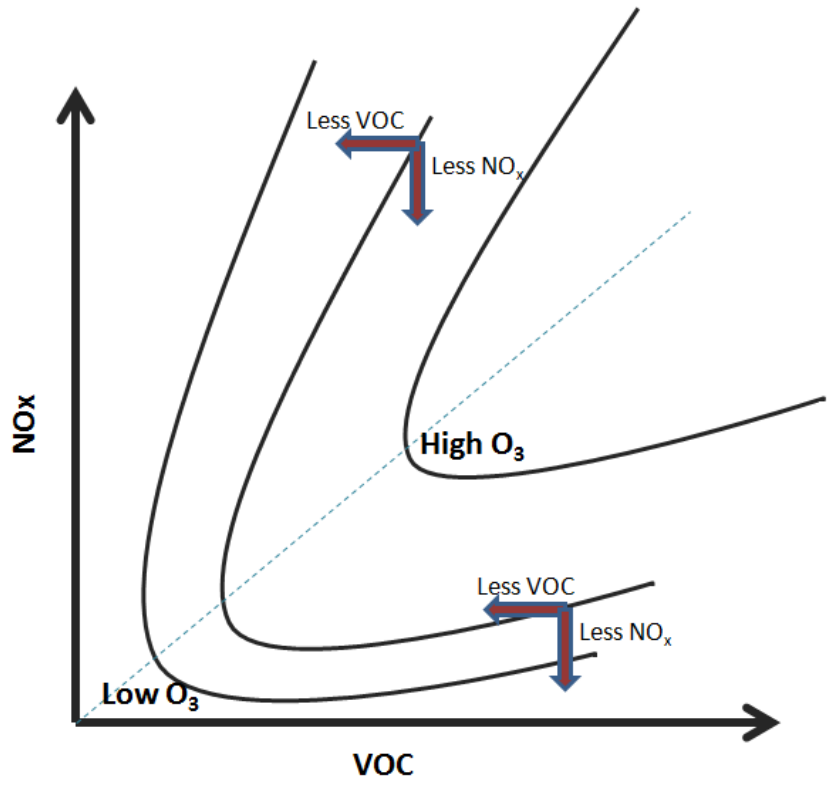

Figure 5.18: Simplified idealised O_3 isopleths as a function of NO_x and VOC levels; the short blue dashed line represents the transition from VOC-sensitive to NO_x-sensitive conditions

The x-axis displays increasing concentrations of VOCs from left to right, while the y-axis represents increasing concentrations of NO_x from bottom to top. The isopleths are the c-shape curves in the body of the graph that present increasing concentrations of O_3 from the bottom left corner to the top right corner, with the concentration of O_3 remaining constant for each isopleth and changes between each isopleth. The top left side of the graph indicates a VOC-sensitive area and the bottom right side an NO_x-sensitive area. The short blue dashed line represents the transition from VOC-sensitive to NO_x-sensitive atmospheric conditions. The central region is the local maximum production of O_3. In the VOC-sensitive regime, the reduction of VOC emissions reduces O_3 production, while the increase in VOC emissions increases the rate of O_3 formation. If NO_x emissions are reduced in the VOC-limited regime, O_3 production will increase and move closer to the maximum O_3 production rate. The opposite effect is seen when NO_x emissions are increased. O_3 production will decrease when moving upwards on the graph, i.e. to a lower O_3 production rate. In the NO_x-sensitive regime (bottom right side), when VOC emissions are

reduced, O_3 production increases as the O_3 production rate trajectory moves towards the local maximum.

In Figure 5.16, an increase in O_3 production is observed when VOC emissions are increased, while O_3 levels decrease when NO_x emissions are increased. Reducing NO_x emissions while keeping VOC emissions constant results in an increase in O_3 concentrations. The changes of O_3 mixing ratios due to the increase in NO_x emissions are lower than the increase of O_3 levels observed when NO_x emissions are reduced. The changes observed with the model can be related to the isopleths in Figure 5.18 in the VOC-sensitive regime.

Chemically, this observation can be explained by the reaction of the $HO^{\bullet}$ radical with NO_2 through Reaction 12 (Chapter 2) that is dominant at high concentrations of NO_x and suppresses the concentration of the $HO^{\bullet}$ radical. The production of $HO_2^{\bullet}$ and $RO_2^{\bullet}$ radicals, which are produced by the oxidation of VOCs with $HO^{\bullet}$ radicals, is slowed down and results in less O_3 production. According to the O_3 isopleths (Figure 5.19), the results shown in Figure 5.17 indicate that the Jhb-Pta megacity is a VOC-limited (or NO_x-saturated) regime. O_3 production in the Jhb-Pta megacity will largely be reduced when the VOC emissions in Jhb-Pta megacity are reduced.

5.3.2.3 Influence of vehicle fleet emissions on O_3 production

As mentioned in Section 5.2.3.1, the current South African vehicular fleet consists of vehicles with emissions classified between Euro-0 and Euro-3. The fuel strategy of the South African government is to only have vehicles on the roads classified as Euro-4 and higher emissions standards in the future (Gazette, 2011). Therefore, in this case study, the effect of reducing vehicular emissions in the Jhb-Pta megacity on the production of O_3 is investigated. Based on the values of emissions associated with each Euro-classified vehicle listed in Table 5.3, a model sensitivity run was performed in which emissions of VOCs, NO_x and CO are reduced from Euro-0 to Euro-3 vehicles. The results are presented in Figure 5.20 and a significant increase in O_3 production of approximately 23ppb is observed. This is consistent with other modelled sensitivity studies of traffic emissions that also predict that future urban O_3 concentrations will increase in many cities by 2050 due to the reduction in NO_x titration of O_3 despite the implementation of O_3 control regulations (Amann *et al.*, 2008). Although these trends were observed with different models for various cities, the reduction in traffic emissions is not the only contributor to the

increase in O_3 levels. Factors such as meteorology, increases in industrial emissions and household combustion can also contribute to the changes in O_3 concentrations.

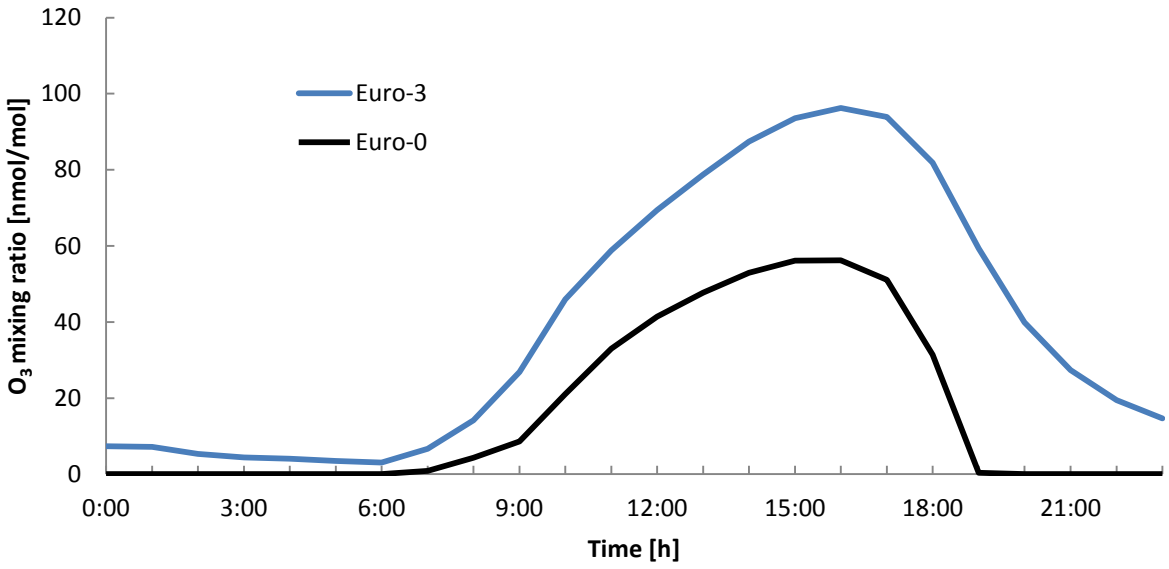

Figure 5.19: Comparison of O_3 production in the Jhb-Pta megacity by changing from Euro-0 to Euro-3 classified vehicles

5.4 CONCLUSION

In this chapter, the MECCA-MCM-UPWIND model, developed based on MECCA-MCM, was used to determine parameters that could potentially be altered in the future to mitigate air pollution in the Jhb-Pta megacity. All of the required input data, i.e. meteorology, emission inventory, ML height and mixing ratios were presented and discussed. The composition of the air masses entering the Jhb-Pta megacity was simulated using MECCA-MCM-UPWIND making use of input data representative of the Mpumalanga Highveld on the eastern border of the Jhb-Pta megacity.

Compared to measured data, MECCA-MCM-UPWIND was able to predict the diurnal variability of NO, NO_2 and O_3 within the Jhb-Pta megacity well. Day-time chemistry was especially well simulated, while small under-predictions were calculated for night-time chemistry. Some of the uncertainties in the model can possibly be attributed to the emission inventories utilised and the deficiency of good NMHC data for the Jhb-Pta megacity. Vertical profiling of tropospheric mixing ratios of pollutant species over the Jhb-Pta megacity would also assist in increasing the accuracy of modelled results.

Sensitivity analyses showed that O_3 mixing ratios decreased with increasing wind speed and increased with decreasing wind speed within the Jhb-Pta megacity. This sensitivity analysis indicated that the Mpumalanga Highveld can potentially be a major source of NO_x in the Jhb-Pta megacity. This implies that if the air quality for the larger surrounding area improves, the concentration of the secondary pollutant O_3 will increase in the Jhb-Pta megacity. This could potentially have health implications in the megacity. A reliable air quality monitoring station located at the boundary region between the Jhb-Pta megacity and the Mpumalanga Highveld would be able to verify the upwind air mass entering the Jhb-Pta megacity.

The influence of NO_x and VOC concentrations on O_3 formation in the Jhb-Pta megacity was also investigated. Results obtained with MECCA-MCM-UPWIND indicated that the Jhb-Pta megacity is a VOC-limited (or NO_x-saturated) regime. Therefore, O_3 levels in the Jhb-Pta megacity will more effectively be reduced if VOC emissions decrease. A reduction of NO_x emissions leads to an increase in O_3 due to a decrease in titration through the reaction with NO. The same effect was observed in various cities world-wide where O_3 levels increased when NO_x emissions were reduced during emission control strategies.

The effect of reducing vehicular emissions in the Jhb-Pta megacity on the instantaneous production of O_3 was also investigated. A significant increase of approximately 23ppb O_3 production was observed when emissions of VOCs, NO_x and CO were reduced from Euro-0 to Euro-3 vehicles. This is consistent with other modelled sensitivity studies of traffic emissions that also predict that future urban O_3 concentrations will increase in many cities by 2050 due to the reduction in NO_x titration of O_3 despite the implementation of O_3 control regulations.

Various measurement studies have indicated that primary pollutant levels decreased during the last decade in cities across Europe and other countries where more strict emission legislation is enforced. In certain cities, especially in cities that were previously NO_x-saturated chemical regimes, this led to an increase in the measured annual average O_3 concentrations (e.g. Keuken *et al.*, 2005; Marr & Harley, 2002; Saavedra *et al.,* 2012; Saikawa *et al.,* 2011; Tang *et al.,* 2012; Xing *et al.,* 2011). This can partly be attributed to less scavenging of O_3 by reduced NO emissions.

Reference

AGENCY, EEA (European Environment. 2009. EMEP/EEA air pollutant emission inventory guidebook.

AMANN, M., ANDERSON, R., ASHMORE, M., DEPLEDGE, M., DERWENT, D., GRENNFELT, P., HEWITT, N., HOV, O., JENKIN, M., KELLY, F., LISS, P., PILLING, M., PYLE, J., SLINGO, J. & STEVENSON, D. 2008. Ground-level ozone in the 21st century: Future trends, impacts and policy implications. London.

BEUKES, J.P., VAKKARI, V., VAN ZYL, P.G., VENTER, A.D., JOSIPOVIC, M., JAARS, K., TIITA, P., LAAKSO, H., KULMALA, D., WORSNOP, D., PIENAAR, J.J., JARVINEN, E., CHELLAPERMAL, R., IGNATIUS, K., MAALICK, Z., CESNULYTE, V., RIPAMONTI, G., LABAN, T.L., SKRABALOVA, L., DU TOIT, M., VIRKKULA, A. & LAAKSO, L. 2013. Source region plume characterisation of the interior of South Africa, as measured at Welgegund. In preparation for submission to Atmospheric Chemistry and Physics.

BLASTING, T.J. 2012. Recent Greenhouse Gas Concentrations. http://cdiac.oml.gov/pns/current_ghg.html Date of access: 15 May 2012.

BLIGNAUT, J.N., CHITTIGA-MABUGU, M.R. & MABUGU, R.M. 2005. Constructing a greenhouse gas emission inventory using energy balances: The case of South Africa for 1998. *Journal of Energy in Southern Africa*, 16(3):21-32.

BUTLER, T.M., LAWRENCE, M.G., TARABORRELLI, D. & LELIEVELD, J. 2011. Tagged Ozone Production Potential (TOPP) of Volatile Organic Compounds. *Atmospheric Environment*, 45:4082-4090.

CARDELINO, C.A. & CHAMEIDES, W.L. 1990. Natural hydrocarbons, urbanization, and urban ozone. *Journal of Geophysical Research Atmosphere*, 95:13971-13979.

CARSLAW, D.C. & BEEVERS, S.D. 2005. Estimations of road vechile primary NO_2 exhaust emission fraction using monitoring data in London. *Atmospheric Environment*, 29:167-177.

CLEMENT, K. & FOSTER, S. 2000. *An investigation into mining as an energy and water using sector and its environmental impacts*.

COLETTE, A., GRANIER, C., HODENBROG, O., JAKOBS, H., MAURIZI, A., NYIRI, A., BESSAGNET, B., D'ANGIOLA, A., D'ISIDORO, M., GAUSS, M., MELEUX, F., MEMMESHEIMER, M., MIEVILLE, A., ROUIL, L., RUSSO, F., SOLBERG, S., STORDAL, F. & TAMPIERI, F. 2011. Air quality trends in Europe over the past decade: A first multi-model assessment. *Atmospheric Chemistry and Physics*, 11:11657-11678.

COLLETT, K.S., PIKETH, S.J. & ROSS, K.E. 2010. An assessment of the atmospheric nitrogen budget on the Highveld. *South African Journal of Science*, 106(5):1-9.

DERWENT, R., JENKIN, M. & SAUNDERS, S. 1996. Photochemical ozone creation potentials for a large number of reactive hydrocarbons under European conditions. *Atmospheric Environment*, 30:181-199.

FOURIE, G.D. 2009. *Personal conversation*. Potchefstroom.

FREEMAN, P.N.W., NAUDE, C.M., PRETORIUS, J., COOVADIA, T. & MATJILA, S.M. 2000. *The transport sector: Energy use and environmental impacts*.

GAFFEN, M., NAUDE, C., LOMBAARD, P., MASSDORP, G., TAYLOR, A. & PRETORUIS, J. 2000. *A quantitive analysis of full cost associated with motor vehicle use in South Africa*.

GAZETTE, Government. 2011. *Department of Energy: Discussion document on the review of fuel specifications and standards for South Africa*.

GONZALEZ, A.G., ALLEN, N.D.C., BERNATH, P.F., BOONE, C.D., MCLEOD, S.D., MANNEY, G.L., TOON, G.C., CAROUGE, C., WANG, Y., WU, S., BARKLEY, M.P., PALMER, P.I., XIAO, Y. & FU, T.M. 2011. Ethane, ethyne and carbon monoxide concentrations in the upper troposphere and lower stratosphere from ACE and GEOS-ChemPa comparison study. *Atmopsheric Chemistry and Physics*, 11:9927-9941.

HEWITT, C.N. 2001. The atmospheric chemistry of sulphur and nitrogen in power station plumes. *Atmopsheric Environment*, 3:387-393.

HURLEY, P. 2002. *The Air Pollution Model (TAPM) Version 2. Part 1: Technical Description*.

JÖCKEL, P., TOST, H., BRÜHL, C., BUCHHOLZ, J., GANZEVELD, L., HOOR, P., KERKWAG, A., LAWRENCE, M.G., SANDER, R., STEIL, G., TANARTHE, M., TARABORRELLI, D., VAN AARDENNE, J. & LELIEVELD, J. 2006. The atmospheric chemistry general circulation model ECHAM5/MESSy1: Consistent simulation of ozone from the surface to the mesosphere. *Atmospheric Chemistry and Physics*, 6:5067-5104.

JORQUERA, H. 2002. Air quality at Santiago, Chile: A box modeling apporach I. Carbon monoxide, nitrogen oxides and sulfur dioxide. *Atmospheric Environment*, 36:315-330.

KEUKEN, M., SANDERSON, E., VAN AALST, R., BORKEN, J. & SCHNEIDER, J. 2005. Contribution of traffic to levels of ambient air pollution in Europe. *In*: *Health effects of transport-related air pollution*, 1st ed. World Health Organization. 54-82 p.

KLEINMAN, L., DAUM, P., LEE, J., LEE, Y., NUNNERMACKER, L., SPRINGSTON, S., NEWMAN, L., WEINSTEINLLOYD, J. & SILLMAN, S. 1997. Dependence of ozone production on NO and hydrocarbons in the troposphere. *Geophysical Research Letters*, 39:575-586.

LIEBENBERG-ENSLIN, H. 2008. *A review of existing information on air quality issues related to vehicle emissions in South Africa*. Johannesburg.

LOGAN, J.A., PRATHER, M.J., WOFSY, S.C. & MCELROY, M.B. 1981. Tropospheric chemistry: A global perspective. *Journal of Geophysical Research*, 86:7210-7254.

LOURENS, A.S.M., BUTLER, T.M., BEUKES, J.P., VAN ZYL, P.G., BEIRLE, S., WAGNER, T., HEUE, K.-P., PIENAAR, J.J., FOURIE, G.D. & LAWRENCE, M.G. 2012. Re-evaluating the NO_2 hotspot over the South African Highveld. *South African Journal of Science*: Submitted.

MARKOVIC, D.M. & MARKOVIC, D.A. 2005. The relationship between some meteorological parameters and the tropospheric concentrations of ozone in the urban area of Belgrade. *Journal of Serbian Chemical Society*, 70(12):1487-1495.

MARR, L.C. & HARLEY, R.A. 2002. Modeling the effect of weekday-weekend differences in motor vehicle emissions on photochemical air pollution in central California. *Environmental Sciences and Technology*, 36:4099-4106.

MCRAE, G.J. & SEINFELD, J.H. 1983. Development of a second-generation mathematical model for urban air pollution: II Evaluation of model performance. *Atmopsheric Environment*, 17:501-522.

MOSCHONAS, M., GLAVAS, S. & KOUIMTZIS, T. 2001. C3 to C9 hydrocarbon measurements in the two largest cities of Greece, Athens and Thessaloniki. Calculations of hydrocarbon emissions by species.Derivation of hydroxyl radical concentrations. *The Science of the Total Environment*, 271:117-133.

ROECKNER, E., BROKOPF, R., ESCH, M., GIORGETTA, M., HAGEMANN, S., KORNBLUEH, L., MANZINI, E., SCHLESE, U. & SCHULZWEIDA, U. 2006. Sensitivity of simulated climate to horizontal and vertical resolution in the ECHAM5 atmosphere model. *Journal of Climate*, 19:3771-3791.

RUDOLPH, J. 1995. The tropospheric distribution and budget of ethane. *Journal of Geophysical Research*, 100:11369-11381.

RUSSEL, A.G., MCCUE, K.F. & CASS, G.R. 1988. Mathematical modeling of the formation of nitrogen-containing air pollutants I. Evaluation of an Eulerian photochemical model. *Environmental Science and Technology*, 22:263-271.

SAAVEDRA, S., RODRIGUEZ, A., SOUTO, J.A., CASARES, J.J., BERMUDEZ, J.L. & SOTO, B. 2012. Trends of rural tropospheric ozone at the Northwest of the Iberian Peninsula. *The Scientific World Journal*, 12:1-15.

SAIKAWA, E., KUROKAWA, J., TAKIGAWA, M., BORKEN-KLEEFELD, J., MAUZERALL, D.L., HOROWITZ, L.W. & OHARA, T. 2011. The impact of China's vehicle emissions on regional air quality in 2000 and 2020: A scenario analysis. *Atmospheric Chemistry and Physics*, 11:9465-9484.

SALBY, M.L. 1996. Fundaments of atmospheric physics. Academic Press.

SCHABERG. 2012. *Personal conversation*. Secunda.

SCHERE, K.L. & DEMERJIAN, K.L. 1984. User's guide for the photochemical box model (PBM).

SCORGIE, Y., ANNEGARN, H.J. & BURGER, L.W. 2004. Fund for research into industrial development growth and equity (FRIDGE). Study to examine the potential socio-economic impact of measures to reduce air pollution from combustion. Pretoria South Africa.

SEINFELD, J.H. & PANDIS, S.N. 1998. Atmospheric chemistry and physics: From air pollution to climate change. New York: Wiley.

SILLMAN, S. 1999. The relation between ozone, NOx and hydrobarbons in urban and polluted rural environments. *Atmospheric Environment*, 33:1821-1845.

SILLMAN, S. & SAMSON, P.J. 1995. Impact of temperature on oxidant photochemistry in urban, polluted rural and remote environments. *Journal of Geophysical Research*, 100:11497-11508.

SOWDEN, M. 2007. Evaluating the ozone potential for the Highveld. Pretirua.

SPALDING-FECHER, R., OKESE, D., EBERHART, R. & DAVIS, M. 2000. Electricity production and the environment.

SWAP, R., GARSTANG, M., MACKO, S.A., TYSON, P.D., MAENHAUT, W., ARTAXO, P., KALLBERG, P. & TALBOT, R. 1996. The long range transport of southern African aerosols to the tropical South Atlantic. *Journal of Geophysical Research*, 101:23777-23791.

TANG, G., WANG, Y., LI, X., JI, D., HSU, S. & GAO, X. 2012. Spatial-temporal variations in surface ozone in Northern China as oberved during 2009-2010 and possible implicatoins for future air quality control strategies. *Atmospheric Chemistry and Physics*, 12:2757-2776.

THOMPSON, A.M., DIAB, R.D., BODEKER, G.E., ZUNCKEL, M., COETZEE, G.J.R., ARHER, C.B., MCNAMARA, D.P., PICKERING, K.E., COMBRINK, J., FISHMAN, J. & NGANGA, D. 1996. Ozone over southern Africa during SAFARI-92/TRACE A. *Journal of Geophysical Research*, D19(101):23793-23807.

TSENG, K-H., WANG, J-L., CHENG, M-T. & TSUANG, B-J. 2009. Assesing the relationship between air mass age and summer ozone episodes based on photochemical indices. *Aerosol and Air Quality Research*, 9(2):148-171.

TYSON, P.D., PRESTON-WHYTE, R.A. & DIAB, R.D. 1976. Towards an inversion climatology of Southern Africa: Part1, Surface inversions. *South African Geographical Journal*, 58(2):151-163.

VENTER, A.D., VAKKARI, V., BEUKES, J.P., VAN ZYL, P.G., LAAKSO, H., MABASO, D., TIITTA, P., JOSIPOVIC, M., KULMALA, M., PIENAAR, J.J. & LAAKSO, L. 2012. An air quality assessment in the industrialized western Bushveld Igneous Complex, South Africa. *South African Journal of Science*, submitted

VOGEL, B., FIEDLER, F. & VOGEL, H. 1995. Influence of topography and biogenic volatile organic compounds emissions in the state of Baen-Wurttemberg on ozone concentrations during episodes of high air temperatures. *Journal of Geophysical Research*, 100:22907-22928.

XING, J., WANG, S.X., JANG, C., ZHU, Y. & HAO, J.M. 2010. Nonlinear response of ozone to precursor emission changes in China: A modeling study using response surface methodology. *Atmospheric Chemistry and Physics*, 11:5027-5044.

Chapter 6
Project evaluation and future perspectives

6.1 INTRODUCTION

As mentioned in Chapter 1, each objective of this study was presented in four separate chapters. Each chapter provided an overview of relevant literature, described the experimental methods utilised, presented the results obtained, as well as discussed and interpreted observations. Each specific objective did, however, form part of the overall objective of this investigation, i.e. to assess ambient air quality in the Jhb-Pta megacity by means of the development of a model for the area. This chapter will evaluate the research project by considering and weighing up the successes and shortcomings encountered for each specific objective. Future perspectives drawn from the results obtained are also discussed.

6.2 PROJECT EVALUATION

Objective 1: **Determine the current air quality in the Jhb-Pta megacity and obtain model input data through:**

a. the establishment of an ambient BTEX, NO_2, SO_2 and O_3 passive sampling network at measurement sites in and around the Jhb-Pta megacity that operated for a period of at least two months;

b. the conducting of active BTEX measurements at some of the sites for eight-hour sample intervals for two consecutive days during each month of sampling.

The main purpose of this objective was to obtain data that could be used as input data in the model developed in this study, as well as to verify the model results. Therefore, the main goal was not to establish a continuous long-term comprehensive field measurement network, but only to collect data that is representative of the Jhb-Pta megacity. A passive sampling network consisting of six sites was successfully established for BTEX, NO_2, SO_2 and O_3 measurements during March and April 2010. At four sites, additional active BTEX

measurements were performed every second week during the same sampling period. Active BTEX sampling was conducted for eight-hour sampling periods between 6:00 and 14:00, 14:00 and 22:00 and 22:00 and 06:00 for two consecutive days. No major logistical problems were experienced during the passive sampling and BTEX active sampling period. One logistical difficulty was experienced for the planned active BTEX sampling during the second week in March 2010. Sampling was rescheduled for the first week in May.

In addition to the passive sampling, active sampling measurements of NO_2, SO_2 and O_3 for three months were also obtained from these monitoring sites. However, due to problems with measurement instruments, data could not be obtained for March and April 2010, but for March, April and May 2009. Although this is not ideal, since passive data could not be compared directly to active measurements, this active data did enable the determination of typical diurnal patterns for NO_2, SO_2 and O_3 during that time of year, which could be used to compare with modelled results.

Objective 2: Contextualise the possible contribution of the Jhb-Pta megacity to the NO_2 hotspot seen over the South African Highveld from satellite retrievals.

It was indicated by the field measurements conducted that the NO_2 Highveld hotspot, which is well known in the international science community due to its prominence in satellite images, is accompanied by a second hotspot over the Jhb-Pta megacity. Peak NO_2 pollution levels in the Jhb-Pta megacity exceeded the maximum daily Highveld ground-level values during the morning and evening rush hours. This result is significant for the more than 10 million people living in the Jhb-Pta megacity. Although satellite instruments have been extremely valuable in pointing out global hotspots, a limitation of satellite retrievals due to their specific overpass times has been presented. This part of the investigation was published in the *South African Journal of Science* (Lourens *et al*., 2012), which emphasises the relevance of this specific objective.

Objective 3: Optimise an existing photochemical box model MECCA (Module Effective Calculating the Chemistry of the Atmosphere) for the Jhb-Pta megacity of South Africa.

An existing photochemical box model, MECCA (Module Effective Calculating Chemistry of the Atmosphere), which was previously improved by including the master chemical

mechanism (MCM) to MECCA-MCM, was further successfully developed in this study to the MECCA-MCM-UPWIND model. This improvement implemented physical processes in the atmosphere, which included advection into and entrainment from the troposphere for a specific area. These processes were included to simulate the advection of upwind air masses into the modelling domain, as well as to determine the entrainment from the troposphere through the diurnal changes of the mixing layer (ML) height. Three processes, i.e. horizontal mixing, vertical mixing and ML height variation, were built into the MECCA-MCM-UPWIND model. These improvements were tested and evaluated. MECCA-MCM-UPWIND proved to be effective to represent mixing processes and all three processes could be simulated.

Objective 4: Utilise the measured data and model to investigate the photochemical processes in the Jhb-Pta megacity and surrounding areas.

The simulation of the composition of air mass entering the Jhb-Pta megacity was accomplished with MECCA-MCM-UPWIND and the data was representative of air mass in the Mpumalanga Highveld. MECCA-MCM-UPWIND was also applied to determine the general air quality in the Jhb-Pta megacity. Although there were uncertainties associated with the input and emissions data used in the model, good comparisons were found between the model runs and observations (field measurements) to within 8% over most of the diurnal cycles. These results indicated that the MECCA-MCM-UPWIND model developed in this study could be used to assess general air quality within the Jhb-Pta megacity. Sensitivity analyses of the model for O_3 production in the Jhb-Pta megacity were also effectively conducted. The influence of changes in wind speeds, emissions within the Jhb-Pta megacity and the vehicle fleet on O_3 levels could be simulated. Results obtained from the sensitivity analyses were in agreement with field measurements and other modelling studies performed in urban areas in the world (Amann *et al.*, 2008).

In general, it can be concluded that this research project was successfully completed, according to the above evaluation of the objectives of this study. A few shortcomings were, however, identified that could be improved upon in future studies.

6.3 FUTURE PERSPECTIVE AND RECOMMENDATIONS

Increased poor urban air quality can have several negative impacts on both humans and the environment, which necessitates the monitoring of pollutants within this area. From the results obtained in this study, the following future perspective can be drawn and recommendations made.

- A comprehensive gridded emission inventory of pollutant species in South Africa is crucial for the assessment of air quality in cities and larger regional areas. This can only be achieved by means of comprehensive long-term ground-based measurements, which are made available to the scientific community, e.g. published in peer-reviewed journals. Data quality must also be assured at monitoring stations. The availability of comprehensive spatial en temporal concentrations of pollutants species will also improve the accuracy of models used for the assessment of air quality in South Africa.

- More comprehensive ground-based and aircraft profile measurements within the Jhb-Pta megacity are required. The actual extent of the contribution of NO2 emissions in the Jhb-Pta megacity to the NO_2 hotspot in the interior of South Africa, in particular, requires direct measurements of tropospheric NO_2 vertical column densities with ground-based or airborne instruments e.g. MAX-DOAS. Airborne DOAS measurements can be used for this type of application. An improved understanding of this pollution hotspot will be valuable, especially in light of eventually determining the consequences of this additional hotspot on health and agriculture, O_3 production and effective mitigation procedures.

- Vertical profiles of pollutant concentrations would also improve the MECC-MCM-UPWIND model by increasing the accuracy of vertical transport estimates.

- Establishing a comprehensive air quality monitoring station at the boundary region between the Jhb-Pta megacity and the Mpumalanga Highveld would assist in verifying air mass advected into the Jhb-Pta megacity determined with MECCA-MCM-UPWIND.

- The influence of the chemical composition of air mass in the Mpumalanga Highveld transported into the Jhb-Pta megacity must also be determined with the MECCA-MCM-UPWIND model. Improved ground-based measurements can also assist to verify modelled results.

- The actual oxidising capacity of the atmosphere in the Jhb-Pta megacity by quantifying O_3 levels must also be determined, to compare the modelled predictions for O_3 concentrations determined in this study.

- Further modelling studies are also required to investigate the relative contributions of the chemistry, mixing and deposition of pollutant species present in the model by performing O_3 budget analyses.

References

LOURENS, A., BUTLER, T., BEUKES, J.P., VAN ZYL, P.G., BEIRLE, S., WAGNER, T., HEUE, K-P., PIENAAR, J., FOURIE, G., LAWRENCE, M. (2012). Re-evaluating the NO_2 hotspot over the South African Highveld. *South African Journal of Science,* 108(11/12):1-6.

AMANN, M., ANDERSON, R., ASHMORE, M., DEPLEDGE, M., DERWENT, D., GRENNFELT, P., HEWITT, N., HOV, O., JENKIN, M., KELLY, F., LISS, P., PILLING, M., PYLE, J., SLINGO, J. & STEVENSON, D. (2008). Ground-level ozone in the 21st century: Future trends, impacts and policy implications. London.

ANNEX A:

Passive (diffusive) sampling

Passive samplers are based on chemical and physical processes, i.e. chemical reactions and laminar diffusion, respectively. The rate at which gases in ambient air diffuses into the sampler is governed by Fick's Law of diffusion, which is influenced by physical parameters, such as gaseous diffusion through a static layer or porous material that is controlled by the diffusion coefficient of the respective gases (Brown, 1999). A graphical representation of the passives samplers used is given in Figure A.1.

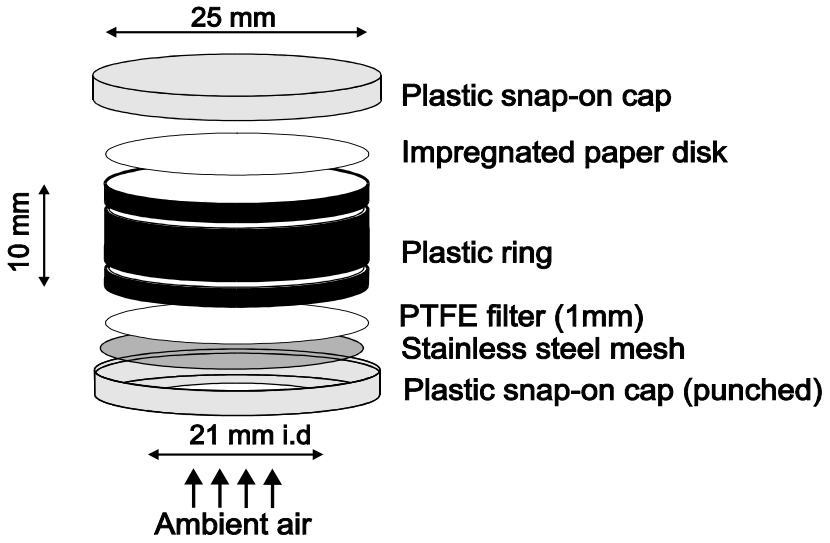

Figure A.1: Schematic representation of a diffusive sampler (Dhammapala, 1996).

The sampler consists of two plastic snap-on caps with a stainless steel mesh (25 mm o.d., thickness of 160 µm and porosity of 40 %) and PTFE Teflon filter (25 mm o.d., 175 µm and porosity of 85 %) to prevent aerosols entering. A Whatman paper filter impregnated with a chemical to specifically react and trap the pollutant of interest, was placed at the rear end of the sampler. The plastic snap-on caps were held together by a plastic ring. Figure A.2 shows the passive samplers used during the study.

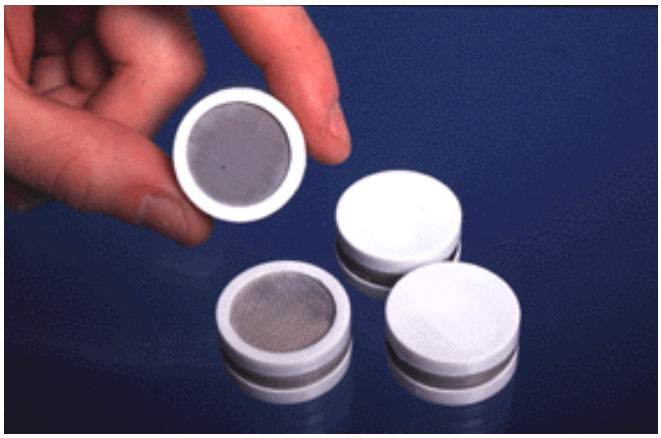

Figure A.2: Passive samplers used during the study.

The equation governing Fick's first law of diffusion (Equation 2.1) states that the flux of matter (rate at which mass transfer occurs) due to diffusion in the direction of the mass flow, is proportional to the concentration gradient of the matter.

$$\emptyset = -D\frac{dC}{dL} \qquad \text{A.1}$$

$\emptyset$ = flux of gas in direction of concentration gradient (µg.m^{-2}s^{-1}),

D = diffusion coefficient of gas (m^{2}s^{-1}),

C = concentration of pollutant (µg m^{-3}),

L = diffusion path length, corrected for the Teflon filter, steel mesh and static air layer (m) and

$\frac{dC}{dL}$= instantaneous concentration gradient of pollutant in direction of air flow.

Given that diffusive sampling is time integrated,

$$\frac{\boldsymbol{dX}}{\boldsymbol{dt}} = \emptyset \qquad \text{A.2}$$

X = amount of pollutant trapped on paper disk corrected for the blank (µg),

A = cross sectional area of diffusion path (m^2) and

t = sampling time (s).

the combination of equation 2.1 and 2.2 results in the elimination of Ø that gives

$$\frac{dX}{dt} = \boldsymbol{A} * \boldsymbol{D}\frac{dC}{dL} \qquad \text{A.3}$$

Integrating and rearranging gives

$$\boldsymbol{C_{avg}} = \frac{\boldsymbol{X}}{\boldsymbol{Dt}} * \frac{\boldsymbol{L}}{\boldsymbol{A}} \qquad \text{A.4}$$

The term L/A is the sum of all L/A contributions from the sampler components, i.e. $L/A=[(L_R/A_R) + (L_F/A_F) + (L_N/A_N) + (L_S/A_R)]$ where L_R and A_R are the thickness and area of the plastic ring respectively, L_F is the thickness of the Teflon filter and A_F is the total area of the pores through wich diffusion takes place, L_N and A_N are the same parameters for the steel net and L_S is the length of the static layer. It must be noted that even though the diameters of the Teflon filter and steel net are both 25 mm, the diffusion takes place through a 21 mm diameter section of it (Dhammapala, 1996).

The results are reported in mixing ratios in order to eliminate the pressure dependency on the diffusion coefficient (Dhammapala, 1996). The ideal gas law is applied to Equation 2.1 and the mixing ratio is given by the formula:

$$C_{avg}(ppb) = \left(\frac{1000*R*T}{Mr*D*t}\right) * \frac{\boldsymbol{L}}{\boldsymbol{A}} \qquad \text{A.5}$$

T = absolute temperature during the sampling period,
Mr = relative molecular mass of the gas in question and
R = gas constant, 8.31 J K^{-1} mol^{-1}.

The amount of the pollutant trapped on the filter (X) can be calculated from the analytical result by multiplying the concentration of the analyte of interest in the sample (μg.dm^{-3}) by the total volume of the sample (dm^3) and then subtracting the blank concentration. The diffusion coefficients for the gas pollutants measured in this study are:

NO_2	1.52 x 10^{10} m^2s^{-1}
SO_2	1.30 x 10^{10} m^2s^{-1}
O_3	1.48 x 10^{10} m^2s^{-1}

The preparation method of passive samplers described by Dhammapala (1996) was used in this study. The same method of preparation was followed for both SO_2 and O_3 passive samplers. All the parts of the passive samplers were washed with EXTRAN, sonicated in de-ionised water and air dried before they were used. The Whatman filters were sonicated at least four times with water and methanol consequently, after which they were air-dried in a vacuum desiccators (Lourens, 2008).

For NO_2 sampling the cellulose filers were impregnated with a solution containing NaOH and NaI dissolved in methanol and water, which was used as absorbent to collect NO_2 in the atmosphere. During the absorption process, NO_2 is converted into nitrite (NO_2^-) and is chemically trapped on the filter by the reaction

$$2NO_2(g) + 3I^- \rightarrow 2NO_2^- + I_3^- \qquad \text{R44}$$

NaOH was added, to ensure a pH of 13 or higher in order to stabilise the NO_2^- species, which can otherwise be oxidised to NO_3^- by O_3 if the pH drop to 12 or lower. I^- was added in excess, to prevent atmospheric oxidants that can oxidise these species to I_2, from diffusing into the sampler (Martins *et al.*, 2007). The absorbing solution was carefully loaded over the surface of the Whatman filter with a micro-pipette and then loaded into the snap-on cap casing, which was then attached to the ring casing. On the other end, the Teflon filter was loaded against the steel mesh inside the snap-on punched cap, and then onto the ring casing as seen in Figure 2.12.

The samples were marked with a date, intended site and gaseous species, before being sealed in a plastic vial for transportation. Laboratory blank samples were also prepared on the same day, to compensate for any systematic errors and contamination present in the reagents, vials, or Whatman filters. This was conducted in exactly the same manner for SO_2 and O_3.

The passive samplers were removed from their vials on arrival at the site and slid into a bracket on an aluminium rail with the front of the sampler facing down (see Figure A.4). After the exposure period, the samples were replaced in their vials and stored below 18°C before analysis.

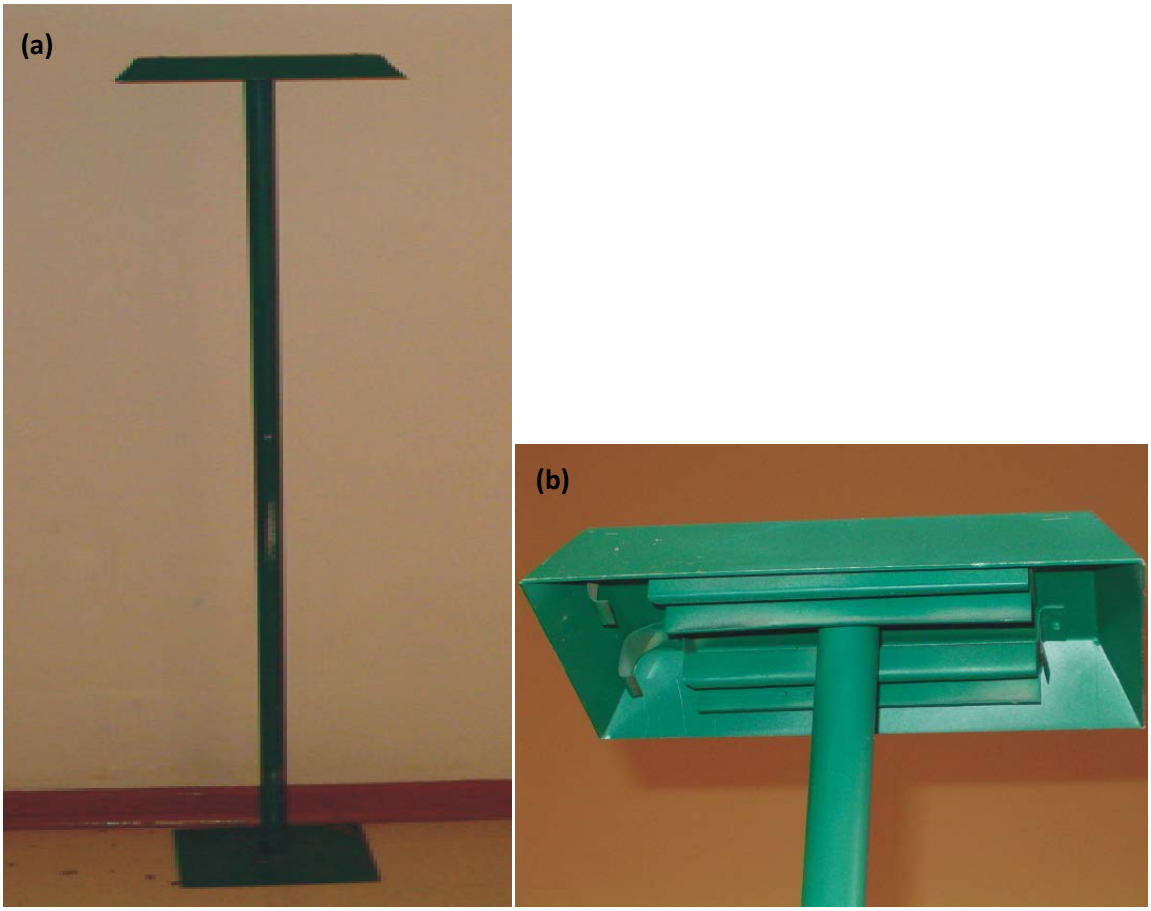

Figure A.4: (a) Sampler hood with aluminium rail (b) Aluminium sampler stand (adopted from Lourens, 2008).